UNIVERSITY OF CALIFORNIA

Santa Barbara

Manipulating Chemistry at the Molecular Level for the Development of Stimuli Responsive Materials

A dissertation submitted in partial satisfaction of the requirements for the degree Doctor of Philosophy in Chemistry

by

Meghan Frances Nichol

Committee in charge:

Professor Javier Read de Alaniz, Chair

Professor Mahdi Abu-Omar

Professor Craig Hawker

Professor Armen Zakarian

December 2020

The dissertation of Meghan Frances Nichol is approved.

_____

Javier Read de Alaniz, Committee Chair

_____

Mahdi Abu-Omar

_____

Craig Hawker

_____

Armen Zakarian

December 2020

This dissertation is dedicated to my parents.

Without your constant love and support, this would not have been possible.

Thank you!

Manipulating Chemistry at the Molecular Level for the

Development of Stimuli Responsive Materials

ACKNOWLEDGEMENTS

As I approach this momentous milestone in my life I have mentally written and rewritten these acknowledgements too many times to count. I have realized there are many people—family, friends, mentors, and colleagues—whom without this would not be possible. In my opinion there are no words that can accurately describe how much every ounce of support has meant to me.

I want to first thank my graduate advisor, Javier. Thank you for taking the chance on me and allowing me to be the fourth student you took on my first year. We have had hard conversations, but in the end, it has all been worthwhile, and I will always appreciate you pushing me to be my best self. With your help I have not only been able to gain skills in lab and grow as a scientist, but I have also grown to be a more confident and stronger person.

I would next like to thank my undergraduate professors who encouraged me to pursue my PhD to begin with. Dr. K and Dr. Crowder there truly are not enough words to tell you each how much you have shaped me as a scientist and a person. I am beyond thankful that you both not only pushed me during my time at Lewis, but you both continue to influence my academic career throughout grad school. I always loved stopping by campus for surprise visits and chatting for hours to catch up. It means the world to me to have both of you present at my defense and watch me finish what you helped me start.

During my time at UCSB I had the privilege to meet and work with an amazing group of people. I want to thank the members of the Read lab, both past and present, for not only helping with my projects but also being willing to answer my dumb questions when I first started. I specifically want to thank Gabby, Helena, José, Kyle, Manny, and Jeff for working on projects alongside me. I also want to give a shout out to Craig Hawker for allowing me to

work in the PSBN 4th floor Hawker lab and Allison for sharing her hood with me for the last couple years. Allison, it has been so much fun to work next to you and I will miss our little gossip sessions.

While living in Santa Barbara I gained lifelong friends who I will miss when I leave. Thank you to the UCSB friends: Manny, Jeff, Kyle, Jake, Allison, Angelique, and Pat. I appreciate all the fun times and adventures we have had, and I am so glad grad school allowed us to cross paths. Outside of UCSB, I have had the pleasure to meet people I know will always be a part of me. I'll miss my MadFit family and Corepower community. Special thank you to Morgan, Aly, Marianne, Rebecca, and Natalie for always giving me a space to chat, vent, and grow. I will miss you all so much, but remember, it is see you later, not goodbye.

Along with the amazing friends I gained these last 5 years, I could not have made it through grad school without the support of my hometown pals—Brandon, Bianca, Phoenix, Daniel, Jake, Frank, and Tony. Hanging out with you all whenever I was home was always a highlight of my visits. Lewis brought us together and I am so glad we stayed in touch and continue to support one another.

My #bestiesfortheresties, Sarah and Alisha, I love you both so much and I cannot thank you both enough for supporting me these last 5 years. You have been there for me on the good days and the bad days. Sarah, I had such a blast living with you these last 3 years, it will be weird not seeing you every day anymore. Alisha, thank you for having an open-door policy for me, I loved my trips to SD.

Manny, you quickly became my best friend in grad school, and I am so happy to have you as my constant support and shoulder to lean on. You have made the hardest days better and I cannot thank you enough. From working in lab to travelling and going on adventures, I

have loved every minute of our time together. Thank you for being there for me and pushing me to continue to grow and realize my potential, I cannot wait to see what the future holds for us.

To my family, you have all been my rock throughout my life. I was never short of cheerleaders and it means more than you can imagine for you all to attend my defense and celebrate with me. From the countless texts, calls, and trips home, I always knew I would be welcomed with excitement and open arms. I know the last 5 years have not been easy on you either and that is why I feel this degree is as much yours as it is mine. I could not have completed this journey without you.

Lastly, Mom and Dad, there really will never be enough words to thank you not only for the support you have offered these last 5 years, but for all of the good and bad days since I was born. You have both been by my side for everything and I dream to be as amazing a parent as you one day. I love you both so much and I am so excited to finish this journey with you both here cheering me on.

Meghan F. Nichol
776 Madrona Walk Apt B, Goleta, CA 93117
1(630) 745-9219
mnichol@ucsb.edu

EDUCATION

Lewis University, Romeoville, IL — Aug 2011 – May 2015
Bachelor of Science in Chemical Physics
Minor in Mathematics
Distinguished Scholar Diploma

University of California, Santa Barbara — Sept 2015 – Present
Doctorate in Chemistry
Focus in Organic Chemistry

RESEARCH EXPERIENCE

Lewis University, Romeoville, IL — Sept 2012 – May 2015
Research– with Dr. Jason Keleher

- Studied the field of chemical mechanical planarization and polished various substrates while working with different nanoparticle solutions to develop new slurries.
- Formulated a novel slurry for nickel-phosphorus CMP alongside Nanophase Technologies Corporation in Romeoville, IL.
- Co-authored 1 manuscript and presented at 4 conferences.

University of California, Santa Barbara — Jan 2016 – Present
Research– with Dr. Javier Read de Alaniz

- Developed and synthesized a new logic-controlled trigger unit for self-immolative polymers (SIP).
- Developed an enantioselective PCCP Brønsted acid-catalyzed aza-Piancatelli rearrangement.
- Working towards the design and development of new novel polymer binders for additive manufacturing.
- Mentored 4 undergraduate student researchers through instrument training, synthetic methods development, and characterization techniques and ensured safe execution.
- Co-authored 2 manuscripts for peer-reviewed journals and presented at 2 conferences.

AWARDS

St. John Baptist de La Salle Scholarship	2011 – 2015
Father John Brennan Endowed Scholarship	2011 – 2014
Dean's List	2011 – 2015

Brother David Delahanty Award	2011 – 2015
2nd Annual Celebration of Scholarship Poster Session Winner	Spring 2012
ACS Organic Student of the Year – Joliet Section	Spring 2012
3rd Annual Celebration of Scholarship Poster Session Winner	Spring 2013
Robert H. DeWolfe Teaching Fellowship in Organic Chemistry	Spring 2017
Mellichamp Academic Initiative in Sustainability Fellowship	Summer 2017
Robert H. DeWolfe Teaching Fellowship in Organic Chemistry	Spring 2018
Outstanding service to the Department Award	Spring 2019

TEACHING EXPERIENCE

University of California, Santa Barbara — Sept 2015 – June 2016

Teaching Assistant – with Dr. Petra Van Koppen

- Supervised and taught the general chemistry lab series.

University of California, Santa Barbara — June 2016 – Aug 2018

Teaching Assistant – with Dr. Morgan Gainer

- Supervised and taught the second section of the organic chemistry lab series.
- Developed a new multi-step synthesis experiment for the third section of the organic chemistry lab series.

University of California, Santa Barbara — Sept 2018 – March 2019

Head Organic Teaching Assistant – with Dr. Morgan Gainer

- Supervised other organic chemistry TAs
- Helped train Tas
- Developed a new experiment for an advanced organic lab

PUBLICATIONS

Patrick G. Murray; Abigail Hooper; Jason Keleher; Jordan Kaiser; Meghan Nichol; Getting the most out of your cerium oxide glass polishing slurry: reducing risk and improving performance with plasma produced particles. Proc. SPIE 8884, Optifab 2013, 88840J (September 6, 2013); doi:10.1117/12.2028868.

"Preparation of Cyclopent-2-enone Derivatives via the Aza-Piancatelli Rearrangement," Nichol, M.; Limon, L.; Read de Alaniz, J. *Organic Syntheses* **2018**, *95*, 46-59.

"Enantioselective PCCP Brønsted Acid-catalyzed Aza-Piancatelli Rearrangement," Hammersley, G. R.; Nichol, M. F.; Steffens, H. C.; Delgado, J. M.; Veits, G. K.; Read de Alaniz, J. *Beilstein J. Org. Chem.* **2019**, *15*, 1569-1574.

"Multi-stimuli Responsive Trigger for Temporally Controlled Depolymerization of Self-immolative Polymers," Nichol, M.F.; Clark, K. D.; Dolinski, N. D.; Read de Alaniz, J. *Polym. Chem.* **2019**, *10*, 4914-4919.

"Discovery-Based S_NAr Experiment in Water Using Micellar Catalysis," Landstrom, E. B.; Nichol, M. F.; Lipshutz, B. H.; Gainer, M. J. *J. Chem. Educ.* **2019**, *96*, 2668-2671.

PRESENTATIONS

"Interferometric Measurements of Liquid Indices of Refraction," M. Moy, M. Munar, M. Nichol, B. Garcia, C. Crowder, Celebration of Scholarship, Romeoville, IL, April 2013.

"Getting the Most Out of Your Cerium Oxide Glass Polishing Slurry: Reducing Risk and Improving Performance with Plasma Produced Particles," P. Murray, A. Hooper, J. Keleher, J. Kaiser, M. Nichol, SPIE 2013 Optifab, Rochester, NY, October 2013.

"Multi-Stimuli Responsive Trigger for Temporally Controlled Depolymerization of Self-Immolative Polymers," M. Nichol, K. Clark, N. Dolinski, J. Read de Alaniz, ACS National Meeting, Orlando, FL, April 2019.

POSTERS

"Evaluation of Mechanisms Relevant to the Chemical Mechanical Planarization of HDD Media," M. Nichol, J. Kaiser, J. Keleher, Celebration of Scholarship, Romeoville, IL, April 2013.

"Evaluation of Mechanisms Relevant to the Chemical Mechanical Planarization of HDD Media," M. Nichol, J. Kaiser, J. Keleher, National Collegiate Honors Council, New Orleans, LA, November 2013.

"Probing Surface Interactions of Copper Substrates with Respect to Activation Energy and Electrochemical Properties," M. Nichol, J. Keleher, Celebration of Scholarship, Romeoville, IL, April 2014.

"Electrochemical Analysis of Film Forming Mechanisms Relevant to Data Storage Chemical Mechanical Planarization," L. Janes, S. Parker, M. Nichol, J. Kaiser, J. Keleher, Celebration of Scholarship, Romeoville, IL, April 2014.

"Electrochemical Analysis of Film Forming Mechanisms Relevant to Data Storage Chemical Mechanical Planarization," L. Janes, S. Parker, M. Nichol, J. Kaiser, J. Keleher, National Collegiate Honors Council, Denver, CO, November 2014.

"Exploring the Chemical Mechanical Planarization Process of Diverse Substrates," A. Mlynarski, M. Nichol, L. Janes, J. Keleher, Argonne National Laboratory Undergraduate Symposium, Argonne, IL, November 2014.

"Advancements Towards the Aza-Piancatelli Rearrangement," M. Nichol, G. Veits, G. Hammersley, H. Steffens, E. Doherty, J. Read de Alaniz, National Organic Symposium, Davis, CA, June 2017.

"Exploring the Mechanical Properties of Organic Photochemical Materials," J. Delgado, F. Stricker, M. Nichol, J. Read de Alaniz, ACS National Meeting, Orlando, FL, April 2019.

MEMBERSHIPS AND OUTREACH

American Chemical Society, Fall 2011 – Present
Society of Physics Students, Lewis University Chapter, Fall 2013 – Spring 2015
Delta Epsilon Sigma (Catholic Honor Society), Fall 2013 – Present
Iota Sigma Pi (Women in Science), Spring 2014 – Present
Graduate Students for Diversity in Science, Fall 2016 – Present
Photographer, Fall 2016 – Present
Treasurer, Fall 2019 – Present

ABSTRACT

Manipulating Chemistry at the Molecular Level for the

Development of Stimuli Responsive Materials

by

Meghan Frances Nichol

The ever-growing field of materials science has utilized its interdisciplinary nature to allow the advancements in research ranging from small molecule uses to polymer material discovery. Specifically, the development of stimuli responsive materials has become of interest while showcasing the importance of small molecule functionality and reactivity. Stimuli responsive materials, or materials that respond to their environment, was derived through studies to understand structure-activity relationships within materials science. Through the use of chemical and physical stimuli, this field has seen growth through the discovery of photoswitches, micelles, self-healing materials, and more. This thesis explores the utilization of acid and heat as tunable stimuli to enable new control and selectivity by which small molecule and materials can be manipulated.

Acid catalysis is a well-studied field within organic chemistry where we see the utilization of the acid for altering reaction kinetics and product formation. Within this area of research, chiral acid catalyst not only take part in affecting kinetics and product formation, but also enable stereochemistry to be controlled. Stereochemistry is vital for organic syntheses due to the relationship between selectivity and reactivity where enantiomers can often have drastically different properties. Through the development of the asymmetric aza-Piancatelli reaction, I developed a new approach using chiral PCCP Brønsted acid catalyst leading to enantioselectivity above 85% ee.

Building on my understanding of the aza-Piancatelli mechanism in small molecules we translated this work into a novel dual-responsive trigger for self-immolative polymers (SIPs). Utilizing the chemistry developed in the aza-Piancatelli rearrangement, we were able to manipulate the reaction's use of acid catalysis and push towards the development of a new temporally controlled trigger unit for SIPs. This class of polymers is unique due to its characteristic ability to undergo end-to-end depolymerization in the presence of a given triggering stimuli. Previously, SIPs were known to undergo this depolymerization spontaneously when triggered; however, through the use of orthogonal chemistry—heat and acid—a trigger unit was developed that can now offer ON/OFF depolymerization control.

The temporal control offered through thermally triggered materials was not only advantageous for work in SIPs, utilizing temperature as a stimulus encouraged the investigation into controlling the reactivity of isocyanates in polyurethane formation. Isocyanates are widely used in polyurethanes found in paints, sealants, adhesives, and polymer binders for energetic materials. Although well studied and used since the 1940's, the processes used for curing of polymer binders is continuing to advance. With goals of pushing materials towards 3D printing, we are developing new formulations utilizing blocked isocyanate chemistry. This class of materials is produced via the addition of a blocking—or protecting—group to the isocyanate functionality to extend material pot life as well as add a handle of control over the isocyanate's reactiveness. While still on going, this thesis will show the progress of these new materials.

Access to new materials has become possible via detailed mechanistic studies of chemistry starting at the small molecule. This thesis presents the development of stimuli

responsive materials through the utilization of chemical and physical stimuli for more control over reaction kinetics and selectivity.

TABLE OF CONTENTS

LIST OF FIGURES

Chapter 1

Chapter 2

Chapter 3

Chapter 4

LIST OF SCHEMES

Chapter 2

Chapter 3

Chapter 4

LIST OF TABLES

Chapter 2

1 Introduction

1.1 Materials Science

The field of materials science was developed through the combination of chemistry, physics, and engineering. Materials science puts an emphasis on researching how the processing of a material later influences the material's properties, structure, and performance.[1] Understanding the connection between these components is vital for designing and creating new materials and advancing current technology. The interdisciplinary nature of materials science allows for these advancements in research to occur in work ranging from small molecules to polymer material development. This thesis will focus on how chemistry at the molecular level can be used to aid in the development of stimuli-responsive materials. These materials will focus on using a) acid stimuli for small molecule rearrangements,[2] b) dual stimuli for the controlled release of small molecules from a polymeric system,[3] and c) thermal stimulus for controlling the reactivity in curing formulations for 3D printing.

1.2 Stimuli Responsive Materials

The materials research in this thesis will focus on stimuli-responsive chemistry, which is defined as chemistry that responds to its environment.[4,5] By studying these reactions and changes, we can begin to understand and probe structure-activity relationships within materials science. Due to the responsive nature of these materials, they can commonly be referred to as "smart" materials. These "smart" materials can be triggered by a range of

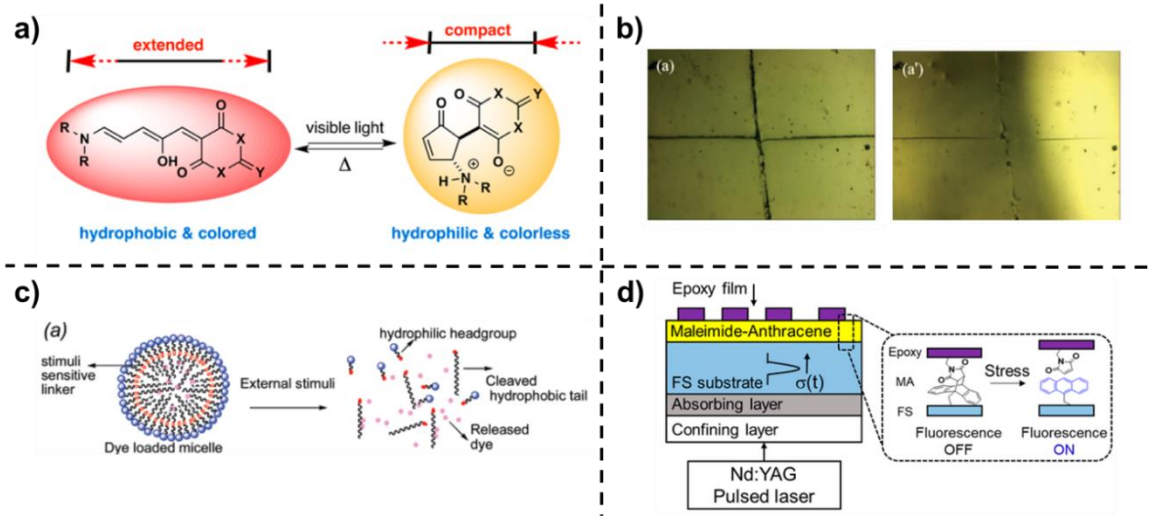

Figure 1. 1

a) Visible light reactive DASA photoswitches (Reprinted with permission from J. Am. Chem. Soc. 2014, 136 (Reference #9) Copyright 2014 American Chemical Society.); b) self-healing polyurethane pre (left) and post (right) heat treatment (Adapted with permission from Macromol. Mater. Eng. 2020, 1900782 (Reference #10) © 2020 John Wiley & Sons, Inc. CCC License Number 4958900819967); c) schematic representation of redox reactive micelle and dye release (Adapted with permission from Langmuir 2007, 23 (Reference #11) Copyright 2007 American Chemical Society.); d) diagram representing the laser-induced stress waves to mechanically activate the material (Reprinted with permission from J. Am. Chem. Soc. 2018, 140 (Reference #12) Copyright 2018 American Chemical Society.)

stimuli. The most common stimuli available fall within two major categories: chemical or physical stimuli.[6,7] Chemical stimuli include acid/base reactions, enzyme chemistry, redox reactions, etc. Physical stimuli include thermal or photo reactivity as the most common, however sonication, mechanical, and electrical stimuli can also be used.[7,8] Some commonly seen examples of stimuli responsive materials and their stimuli include: photoswitches (light),[9] self-healing materials (heat),[10] micelle assembly and disassembly (redox chemistry),[11] and mechanical work on polymers (electrical energy).[12] (Figure 1.1) Of these, acid and heat offer greater tunability. For example, in acid catalysis we can alter the reactivity of the material by changing our acid catalyst between Brønsted and Lewis acids as well as selecting acids based upon their pK_a values. This reactivity difference from acid pK_a values is displayed in work done by our group on Brønsted acid catalyzed vitrimers (Figure

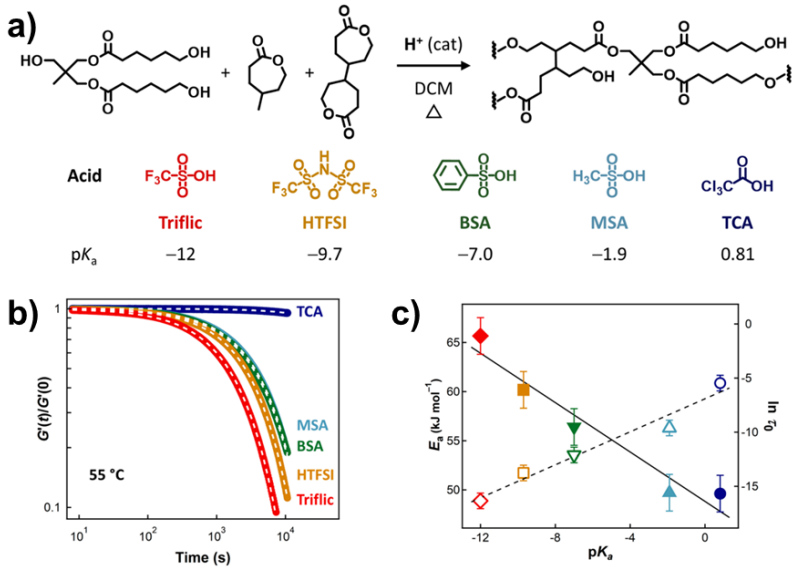

Figure 1. 2

a) synthesis of polyester vitrimers and acid catalysts to promote transesterification; b) oscillatory rheology step-strain stress relaxation of polyester vitrimers containing differing acid catalysts; c) Activation energy (filled symbols) and Arrhenius prefactor (open symbols) correlated to acidity of catalyst. Adapted with permission from ACS Macro Lett. 2018, 7 (Reference #13) Copyright 2018 American Chemical Society.

1.2).[13] In this work, Self et al. demonstrates how the difference in the acid catalyst's pK_a can alter various properties of his dynamic covalent networks including relaxation time and activation energy.[13] Meanwhile, heat is also an advantageous stimulus due to the ability to impart temporal control into a reaction. By exploiting a reaction's kinetics and activation energy we can begin to study the possibilities of selective reactivity within a material. A great example of this control is seen in our group's previous work on temperature-tunable polymer functionalization where Discekici et al. were able to utilize the difference between *endo* and *exo* retro-Diels–Alder activation temperatures (Figure 1.3).[14]

As the application of stimuli responsive materials has grown more complex and sophisticated, it has become apparent that there is a need to enable more precise spatial and temporal control over the activation from the stimuli. To address this need, investigations

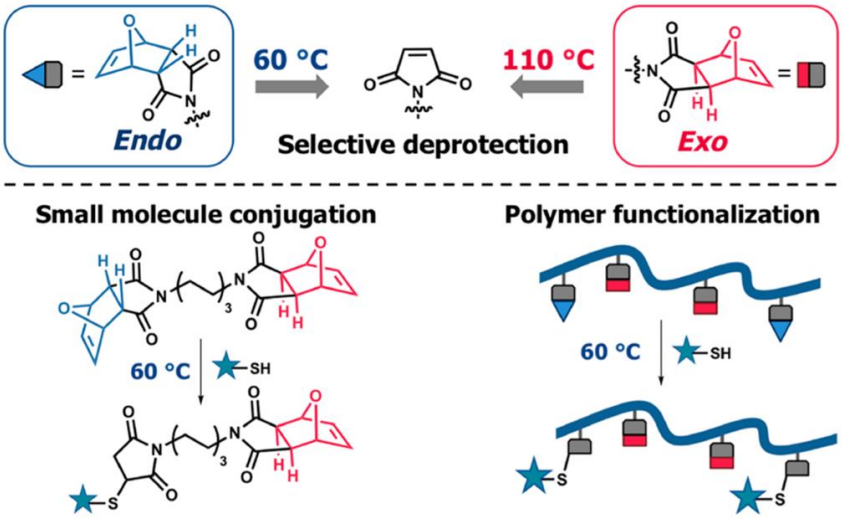

Figure 1. 3

***Endo* and *exo* isomers for temperature-dependent deprotection and selective functionalization. Reprinted with permission from J. Am. Chem. Soc. 2018, 140 (Reference #14) Copyright 2018 American Chemical Society.**

into different forms of stimulus have revealed that multi-stimuli-responsive materials enable greater control and facilitate the development of more intricate materials. In this context, researchers have developed three main classes of dual-stimulus materials: chemical-chemical, physical-chemical, and physical-physical stimuli systems.[6] In 2015 Phillips's group shows an example of a chemical-chemical system in which they have three layers of poly(4,5-dichlorophthalaldehyde) containing different end caps (Figure 1.4).[15] These endcaps—allyloxycarbonyl, *t*-butyldimethylsilyl ether, acetyl—undergo cleavage when exposed to different chemical stimuli. By undergoing sequential exposure, Phillips was able to show the sequential triggering and depolymerization of the polymer layers.[15] More recently, an example from Gillies group was reported in which they observe a change in their material under irradiation or change in temperature.[16] This use of physical stimuli offers some control over the rate at which they observe their depolymerization. Under irradiation the SIP undergoes a quicker depolymerization due to the removal of the UV

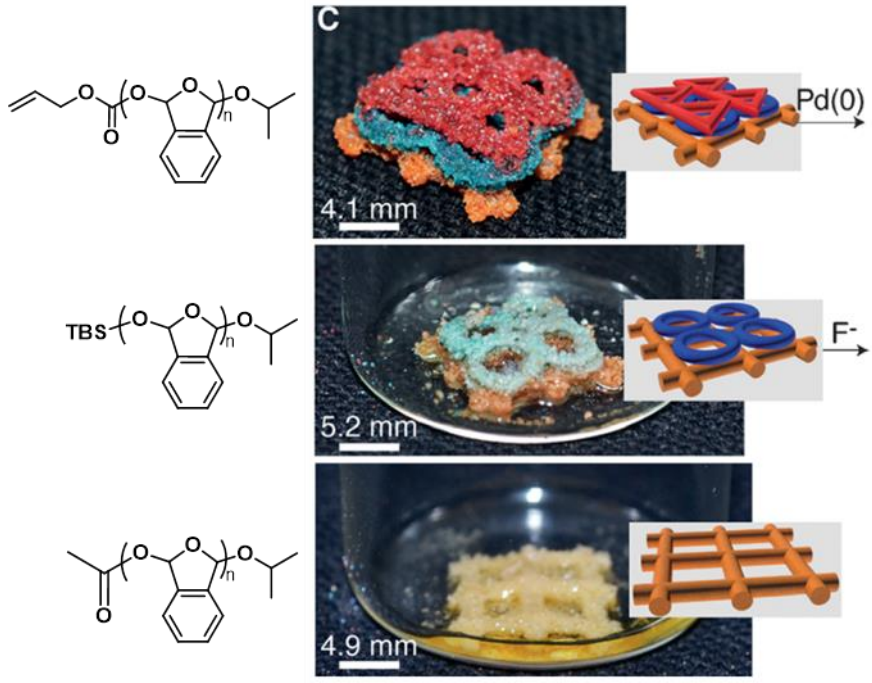

Figure 1. 4

Layered polymer samples undergo selective triggering and depolymerization. Figured reprinted with permission from Angew. Chem. Int. Ed. 2015, 54 (Reference #15) © John Wiley & Sons, Inc. CCC License Number 4958910751935.

light-responsive trigger.[16] This same material can undergo depolymerization at a slower rate when the temperature is above the material's lower critical solution temperature (LCST).[16] Having this difference in depolymerization rates based on stimuli builds in a handle to offer greater control over the polymer's reactivity.

This thesis will explore the utilization of chemical, physical, and multi-stimuli-responsive materials. For chemical stimuli, the focus will center on small molecule activation with chiral Brønsted acids, discussed in detail in Chapter 2. By leveraging the reactivity developed in Chapter 2, we developed a new class of self-immolative polymers (SIPs) using the combination of acid and heat. This new SIP offers temporal control not previously seen. This added ability to control the amount of material released can be integral in the development of new controlled

cargo release applications such as on-demand drug delivery. This controllable trigger will be discussed further in greater detail in Chapter 3. Finally, Chapter 4 discusses the use of heat to "unmask" a protecting group and trigger the formation of polyurethane networks between polyols and isocyanates. Given that both acid and heat are central to the research in this thesis, below you will find a brief introduction into the background and use of the stimuli for both small molecule and materials.

1.3 Utilizing Acid as a Stimulus

1.3.1 Acid as a Reaction Catalyst

Acid catalysts have been utilized in a range of organic reactions, for example, esterification and alkylation due to the broad selection of acids available.[17,18] Acid catalysis is comprised of both Lewis and Brønsted acids. Lewis acids, also known as electron acceptors, are comprised of main group, d-block, and f-block metals.[18] Brønsted acids, or proton donors, are acids that can dissociate to release a proton and form its conjugate base.[18] Having such a variety of acids available for catalysis is advantageous for selecting a catalyst that would fit within the parameters of the reaction whether it is in organic or aqueous media as well as the temperature at which the reaction will be run. Another advantage of acid catalysts is the ability to synthesize materials that contain specific stereochemistry. These catalysts, classified as chiral catalysts, can control the stereochemistry of the reaction's product. This ability for stereoselectivity is heavily utilized in natural product synthesis.

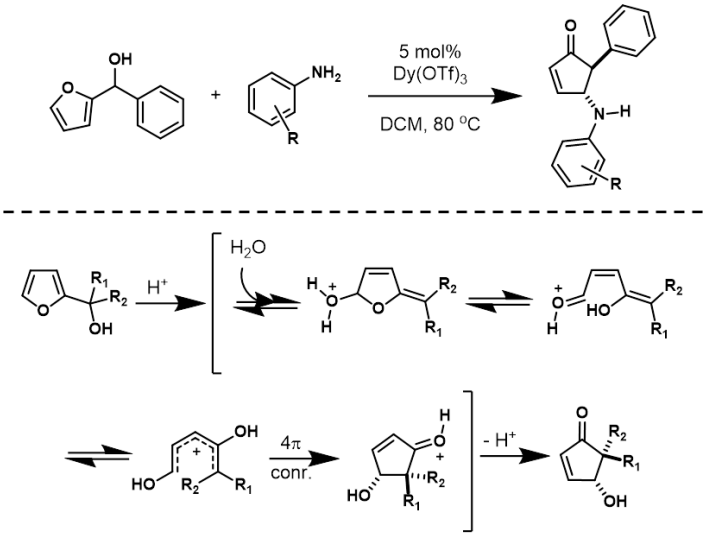

Figure 1. 5

General scheme and mechanism of the first developed aza-Piancatelli rearrangement.

1.3.2 Role of Acid Stimulus in the Piancatelli Rearrangement

The Piancatelli rearrangement, developed in 1976 by Piancatelli and coworkers, is a cascade reaction resulting in the synthesis of a 4-hydroxycyclopentenone via acid catalysis.[19] Although the Piancatelli rearrangement is an optimal route to obtain 4-hydroxycyclopentenones, interest in this reaction was mainly focused on its application toward the synthesis of prostaglandins. The original development of the Piancatelli rearrangement was utilizing a furylcarbinol substrate that undergoes an acid catalyzed transformation in the presence of water to afford a 5-membered ring scaffold.[19] This cyclopentenone privileged scaffold is present in many natural products; however, there was

still a need to advance this rearrangement further to allow for more heteroatom containing nucleophiles to be utilized. In 2010, our group developed the aza-Piancatelli rearrangement allowing for the formation of 4,5-disubstituted cyclopentenones through the use of aniline nucleophiles (Figure 1.5).[20] Through mechanistic studies it was determined that the cascade

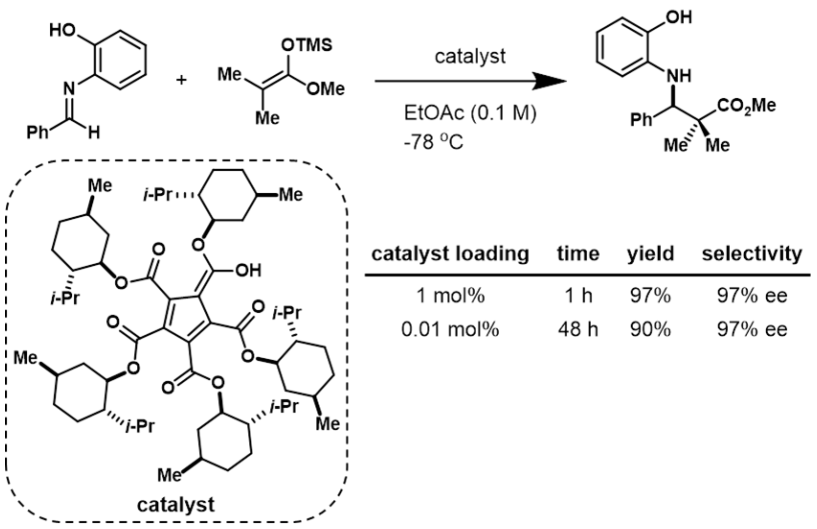

catalyst loading	time	yield	selectivity
1 mol%	1 h	97%	97% ee
0.01 mol%	48 h	90%	97% ee

Figure 1. 6

Lambert et al. PCCP catalyst affording 97% ee at catalyst loading as low as 0.01 mol%.

reaction undergoes a 4π conrotatory electrocyclization ring closure.[21] In this key mechanism step the product's stereochemistry is determined to be in a *trans* orientation. During natural product synthesis, one needs the ability to control a material's stereochemistry and though the aza-Piancatelli rearrangement offers control for a *trans* substitution relationship, the ability to have absolute control on the exact enantiomer obtained is crucial. Through the use of chiral acid catalysts, an enantioselective aza-Piancatelli rearrangement was first reported in 2016.[22,23] In this work, chiral phosphoric acids were used to afford enantioselectivity up to 96% ee.[23] The success in enabling stereocontrol inspired our group to investigate other chiral acid catalysts and thus develop the enantioselective aza-Piancatelli rearrangement via a chiral PCCP Brønsted acid.[2] Lambert and coworkers published work that utilized a chiral pentacarboxycyclopentadiene (PCCP) Brønsted acid catalyst.[24] This new PCCP catalyst was shown to successfully afford a 97% ee at low catalyst loading for their enantioselective Mukaiyama-Mannich reaction (Figure 1.6).[24] Due to the proposed hydrogen bonding mechanism that aids in the stereocontrol of the reaction, we believed that this can be translated

into our group's work on the aza-Piancatelli rearrangement. Discussed further in Chapter 2, we were able to synthesize and use Lambert's chiral PCCP Brønsted acid to develop an enantioselective aza-Piancatelli rearrangement.[2]

1.3.3 Translating small molecule catalysis to materials

Translating discoveries in small molecule chemistry to materials has allowed the field of materials chemistry to expand and offer new advancements. For example, Grubbs catalysts are exceptional reagents to use in both small molecule and polymer synthesis. Originally developed for small molecule olefin metathesis, Grubbs catalysts are now well known for being used in ring-opening-metathesis polymerization (ROMP), for example. We see similar small molecule chemistry adaptations with the Diels–Alder reaction. Although no catalyst is typically used during this reaction, this transformation along with its reversion—the retro-Diels–Alder—has found wide-spread use in both small molecule and polymer systems. Being able to manipulate small molecule chemistry into systems for materials science is key in our group's work. Notably, the use of Diels–Alder chemistry in polymers and the aza-Piancatelli rearrangement served as inspiration for our development of a new trigger unit for self-immolative polymers (SIPs).[3] By utilizing the thermal reactivity of the Diels–Alder reaction, we were able to design a temporally controlled trigger unit for the depolymerization of SIPs. Along with the use of Diels–Alder chemistry, we translated our group's work on the aza-Piancatelli rearrangement into an additional portion for our new SIP trigger.[3]

The initial step in the Piancatelli rearrangement – activation with acid and subsequent elimination of water – served as the inspiration for the development of a new acid trigger for

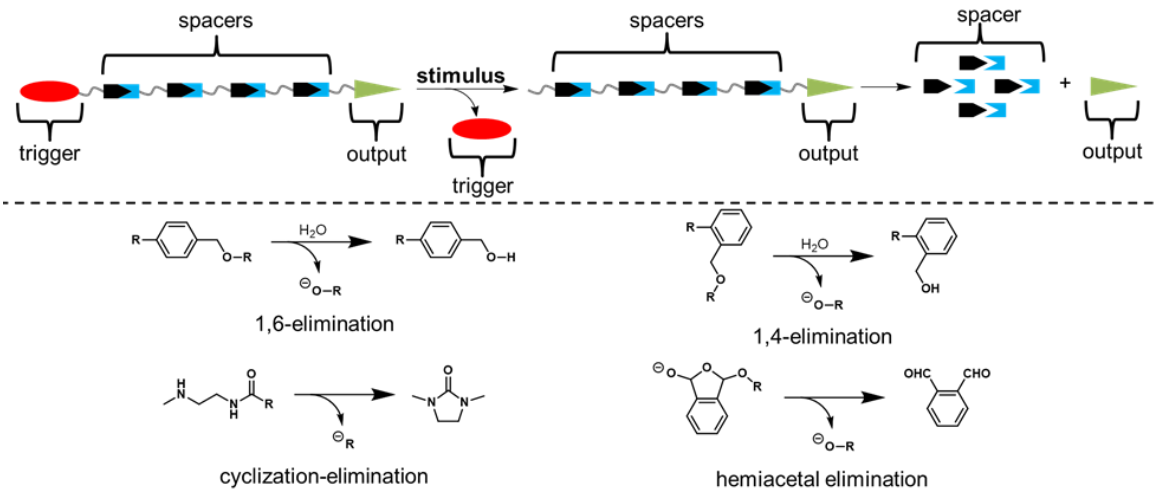

Figure 1. 7

Traditional SIP architecture and commonly seen depolymerization pathways.

SIPs. Self-immolative polymers are a class of materials that when exposed to a predetermined external stimulus will undergo endcap cleavage and complete end-to-end depolymerization.[8,25,26] These materials are a new and growing field that utilizes known chemistry to offer new uses of polymers. SIP architecture contains three main portions—trigger unit, spacers, and output/cargo (Figure 1.7). The trigger unit of a SIP can be seen as a protecting group for the polymer. It is this unit that when cleaved exposes a reactive site that then catalyzes a depolymerization to occur.[8] The polymer's size, scaffold, and depolymerization mechanism is then determined by the spacer units used. Spacers can offer linear or branched/dendritic type polymers that undergo one of three possible depolymerization mechanisms—1,4-elimination, 1,6-elimination, cyclization-elimination, or hemiacetal elimination.[8,26] Lastly, SIPs contain an output unit; this unit is what identifies the material's end application.[25]

SIPs differentiate from any other stimuli responsive material due to their end-to-end depolymerization that takes place after the cleavage of the trigger moiety.[8,27] This depolymerization allows for self-immolative polymers to be used for on-demand drug

delivery,[28] degradable materials,[29] and analyte detection. Amongst these three SIP portions, the trigger unit is the most of interest to us and is studied further in Chapter 3. SIP trigger units are comparable to small molecule protecting groups. The most common types of triggers fall within the following reactivity classes: redox, nucleophile, acid/base, enzyme, photo, and thermal.[30] When designing SIPs, these materials typically contain only one reactivity and thus once the polymer is exposed to its designated stimuli the SIP will undergo complete depolymerization. A major gap in the SIP literature is the ability to impart temporal control into the depolymerization and release of material. SIPs have classically been single stimuli based; however, in more recent studies, the use of multi-stimuli systems has emerged.[6,7,15,16,31] Our work focuses on the use of a dual-stimuli-responsive system that harnesses the orthogonality of a physical-chemical stimuli partnership to impart the ability for temporally controlled depolymerization.[3]

1.4 Using Temperature as a Stimulus

1.4.1 Utilizing Temperature in Self-Immolative Polymers

Within our work on SIPs, heat is utilized as a physical stimulus for triggering the depolymerization of a self-immolative polymer system. Physical stimuli such as light and temperature are advantageous chemistries due to the temporal control, they both offer, something not typically seen with chemical stimuli like acid. Using temperature to control reactivity is seen throughout chemistry whether it be to cool a reaction for better selectivity by slowing the reaction kinetics or heating a reaction to overcome the activation energy needed for product formation. This idea of overcoming activation energies via heated reactions will be the focus of thermal stimuli in our work.

The Diels–Alder reaction is a well-studied thermally driven reaction in organic chemistry. Within Diels–Alder chemistry, furan-maleimide chemistry is among the most commonly studied.[32] Diels–Alder reactions are known to be thermally reversible and it is this reactivity that is of interest for designing new thermal SIP triggers. By taking advantage of this reversibility, we were able to design and develop a new trigger moiety for self-immolative polymers that utilizes a furan-maleimide Diels–Alder adduct as a lock. Furan-maleimide adducts have been studied in polymers;[14,33,34] however, utilizing this material to impart temporal control into SIPs is a novel application that has not been previously explored. This furan-maleimide Diels-Alder adduct would be instrumental in our trigger design to allow for long term stability when exposed to other stimulus environments.

1.4.2 Heat Responsive Compounds for 3D Printing of Polyurethanes

Polyurethanes are a class of polymers was first discovered via reaction of a polyester diol with a diisocyanate in 1937 by Bayer and coworkers.[35] These polymers have since become one of the most versatile and widely produced materials. The typical synthesis of a polyurethane is carried out with a polyol and isocyanate source; depending on the functionality content of each of these components, various architectures—linear, branched, cross-linked—can be obtained. Due to the variety available, polyurethanes have been used in foams, coatings, adhesives, and polymer binders.[35,36] Our interest lies in its use for polymer binder materials.

Polymer binders are utilized in energetic materials as composite materials that contain oxidizers and fuel components. Commonly used in rocket propellants, this polyurethane composite forms an elastic material that can withstand many stressors to maintain its integrity to avoid activation of the oxidizers held within the network.[36] One of the most commonly

utilized polyols for polymer binders is hydroxyl terminated polybutadiene (HTPB). HTPB is an advantageous material that has been used throughout time due to its ideal physical properties that allow for a high solids loading without losing its processability and strength once cross-linked.[36] The chemistry of using HTPB in polymer binders is well studied;[36–42] however, the technology in which these materials are processed and created is continuing to advance. Typically, polymer binders are created via molds; however, due to the need for more novel methods, we are aiming to combine the known chemistry of polymer binders with the recent advancements in 3D printing. 3D printing is becoming a popular method for fabricating new materials based off digital designs and concepts. The motivation for creating 3D printing methods for polymer binders comes from a need for more shape and form availability as well as the want for more on-demand and point-of-use material production.

Currently, polymer binders containing HTPB are created via reaction with a diisocyanate. This reaction is advantageous due to the high reactivity of isocyanates and the quick kinetics for polyurethane formation. Alternatively, though, the quick kinetics prove to be a downfall to this chemistry when moving into 3D printing. Polymer binders typically contain a high solids loading (86-88%)[36] and thus need time to allow for homogenous mixing and curing; the high reactivity between the polyol and isocyanate often causes inconsistent materials. Due to the need for more homogenous materials that can undergo 3D

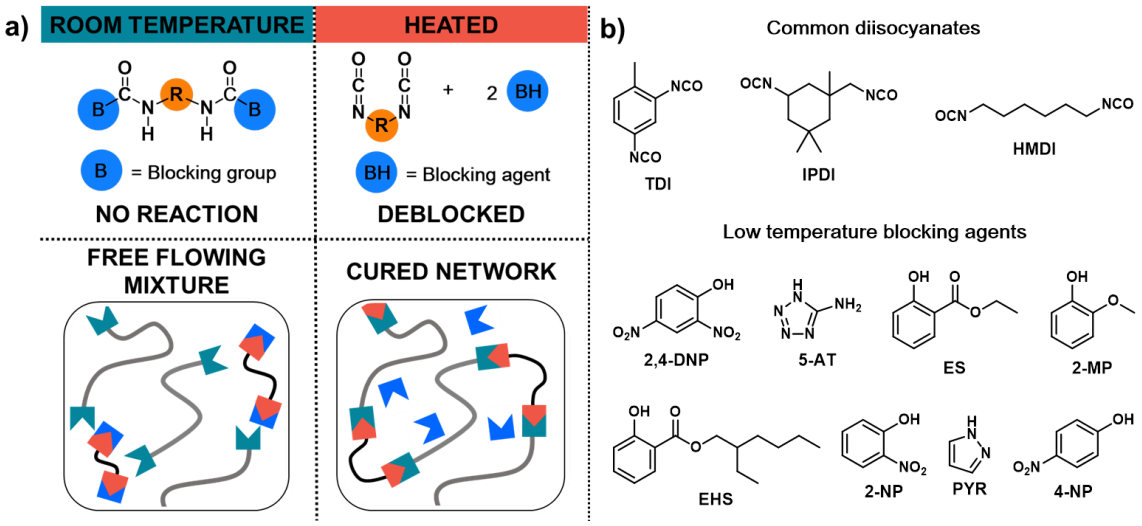

Figure 1. 8

a) Schematic depiction of using blocked isocyanates in polymer networks pre and post heating affording the polyurethane formation; b) common isocyanate and blocking groups used for low temperature activated materials.

printing, we aim to develop new chemistry for polymer binders that allows for on-demand curing.

One potential solution to address this need is the use of blocked isocyanates (BICs). Blocked isocyanates are a class of materials derived from the reaction of an isocyanate and a protecting group containing an active hydrogen with the goals of procuring better pot-life and imparting control over the isocyanate reactivity (Figure 1.8a).[43] Via a facile synthesis, isocyanates can undergo a blocking reaction with a variety of blocking groups including phenols[44], anilines[45], pyrazoles[43], and more[43] forming a new carbonate or carbamate functional group (Figure 1.8b). Currently BICs are already being used in materials such as coatings and polyurethane foams.[43]

Specifically, BICs are commonly seen in organic powder coatings within the automotive industry for topcoats and primers.[46] Typical coatings are comprised of oxime blocked isocyanates with a hydroxyl functionalized acrylic or polyester to then be cured at

temperatures of 130-150 °C.[46,47] These deblocking temperatures are normal for industrial applications of BICs, with their considerations of low temperature deblocking being 120 °C.[48] Unfortunately, temperatures above 100 °C are not viable deblocking temperatures for materials such as polymer binders containing energetic materials. Due to the inclusion of energetic materials within the binder network, deblocking and processing temperatures must be below 100 °C and ideally under 70 °C.[40,49] With this limitation in mind, we set forth in designing and building a library of a new class of low temperature BICs.

The thermal stability achieved by blocked isocyanates is advantageous due to the extended pot-life of isocyanates as well as the decreased occurrence of unwanted reactions. This new material is well suited for producing bulk materials in which isocyanates can be used as crosslinking agents. Isocyanates are utilized in polyurethane crosslinking reactions due to the quick reaction between a polyol chain end and the isocyanate.[49,50] However, because of the rapid reaction, premature curing as well as undesired side reactions tends to occur during the mixing stage resulting in incomplete curing as well as non-homogenous materials. The thermal stability of the blocked isocyanate materials is ideal for these types of materials as all reagents for a material can undergo homogenous mixing and molding prior to any curing. Once the material is ready for curing, the material can be heated to a designated deblocking temperature, thus releasing the isocyanate functionality, and allowing the curing reaction to take place.

Isocyanates are already heavily used in polymer networks where curing takes place, specifically in coatings and polymer binders.[46,48,49] By switching to the use of blocked isocyanates, not only will there be more control over the curing reactions between the isocyanate and the polyol, but now there can be new applications for these isocyanate based

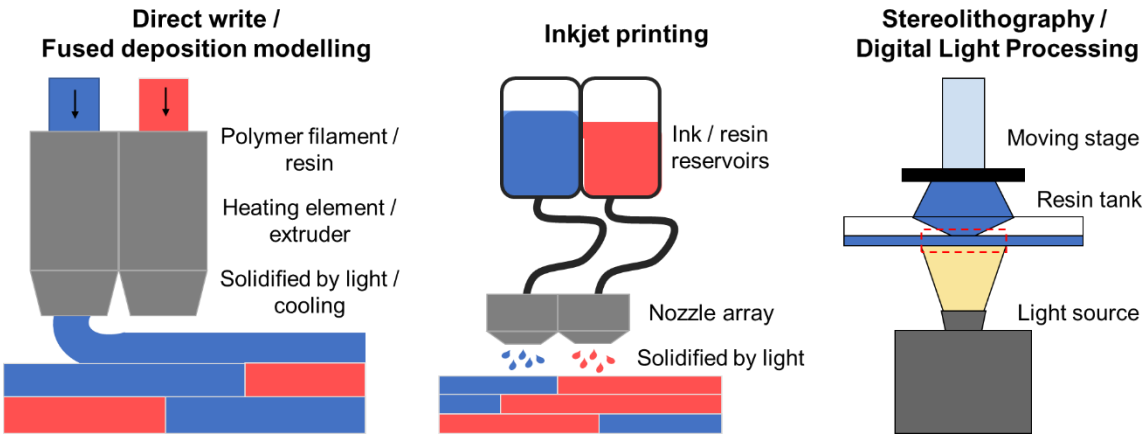

Figure 1. 9

Graphic portrayal of common 3D printing techniques available.

polyurethane systems. Utilizing the control given by blocked isocyanates, the methods of 3D printing can be accessible. There are many types of 3D printing available, including stereolithography (SLA), direct ink write/fused deposition modeling (FDM), and inkjet printing.[51] (Figure 1.9) Many of these systems use either light or heat to aid in the curing/solidifying of the materials. By using blocked isocyanates, we can further utilize the heat already used in 3D printing to activate and cure these new materials. FDM is known specifically for using elevated temperatures during the printing process. This is also known as extrusion printing where a solid polymer filament is fed into a nozzle head where it is heated and extruded onto a build table.[51] The printing here is done in layers and the material cures into its final shape as the filament is cooled. Powder bed fusion and liquid additive manufacturing (LAM) are other 3D printing approaches that utilize heat for curing.[51] Due to the fluid nature of isocyanate based polyurethane materials pre-curing, LAM would be most advantageous rather than FDM and powder bed fusion. LAM is a printing technique that will deposit a liquid or highly viscous material onto the build table and heat is used to then cure and solidify the material into the desired shape.[51]

By incorporating BICs into 3D printing, materials science can begin to expand the current applications in which isocyanate crosslinking is used. This thesis will specifically discuss the development of "low temperature" BICs for future 3D printing applications. This range of low temperature BICs, 60-100 °C, is especially of interest due to the instability of polymer binder contents that require low processing temperatures.[36,49] Most BICs currently used in industry have deblocking temperature above 150 °C[43,47,52], allowing for this investigation into the structure-activity relationship of the BIC and designing materials that fit within our desired temperature range.

1.5 References

1 P. Mestecky, *Mater. Today*, 1998, **1**, 1.

2 G. R. Hammersley, M. F. Nichol, H. C. Steffens, J. M. Delgado, G. K. Veits and J. Read de Alaniz, *Beilstein J. Org. Chem.*, 2019, **15**, 1569–1574.

3 M. F. Nichol, K. D. Clark, N. D. Dolinski and J. Read De Alaniz, *Polym. Chem.*, 2019, **10**, 4914–4919.

4 M. Wei, Y. Gao, X. Li and M. J. Serpe, *Polym. Chem.*, 2017, **8**, 127–143.

5 D. Wang, M. D. Green, K. Chen, C. Daengngam and Y. Kotsuchibashi, *Int. J. Polym. Sci.*, 2016, **2016**, 2–4.

6 J. Zhuang, M. Gordon, J. Ventura, L. Li and S. Thayumanavan, *Chem. Soc. Rev.*, 2013, **42**, 7421–7435.

7 P. Schattling, F. D. Jochum and P. Theato, *Polym. Chem.*, 2014, **5**, 25–36.

8 G. I. Peterson, M. B. Larsen and A. J. Boydston, *Macromolecules*, 2012, **45**, 7317–7328.

9 S. Helmy, F. A. Leibfarth, S. Oh, J. E. Poelma, C. J. Hawker and J. R. De Alaniz, *J. Am.*

Chem. Soc., 2014, **136**, 8169–8172.

10 F. Han, B. Xu, S. Asim, A. Shah, J. Zhang and J. Cheng, 2020, **1900782**, 1–9.

11 S. Ghosh, K. Irvin and S. Thayumanavan, *Langmuir*, 2007, **23**, 7916–7919.

12 J. Sung, M. J. Robb, S. R. White, J. S. Moore and N. R. Sottos, *J. Am. Chem. Soc.*, 2018, **140**, 5000–5003.

13 J. L. Self, N. D. Dolinski, M. S. Zayas, J. Read De Alaniz and C. M. Bates, *ACS Macro Lett.*, 2018, **7**, 817–821.

14 E. H. Discekici, A. H. St. Amant, S. N. Nguyen, I. H. Lee, C. J. Hawker and J. Read De Alaniz, *J. Am. Chem. Soc.*, 2018, **140**, 5009–5013.

15 A. M. Dilauro, G. G. Lewis and S. T. Phillips, *Angew. Commun.*, 2015, **54**, 6200–6205.

16 R. E. Yardley and E. R. Gillies, *J. Polym. Sci.*, 2018, **56**, 1868–1877.

17 J. N. Brönsted, *Chem. Rev.*, 1928, **5**, 231–338.

18 H. Yamamoto, *Proc. Japan Acad. Ser. B Phys. Biol. Sci.*, 2008, **84**, 134–146.

19 G. Piancatelli, A. Scettri and S. Barbadoro, *Tetrahedron Lett.*, 1976, **17**, 3555–3558.

20 G. K. Veits, D. R. Wenz and J. Read De Alaniz, *Angew. Chem. Int. Ed.*, 2010, **49**, 9484–9487.

21 S. W. Li and R. A. Batey, *Chem. Commun.*, 2007, **8**, 3759–3761.

22 H. Li, R. Tong and J. Sun, *Angew. Chem. Int. Ed.*, 2016, **55**, 15125–15128.

23 Y. Cai, Y. Tang, I. Atodiresei and M. Rueping, *Angew. Chem. Int. Ed.*, 2016, **55**, 14126–14130.

24 C. D. Gheewala, B. E. Collins and T. H. Lambert, *Science (80-.).*, 2016, **351**, 961–966.

25 M. E. Roth, O. Green, S. Gnaim and D. Shabat, *Chem. Rev.*, 2016, **116**, 1309–1352.

26 D. Sagi, A.; Weinstain, R.; Karton, N.; Shabat, *J. Am. Chem. Soc.*, 2008, **130**, 5434–

5435.

27 R. A. McBride and E. R. Gillies, *Macromolecules*, 2013, **46**, 5157–5166.

28 M. Gisbert-Garzarán, D. Lozano, M. Vallet-Regí and M. Manzano, *RSC Adv.*, 2017, **7**, 132–136.

29 A. P. Esser-Kahn, N. R. Sottos, S. R. White and J. S. Moore, *J. Am. Chem. Soc.*, 2010, **132**, 10266–10268.

30 G. I. Peterson, M. B. Larsen and A. J. Boydston, *Macromolecules*, 2012, **45**, 7317–7328.

31 R. Cheng, F. Meng, C. Deng, H. Klok and Z. Zhong, *Biomaterials*, 2013, **34**, 3647–3657.

32 A. Gandini, *Prog. Polym. Sci.*, 2013, **38**, 1–29.

33 E. R. Gillies, B. Fan, J. F. Trant and E. R. Gillies, *Chem. Comm.*, 2017, **53**, 12068–12071.

34 S. M. Taimoory, S. I. Sadraei, R. A. Fayoumi, S. Nasri, M. Revington and J. F. Trant, *J. Org. Chem.*, 2018, **83**, 4427–4440.

35 E. Delebecq, J. P. Pascault, B. Boutevin and F. Ganachaud, *Chem. Rev.*, 2012, **113**, 80–118.

36 A. K. Mahanta and D. D. Pathak, *Polyurethane*.

37 S. Cerri, M. A. Bohn, K. Menke and L. Galfetti, *Propellants, Explos. Pyrotech.*, 2013, **38**, 190–198.

38 W. M. ADEL and G. LIANG, *Chinese J. Aeronaut.*, 2019, **32**, 361–368.

39 M. Kivity, G. Hartman and A. Achlama, 2005, 1–6.

40 J. K. Chen and T. B. Brill, *Combust. Flame*, 1991, **87**, 217–232.

41 S. Cerri, M. Bohn, L. Galfetti and K. Menke, *Cent. Eur. J. Energ. Mater.*, 2009, **Vol. 6**,

149–165.

42 X. Yang, C. Sun, J. Zhang, J. Xu and B. Tan, *AIP Conf. Proc.*, , DOI:10.1063/1.4981578.

43 M. S. Rolph, A. L. J. Markowska, C. N. Warriner and R. K. O'Reilly, *Polym. Chem.*, 2016, **7**, 7351–7364.

44 A. S. Nasar and S. Kalaimani, *RSC Adv.*, 2016, **6**, 76802–76812.

45 A. S. Nasar, S. Subramani and G. Radhakrishnan, *J. Polym. Sci. Part A Polym. Chem.*, 1999, **37**, 1815–1821.

46 D. A. Wicks and Z. W. Wicks, *Prog. Org. Coatings*, 2001, **41**, 1–83.

47 D. A. Wicks and Z. W. Wicks, *Prog. Org. Coatings*, 1999, **36**, 148–172.

48 R. Jones, *Trans. Inst. Met. Finish.*, 2008, **86**, 75–79.

49 W. H. Graham and R. E. Boothe, *Control of the Urethane Cure Reaction with Solid, Blocked Isocyanates*, 1986.

50 A. Olejnik, K. Gosz and Ł. Piszczyk, *Thermochim. Acta*, 2020, **683**, 178435.

51 K. V. Wong and A. Hernandez, *ISRN Mech. Eng.*, 2012, **2012**, 1–10.

52 M. L. Jung, S. Subramani, S. L. Young and H. K. Jung, *Macromol. Res.*, 2005, **13**, 427–434.

2 Enantioselective PCCP Brønsted Acid-catalyzed Aza-Piancatelli Rearrangement

2.1 Abstract

An enantioselective aza-Piancatelli rearrangement has been developed using a chiral Brønsted acid based on pentacarboxycyclopentadiene (PCCP). This reaction provides rapid access to valuable chiral 4-amino-2-cyclopentenone building blocks from readily available starting material and is operationally simple.

2.2 Introduction

The discovery of a wide range of cyclopentane containing natural products[53,54] and biologically active molecules such as palau'amine,[55,56] agelastatin A,[57–59] pactamycin,[60–62] and aristeromycin,[63,64] has created a demand for new methodologies to construct this privileged scaffold (Figure 2.1). The aza-Piancatelli reaction has recently emerged as a particularly attractive method to access densely functionalized cyclopentene cores bearing nitrogen substituents directly from readily available 2-furylcarbinols.[65–67]

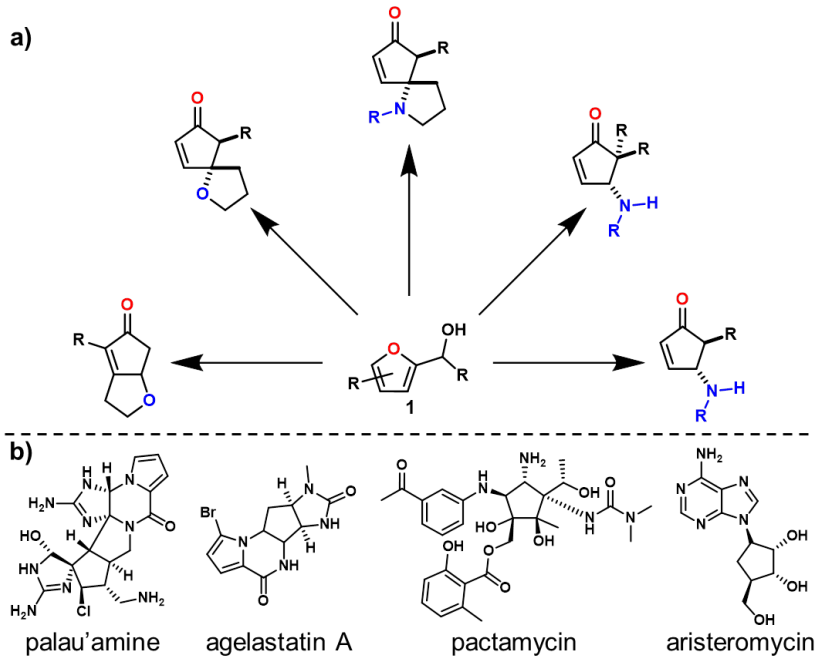

Figure 2. 1

5 membered ring privileged scaffolds commonly seen in natural products, specifically shown in palau'amine,[55,56] agelastatin A,[57–59] pactamycin,[60–62] and aristeromycin[63,64].

Inspired by Piancatelli's original work in 1976,[19] our group has developed both the inter- and intramolecular aza-Piancatelli reaction using commercially available dysprosium trifluoromethanesulfonate ($Dy(OTf)_3$) as a catalyst with a range of nitrogen nucleophiles.[20,68–73] The range of catalytic systems facilitating this reaction has been extended to include other Brønsted and Lewis acids, such as phosphomolybdic acid (PMA),[74] $Ca(NTf_2)_2$,[75] $In(OTf)_3$,[76] $La(OTf)_3$,[77] and BF_3•OEt_2,[78] as well as other nucleophiles.[79–81]

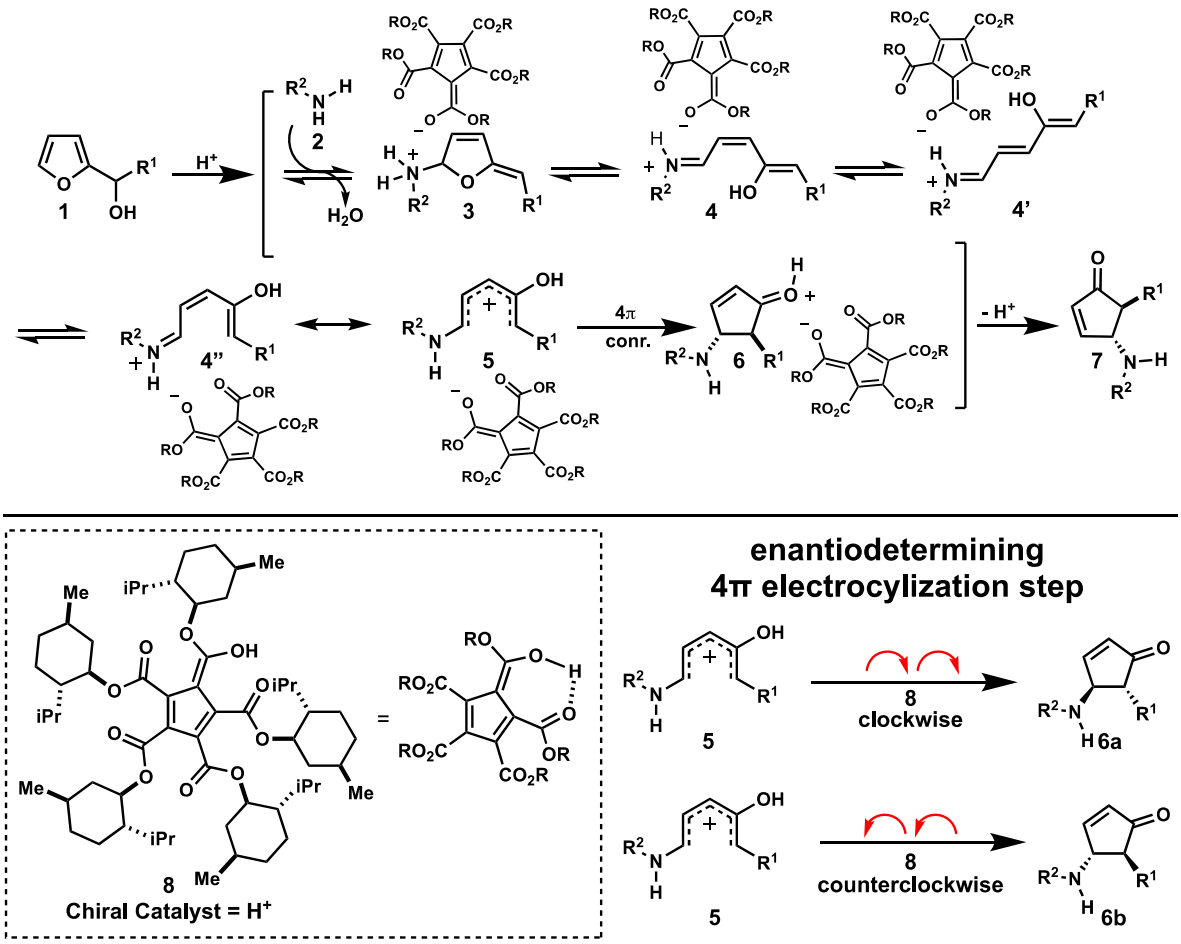

Figure 2. 2

Proposed mechanism of the asymmetric aza-Piancatelli reaction. Figure reproduced with permission from Beilstein Journal of Organic Chemistry.

In all cases examined, the products of the aza-Piancatelli reaction have a *trans* relationship between the C4 and C5 substituents.[65–67] It is believed that the 4π conrotatory electrocyclization step that converts the pentadienyl cation **5** into the corresponding cyclopentenone adduct **6** is responsible for controlling the relative diastereoselectivity in this cascade rearrangement (Figure 2.2). Analogous to the Nazarov cyclization, controlling the absolute stereochemistry can be achieved by governing the direction of the conrotatory electrocyclization, clockwise vs counterclockwise.[82–84] The Nazarov cyclization utilizes

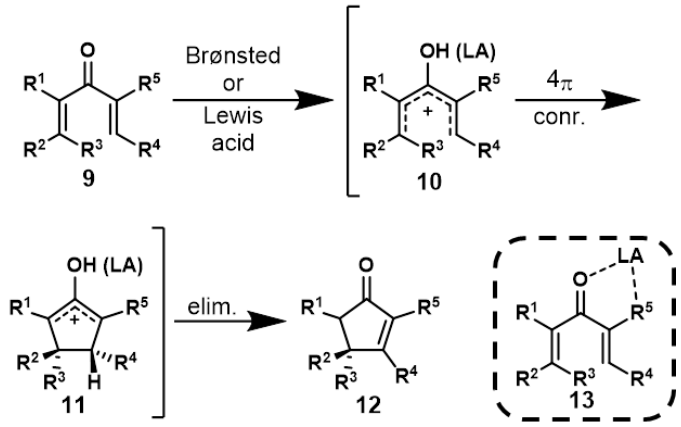

Figure 2. 3

Nazarov cyclization mechanism showcasing the coordination between the catalyst and substrate and the carbonyl oxygen and α-substituent.

divinyl ketones to achieve cyclopentenones while being able to construct quaternary stereocenters in its ring closing step.[66] Shown in Figure 2.3, the overall transformation and mechanism is similar to that of the Piancatelli reaction focusing on the conrotatory electrocyclization step. During this step, it was shown that coordination of the catalyst with the carbonyl oxygen and the functional group in the α-position aids in driving the cyclization and provides a handle to impart stereoselectivity.[83]

Despite the direct relationship to the asymmetric Nazarov cyclization, however, it was not until 2016 that the first asymmetric aza-Piancatelli reaction was reported in the literature. To control the absolute stereochemistry of the aza-Piancatelli rearrangement, Rueping,[23] Sun,[22] and Patil[85] independently demonstrated that chiral phosphoric acids can be used as an enantioselectivity-inducing element capable of controlling the clockwise or counterclockwise conrotation of the key 4π electrocyclization step (Table 2.1).

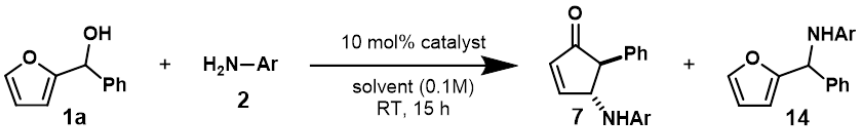

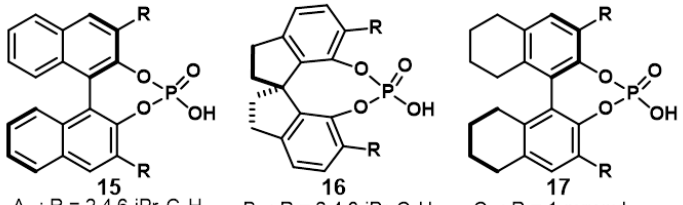

A_1 : R = 2,4,6-$iPr_3C_6H_2$
A_2 : R = 1-pyrenyl
A_3 : R = 2,4,6-$Cy_3C_6H_2$

B_1 : R = 2,4,6-$iPr_3C_6H_2$
B_2 : R = 9-anthryl
B_3 : R = 9-phenanthyl
B_4 : R = 1-pyrenyl

C_1 : R = 1-pyrenyl

Catalyst	Solvent	Conv. (%)	Yield (%) **7**	Yield (%) **14**	ee (%) **7**
(R)-A_1	DCM	80	3	77	34
(S)-B_1	DCM	66	26	40	37
(S)-B_2	DCM	100	26	74	46
(S)-B_4	DCM	100	62	35	84
(R)-C_1	DCM	100	70	0	73
(S)-B_4	DCE	100	49	33	86
(S)-B_4	DCE	100	44	55	90
(S)-B_4	DCE	100	74	14	90

Table 2. 1

Examples of chiral phosphoric acids used in the synthesis of enantioselective cyclopentenone structures via the aza-Piancatelli rearrangement. Figure reproduced with permission from Angew. Chem. Int. Ed. 2016, 55, 15125-15128 (Reference #36) © 2016 John Wiley & Sons, Inc. CCC License Number 4946710764940.

Although the utility of these asymmetric catalytic systems is unquestionable, the ability to identify the optimal catalyst is not straightforward. In each case, extensive optimization of the reaction conditions was required to achieve high enantioselectivity and good yield, with small variations to the catalyst architecture or solvent having dramatic effects on enantioselectivity or yield. In fact, our group first explored the use of chiral phosphoric acids to control the aza-Piancatelli rearrangement in 2012.[86]

We approached this investigation through the similarities of the Nazarov cyclization and Piancatelli rearrangement. We hypothesized that a chiral unit either bonded or in close proximity to the pentadienyl cation would aid in rendering an enantioselective substrate. Our

group's initial studies focused on the use of chiral Lewis acids, specifically rare earth triflates with chiral ligands. Unfortunately chiral Lewis acids did not result in any promising results and we shifted to study chiral Brønsted acids.[86] Inspired by the chiral Nazarov cyclization work done by Rueping, Gesine Veits in our group began by studying chiral phosphoric acids as potential catalysts.[87] Through these studies we found that the bulky chiral catalyst (R)-TRIP not only was an effective catalyst for the aza-Piancatelli rearrangement, but it also afforded a 46% and 49% ee in acetonitrile (MeCN) and nitromethane ($MeNO_2$), respectively (Figure 2.4). Although the enantioselectivity were modest, these results highlighted that chiral Brønsted acids could be used to control the absolute stereochemistry of the asymmetric aza-Piancatelli rearrangement.[86] Our group continued studies with (R)-TRIP including the addition of various additives to enhance selectivity ending with the best result of 59% ee using a combination of 20 mol% (R)-TRIP and 20 mol% DTBMP in $MeNO_2$.[86] The main challenges that prevented the rapid optimization of these encouraging results was the lengthy synthesis of the chiral phosphoric acids and the lack of a model to help guide catalyst development.

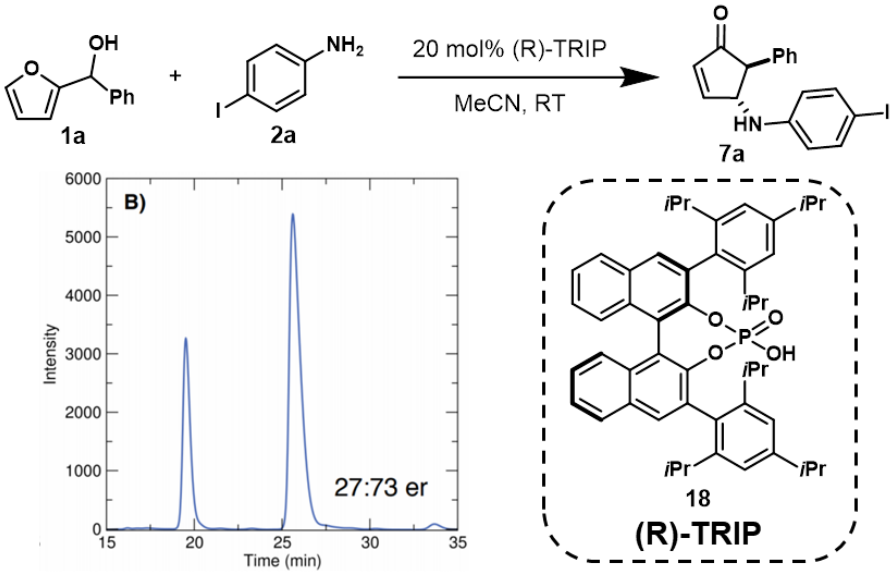

Figure 2. 4

Asymmetric aza-Piancatelli rearrangement utilizing (R)-TRIP as a catalyst to afford a 46% ee in MeCN.

Because of these challenges and less than ideal selectivity, our group's ongoing interest in further developing the aza-Piancatelli reaction sought to identify other asymmetric catalytic systems capable of controlling the absolute stereochemistry. To this end, we envisioned that the chiral pentacarboxy-cyclopentadiene (PCCP) Brønsted acid catalyst **8** recently developed by the Lambert lab might be suitable (Figure 2.2).[24] First, the pK_a values measured in acetonitrile (MeCN) are lower than chiral phosphoric acids (Brønsted acid $pK_a = 8.85$ vs. chiral phosphoric acids $pK_a = 12\text{-}14$).[24] Given the enhanced acidity, we reasoned that this type of chiral Brønsted acid catalyst could facilitate the dehydration reaction of the furylcarbinol to generate the oxocarbenium intermediate. Second, by analogy to asymmetric induction in aza-Piancatelli reactions with chiral phosphoric acids, where enantioselectivity has generally been achieved by strategically installing bulky groups on the hydrogen-bonding catalysts, we hypothesized that a PCCP-derived catalyst could be used. Currently, we do not know the exact interaction between the substrate and our PCCP catalyst that allows for the stereocontrol, however, it is proposed that the chiral moieties serve to interact with the key intermediate **5** during the enantiodetermining electrocyclization step.[22,23,85] Finally, this new catalyst can be produced inexpensively and on scale, features that are attractive for developing a wide range of asymmetric transformations.

2.3 Results and Discussion

Our investigations began by examining the reaction of *para*-iodoaniline **2a** with furylcarbinol **1a** in dichloromethane (DCM) in the presence of 5 mol % chiral Brønsted acid **8** (Table 2.2). We were pleased to find that **8** catalyzed the desired asymmetric transformation at

40 °C, affording 4-aminocyclopentenone **7a** in 78% yield and a moderate 65% ee. At lower temperatures (30 °C and 23 °C (RT)) the selectivity increased to 73% and 78% ee, respectively. For consistency, the optimization studies were all allowed to run for 48 h with higher temperatures being more efficient (entries 1-3). Importantly, the catalytic activity did not diminish with extended reaction time and the yield of the room temperature reaction could be increased to 70% by extending the reaction time from 48 h to 120 h (entry 4). The asymmetric reaction was found to be most effective at 23 °C (entries 3 and 4). Unfortunately, attempts to lower the temperature further resulted in exceedingly long reaction times, greater than 5 days, and thus were not pursued. Next the effects of aromatic and halogenated solvents were evaluated (entries 5–7), with DCM proving optimal. We developed the reaction using 5 mol % catalyst in (DCM) at 23 °C as the optimized reaction conditions.

With optimized reaction conditions in hand, we set out to explore the scope and limitations of the asymmetric reaction (Scheme 2.1). Initially, we examined the reaction of

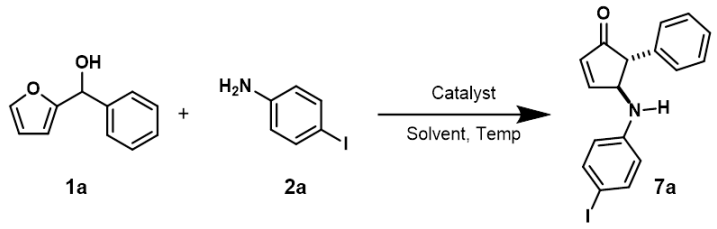

1a 2a 7a

Entry	Catalyst (mol%)	Solvent	Temp (°C)	ee (%)	Yield (%)
1	5	DCM	40	65	78
2	5	DCM	30	73	46
3	5	DCM	RT	78	26
4	5	DCM	RT	75	70
5	5	DCE	RT	68	23
6	5	fluorobenzene	RT	76	20
7	5	toluene	RT	75	12

[a] This reaction was run for 5 days whereas the rest of the reactions were run for 2 days.

Table 2. 2

Initial optimization studies. Figure reproduced with permission from Beilstein Journal of Organic Chemistry.

various anilines with furylcarbinol **1a**. Using the optimized reaction conditions, we investigated the scope of this reaction with different anilines. Scheme 2.1 summarizes results obtained with *ortho-*, *meta-*, and *para*-substituted aniline derivatives. The reaction of anilines bearing an electron withdrawing group at the *para*-position afforded the optimal balance between efficiency and enantioselectivity. Consistent with Rueping's work,[23] *ortho*-aminobenzoic acid, which contains an additional hydrogen bond group afforded the best selectivity (**7k**). To simplify the purification process, all acid products were transformed into the corresponding methyl ester *in situ* using (trimethylsilyl)diazomethane. A slight drop in enantioselectivity is observed when benzoic acid group was moved to the *meta*-position or when using the methyl ester (**7i** and **7j**)**.** The absolute stereochemistry of the product **7k** was assigned by comparison to literature[23] and the other products were assigned by analogy.

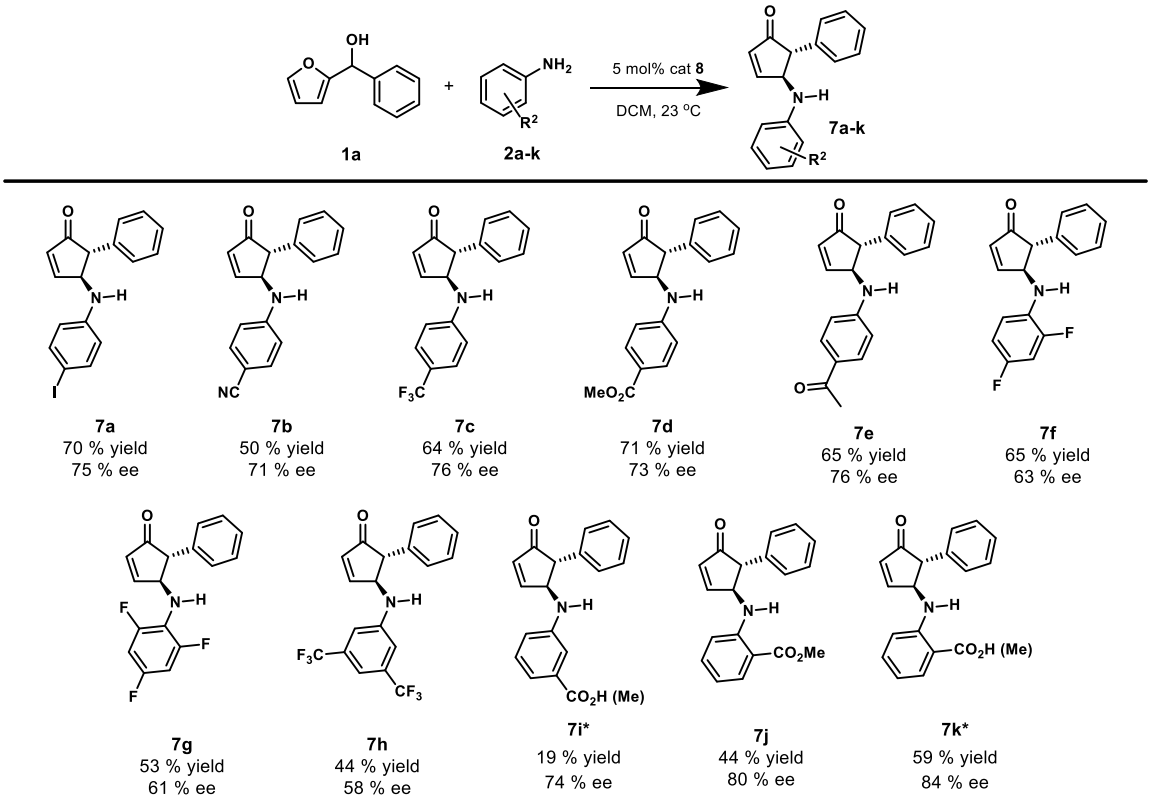

Scheme 2. 1

Asymmetric aza-Piancatelli with a range of substituted anilines. *To simplify the purification process, carboxylic acids were transformed *in situ* into the corresponding methyl ester using (trimethylsilyl)diazomethane. Figure reproduced with permission from Beilstein Journal of Organic Chemistry.

To further expand the substrate scope, we investigated the effects on both reactivity and enantioselectivity when substituted furylcarbinols were used with either *para*-iodoaniline (**2a**) or *ortho*-aminobenzoic acid (**2k**) (Scheme 2.2). In every case examined, the *ortho*-aminobenzoic acid gave higher selectivity compared to the corresponding *para*-iodoaniline, which supports the importance of the additional hydrogen bonding capability of the carboxylic acid group. In contrast, with the exception of **7p** and **7q**, a lower yield was obtained when *ortho*-aminobenzoic acid was used. Presumably, this decrease in efficiency is due to the increased steric bulk on the aniline, which slows the initial nucleophilic attack on the furan ring required to initiate the cascade sequence. This highlights that a balance between nucleophilicity and hydrogen bond capabilities are required to obtain an efficient and selective reaction. Compared to the rearrangement of furylcarbinol **1a**, sterically bulky aryl groups attached to the furylcarbinol resulted in significantly diminished enantioselectivity (**7l** and **7m**). In contrast, placing a substituent at either the *meta*- or *para*-position showed no effect on the selectivity when compared to an unsubstituted phenyl group. For example, **1a** afforded the desired product in 75% ee, while **1n** and **1p** afforded the cyclopentenone product in 76% ee and 75% ee, respectively. In general, the enantioselectivity of the reactions with *para*-iodoaniline and *ortho*-aminobenzoic acid behaved similarly, with the selectivity being influenced most obviously by changes in the furylcarbinol. However, a dramatic difference in selectivity was observed when employing a tertiary furylcarbinol (**7r** and **7s**). In this case, *ortho*-aminobenzoic acid resulted in the desired product with good enantioselectivity (72% ee), while *para*-iodoaniline only gave

a modest 41% ee. The exact nature for the decrease in enantioselectivity in this case with *para*-iodoaniline is not clear.

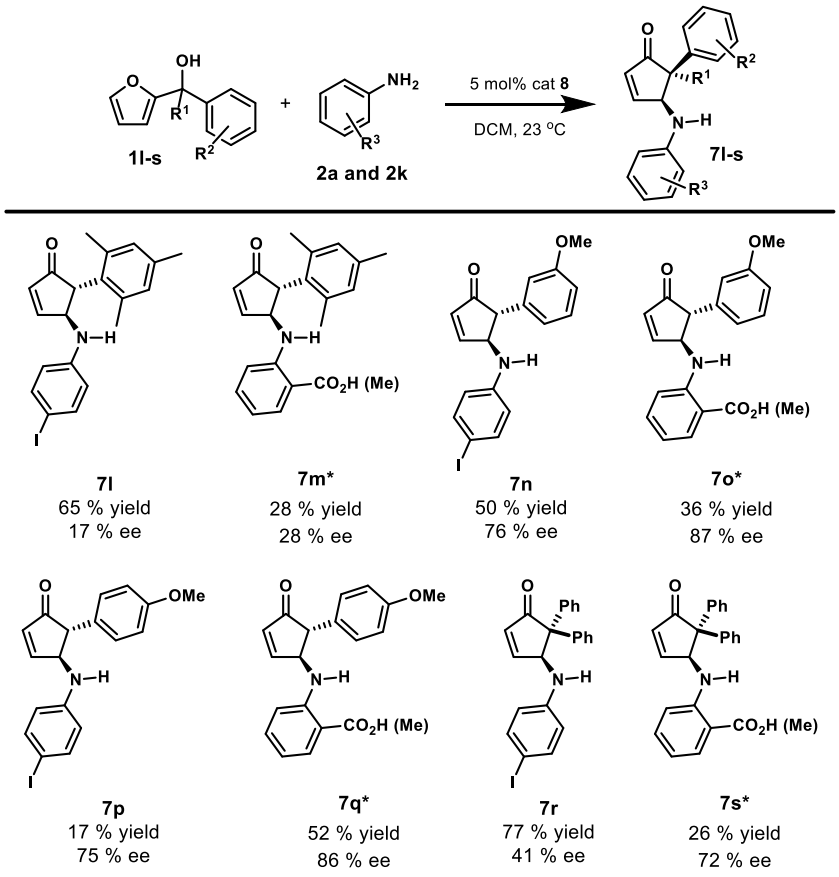

Scheme 2. 2

Asymmetric aza-Piancatelli with a range of substituted furylcarbinols. *To simply the purification process, carboxylic acids were transformed *in situ* into the corresponding methyl ester using (trimethylsilyl)diazomethane. Figure reproduced with permission from Beilstein Journal of Organic Chemistry.

2.4 Conclusion

In summary, we have developed an efficient asymmetric aza-Piancatelli rearrangement that constructs a carbon–carbon bond plus a carbon–nitrogen bond and controls the absolute stereochemistry of the two stereocenters, through control of the direction of conrotation, in a

single operation. This strategy offers a practical alternative to using chiral phosphoric acids and demonstrates that chiral PCCP-based Brønsted acid catalysts can be used to control the absolute stereochemistry of the aza-Piancatelli rearrangement. The PCCP chiral Brønsted acid catalyzed reaction shows good substrate scope and proceeds well with a range of aniline and furylcarbinol derivatives. The ability to control the absolute stereochemistry of the 4π electrocyclization using an inexpensive and easy to prepare chiral Brønsted acid catalyst holds tremendous promise for the aza-Piancatelli and related rearrangements.

2.5 Experimental

2.5.1 Materials and Methods

Unless stated otherwise, reactions were conducted in oven dried glassware under an atmosphere of N_2 using reagent grade solvents. All commercially obtained reagents were used as received. Reaction temperatures were controlled using a Heidolph temperature modulator, and unless otherwise, reactions were performed at room temperature (RT, approximately 23 °C). Thin-layer chromatography (TLC) was conducted with E. Merck silica gel 60 F254 pre-coated plates (0.25 mm) and visualized by exposure to UV light (254 nm) or stained with potassium permanganate or p-anisaldehyde. Flash chromatography was preformed using normal phase silica gel (60 Å, 230–240 mesh, Geduran®) ^{1}H NMR spectra were recorded on Varian Spectrometers (at 400, 500, and 600 MHz) and are reported relative to deuterated solvent signals. Data for ^{1}H NMR spectra are reported as follows: chemical shift (δ ppm), multiplicity, coupling constant (Hz) and integration. ^{13}C NMR spectra were recorded on Varian spectrometers (at 100, 125, and 150 MHz). Data for ^{13}C NMR spectra are reported in terms of chemical shift. IR spectra were recorded on a Perkin Elmer Spectrum 100 FTIR and a Bruker

Alpha FTIR and are reported in terms of frequency of absorption (cm^{-1}). High resolution mass spectra were obtained from the UC Santa Barbara Mass Spectrometry Facility. Enantiomeric excess was determined by use of a Shimadzu Prominence high-performance liquid chromatography (HPLC) system. Furylcarbinols 1a, 1b, 1c, 1d, and 1e were prepared according to literature precedent by reacting furfural with the corresponding Grignard reagent.[39] The PCCP catalyst **8** was prepared according to literature precedent.[38]

2.5.2 Experimental Procedures and Data

2.5.2.1 General Procedures

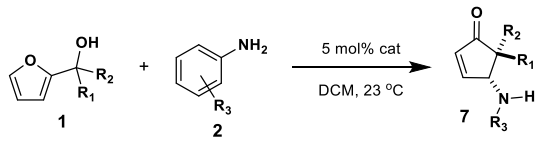

General procedure for the rearrangement: Furylcarbinol **1** and aniline **2** were dissolved in DCM. At 23 °C, 5 mol % of the catalyst was added to the reaction mixture. Once capped, the reaction was allowed to stir for 5 days. The reaction was then quenched with saturated aqueous sodium bicarbonate and extracted with DCM (3 x 5 mL). The combined organic layers were dried over $MgSO_4$, filtered, and concentrated *in vacuo*. The residue was then purified via column chromatography to afford the cyclopentenone **7**.

2.5.2.2 Synthesis Procedures

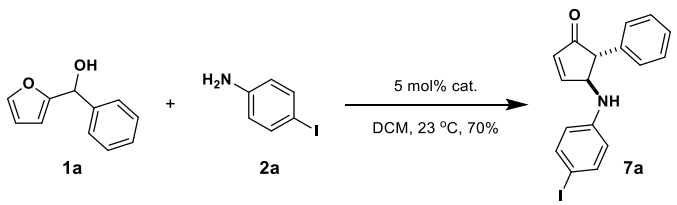

(4S,5R)-4-((4-iodophenyl)amino)-5-phenylcyclopent-2-en-1-one (7a): According to the general procedure, the catalyst **8** (4.7 mg, 0.005 mmol, 0.05 eq) was added to furan-2-yl(phenyl)methanol **1a** (20.0 mg, 0.11 mmol, 1.2 eq) and 4-iodoaniline **2a** (21.0 mg, 0.10 mmol, 1.0 eq) in 1 mL of anhydrous DCM. The resulting reaction mixture was allowed to stir at room temperature for 5 days before being quenched with 5 mL of saturated aqueous sodium bicarbonate and extracted with DCM (3 x 5 mL). The combined organic layers were dried over $MgSO_4$, filtered, and concentrated *in vacuo*. The residue was purified via column chromatography to afford cyclopentenone **7a** (25.1 mg, 70%) as a solid. Spectral data matches literature values[17]; The enantiomeric purity of the product determined by HPLC: 75 % ee (Chiralpak IB column, *n*-hexane/*i*-PrOH = 90/10, flow rate 1.0 mL/min, $\lambda = 254$ nm), t_r (minor) = 19.5 min, t_r (major) = 25.0 min; $[\alpha]^{RT}_D = 87.4$ (*c* = 0.53 in CH_2Cl_2).

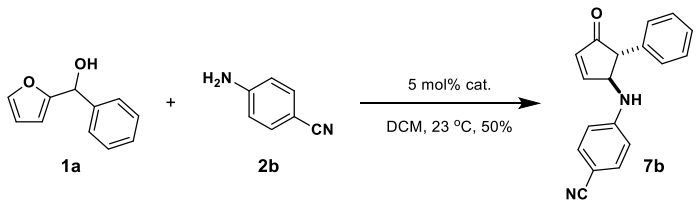

4-(((1S,5R)-4-oxo-5-phenylcyclopent-2-en-1-yl)amino)benzonitrile (7b): According to the general procedure, the catalyst **8** (4.7 mg, 0.005 mmol, 0.05 eq) was added to **1a** (20.0 mg, 0.11 mmol, 1.2 eq) and 4-aminobenzonitrile **2b** (11.3 mg, 0.10 mmol, 1.0 eq) in 1 mL of anhydrous DCM. The resulting reaction mixture was allowed to stir at room temperature for 5 days before being quenched with 5 mL of saturated aqueous sodium bicarbonate and extracted with DCM (3 x 5 mL). The combined organic layers were dried over $MgSO_4$, filtered, and concentrated *in vacuo*. The residue was purified via column chromatography to afford cyclopentenone **7b** (13.1 mg, 50%) as a solid. Spectral data matches literature values[25]; The enantiomeric purity of the product determined by HPLC: 71 % ee (Chiralpak IB column, *n*-hexane/*i*-PrOH = 90/10, flow

rate 1.0 mL/min, λ = 254 nm), t_r (minor) = 30.2 min, t_r (major) = 38.4 min; $[\alpha]^{RT}_D$ = 87.0 (*c* = 0.53 in CH_2Cl_2).

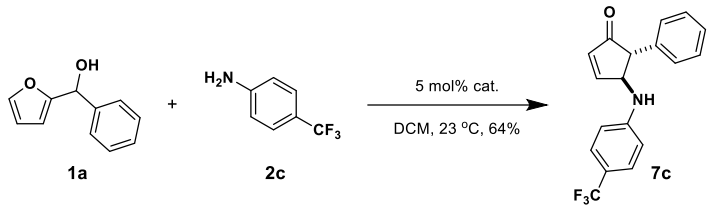

(4S,5R)-5-phenyl-4-((4-(trifluoromethyl)phenyl)amino)cyclopent-2-en-1-one (7c): According to the general procedure, the catalyst **8** (4.7 mg, 0.005 mmol, 0.05 eq) was added to **1a** (20.0 mg, 0.11 mmol, 1.2 eq) and 4-(trifluoromethyl)aniline **2c** (12 μL, 0.10 mmol, 1.0 eq) in 1 mL of anhydrous DCM. The resulting reaction mixture was allowed to stir at room temperature for 5 days before being quenched with 5 mL of saturated aqueous sodium bicarbonate and extracted with DCM (3 x 5 mL). The combined organic layers were dried over $MgSO_4$, filtered, and concentrated *in vacuo*. The residue was purified via column chromatography to afford cyclopentenone **7c** (19.4 mg, 64%) as a solid. Spectral data matches literature values[35]; The enantiomeric purity of the product determined by HPLC: 76 % ee (Chiralpak IB column, *n*-hexane/*i*-PrOH = 90/10, flow rate 1.0 mL/min, λ = 254 nm), t_r (minor) = 15.0 min, t_r (major) = 19.3 min; $[\alpha]^{RT}_D$ = 30.5 (*c* = 0.24 in CH_2Cl_2).

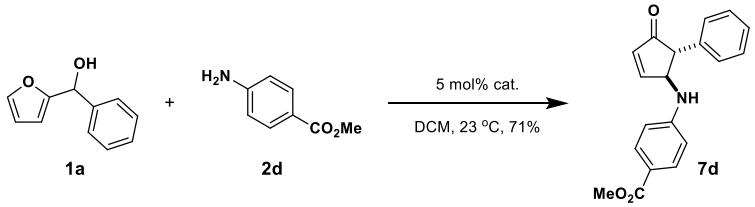

Methyl 4-(((1S,5R)-4-oxo-5-phenylcyclopent-2-en-1-yl)amino)benzoate (7d): According to the general procedure, the catalyst **8** (4.7 mg, 0.005 mmol, 0.05 eq) was added to **1a** (20.0 mg, 0.11 mmol, 1.2 eq) and methyl 4-aminobenzoate **2d** (14.5 mg, 0.10 mmol, 1.0 eq) in 1 mL of

anhydrous DCM. The resulting reaction mixture was allowed to stir at room temperature for 5 days before being quenched with 5 mL of saturated aqueous sodium bicarbonate and extracted with DCM (3 x 5 mL). The combined organic layers were dried over $MgSO_4$, filtered, and concentrated *in vacuo*. The residue was purified via column chromatography to afford cyclopentenone **7d** (20.9 mg, 71%) as a solid. Spectral data matches literature values[17]; The enantiomeric purity of the product determined by HPLC: 73 % ee (Chiralpak IB column, *n*-hexane/*i*-PrOH = 90/10, flow rate 1.0 mL/min, λ = 254 nm), t_r (minor) = 27.0 min, t_r (major) = 31.9 min; $[\alpha]^{RT}_D$ = 76.6 (*c* = 0.50 in CH_2Cl_2).

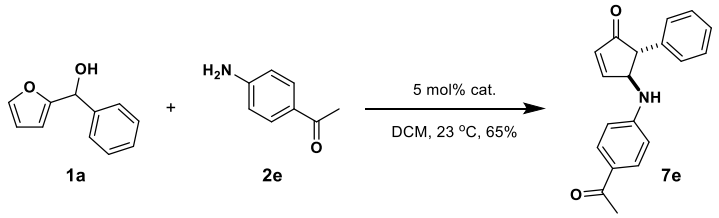

(4S,5R)-4-((4-acetylphenyl)amino)-5-phenylcyclopent-2-en-1-one (7e): According to the general procedure, the catalyst **8** (4.7mg, 0.005 mmol, 0.05 eq) was added to **1a** (20.0 mg, 0.11 mmol, 1.2 eq) and 4-aminoacetophenone **2e** (12.9 mg, 0.10 mmol, 1.0 eq) in 1 mL of anhydrous DCM. The resulting reaction mixture was allowed to stir at room temperature for 5 days before being quenched with 5 mL of saturated aqueous sodium bicarbonate and extracted with DCM (3 x 5 mL). The combined organic layers were dried over $MgSO_4$, filtered, and concentrated *in vacuo*. The residue was purified via column chromatography to afford cyclopentenone **7e** (18.1 mg, 65%) as a solid. ^{1}H NMR (500 MHz, Chloroform-*d*) δ 7.79 – 7.74 (m, 3H), 7.40 – 7.29 (m, 3H), 7.14 (dt, *J* = 7.7, 1.6 Hz, 2H), 6.52 – 6.45 (m, 3H), 4.84 (t, *J* = 2.2 Hz, 1H), 4.54 (s, 1H), 3.41 (q, *J* = 2.3 Hz, 1H), 2.48 (d, *J* = 1.9 Hz, 3H); ^{13}C NMR (125 MHz, Chloroform-*d*) δ 196.4, 160.6, 150.3, 137.7, 135.6, 130.9, 129.3, 128.2, 128.0, 127.8, 112.6, 62.8, 60.4, 26.2;

IR 3328, 3068, 3000, 2921, 1713, 1648, 1569, 1525, 1339, 1275, 1165, 824, 700, 532 cm^{-1}; HRMS (ESI), calculated for $C_{19}H_{17}NO_2$: (M^+) 291.1259; observed 291.1270; The enantiomeric purity of the product determined by HPLC: 76 % ee (Chiralpak IB column, *n*-hexane/*i*-PrOH = 90/10, flow rate 1.0 mL/min, λ = 254 nm), t_r (minor) = 39.3 min, t_r (major) = 43.8 min; $[\alpha]^{RT}_D$ = 76.0 (*c* = 0.51 in CH_2Cl_2).

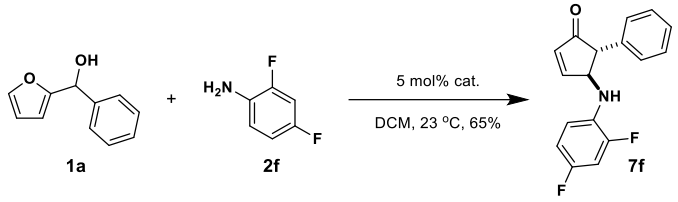

(4S,5R)-4-((2,4-difluorophenyl)amino)-5-phenylcyclopent-2-en-1-one (7f): According to the general procedure, the catalyst **8** (4.7 mg, 0.005 mmol, 0.05 eq) was added to **1a** (20.0 mg, 0.11 mmol, 1.2 eq) and 2,4-difluoroaniline **2f** (9.7 μL, 0.10 mmol, 1.0 eq) in 1 mL of anhydrous DCM. The resulting reaction mixture was allowed to stir at room temperature for 5 days before being quenched with 5 mL of saturated aqueous sodium bicarbonate and extracted with DCM (3 x 5 mL). The combined organic layers were dried over $MgSO_4$, filtered, and concentrated *in vacuo*. The residue was purified via column chromatography to afford cyclopentenone **7f** (17.7 mg, 65%) as a solid. ^{1}H NMR (500 MHz, Chloroform-*d*) δ 7.76 (dd, *J* = 5.7, 2.3 Hz, 1H), 7.38 – 7.27 (m, 3H), 7.14 – 7.09 (m, 2H), 6.80 (ddd, *J* = 11.3, 8.4, 2.8 Hz, 1H), 6.63 – 6.57 (m, 1H), 6.45 (dd, *J* = 5.7, 1.7 Hz, 1H), 6.38 (td, *J* = 9.2, 5.3 Hz, 1H), 4.72 (q, *J* = 2.3 Hz, 1H), 4.03 (s, 1H), 3.38 (d, *J* = 2.6 Hz, 1H); ^{13}C NMR (125 MHz, Chloroform-*d*) δ 206.1, 161.1, 156.1, 137.9, 135.3, 129.6, 129.2, 128.7, 128.7, 128.1, 127.7, 114.1, 114.0, 114.0, 114.0, 111.0, 111.0, 110.9, 110.9, 105.1, 104.2, 104.0, 104.0, 103.8, 63.8, 60.4; IR 3374, 3063, 3029, 2919, 1703, 1600, 1516, 1431, 1265, 1142, 959, 698 cm^{-1}; HRMS (ESI), calculated for $C_{17}H_{13}F_2NO$: (M^+) 285.0965; observed 285.0961; The enantiomeric purity of the product determined by HPLC:

63 % ee (Chiralpak IB column, *n*-hexane/*i*-PrOH = 90/10, flow rate 1.0 mL/min, λ = 254 nm), t_r (minor) = 13.4 min, t_r (major) = 18.0 min; $[\alpha]^{RT}_D$ = 76.8 (*c* = 0.47 in CH_2Cl_2).

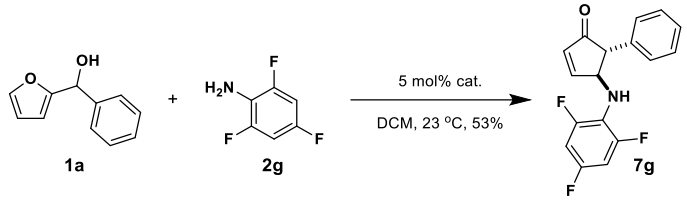

(4S,5R)-5-phenyl-4-((2,4,6-trifluorophenyl)amino)cyclopent-2-en-1-one (7g): According to the general procedure, the catalyst **8** (4.7 mg, 0.005 mmol, 0.05 eq) was added to **1a** (20.0 mg, 0.11 mmol, 1.2 eq) and 2,4,6-trifluoroaniline **2g** (14.1 mg, 0.10 mmol, 1.0 eq) in 1 mL of anhydrous DCM. The resulting reaction mixture was allowed to stir at room temperature for 5 days before being quenched with 5 mL of saturated aqueous sodium bicarbonate and extracted with DCM (3 x 5 mL). The combined organic layers were dried over $MgSO_4$, filtered, and concentrated *in vacuo*. The residue was purified via column chromatography to afford cyclopentenone **7g** (15.4 mg, 53%) as a solid. Spectral data matches literature values[17]; The enantiomeric purity of the product determined by HPLC: 61 % ee (Chiralpak IB column, *n*-hexane/*i*-PrOH = 90/10, flow rate 1.0 mL/min, λ = 254 nm), t_r (minor) = 12.6 min, t_r (major) = 14.7 min; $[\alpha]^{RT}_D$ = 97.4 (*c* = 0.50 in CH_2Cl_2).

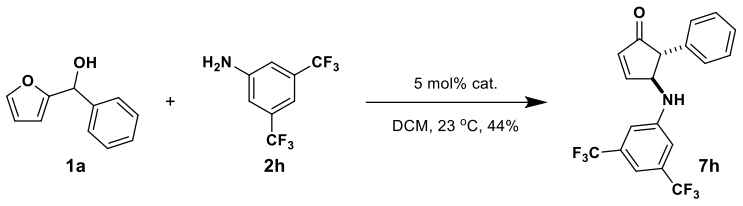

(4S,5R)-4-((3,5-bis(trifluoromethyl)phenyl)amino)-5-phenylcyclopent-2-en-1-one (7h): According to the general procedure, the catalyst **8** (4.7 mg, 0.005 mmol, 0.05 eq) was added to **1a** (20.0 mg, 0.11 mmol, 1.2 eq) and 3,5-bis(trifluoromethyl)aniline **2h** (14.9 μL, 0.10 mmol,

1.0 eq) in 1 mL of anhydrous DCM. The resulting reaction mixture was allowed to stir at room temperature for 5 days before being quenched with 5 mL of saturated aqueous sodium bicarbonate and extracted with DCM (3 x 5 mL). The combined organic layers were dried over $MgSO_4$, filtered, and concentrated *in vacuo*. The residue was purified via column chromatography to afford cyclopentenone **7h** (16.2 mg, 44%) as a solid. Spectral data matches literature values[17]; The enantiomeric purity of the product determined by HPLC: 58 % ee (Chiralpak IB column, *n*-hexane/*i*-PrOH = 90/10, flow rate 1.0 mL/min, $\lambda = 254$ nm), t_r (minor) = 20.4 min, t_r (major) = 24.3 min; $[\alpha]^{RT}_D = 14.7$ (*c* = 1.10 in CH_2Cl_2).

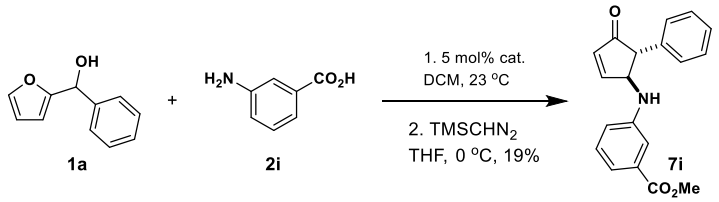

Methyl 3-(((1S,5R)-4-oxo-5-phenylcyclopent-2-en-1-yl)amino)benzoate (7i): According to the general procedure, the catalyst **8** (4.7 mg, 0.005 mmol, 0.05 eq) was added to **1a** (20.0 mg, 0.11 mmol, 1.2 eq) and 3-aminobenzoic acid **2i** (13.1 mg, 0.10 mmol, 1.0 eq) in 1 mL of anhydrous DCM. The resulting reaction mixture was allowed to stir at room temperature for 5 days before being concentrated *in vacuo*. The residue is dissolved into 0.5 mL of anhydrous THF and cooled to 0 °C. (Trimethylsilyl)diazomethane (2 M in hexanes; 0.19 mL, 0.38 mmol, 4.0 eq) was added dropwise to the reaction and allowed to stir for 15 minutes before being quenched with MeOH. The reaction was then extracted with DCM and water (3 x 10 mL). The combined organic layers were dried over $MgSO_4$, filtered, and concentrated *in vacuo*. The residue was purified via column chromatography to afford cyclopentenone **7i** (5.6 mg, 19%) as a solid. ^{1}H NMR (500 MHz, Chloroform-*d*) δ 7.78 (dd, *J* = 5.8, 2.3 Hz, 1H), 7.43 – 7.40 (m, 1H), 7.38 – 7.28 (m, 3H), 7.21 – 7.12 (m, 4H), 6.70 (ddd, *J* = 8.2, 2.6, 1.0 Hz, 1H), 6.45 (dd, *J*

= 5.8, 1.7 Hz, 1H), 4.81 (s, 1H), 4.11 (d, *J* = 8.7 Hz, 1H), 3.83 (s, 3H), 3.39 (d, *J* = 2.7 Hz, 1H); ^{13}C NMR (125 MHz, Chloroform-*d*) δ 206.2, 167.2, 161.2, 146.3, 137.9, 135.2, 131.5, 129.6, 129.2, 128.1, 127.6, 120.1, 118.3, 114.6, 105.2, 63.4, 60.4, 52.2; IR 3378, 3329, 3028, 2949, 1698, 1605, 1585, 1530, 1337, 1276, 1110, 744, 699, 545 cm^{-1}; HRMS (ESI), calculated for $C_{19}H_{17}NO_3$: (M^+) 307.1208; observed 307.1218; The enantiomeric purity of the product determined by HPLC: 74 % ee (Chiralpak IB column, *n*-hexane/*i*-PrOH = 90/10, flow rate 1.0 mL/min, λ = 254 nm), t_r (minor) = 47.5 min, t_r (major) = 53.9 min; $[\alpha]^{RT}_D$ = 46.3 (*c* = 0.45 in CH_2Cl_2).

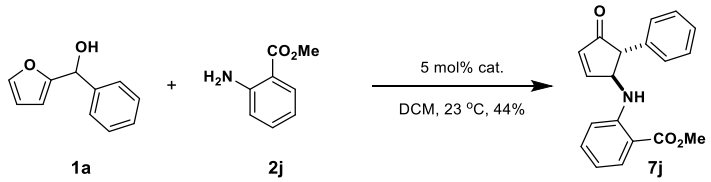

Methyl 2-(((1S,5R)-4-oxo-5-phenylcyclopent-2-en-1-yl)amino)benzoate (7j): According to the general procedure, the catalyst **8** (4.7 mg, 0.005 mmol, 0.05 eq) was added to **1a** (20.0 mg, 0.11 mmol, 1.2 eq) and methyl 2-aminobenzoate **2j** (12.4 μL, 0.10 mmol, 1.0 eq) in 1 mL of anhydrous DCM. The resulting reaction mixture was allowed to stir at room temperature for 5 days before being quenched with 5 mL of saturated aqueous sodium bicarbonate and extracted with DCM (3 x 5 mL). The combined organic layers were dried over $MgSO_4$, filtered, and concentrated *in vacuo*. The residue was purified via column chromatography to afford cyclopentenone **7j** (12.9 mg, 44%) as a solid. Spectral data matches literature values[17]; The enantiomeric purity of the product determined by HPLC: 80 % ee (Chiralpak IB column, *n*-hexane/*i*-PrOH = 90/10, flow rate 1.0 mL/min, λ = 254 nm), t_r (minor) = 14.3 min, t_r (major) = 16.2 min; $[\alpha]^{RT}_D$ = 235.1 (*c* = 0.49 in CH_2Cl_2).

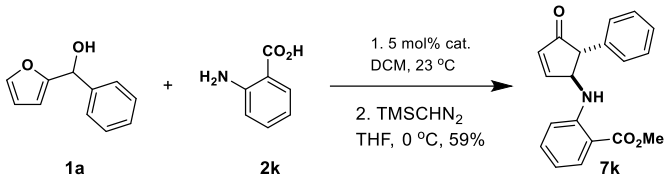

Methyl 2-(((1S,5R)-4-oxo-5-phenylcyclopent-2-en-1-yl)amino)benzoate (7k): According to the general procedure, the catalyst **8** (4.7 mg, 0.005 mmol, 0.05 eq) was added to **1a** (20.0 mg, 0.11 mmol, 1.2 eq) and 2-aminobenzoic acid **2k** (13.1 mg, 0.10 mmol, 1.0 eq) in 1 mL of anhydrous DCM. The resulting reaction mixture was allowed to stir at room temperature for 5 days before being concentrated *in vacuo*. The residue is dissolved into 0.5 mL of anhydrous THF and cooled to 0 °C. (Trimethylsilyl)diazomethane (2 M in hexanes; 0.19 mL, 0.38 mmol, 4.0 eq) was added dropwise to the reaction and allowed to stir for 15 minutes before being quenched with MeOH. The reaction was then extracted with DCM and water (3 x 10 mL). The combined organic layers were dried over $MgSO_4$, filtered, and concentrated *in vacuo*. The residue was purified via column chromatography to afford cyclopentenone **7k** (17.3 mg, 59%) as a solid. Spectral data matches literature values[35]; The enantiomeric purity of the product determined by HPLC: 84 % ee (Chiralpak IB column, *n*-hexane/*i*-PrOH = 90/10, flow rate 1.0 mL/min, λ = 254 nm), t_r (minor) = 13.9 min, t_r (major) = 15.5 min; $[\alpha]^{RT}_D$ = 254.0 (*c* = 0.42 in CH_2Cl_2).

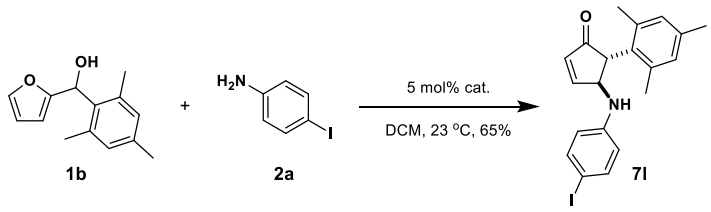

(4S,5R)-4-((4-iodophenyl)amino)-5-mesitylcyclopent-2-en-1-one (7l): According to the general procedure, the catalyst **8** (3.8 mg, 0.004 mmol, 0.05 eq) was added to furan-2-

yl(mesityl)methanol **1b** (20.0 mg, 0.09 mmol, 1.2 eq) and **2a** (16.9 mg, 0.08 mmol, 1.0 eq) in 1 mL of anhydrous DCM. The resulting reaction mixture was allowed to stir at room temperature for 5 days before being quenched with 5 mL of saturated aqueous sodium bicarbonate and extracted with DCM (3 x 5 mL). The combined organic layers were dried over $MgSO_4$, filtered, and concentrated *in vacuo*. The residue was purified via column chromatography to afford cyclopentenone **7l** (20.9 mg, 65%) as a solid. ^{1}H NMR (500 MHz, Chloroform-*d*) δ 7.62 (dt, *J* = 5.8, 1.6 Hz, 1H), 7.34 – 7.28 (m, 2H), 6.83 (d, *J* = 13.6 Hz, 2H), 6.45 (dt, *J* = 5.9, 1.5 Hz, 1H), 6.27 – 6.20 (m, 2H), 4.75 (dt, *J* = 7.6, 2.4 Hz, 1H), 4.07 (d, *J* = 8.3 Hz, 1H), 3.82 (d, *J* = 3.5 Hz, 1H), 2.25 (s, 3H), 2.11 (s, 3H), 1.99 (s, 3H); ^{13}C NMR (125 MHz, Chloroform-*d*) δ 206.4, 160.0, 146.0, 138.3, 138.0, 137.2, 135.8, 134.9, 131.2, 130.5, 129.5, 115.7, 79.6, 62.2, 56.9, 21.3, 21.0, 20.5, 1.2; IR 3359, 2961, 2919, 2858, 1702, 1587, 1484, 1291, 1248, 1129, 904, 810, 728, 500 cm^{-1}; HRMS (ESI), calculated for $C_{20}H_{20}INO$: ($M+Na^+$) 440.0487; observed 440.0473; The enantiomeric purity of the product determined by HPLC: 17 % ee (Chiralpak IB column, *n*-hexane/*i*-PrOH = 90/10, flow rate 1.0 mL/min, λ = 254 nm), t_r (minor) = 15.7 min, t_r (major) = 20.6 min; $[\alpha]^{RT}_D$ = 12.8 (*c* = 0.48 in CH_2Cl_2).

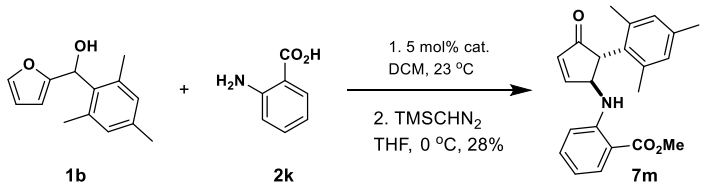

Methyl 2-(((1S,5R)-5-mesityl-4-oxocyclopent-2-en-1-yl)amino)benzoate (7m): According to the general procedure, the catalyst **8** (3.8 mg, 0.004 mmol, 0.05 eq) was added to **1b** (20.0 mg, 0.09 mmol, 1.2 eq) and **2k** (10.6 mg, 0.08 mmol, 1.0 eq) in 1 mL of anhydrous DCM. The resulting reaction mixture was allowed to stir at room temperature for 5 days before being concentrated *in vacuo*. The residue is dissolved into 0.5 mL of anhydrous THF and cooled to

0 °C. (Trimethylsilyl)diazomethane (2 M in hexanes; 0.15 mL, 0.31 mmol, 4.0 eq) was added dropwise to the reaction and allowed to stir for 15 minutes before being quenched with MeOH. The reaction was then extracted with DCM and water (3 x 10 mL). The combined organic layers were dried over $MgSO_4$, filtered, and concentrated *in vacuo*. The residue was purified via column chromatography to afford cyclopentenone **7m** (7.5 mg, 28%) as a solid. ^{1}H NMR (500 MHz, Chloroform-*d*) δ 8.25 (d, *J* = 7.7 Hz, 1H), 7.91 (dd, *J* = 8.0, 1.7 Hz, 1H), 7.66 (dd, *J* = 5.8, 2.0 Hz, 1H), 7.16 (ddd, *J* = 8.6, 7.1, 1.7 Hz, 1H), 6.85 (s, 1H), 6.81 (s, 1H), 6.61 (ddd, *J* = 8.1, 7.1, 1.0 Hz, 1H), 6.47 (dd, *J* = 5.8, 1.8 Hz, 1H), 6.43 (d, *J* = 8.5 Hz, 1H), 4.91 (ddt, *J* = 7.5, 3.5, 1.8 Hz, 1H), 3.90 (d, *J* = 3.6 Hz, 1H), 3.87 (s, 3H), 2.25 (s, 3H), 2.20 (s, 3H), 2.04 (s, 3H); ^{13}C NMR (125 MHz, Chloroform-*d*) δ 206.4, 169.2, 159.6, 149.8, 138.5, 137.0, 135.8, 134.7, 134.7, 131.9, 131.2, 130.4, 129.4, 116.0, 111.7, 110.8, 60.8, 57.4, 51.8, 21.3, 21.0, 20.9, 20.5; IR 3331, 2951, 2921, 2854, 1705, 1584, 1511, 1316, 1243, 1164, 810, 747, 487 cm^{-1}; HRMS (ESI), calculated for $C_{22}H_{23}NO_3$: ($M+Na^+$) 372.1576; observed 372.1589; The enantiomeric purity of the product determined by HPLC: 28 % ee (Chiralpak IB column, *n*-hexane/*i*-PrOH = 90/10, flow rate 1.0 mL/min, λ = 254 nm), t_r (minor) = 15.1 min, t_r (major) = 11.1 min; $[\alpha]^{RT}_D$ = 69.7 (*c* = 0.49 in CH_2Cl_2).

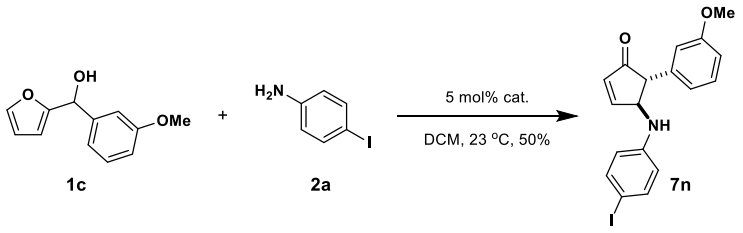

(4S,5R)-4-((4-iodophenyl)amino)-5-(3-methoxyphenyl)cyclopent-2-en-1-one (7n): According to the general procedure, the catalyst **8** (4.0 mg, 0.004 mmol, 0.05 eq) was added to furan-2-yl(3-methoxyphenyl)methanol **1c** (20.0 mg, 0.10 mmol, 1.2 eq) and **2a** (17.9 mg, 0.08

mmol, 1.0 eq) in 1 mL of anhydrous DCM. The resulting reaction mixture was allowed to stir at room temperature for 5 days before being quenched with 5 mL of saturated aqueous sodium bicarbonate and extracted with DCM (3 x 5 mL). The combined organic layers were dried over $MgSO_4$, filtered, and concentrated *in vacuo*. The residue was purified via column chromatography to afford cyclopentenone **7n** (16.5 mg, 50%) as a solid. ^{1}H NMR (500 MHz, Chloroform-*d*) δ 7.74 (dd, *J* = 5.7, 2.4 Hz, 1H), 7.40 – 7.35 (m, 2H), 7.29 – 7.23 (m, 1H), 6.84 (ddd, *J* = 8.3, 2.6, 0.9 Hz, 1H), 6.70 (dt, *J* = 7.6, 1.2 Hz, 1H), 6.65 (dd, *J* = 2.5, 1.7 Hz, 1H), 6.42 (dd, *J* = 5.7, 1.7 Hz, 1H), 6.33 – 6.27 (m, 2H), 4.71 (s, 1H), 4.02 (s, 1H), 3.78 (s, 3H), 3.32 (d, *J* = 2.5 Hz, 1H); ^{13}C NMR (125 MHz, Chloroform-*d*) δ 206.0, 161.2, 160.1, 145.9, 139.4, 138.1, 135.3, 130.3, 120.3, 116.1, 114.0, 112.9, 79.8, 63.3, 60.1, 55.4; IR 3367, 2923, 2834, 1703, 1584, 1486, 1315, 1248, 1151, 1038, 806, 755, 696, 497 cm^{-1}; HRMS (ESI), calculated for $C_{18}H_{16}INO_2$: ($M+Na^+$) 428.0124; observed 428.0121; The enantiomeric purity of the product determined by HPLC: 76 % ee (Chiralpak IB column, *n*-hexane/*i*-PrOH = 90/10, flow rate 1.0 mL/min, λ = 254 nm), t_r (minor) = 23.4 min, t_r (major) = 33.0 min; $[\alpha]^{RT}_D$ = 37.7 (*c* = 0.51 in CH_2Cl_2).

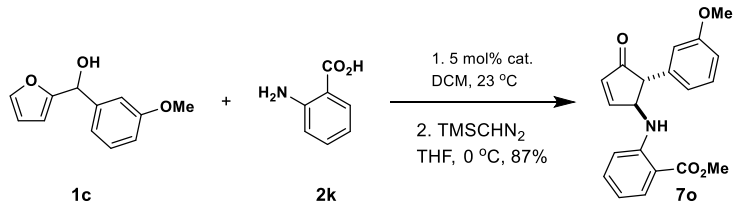

Methyl 2-(((1S,5R)-5-(3-methoxyphenyl)-4-oxocyclopent-2-en-1-yl)amino)benzoate (7o): According to the general procedure, the catalyst **8** (4.0 mg, 0.004 mmol, 0.05 eq) was added to **1c** (20.0 mg, 0.10 mmol, 1.2 eq) and **2k** (11.2 mg, 0.08 mmol, 1.0 eq) in 1 mL of anhydrous DCM. The resulting reaction mixture was allowed to stir at room temperature for 5 days before

being concentrated *in vacuo*. The residue is dissolved into 0.5 mL of anhydrous THF and cooled to 0 °C. (Trimethylsilyl)diazomethane (2 M in hexanes; 0.16 mL, 0.33 mmol, 4.0 eq) was added dropwise to the reaction and allowed to stir for 15 minutes before being quenched with MeOH. The reaction was then extracted with DCM and water (3 x 10 mL). The combined organic layers were dried over $MgSO_4$, filtered, and concentrated *in vacuo*. The residue was purified via column chromatography to afford cyclopentenone **7o** (9.9 mg, 36%) as a solid. ^{1}H NMR (500 MHz, Chloroform-*d*) δ 8.18 (d, *J* = 7.6 Hz, 1H), 7.92 (dd, *J* = 8.0, 1.7 Hz, 1H), 7.78 (dd, *J* = 5.7, 2.4 Hz, 1H), 7.30 – 7.24 (m, 1H), 7.22 (ddd, *J* = 8.7, 7.1, 1.8 Hz, 1H), 6.84 (ddd, *J* = 8.3, 2.6, 0.9 Hz, 1H), 6.75 (dt, *J* = 7.6, 1.2 Hz, 1H), 6.70 (t, *J* = 2.1 Hz, 1H), 6.64 (ddd, *J* = 8.1, 7.1, 1.1 Hz, 1H), 6.48 – 6.42 (m, 2H), 4.83 (dq, *J* = 7.4, 2.2 Hz, 1H), 3.87 (s, 3H), 3.78 (s, 3H), 3.39 (d, *J* = 2.6 Hz, 1H); ^{13}C NMR (125 MHz, Chloroform-*d*) δ 206.2, 169.2, 161.2, 160.1, 149.6, 139.6, 135.2, 134.8, 132.0, 130.2, 120.4, 116.1, 114.0, 113.0, 112.4, 111.1, 111.1, 62.3, 60.7, 55.4, 51.8; IR 3333, 3000, 2951, 2837, 1713, 1680, 1581, 1513, 1436, 1318, 1238, 1150, 1046, 747, 699 cm^{-1}; HRMS (ESI), calculated for $C_{20}H_{19}NO_4$: ($M+Na^+$) 360.1212; observed 360.1229; The enantiomeric purity of the product determined by HPLC: 87 % ee (Chiralpak IB column, *n*-hexane/*i*-PrOH = 90/10, flow rate 1.0 mL/min, λ = 254 nm), t_r (minor) = 16.3 min, t_r (major) = 20.5 min; $[\alpha]^{RT}_D$ = 217.8 (*c* = 0.53 in CH_2Cl_2).

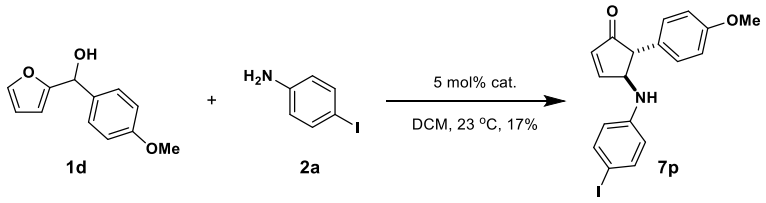

(4S,5R)-4-((4-iodophenyl)amino)-5-(4-methoxyphenyl)cyclopent-2-en-1-one (7p): According to the general procedure, the catalyst **8** (4.0 mg, 0.004 mmol, 0.05 eq) was added to furan-2-yl(4-methoxyphenyl)methanol **1d** (20.0 mg, 0.10 mmol, 1.2 eq) and **2a** (17.9 mg, 0.08 mmol, 1.0 eq) in 1 mL of anhydrous DCM. The resulting reaction mixture was allowed to stir at room temperature for 5 days before being quenched with 5 mL of saturated aqueous sodium bicarbonate and extracted with DCM (3 x 5 mL). The combined organic layers were dried over $MgSO_4$, filtered, and concentrated *in vacuo*. The residue was purified via column chromatography to afford cyclopentenone **7p** (5.6 mg, 17%) as a solid. Spectral data matches literature values[17]; The enantiomeric purity of the product determined by HPLC: 75 % ee (Chiralpak IB column, *n*-hexane/*i*-PrOH = 90/10, flow rate 1.0 mL/min, $\lambda = 254$ nm), t_r (minor) = 27.1 min, t_r (major) = 38.0 min; $[\alpha]^{RT}_D = 26.6$ (*c* = 0.51 in CH_2Cl_2).

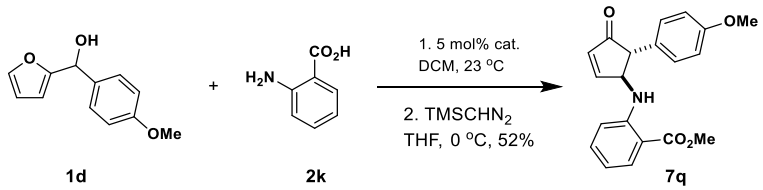

Methyl 2-(((1S,5R)-5-(4-methoxyphenyl)-4-oxocyclopent-2-en-1-yl)amino)benzoate (7q): According to the general procedure, the catalyst **8** (4.0 mg, 0.004 mmol, 0.05 eq) was added to **1d** (20.0 mg, 0.10 mmol, 1.2 eq) and **2k** (11.2 mg, 0.08 mmol, 1.0 eq) in 1 mL of anhydrous DCM. The resulting reaction mixture was allowed to stir at room temperature for 5 days before being concentrated *in vacuo*. The residue is dissolved into 0.5 mL of anhydrous THF and cooled to 0 °C. (Trimethylsilyl)diazomethane (2 M in hexanes; 0.16 mL, 0.33 mmol, 4.0 eq) was added dropwise to the reaction and allowed to stir for 15 minutes before being quenched with MeOH. The reaction was then extracted with DCM and water (3 x 10 mL). The combined organic layers were dried over $MgSO_4$, filtered, and concentrated *in vacuo*. The residue was

purified via column chromatography to afford cyclopentenone **7q** (14.3 mg, 52%) as a solid. ^{1}H NMR (500 MHz, Chloroform-*d*) δ 8.18 (d, *J* = 7.5 Hz, 1H), 7.92 (dt, *J* = 8.0, 1.4 Hz, 1H), 7.76 (ddd, *J* = 5.9, 2.4, 1.0 Hz, 1H), 7.22 (ddd, *J* = 8.5, 7.1, 1.6 Hz, 1H), 7.11 – 7.06 (m, 2H), 6.91 – 6.86 (m, 2H), 6.63 (ddt, *J* = 8.2, 7.1, 1.1 Hz, 1H), 6.47 – 6.41 (m, 2H), 4.81 – 4.75 (m, 1H), 3.86 (s, 3H), 3.80 (s, 3H), 3.38 (d, *J* = 2.6 Hz, 1H); ^{13}C NMR (125 MHz, Chloroform-*d*) δ 169.2, 161.0, 159.1, 149.7, 135.1, 134.8, 132.0, 130.1, 129.2, 116.1, 114.7, 112.4, 111.0, 62.4, 60.0, 55.5, 51.8; IR 3331, 2996, 2950, 2836, 1716, 1677, 1582, 1511, 1436, 1239, 1178, 1032, 746, 524 cm^{-1}; HRMS (ESI), calculated for $C_{20}H_{19}NO_4$: ($M+Na^+$) 360.1212; observed 360.1215; The enantiomeric purity of the product determined by HPLC: 86 % ee (Chiralpak IB column, *n*-hexane/*i*-PrOH = 90/10, flow rate 1.0 mL/min, λ = 254 nm), t_r (minor) = 18.0 min, t_r (major) = 22.7 min; $[\alpha]^{RT}_D$ = 300.3 (*c* = 0.38 in CH_2Cl_2).

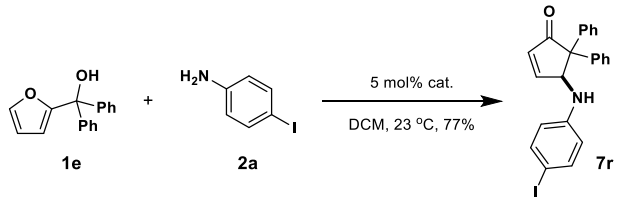

(S)-4-((4-iodophenyl)amino)-5,5-diphenylcyclopent-2-en-1-one (7r): According to the general procedure, the catalyst **8** (3.3 mg, 0.003 mmol, 0.05 eq) was added to furan-2-yldiphenylmethanol **1e** (20.0 mg, 0.08 mmol, 1.2 eq) and **2a** (14.6 mg, 0.07 mmol, 1.0 eq) in 1 mL of anhydrous DCM. The resulting reaction mixture was allowed to stir at room temperature for 5 days before being quenched with 5 mL of saturated aqueous sodium bicarbonate and extracted with DCM (3 x 5 mL). The combined organic layers were dried over $MgSO_4$, filtered, and concentrated *in vacuo*. The residue was purified via column chromatography to afford cyclopentenone **7r** (23.1 mg, 77%) as a solid. ^{1}H NMR (500 MHz, Chloroform-*d*) δ 7.73 (dd, *J* = 5.9, 2.3 Hz, 1H), 7.46 (dd, *J* = 7.5, 1.9 Hz, 2H), 7.37 – 7.22 (m,

8H), 7.00 – 6.95 (m, 2H), 6.47 (dd, *J* = 5.8, 1.8 Hz, 1H), 6.22 (d, *J* = 8.6 Hz, 2H), 5.49 (dt, *J* = 10.0, 2.2 Hz, 1H), 3.35 (d, *J* = 9.9 Hz, 1H); ^{13}C NMR (125 MHz, Chloroform-*d*) δ 206.8, 161.3, 145.7, 140.7, 140.3, 138.1, 134.2, 129.9, 128.7, 128.4, 128.4, 127.7, 127.6, 115.7, 79.2, 65.1, 63.5; IR 3381, 3024, 2920, 1697, 1587, 1482, 1315, 1157, 805, 742, 701, 507 cm^{-1}; HRMS (ESI), calculated for $C_{23}H_{18}INO$: ($M+Na^+$) 474.0331; observed 474.0347; The enantiomeric purity of the product determined by HPLC: 41 % ee (Chiralpak IB column, *n*-hexane/*i*-PrOH = 90/10, flow rate 1.0 mL/min, λ = 254 nm), t_r (minor) = 15.0 min, t_r (major) = 20.9 min; $[\alpha]^{RT}_D$ = 136.9 (*c* = 0.46 in CH_2Cl_2).

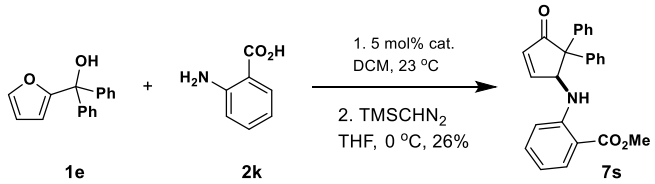

Methyl (S)-2-((4-oxo-5,5-diphenylcyclopent-2-en-1-yl)amino)benzoate (7s): According to the general procedure, the catalyst **8** (3.3 mg, 0.003 mmol, 0.05 eq) was added to **1e** (20.0 mg, 0.08 mmol, 1.2 eq) and **2k** (9.1 mg, 0.07 mmol, 1.0 eq) in 1 mL of anhydrous DCM. The resulting reaction mixture was allowed to stir at room temperature for 5 days before being concentrated *in vacuo*. The residue is dissolved into 0.5 mL of anhydrous THF and cooled to 0 °C. (Trimethylsilyl)diazomethane (2 M in hexanes; 0.13 mL, 0.27 mmol, 4.0 eq) was added dropwise to the reaction and allowed to stir for 15 minutes before being quenched with MeOH. The reaction was then extracted with DCM and water (3 x 10 mL). The combined organic layers were dried over $MgSO_4$, filtered, and concentrated *in vacuo*. The residue was purified via column chromatography to afford cyclopentenone **7s** (6.6 mg, 26%) as a solid. ^{1}H NMR (500 MHz, Chloroform-*d*) δ 7.78 (dd, *J* = 5.8, 2.5 Hz, 1H), 7.75 (dd, *J* = 8.0, 1.7 Hz, 1H), 7.49 – 7.45 (m, 3H), 7.37 – 7.27 (m, 4H), 7.16 – 7.11 (m, 3H), 7.00 – 6.96 (m, 2H), 6.75 (d, *J* = 8.5

Hz, 1H), 6.58 (ddd, *J* = 8.1, 7.1, 1.0 Hz, 1H), 6.47 (dd, *J* = 5.8, 1.8 Hz, 1H), 5.70 (dt, *J* = 9.6, 2.2 Hz, 1H), 3.66 (s, 3H); ^{13}C NMR (125 MHz, Chloroform-*d*) δ 207.1, 168.3, 161.1, 149.1, 141.0, 140.1, 134.5, 134.1, 132.0, 130.2, 128.7, 128.3, 128.0, 127.5, 127.2, 115.8, 112.0, 111.5, 65.6, 63.3, 51.6; IR 3313, 2923, 2853, 1691, 1577, 1495, 1439, 1259, 1236, 745, 698 cm^{-1}; HRMS (ESI), calculated for $C_{25}H_{21}NO_3$: (M+Na$^+$) 406.1419; observed 406.1405; The enantiomeric purity of the product determined by HPLC: 72 % ee (Chiralpak IB column, *n*-hexane/*i*-PrOH = 90/10, flow rate 1.0 mL/min, λ = 254 nm), t_r (minor) = 11.7 min, t_r (major) = 14.7 min; $[\alpha]^{RT}_D$ = 161.0 (*c* = 0.50 in CH_2Cl_2).

2.5.3 ^{1}H NMR and ^{13}C NMR Spectra

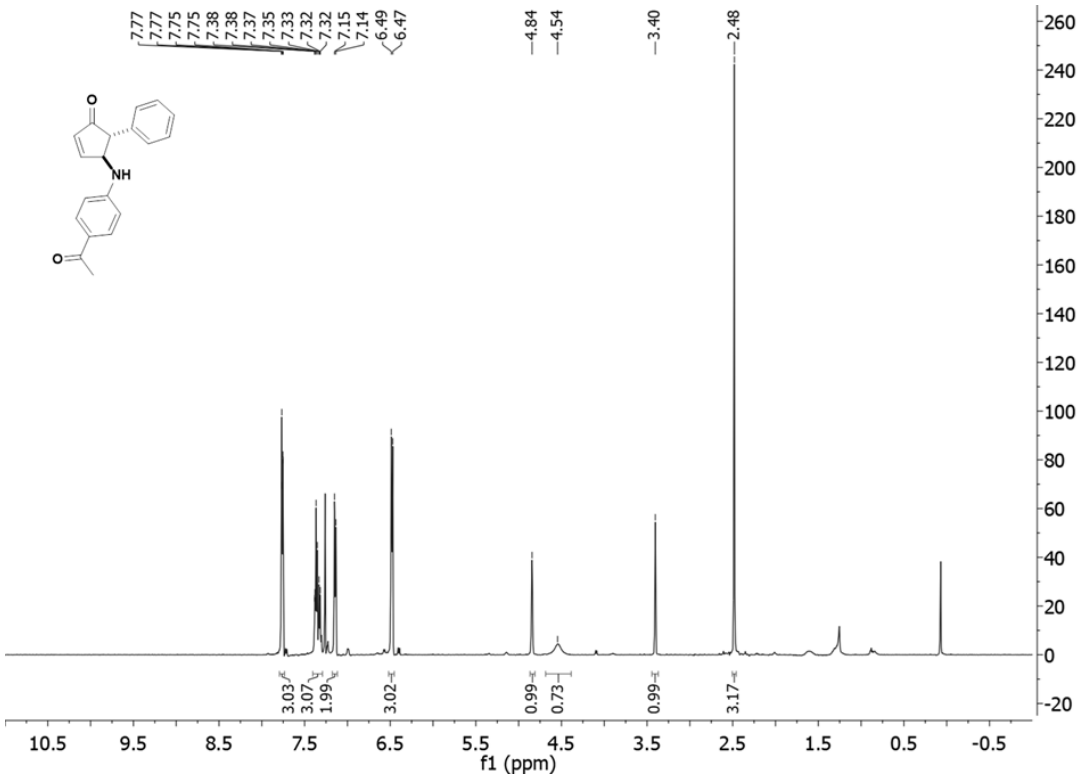

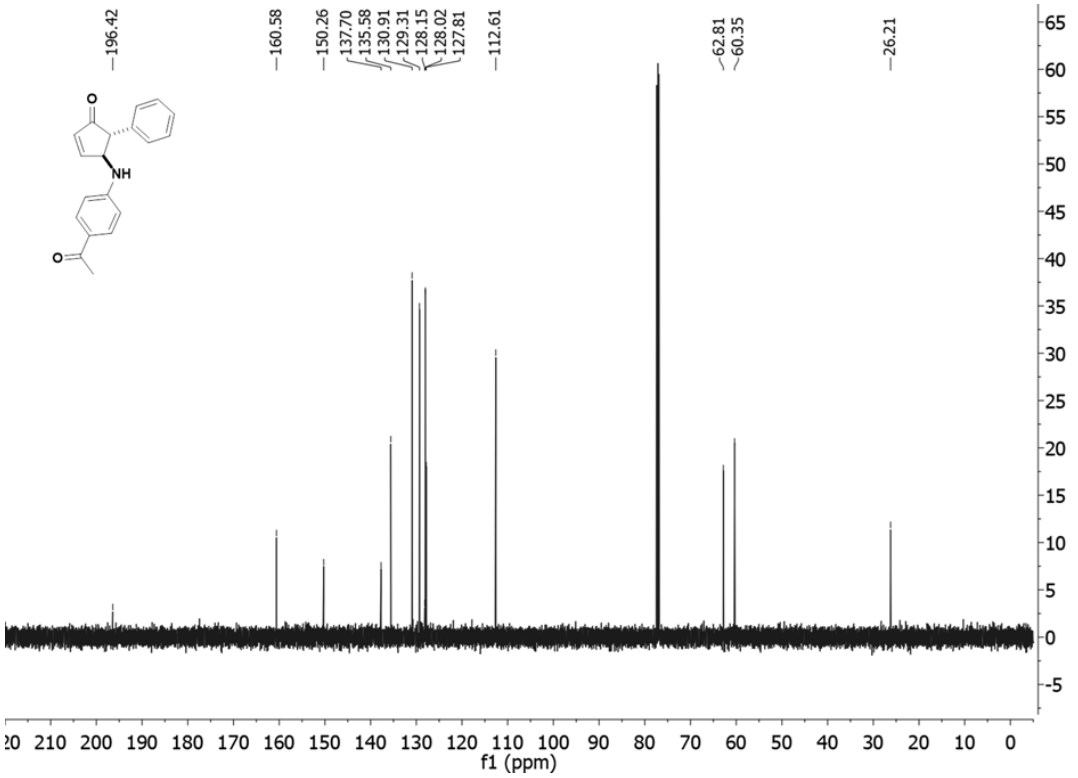
196.42
160.58
150.26
137.70
135.58
130.91
129.31
128.15
128.02
127.81
112.61
62.81
60.35
26.21
O
NH
O
f1 (ppm)

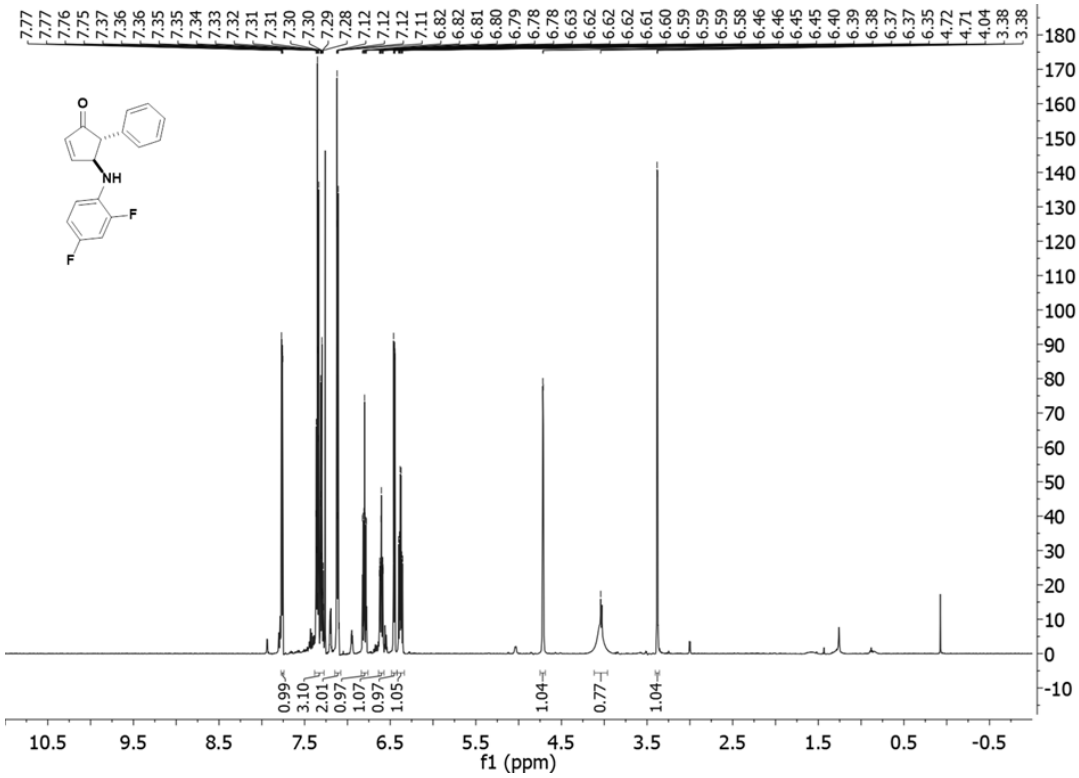
O
NH
F
F
0.99
3.10
2.01
0.97
1.07
0.97
1.05
1.04
0.77
1.04
f1 (ppm)

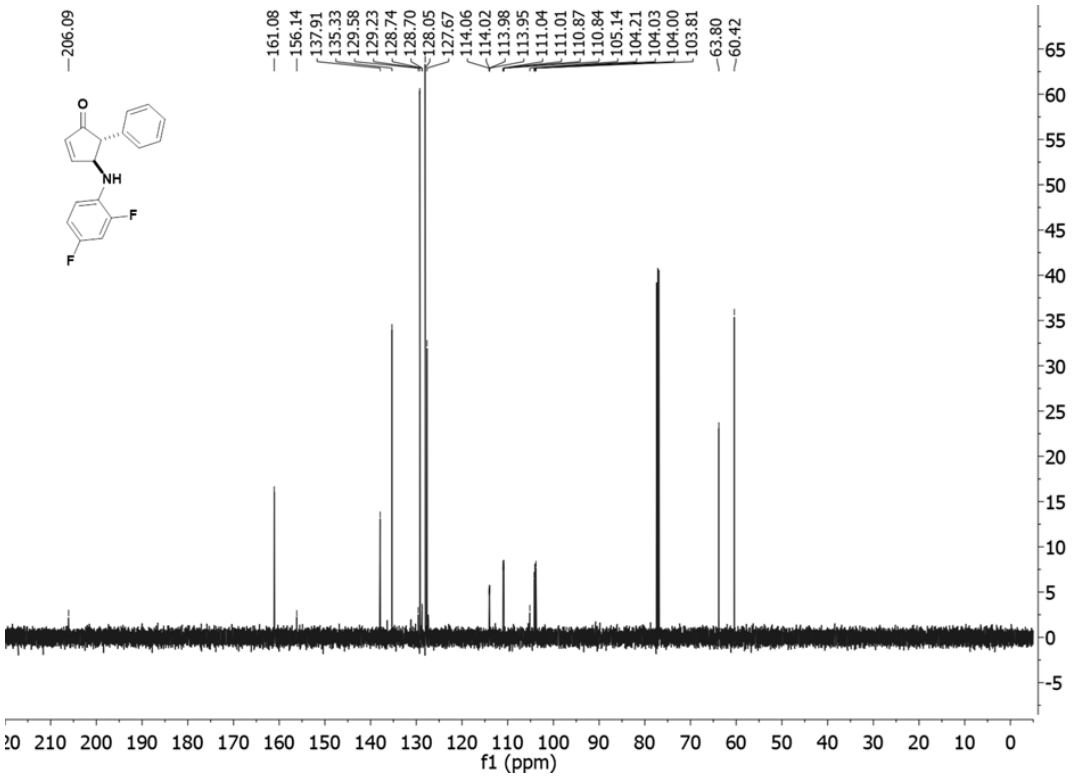
206.09
161.08
156.14
137.91
135.33
129.58
129.23
128.74
128.70
128.05
127.67
114.06
114.02
113.98
113.95
111.04
111.01
110.87
110.84
105.14
104.21
104.03
104.00
103.81
63.80
60.42
O
NH
F
F
f1 (ppm)

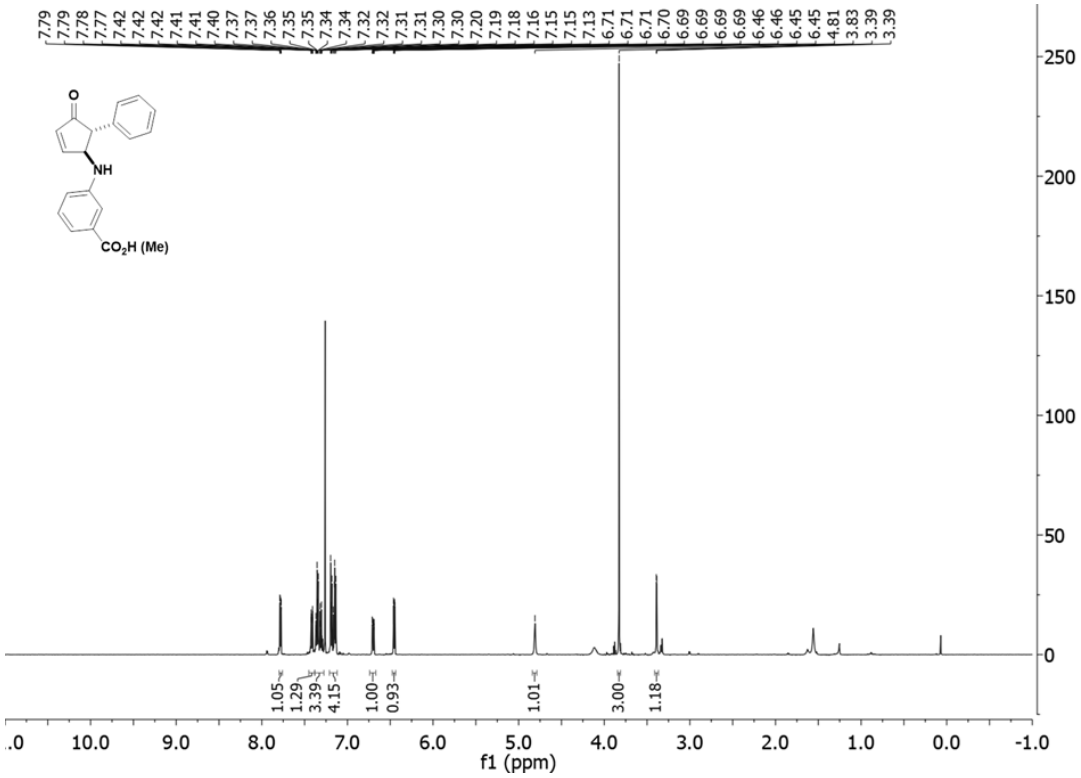
7.79
7.79
7.78
7.77
7.42
7.42
7.42
7.41
7.41
7.40
7.37
7.37
7.36
7.35
7.35
7.34
7.34
7.32
7.31
7.31
7.30
7.30
7.20
7.19
7.18
7.16
7.15
7.15
7.13
6.71
6.71
6.70
6.69
6.69
6.69
6.69
6.46
6.46
6.45
6.45
4.81
3.83
3.39
3.39
O
NH
CO2H (Me)
1.05
1.29
3.39
4.15
1.00
0.93
1.01
3.00
1.18
f1 (ppm)

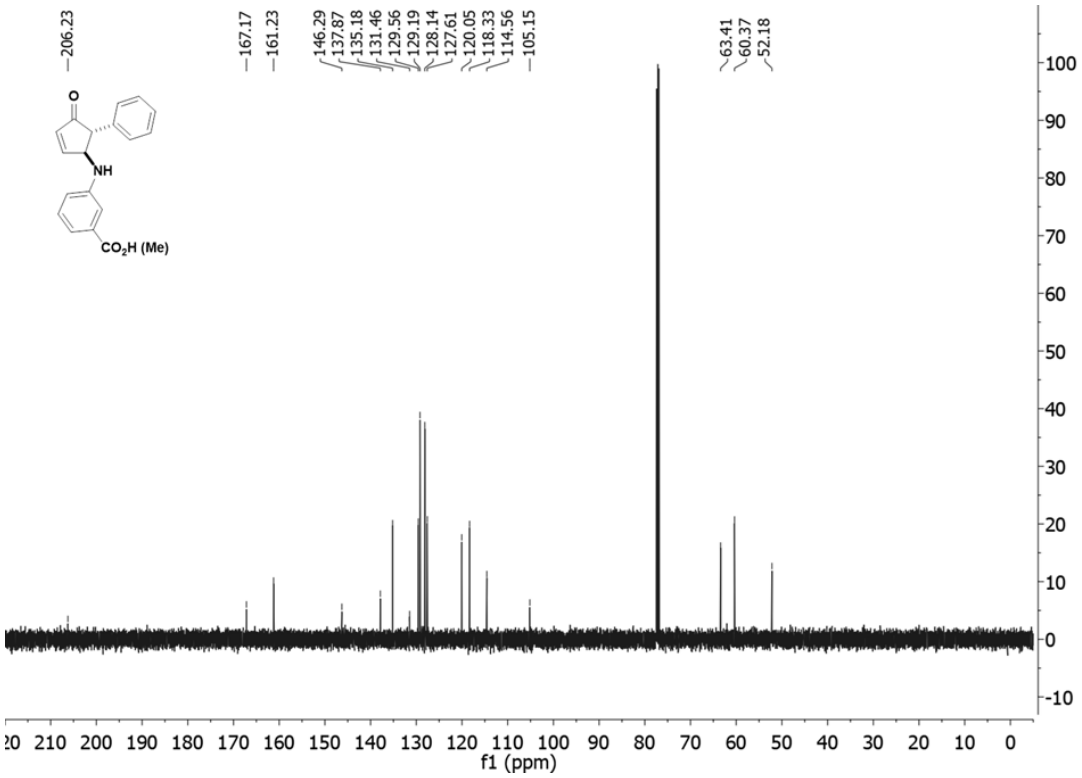
206.23
167.17
161.23
146.29
137.87
135.18
131.46
129.56
129.19
128.14
127.61
120.05
118.33
114.56
105.15
63.41
60.37
52.18
O
NH
CO2H (Me)
f1 (ppm)

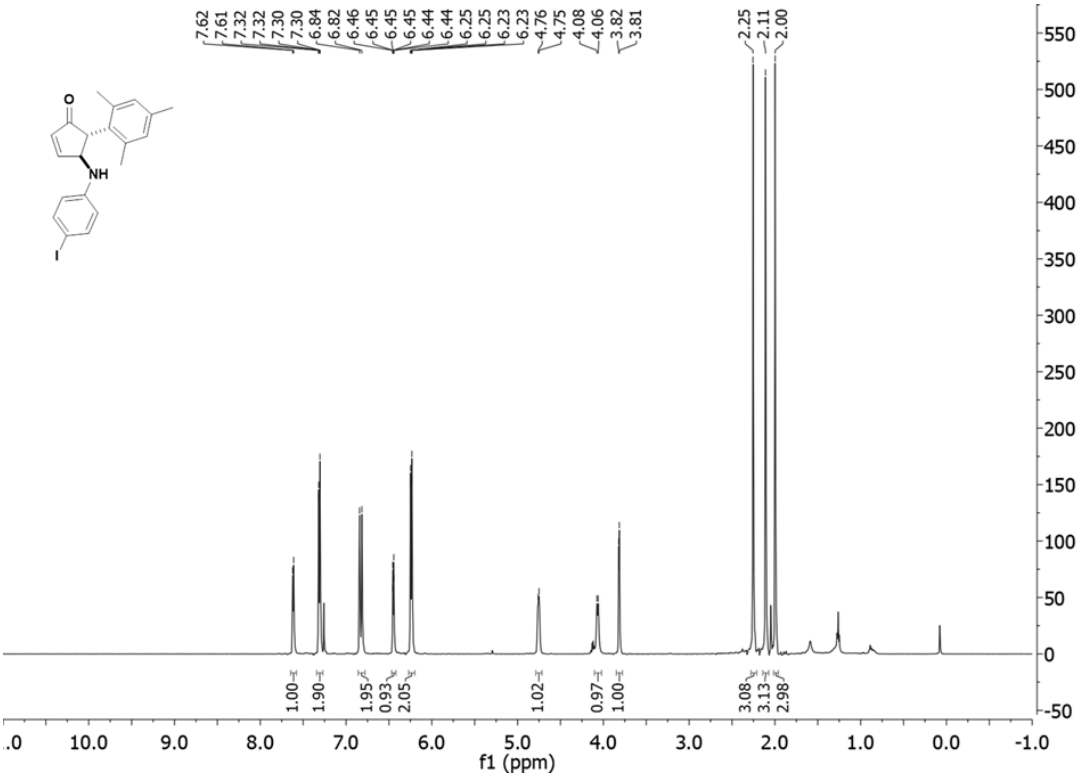
7.62
7.61
7.32
7.32
7.30
7.30
6.84
6.82
6.46
6.45
6.45
6.45
6.44
6.44
6.25
6.25
6.23
4.76
4.75
4.08
4.06
3.82
3.81
2.25
2.11
2.00
1.00
1.90
1.95
0.93
2.05
1.02
0.97
1.00
3.08
3.13
2.98
O
NH
I
f1 (ppm)

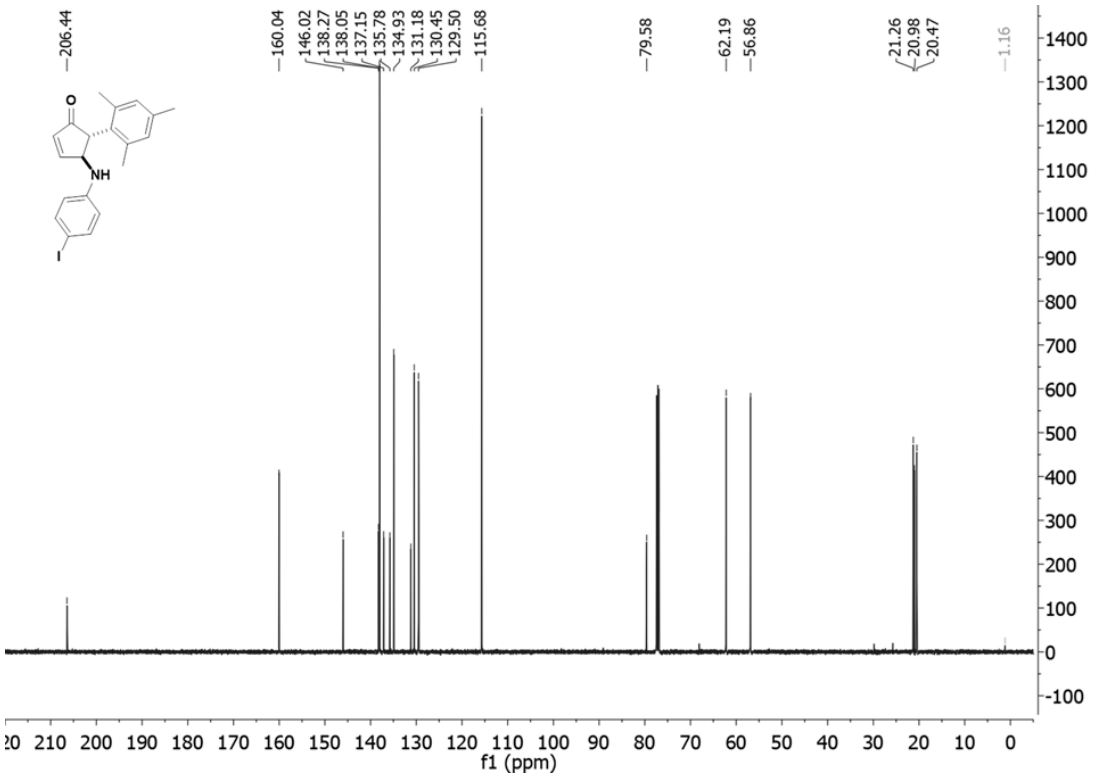
206.44
160.04
146.02
138.27
138.05
137.15
135.78
134.93
131.18
130.45
129.50
115.68
79.58
62.19
56.86
21.26
20.98
20.47
1.16
O
NH
I
f1 (ppm)

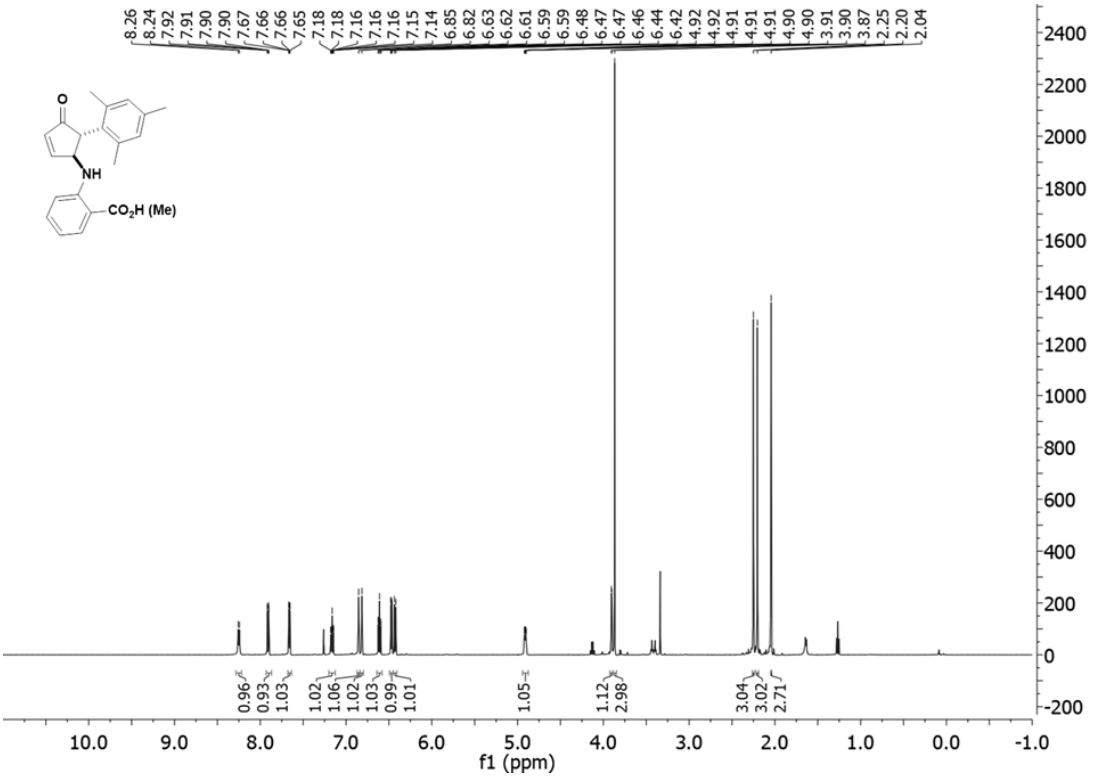
8.26
8.24
7.92
7.91
7.90
7.90
7.67
7.66
7.66
7.65
7.18
7.18
7.16
7.16
7.16
7.15
7.14
6.85
6.82
6.63
6.62
6.61
6.59
6.59
6.48
6.47
6.47
6.46
6.44
6.42
4.92
4.92
4.91
4.91
4.91
4.90
4.90
3.91
3.90
3.87
2.25
2.20
2.04
O
NH
CO2H (Me)
0.96
0.93
1.03
1.02
1.06
1.02
1.03
0.99
1.01
1.05
1.12
2.98
3.04
3.02
2.71
f1 (ppm)

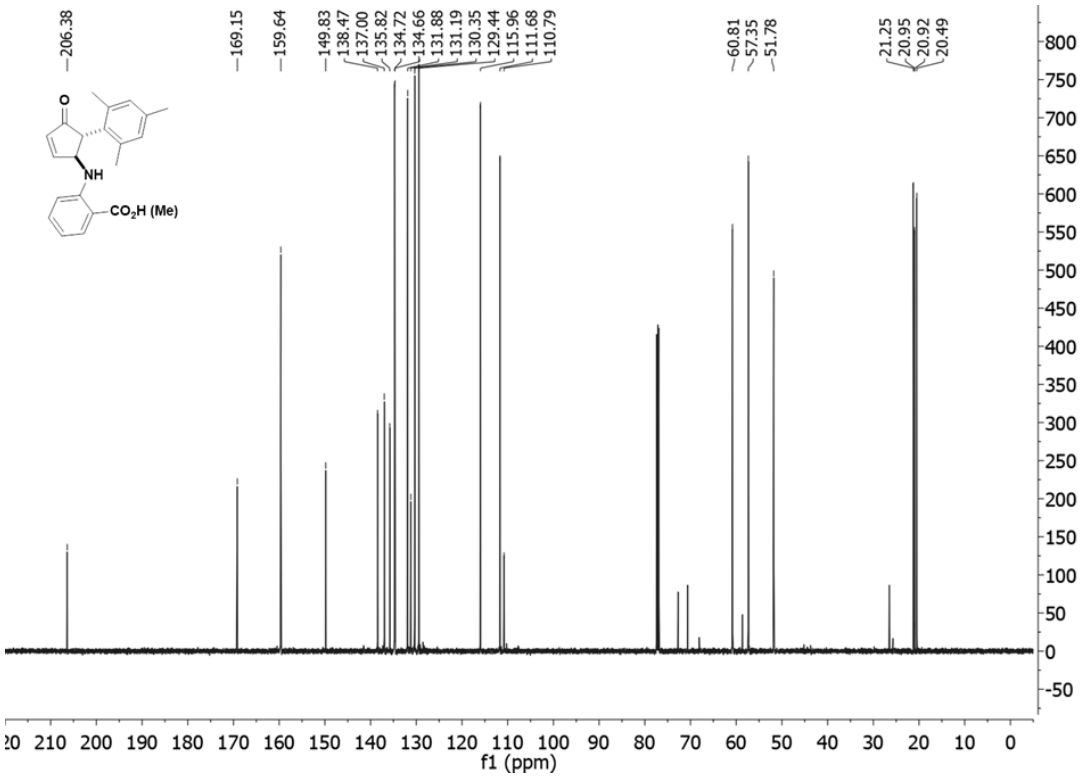
206.38
169.15
159.64
149.83
138.47
137.00
135.82
134.72
134.66
131.88
131.19
130.35
129.44
115.96
111.68
110.79
60.81
57.35
51.78
21.25
20.95
20.92
20.49
O
NH
CO2H (Me)
f1 (ppm)

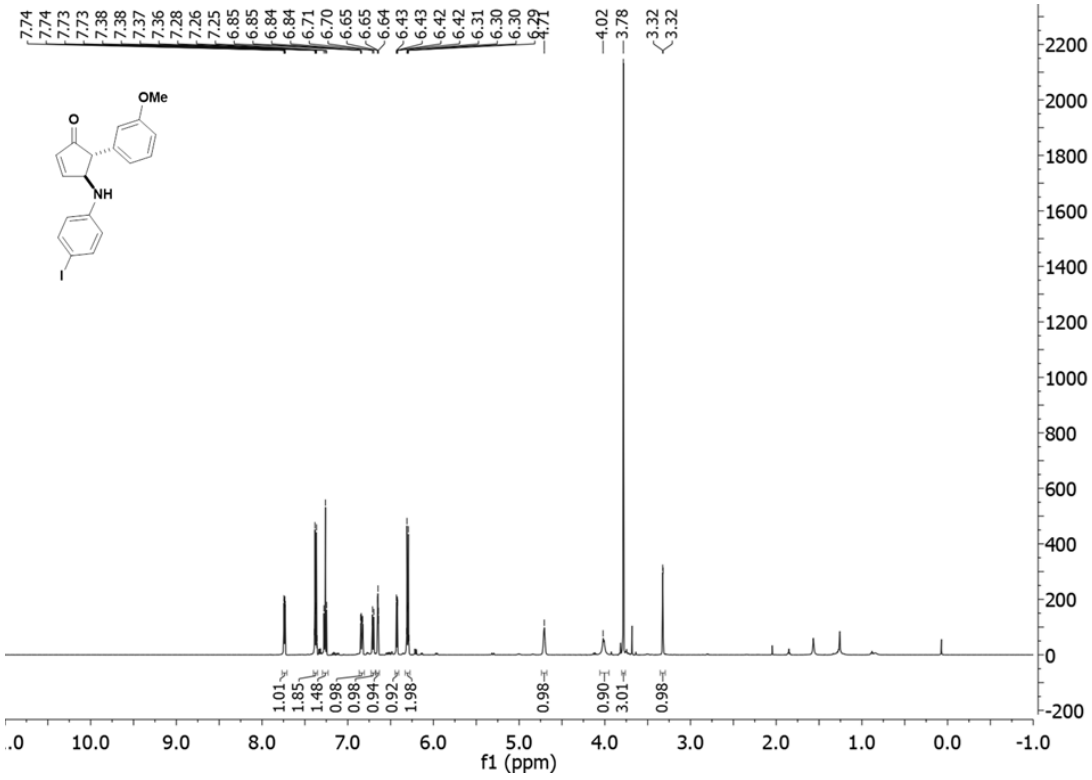
7.74
7.74
7.73
7.73
7.38
7.38
7.37
7.36
7.28
7.26
7.25
6.85
6.85
6.84
6.84
6.71
6.70
6.65
6.65
6.64
6.43
6.43
6.42
6.42
6.31
6.30
6.30
4.02
3.78
3.32
3.32
OMe
O
NH
I
1.01
1.85
1.48
0.98
0.98
0.94
0.92
1.98
0.98
0.90
3.01
0.98
f1 (ppm)

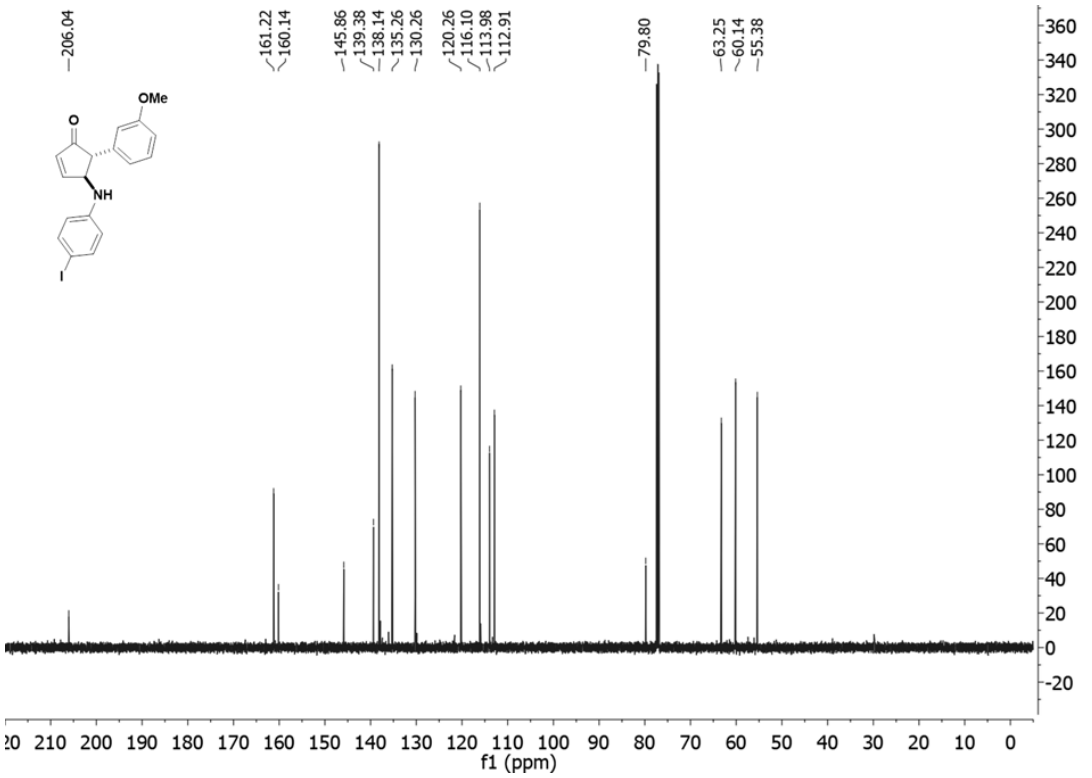
206.04
161.22
160.14
145.86
139.38
138.14
135.26
130.26
120.26
116.10
113.98
112.91
79.80
63.25
60.14
55.38
OMe
O
NH
I
f1 (ppm)

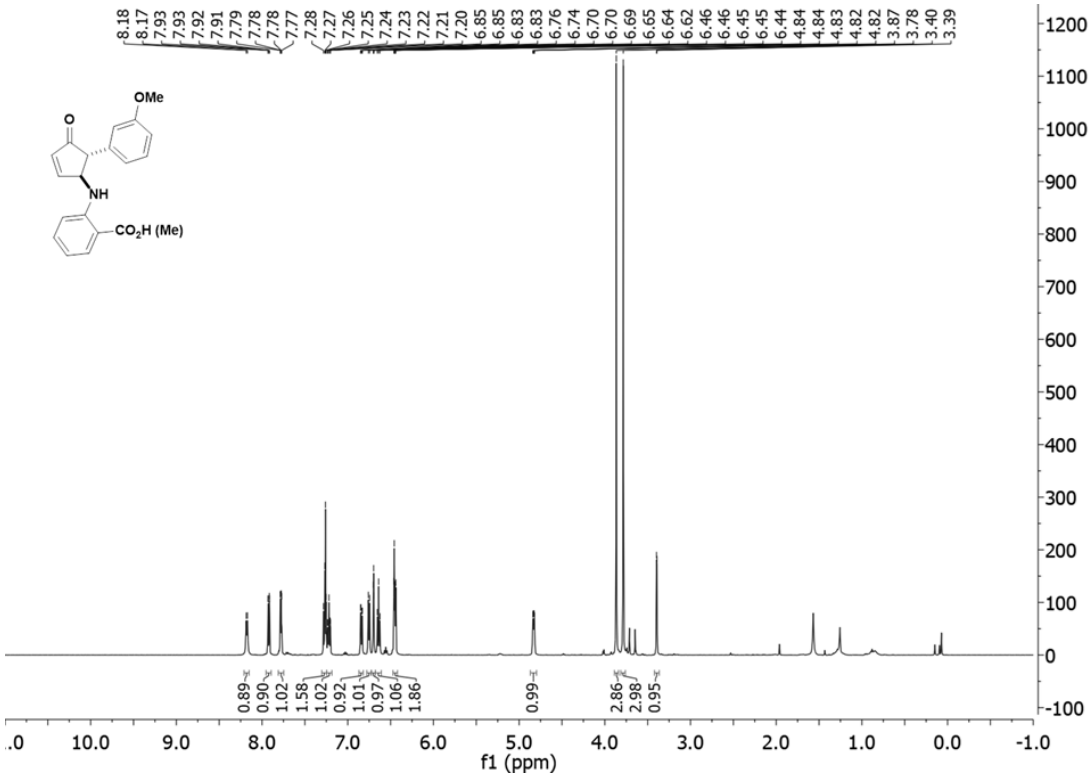
8.18
8.17
7.93
7.93
7.92
7.91
7.79
7.78
7.78
7.77
7.28
7.27
7.26
7.25
7.24
7.23
7.22
7.21
7.20
6.85
6.85
6.83
6.83
6.76
6.74
6.70
6.70
6.69
6.65
6.64
6.62
6.46
6.46
6.45
6.45
6.44
4.84
4.84
4.83
4.82
4.82
3.87
3.78
3.40
3.39
OMe
O
NH
CO2H (Me)
0.89
0.90
1.02
1.58
1.02
0.92
1.01
0.97
1.06
1.86
0.99
2.86
2.98
0.95
f1 (ppm)

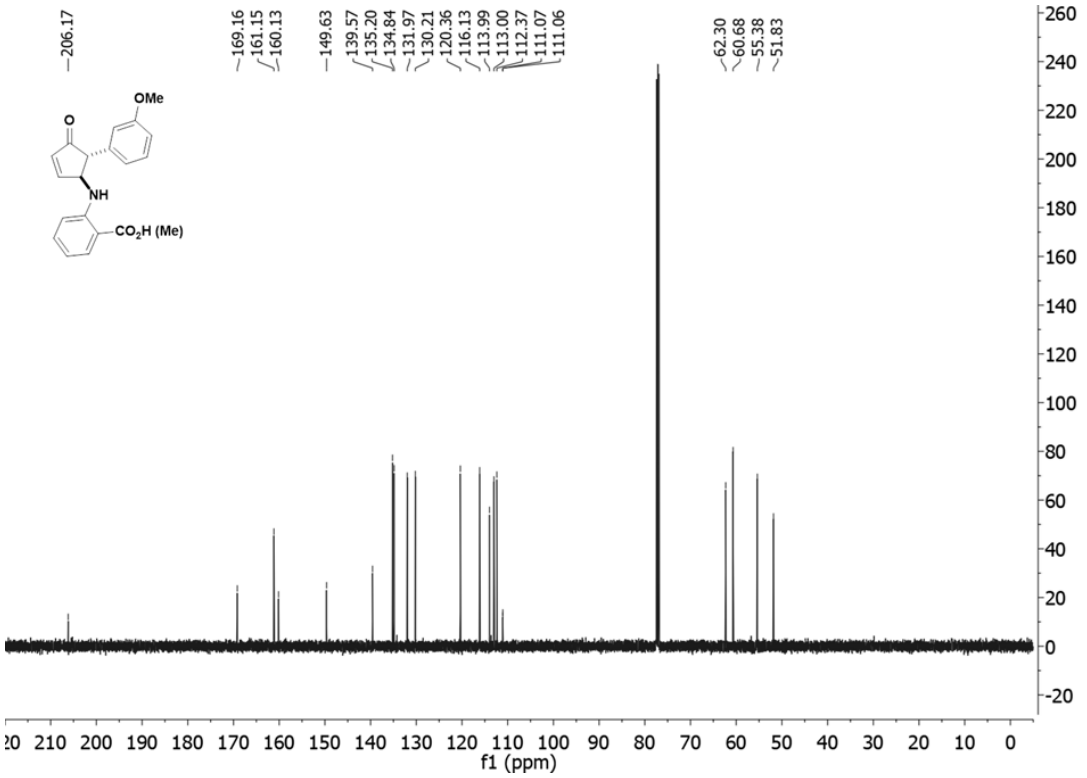
206.17
169.16
161.15
160.13
149.63
139.57
135.20
134.84
131.97
130.21
120.36
116.13
113.99
113.00
112.37
111.07
111.06
62.30
60.68
55.38
51.83
OMe
O
NH
CO2H (Me)
f1 (ppm)

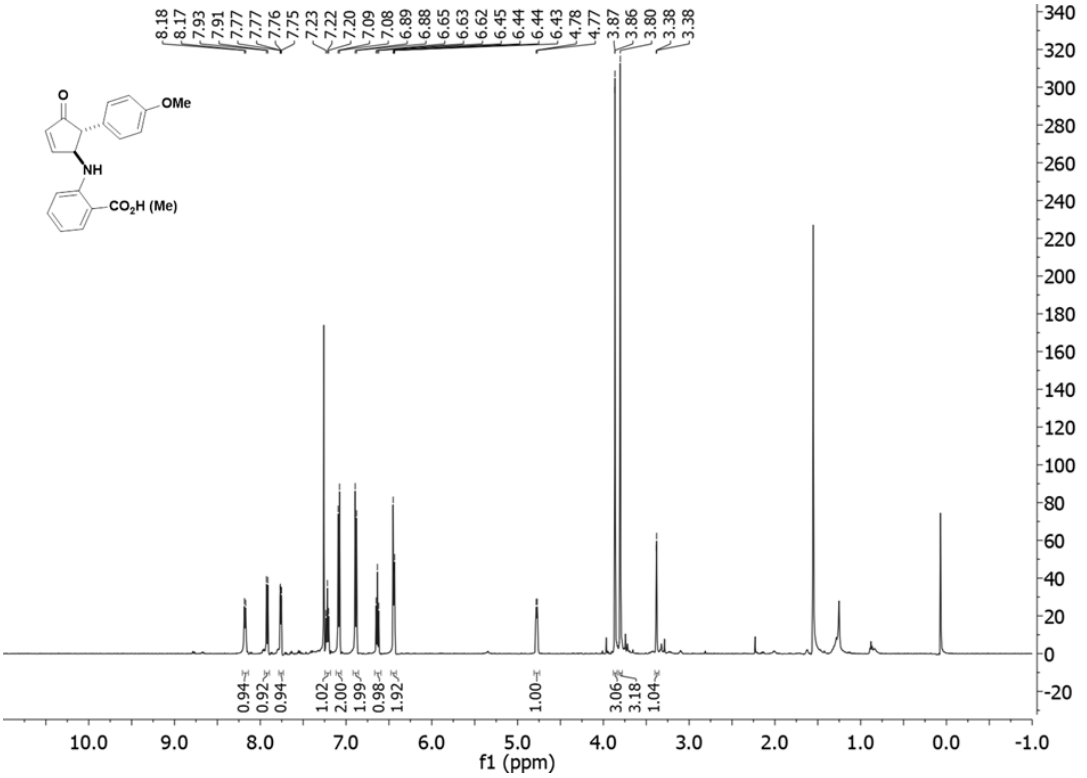
8.18
8.17
7.93
7.91
7.77
7.77
7.76
7.75
7.23
7.22
7.20
7.09
7.08
6.89
6.88
6.65
6.63
6.62
6.45
6.44
6.44
6.43
4.78
4.77
3.87
3.86
3.80
3.38
3.38
OMe
O
NH
CO2H (Me)
0.94
0.92
0.94
1.02
2.00
1.99
0.98
1.92
1.00
3.06
3.18
1.04
f1 (ppm)

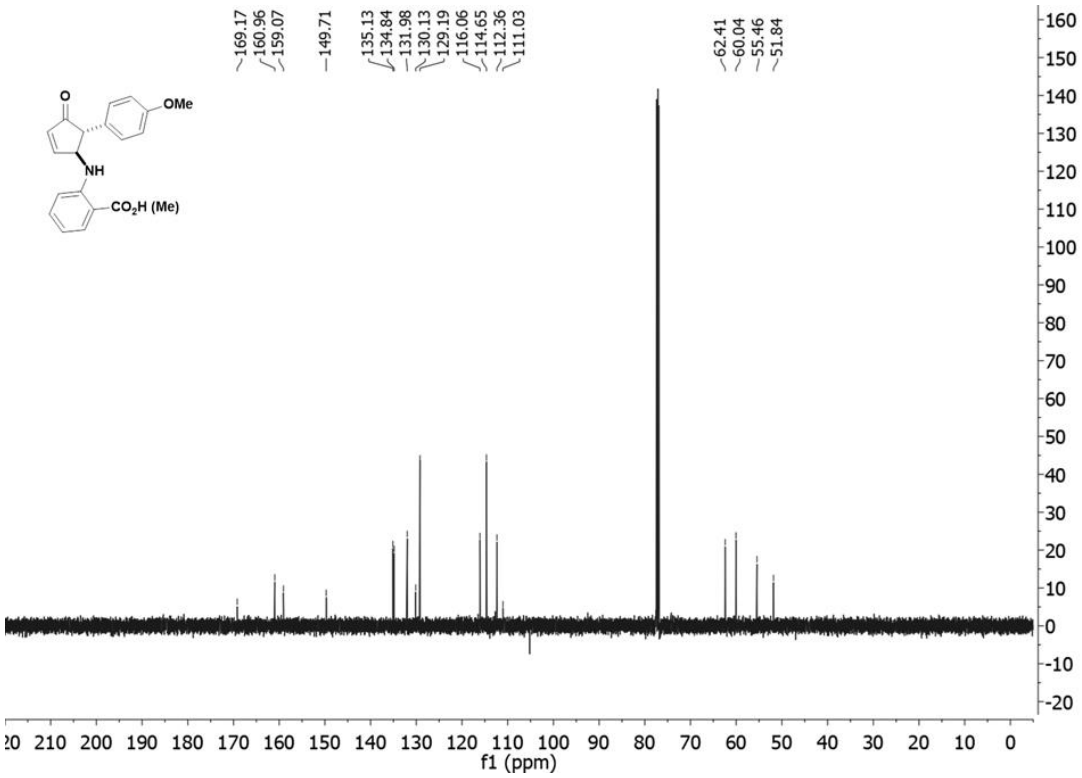
169.17
160.96
159.07
149.71
135.13
134.84
131.98
130.13
129.19
116.06
114.65
112.36
111.03
62.41
60.04
55.46
51.84
O
OMe
NH
CO2H (Me)
f1 (ppm)

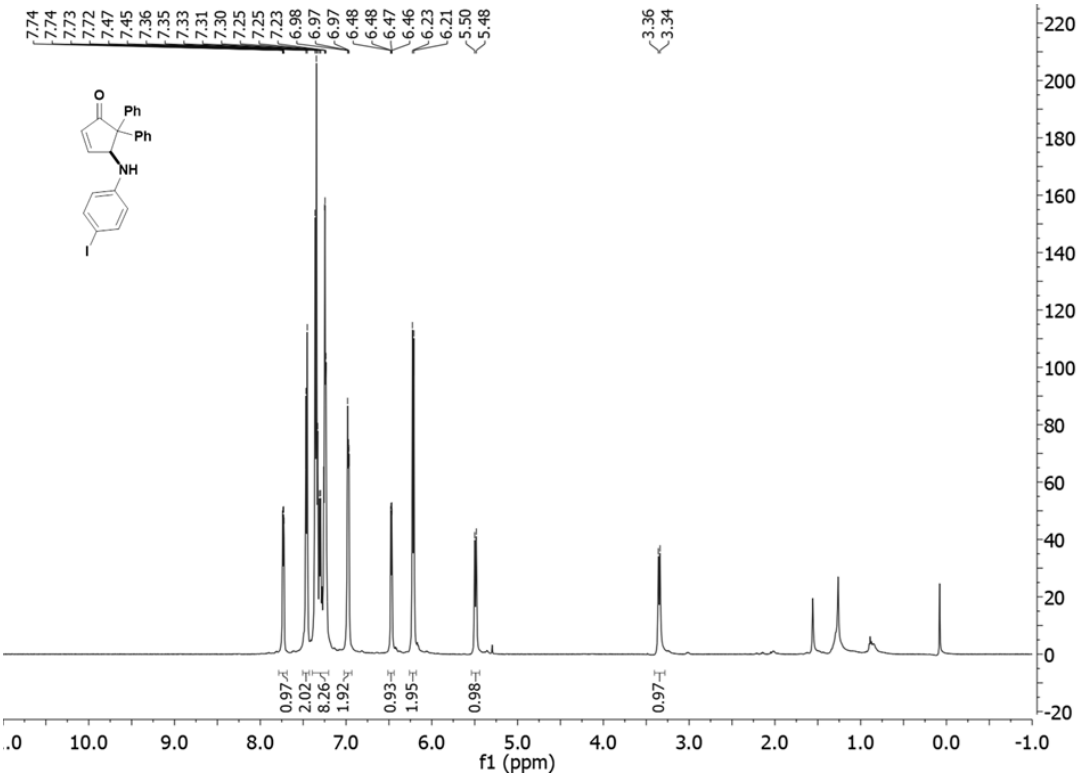
7.74
7.74
7.73
7.72
7.47
7.45
7.36
7.35
7.33
7.31
7.30
7.25
7.25
7.23
6.98
6.97
6.97
6.48
6.48
6.47
6.46
6.23
6.21
5.50
5.48
3.36
3.34
O
Ph
Ph
NH
I
0.97
2.02
8.26
1.92
0.93
1.95
0.98
0.97
f1 (ppm)

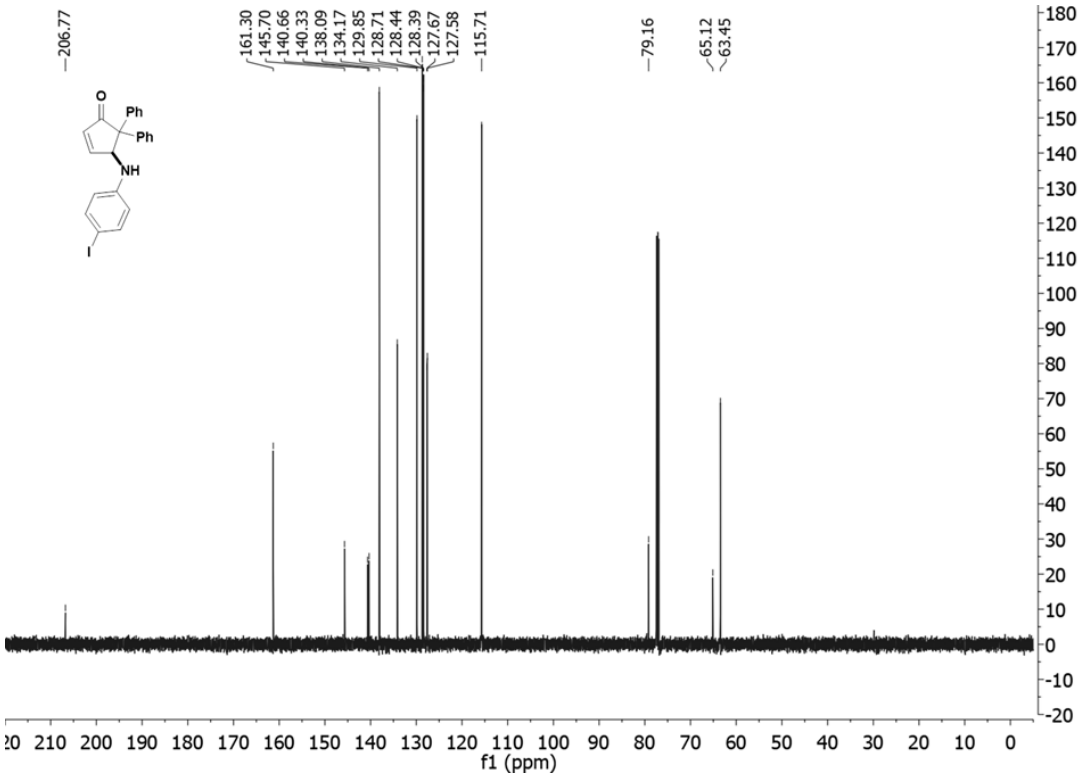
206.77
161.30
145.70
140.66
140.33
138.09
134.17
129.85
128.71
128.44
128.39
127.67
127.58
115.71
79.16
65.12
63.45
O
Ph
Ph
NH
I
f1 (ppm)

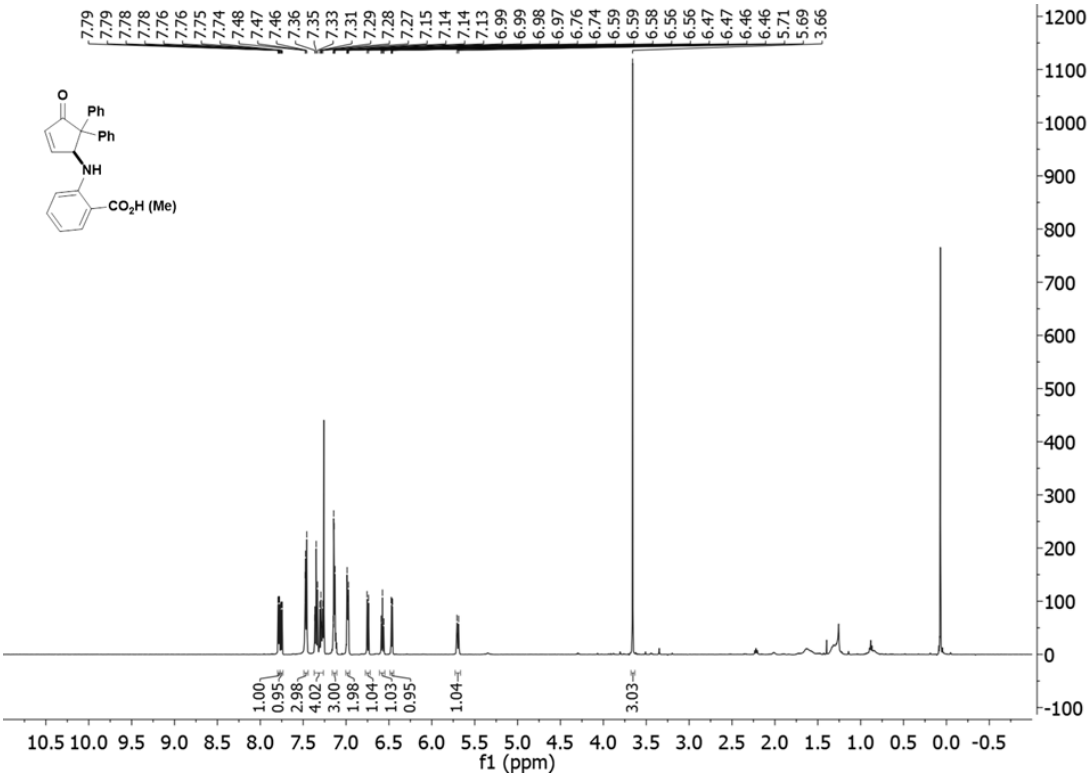
7.79
7.79
7.78
7.78
7.76
7.76
7.75
7.74
7.48
7.47
7.46
7.36
7.35
7.33
7.31
7.29
7.28
7.27
7.15
7.14
7.14
7.13
6.99
6.99
6.98
6.97
6.76
6.74
6.59
6.59
6.58
6.56
6.56
6.47
6.47
6.46
6.46
5.71
5.69
3.66
O
Ph
Ph
NH
CO2H (Me)
1.00
0.95
2.98
4.02
3.00
1.98
1.04
1.03
0.95
1.04
3.03
f1 (ppm)

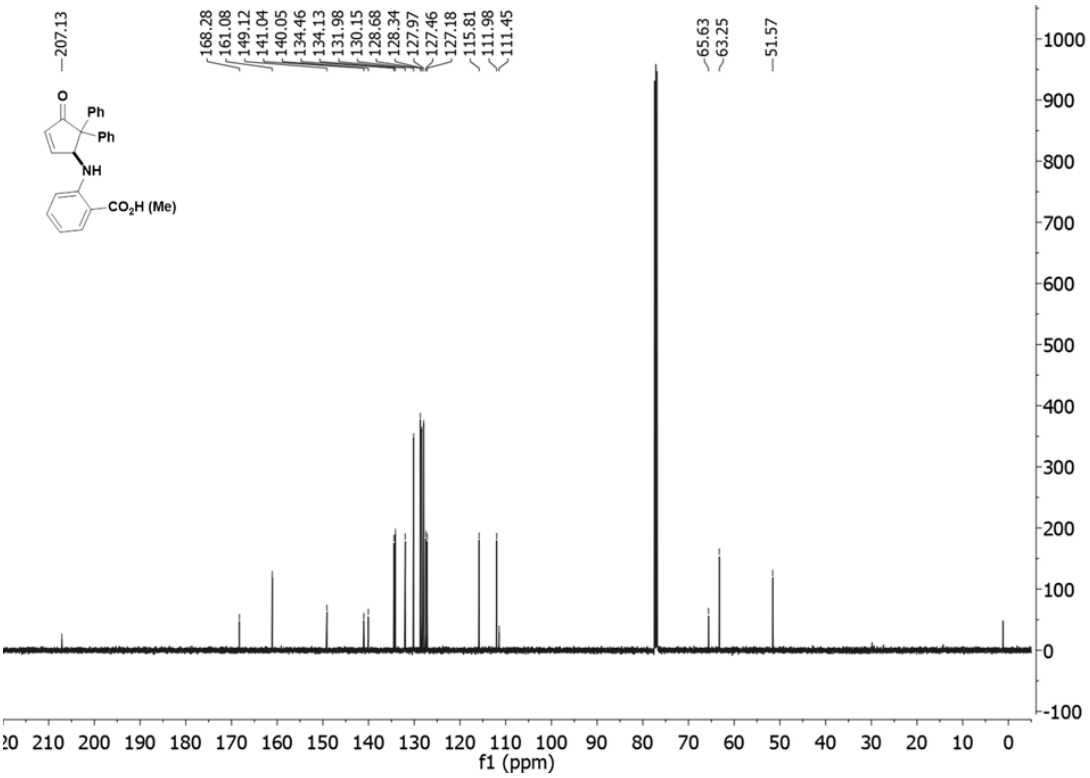

2.6 References

1 G. Liu, M. E. Shirley, K. N. Van, R. L. Mcfarlin and D. Romo, *Nat. Chem.*, 2013, **5**, 1049–1057.

2 B. Heasley, J. Wan, Y. Lin and Y. Liu, *Curr. Org. Chem.*, 2014, **18**, 641.

3 M. Köck, A. Grube, I. B. Seiple and P. S. Baran, *Angew. Chemie - Int. Ed.*, 2007, **46**, 6586–6594.

4 I. B. Seiple, S. Su, I. S. Young, C. A. Lewis, J. Yamaguchi and P. S. Baran, *Angew. Chemie - Int. Ed.*, 2010, **49**, 1095–1098.

5 B. M. Trost and G. Dong, *J. Am. Chem. Soc.*, 2006, **128**, 6054–6055.

6 T. Yoshimitsu, T. Ino and T. Tanaka, 2008, **10**, 5457–5460.

7 P. A. Duspara and R. A. Batey, *Angew. Chemie - Int. Ed.*, 2013, **52**, 10862–10866.

8 S. Hanessian, R. R. Vakiti, S. Dorich, S. Banerjee, F. Lecomte, J. R. DelValle, J. Zhang and B. Deschênes-Simard, *Angew. Chemie - Int. Ed.*, 2011, **50**, 3497–3500.

9 J. T. Malinowski, R. J. Sharpe and J. S. Johnson, *Science (80-.).*, 2013, **340**, 180–182.

10 R. J. Sharpe, J. T. Malinowski and J. S. Johnson, *J. Am. Chem. Soc.*, 2013, **135**, 17990–17998.

11 B. M. Trost, G. H. Kuo and T. Benneche, *J. Am. Chem. Soc.*, 1988, **110**, 621–622.

12 A. Mieczkowski, V. Roy and L. A. Agrofoglio, *Chem. Rev.*, 2010, **110**, 1828–1856.

13 C. Piutti and F. Quartieri, *Molecules*, 2013, **18**, 12290–12312.

14 D. R. Wenz and J. R. De Alaniz, *European J. Org. Chem.*, 2015, 23–37.

15 R. F. A. Gomes, J. A. S. Coelho and C. A. M. Afonso, *Chem. - A Eur. J.*, 2018, **24**, 9170–9186.

16 G. Piancatelli, A. Scettri and S. Barbadoro, *Tetrahedron Lett.*, 1976, **17**, 3555–3558.

17 G. K. Veits, D. R. Wenz and J. Read De Alaniz, *Angew. Chemie - Int. Ed.*, 2010, **49**, 9484–9487.

18 D. Iii, T. Catalyzed, L. I. Palmer and J. R. De Alaniz, *Angew. Chemie - Int. Ed.*, 2011, **50**, 7167–7170.

19 L. I. Palmer and J. R. De Alaniz, *Org. Lett.*, 2013, **15**, 476–479.

20 D. Yu, V. T. Thai, L. I. Palmer, G. K. Veits, J. E. Cook, J. R. De Alaniz and J. E. Hein, *J. Org. Chem.*, 2013, **78**, 12784–12789.

21 L. I. Palmer and J. R. De Alaniz, *SynLett*, 2014, **25**, 8–11.

22 D. Fisher, L. I. Palmer, J. E. Cook, J. E. Davis and J. R. De Alaniz, *Tetrahedron*, 2014, **70**, 4105–4110.

23 G. K. Veits, D. R. Wenz, L. I. Palmer, A. H. S. Amant, J. E. Hein and J. R. De Alaniz, *Org. Biomol. Chem.*, 2015, **13**, 8465–8469.

24 B. V. Subba Reddy, G. Narasimhulu, P. Subba Lakshumma, Y. Vikram Reddy and J. S. Yadav, *Tetrahedron Lett.*, 2012, **53**, 1776–1779.

25 D. Leboeuf, E. Schulz and V. Gandon, *Org. Lett.*, 2014, **16**, 6464–6467.

26 B. V. Subba Reddy, Y. Yikram Reddy, P. Subba Lakshumma, G. Narasimhulu, J. S. Yadav, B. Sridhar, P. Purushotham Reddy and A. C. Kunwar, *RSC Adv.*, 2012, **2**, 10661–10666.

27 J. Liu, Q. Shen, J. Yu, M. Zhu, J. Han and L. Wang, *European J. Org. Chem.*, 2012, **2012**, 6933–6939.

28 J. P. M. Nunes, C. A. M. Afonso and S. Caddick, *RSC Adv.*, 2013, **3**, 14975–14978.

29 B. Yin, L. Huang, X. Wang, J. Liu and H. Jiang, *Adv. Synth. Catal.*, 2013, **355**, 370–376.

30 C. Wang, C. Dong, L. Kong, Y. Li and Y. Li, *Chem. Commun.*, 2014, **50**, 2164–2166.

31 J. Xu, Y. Luo, H. Xu, Z. Chen, M. Miao and H. Ren, *J. Org. Chem.*, 2017, **82**, 3561–3570.

32 M. A. Tius, *European J. Org. Chem.*, 2005, **2005**, 2193–2206.

33 A. J. Frontier and C. Collison, *Tetrahedron*, 2005, **61**, 7577–7606.

34 N. Shimada, C. Stewart and M. A. Tius, *Tetrahedron*, 2011, **67**, 5851–5870.

35 Y. Cai, Y. Tang, I. Atodiresei and M. Rueping, *Angew. Chemie - Int. Ed.*, 2016, **55**, 14126–14130.

36 H. Li, R. Tong and J. Sun, *Angew. Chemie - Int. Ed.*, 2016, **55**, 15125–15128.

37 A. B. Gade and N. T. Patil, *Synlett*, , DOI:10.1055/s-0036-1558952.

38 G. K. Veits, University of California, Santa Barbara, 2014.

39 M. Rueping, W. Ieawsuwan, A. P. Antonchick and B. J. Nachtsheim, *Angew. Chemie - Int. Ed.*, 2007, **46**, 2097–2100.

40 C. D. Gheewala, B. E. Collins and T. H. Lambert, *Science (80-.).*, 2016, **351**, 961–966.

3 Multi-stimuli Responsive Trigger for Temporally Controlled Depolymerization of Self-immolative Polymers

3.1 Abstract

For many decades, stimuli responsive materials have been studied and utilized in various fields, ranging from chemical sensors to controlled drug release. Among those responsive materials are self-immolative polymers (SIP) that allow for end-to-end depolymerization and the ability to release a desired cargo on demand or amplify analyte detection. However, in typical SIP systems, the triggering event leads to a relatively uncontrolled degradation process. Herein we present a multi-stimuli trigger that utilizes the combination of heat and acid to impart control over the trigger event and thus the degradation process. By controlling this reaction, we achieve temporal control over the trigger cleavage and subsequent depolymerization and release of cargo from the SIP.

3.2 Introduction

Chemical strategies that rely on self-immolative polymers (SIPs) to enable the development of on-demand drug delivery systems,[1] degradable materials,[2] and analyte detection[3] have expanded significantly in the past decade. Within SIPs there are three major components establishing their anatomy: trigger, spacer, and output.[4,5] These variables can independently be tuned to influence the macroscopic behavior and application of the SIP. For example, trigger units are stimuli reactive endcaps that, when cleaved, allow for the end-to-end depolymerization of the SIP. The spacer units within the polymer dictate the chemical and physical properties of the polymer for desired structure and function. The last component to

SIPs, the output, can be tailored to maximize the impact of the desired application. Output units can range from photodynamic therapy moieties to fluorescence signaling compounds and antibodies.[4,5] The combination of these features and flexibility to modify each component have made SIPs an attractive and versatile platform for stimuli responsive materials.

One distinguishing feature of SIPs compared to other stimuli-responsive materials is the end-to-end depolymerization facilitated by cleavage of the trigger unit. The design of these triggers can be traced back to protecting group strategies in small molecule synthesis where "deprotection" of the trigger occurs upon treatment with the appropriate stimuli. The main classes of stimuli include nucleophilic,[6-8] redox,[9-11] enzymatic,[12,13] acid/base,[14] light,[15,16] and heat.[17-19] Upon subjection to one of these given stimuli, "deprotection" of the trigger reveals an electron-rich functional group at the polymer terminus that initiates an end-to-end-depolymerization. In many cases, the structure of the polymer backbone and chemical environment can be used to alter the rate of degradation of the polymer. For example, trigger deprotection from polycarbamate derived SIPs reveal a carbamate functional group that can subsequently undergo a decarboxylation reaction to release CO_2 and the corresponding amine. Once the amine group is revealed, there are three commonly used cascade reactions leading to depolymerization: 1,4-elimination; 1,6-elimination; and cyclization-elimination.[4,5] Due to the basicity of the amine group and nature of the elimination process, pH, solvent, and composition of the polymer (e.g., length and architecture) can each be used to alter the rate of degradation of the polymer backbone.[20] However, these approaches do not readily enable the degradation rate to be controlled once the trigger is removed.

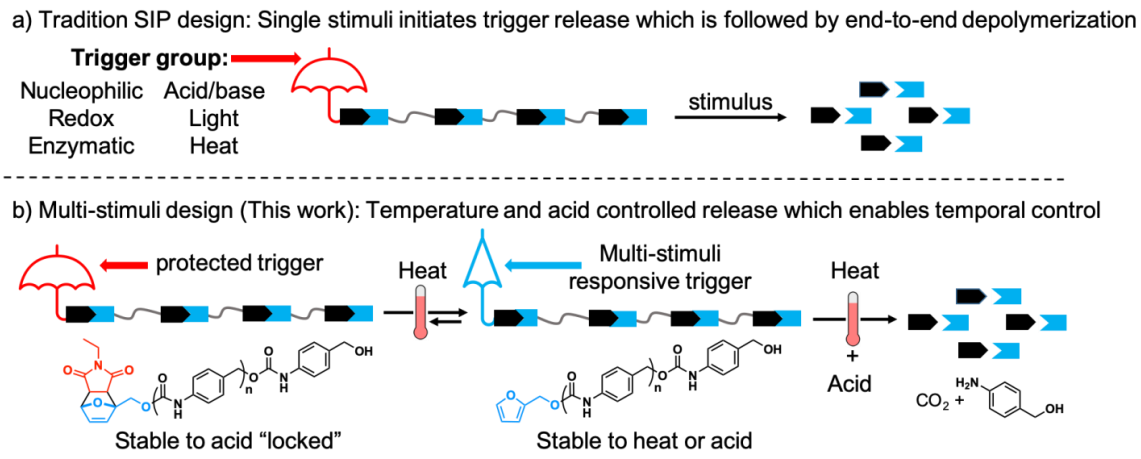

Figure 3. 1

a) Traditional SIP approaches often rely on a single stimulus trigger that when removed causes the SIP to undergo complete depolymerization. b) In the work shown here, we have a logic-controlled approach that enables temporal control of the trigger release and subsequent depolymerization of the SIP. For this multi-stimuli approach the chemistry utilizes heat and acid as the orthogonal stimuli, where neither stimulus facilitates a response alone. Reproduced from Polym. Chem. 2019, 10 with permission from the Royal Society of Chemistry.

The use of a multi-stimuli trigger unit has emerged as the attractive solution to impart temporal control to the depolymerization of SIPs and to enrich the molecular toolbox which one can use to affect the physical properties of SIPs. In an early example, Phillips and co-workers demonstrated that pre-patterned 3D objects could be selectively depolymerized by varying the nature of the applied stimuli.[7,8] More recently, Gillies and co-workers introduced a multi-stimuli approach using thermos-responsive polymers that undergo a change in their physical properties when exposed to changes in temperature.[19] In this case, slower depolymerization occurred when the material was above the lower critical solution temperature (LCST). Despite these advances, the development of systems that regulate depolymerization of SIPs using multiple external stimuli remains largely unexplored. The use of a "logic-controlled" SIP, where depolymerization only begins in response to two simultaneous external

stimuli, neither of which would provoke a response alone, would represent an attractive approach to imbue SIPs with temporal control.

Herein we report our design of a multi-stimuli trigger that utilizes the combination of heat and acid to control trigger release and subsequent depolymerization of a SIP. When one of the stimuli is not applied the depolymerization can be "paused", thus enabling temporal control. Inspired by our extensive studies of the Piancatelli[21,22] and aza-Piancatelli rearrangement,[23-25] we envisioned that 2-furylcarbinols could serve as a multi-stimuli trigger for SIPs (Figure 3.1). In the presence of an acidic environment (often elevated temperatures, typically above 80 °C are also used) the furylcarbinol forms a highly reactive oxocarbenium ion upon the loss of water;[26,27] we identified this first step in the Piancatelli cascade reaction mechanism as a potentially tunable Brønsted or Lewis acid sensitive trigger. The net transformation may be viewed as an acid catalyzed elimination of the hydroxyl functional group. Based on these observations, we postulated that attachment of a polymeric system in place of the alcohol would result in a versatile multi-stimulus trigger for self-immolative polymers. Furthermore, to "lock" the trigger we envisioned using the well-known Diels–Alder (DA) cyclization of furans and maleimides.[28] Upon exposure to heat, a retro-Diels– Alder (rDA) reaction would reveal the acid sensitive furylcarbinol trigger. We envisioned that the Diels–Alder adduct could impart long term stability for potential applications where depolymerization in acidic environment is not desired. In addition, the heat used to promote the Diels–Alder cycloreversion could also be used as one of the stimuli to promote the release of the furylcarbinol trigger.

Thus far only Gillies[18] and Trant[29] have explored the use of a furylcarbinol based trigger for SIPs. Using a carbonate ester to link the furylcarbinol to the polymer, the furylcarbinol was

protected as the DA adduct using maleimide. For this system, a single stimuli, heat, is used to initiate the retro-Diels–Alder reaction to generate an unstable furfuryl carbonate that spontaneously undergoes an elimination reaction releasing an uncapped poly(ethyl glyoxylate) PEtG SIP; as these polymers degrade rapidly at elevated temperatures the rate limiting step is trigger removal.[30] Although this work elegantly demonstrates that furylcarbinols and their corresponding DA adduct can act as a new trigger system for SIPs, the exploration of a multi-stimuli approach based on furylcarbinol triggers was not investigated.

3.3 Results and Discussion

3.3.1 Orthogonal Chemistry Testing with Small Molecules

Our initial approach focused on the use of orthogonal physical-chemical chemistry, specifically heat and acid. Thayumanavan and co-workers recently reviewed the use of orthogonal chemistry in multi-stimuli systems and categorized them into three classes: physical (heat and light), chemical (pH and redox), and biological.[31] We chose to utilize the furan-maleimide adduct because the temperature of the retro-Diels–Alder reaction can be tuned by using either the *endo* or *exo* furan-maleimide adduct[32] or by altering the substituent on the furan or maleimide moiety.[29] To connect the furylcarbinol to the terminal end of the polymer we used a urethane linkage (Scheme 3.1). Utilizing the urethane polymer backbone, we created a SIP-like model system that undergoes a 1,6-elimination pathway during its degradation, with 4-methylaniline serving as the output.

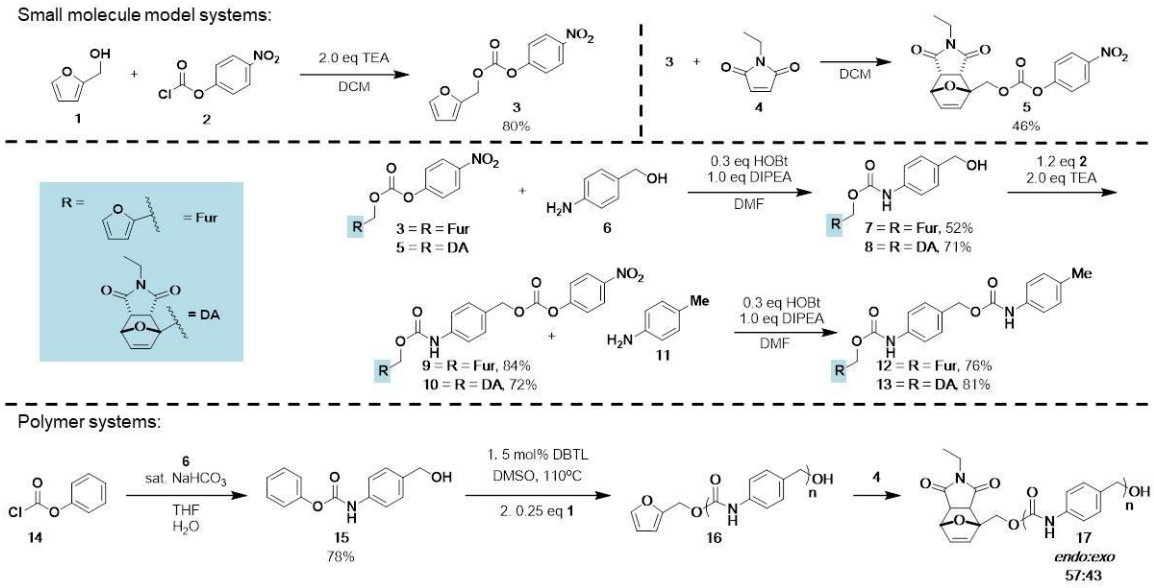

Scheme 3. 1

Overall synthesis of the small molecule models to test the use of the multi-stimuli trigger unit as well as the synthesis and polymerization of the SIP used to demonstrate the temporal control given by the multi-stimuli trigger. Reproduced from Polym. Chem. 2019, 10 with permission from the Royal Society of Chemistry.

To validate our approach using the furylcarbinol tethered to a urethane linkage, we began our studies by testing the thermal stability using a small molecule model system (**12**). Compound **12** in acetonitrile-d_3 was heated at 80 °C for 6 h. No change was observed via ^{1}H NMR spectroscopy of the material over a 6 h period (Figure 3.2a). This result supports that furylcarbinol **12** bearing a urethane linkage is thermally stable up to 80 °C. Next, we tested the efficiency of the rDA (Figure 3.2b) at this same temperature. Quantitative rDA was determined via ^{1}H NMR spectroscopy of **13** in acetonitrile-d_3 when heated at 80 °C for 6 h. It should be noted that at higher temperatures some decomposition of the trigger was observed and when tested below 80 °C the rDA rate was notably diminished. As such, 80 °C was selected as the temperature for the rDA reaction because it was efficient yet did not afford undesired side reactions.

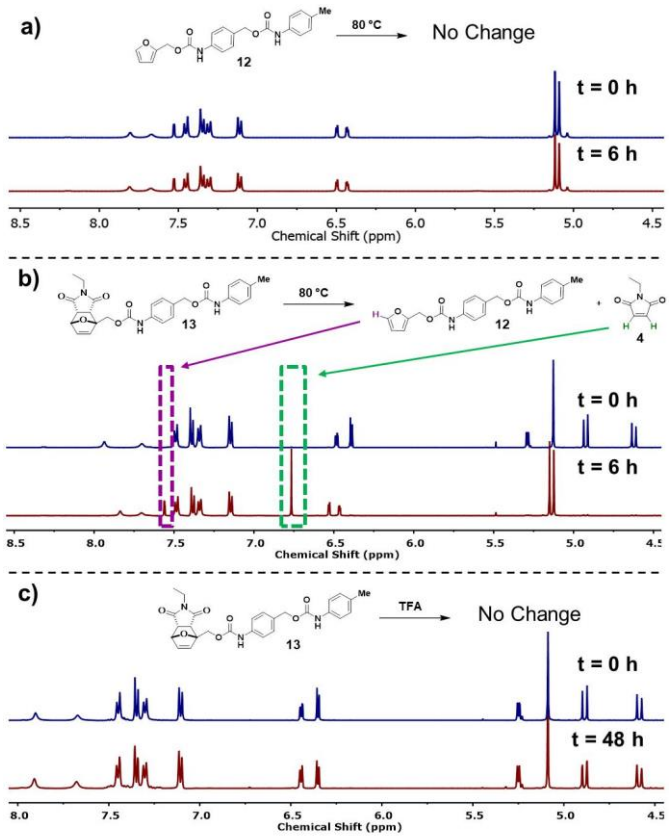

Figure 3. 2

a) Thermal stability of 12 is shown via ^{1}H NMR spectroscopy before heating and after 6 h of heating at 80 °C. b) ^{1}H NMR spectroscopy demonstrating the quantitative rDA of 13 to afford 12 after subjection to 80 °C for a 6 h period. c) No degradation of 13 is observed by ^{1}H NMR spectroscopy after treating with excess TFA at room temperature for 48 h. Reproduced from Polym. Chem. 2019, 10 with permission from the Royal Society of Chemistry.

Given the thermal stability of the furan moiety at the selected rDA temperature of 80 °C, we next studied the Lewis and Brønsted acid stability of the furan-maleimide DA adduct to ensure no premature depolymerization would occur. Treatment of **13** in acetonitrile-d_3 with 10 mol% $Sc(OTf)_3$ (a common Lewis acid used for the aza-Piancatelli reaction)[26,27] showed no change in the ^{1}H NMR spectrum over 48 h indicating that the DA adduct prevents the acid catalyzed Piancatelli reaction that mediates the trigger release (Figure S3.3). In addition to Lewis acids, **13** was also stable to acidic conditions using a Brønsted acid, trifluoroacetic acid

(TFA). Furan-maleimide DA adduct **13** was treated with 7:1 DMSO-d_6:TFA-*d* solution and monitored via ^{1}H NMR spectroscopy. Analogous to the Lewis acid studies, the use of TFA showed no change over 48 h (Figure 3.2c). These results demonstrate the ability of the Diels–Alder adduct to prevent premature depolymerization when exposed to an acidic environment. With quantitative rDA and stability of the trigger moieties established, we next sought to study the kinetics of the elimination process using the model system. By monitoring the cleavage of **5** at various temperatures an activation energy (E_a) of 112 ± 3 kJ/mol was determined (Figure S3.7), which is consistent with kinetic work previously done by Boydston on a related thermal DA trigger system.[17]

3.3.2 Trigger Studies in Polymer Systems

Following our small molecule studies, we evaluated the self-immolative polymer system (**16** and **17**). Initially the degradation of the SIP polymer **16** bearing the furylcarbinol based trigger was determined by monitoring the decrease in the degree of polymerization (DP) by ^{1}H NMR spectroscopy. Complete depolymerization was achieved after 10 days upon treatment of **16** with a solution of 7:1 DMSO-d_6:TFA-*d* at 50 °C (Figure S3.17). Boydston observed similar rates of depolymerization using a thermally responsive 1,2-oxazine based trigger.[17]

To validate the temporal control on the SIP system, ON/OFF studies were conducted independently on polymer **16** and **17**. However, **17** was chosen for initial studies due to the known stability of the DA adduct to acidic conditions. The DA capped polymer, **17**, was subjected to an acidic 7:1 DMSO-d_6:TFA-*d* solution at ambient temperatures. The sample was then heated to 80 °C for 1 h to mediate the rDA reaction and reveal the stimuli responsive furylcarbinol trigger. In the presence of both heat and acid, the furylcarbinol forms a highly

reactive oxocarbenium ion and initiates depolymerization. To "pause" the depolymerization, the reaction flask containing the polymer sample was then placed in an ice-bath for 1 min to rapidly cool the reaction mixture, upon which it was held at 25 °C for 1 h. At this temperature, the DA endcap is stable to the acidic conditions and "locked". This process was repeated with successive periods of heating and cooling for a total of 6 cycles over a 12 h period. Using ^{1}H NMR spectroscopy, excellent ON/OFF control was observed (Figure 3.3a), where depolymerization only occurred in the presence of both stimuli and when heat is removed depolymerization was not observed. Next, the furylcarbinol end-capped polymer **16** was subjected to the same acidic conditions and a similar heat cycling sequence as **17**. To our surprise, as shown in Figure 3.3b, the ability to "pause" the trigger cleavage and depolymerization was still observed without the DA lock present. In fact, the rates of depolymerization of **16** and **17** are nearly identical when subjected to acidic condition at 50 °C and 80 °C (Figure S3.15). This implies that the rate limiting step is end-cap removal and not the rDA reaction. However, it is also possible that the pausing effect observed is caused by simply slowing the depolymerization rate down enough to appear as a temporary pause; depolymerizations of polycarbamates is known to be slow and highly sensitive to pH and solvent.[20] As such, we tested the depolymerization of a similar polycarbamate derived SIP backbone bearing a known acid sensitive N-Boc-derived trigger (Figure S3.19). In contrast, to the furylcarbinol and corresponding DA adduct derived triggers, the polycarbamate derived SIP bearing a N-Boc protecting group resulted in a near spontaneously depolymerization at ambient temperature. This suggests that the ability to

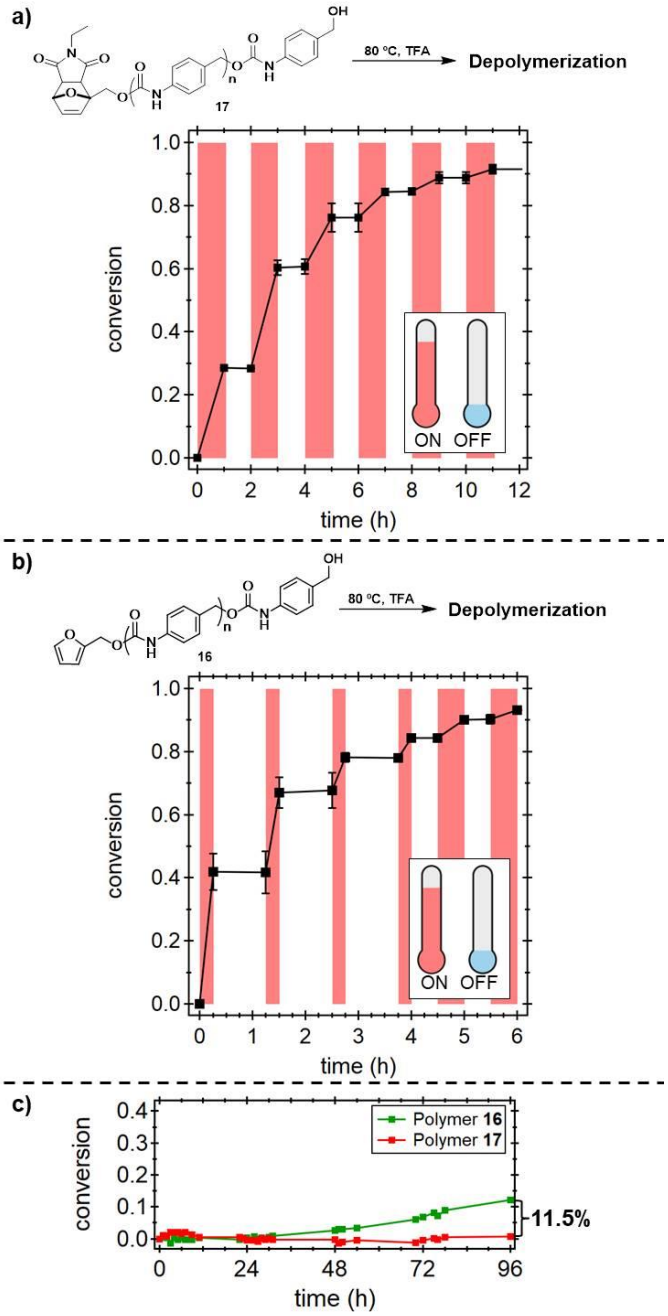

Figure 3. 3

a) Temporal ON/OFF studies of SIP 17. ^{1}H NMR spectroscopy was used to monitor the depolymerization upon subjection of the SIP to 6 cycles of heating and cooling over a period of 12 h. Red bars are heating cycles where the flask containing the polymer was heated to 80 °C. White bars are cooling cycles where the flask was held at room temperature. b) Temporal ON/OFF studies of SIP 16 subjected to similar heating heat cycling sequence. c) 4-day stability test to evaluate the stability of the trigger endcap toward acidic environment. Reproduced from Polym. Chem. 2019, 10 with permission from the Royal Society of Chemistry.

impart temporal control for polymer **16** and **17** is due to the trigger unit and not environmental factors or the nature of the polycarbamate backbone.

Given that excellent temporal control is observed even without the DA lock, long term stability studies on polymer **16** and **17** were conducted to determine if the Diels–Alder adduct provided enhanced stability toward an acidic environment at ambient temperature (Figure 3.3c). Polymer **16** was subjected to the acidic 7:1 DMSO-d_6:TFA-*d* solution at ambient temperature and the stability of the polymer was monitored via ^{1}H NMR spectroscopy over a 4-day period. As shown in Figure 3.3c, we observed less than 1% depolymerization for the first 24 h. However, after 4 days, 12% depolymerization was observed. Under identical conditions, **17**, was observed to be more stable with less than 1% depolymerization detected after 4 days. Even though the DA adduct is not necessary to impart temporal control, we favor this approach due to the added stability toward an acidic environment and because the heat used to promote the Diels–Alder cycloreversion can also be used as one of the stimuli to promote the release of the furylcarbinol trigger. The orthogonality of this multi-stimuli process combined with the facile, user-friendly nature of the reaction establishes the potential use of this system as a promising platform for more complex SIP applications.

3.4 Conclusion

In conclusion, we have shown that a physical-chemical multi-stimuli trigger unit for SIPs can be used to control the trigger release rate and thus the rate of depolymerization. Excellent temporal control was observed for both the furylcarbinol and corresponding DA derived triggers. For long term stability, the furan-maleimide derived trigger was found to be more stable to the acidic conditions and premature depolymerization was not observed in the absence

of heat. We envision this strategy will enable SIP to impart an additional level of control to applications that range from drug delivery to degradable materials.

3.5 Experimental

3.5.1 Materials and Methods

Unless stated otherwise, reactions were conducted in oven dried glassware under an atmosphere of N_2 using reagent grade solvents. All commercially obtained reagents were used as received. Reaction temperatures were controlled using a Heidolph temperature modulator, and unless otherwise, reactions were performed at room temperature (RT, approximately 23 °C). Thin-layer chromatography (TLC) was conducted with E. Merck silica gel 60 F254 pre-coated plates (0.25 mm) and visualized by exposure to UV light (254 nm) or stained with potassium permanganate or p-anisaldehyde. Flash chromatography was preformed using normal phase silica gel (60 Å, 230-240 mesh, Geduran®) ^{1}H NMR spectra were recorded on Varian Spectrometers (at 400, 500, and 600 MHz) and are reported relative to deuterated solvent signals. Data for ^{1}H NMR spectra are reported as follows: chemical shift (δ ppm), multiplicity, coupling constant (Hz) and integration. ^{13}C NMR spectra were recorded on Varian Spectrometers (at 100, 125, and 150 MHz). Data for ^{13}C NMR spectra are reported in terms of chemical shift. IR spectra were recorded on a Perkin Elmer Spectrum 100 FT/IR and a Bruker Alpha FT/IR and are reported in terms of frequency of absorption (cm^{-1}). High resolution mass spectra were obtained from the UC Santa Barbara Mass Spectrometry Facility.

3.5.2 Synthesis Procedures

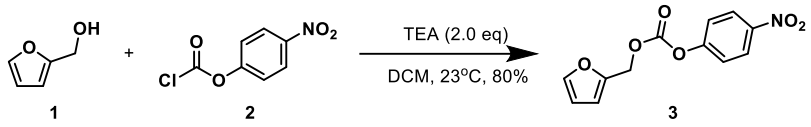

Furan-2-ylmethyl (4-nitrophenyl) carbonate (3): To a 100 mL oven dried round bottom flask is added 4-nitrophenyl chloroformate **2** (2.8 g, 13.8 mmol, 1.2 eq) in DCM (anhydrous, 30 mL). While under an atmosphere of nitrogen furfuryl alcohol **1** (1 mL, 11.5 mmol, 1.0 eq) is added via syringe to the flask. Triethylamine (3.2 mL, 23 mmol, 2.0 eq) is added dropwise to the reaction via syringe. The reaction is allowed to stir for one hour before being quenched with 1 M HCl (1 x 30 mL) and saturated potassium carbonate (3 x 30 mL).The organic layer was dried over magnesium sulfate prior to being concentrated *in vacuo* to afford a pale yellow solid (2.42 g, 80%). ^{1}H NMR (500 MHz, Chloroform-*d*) δ 8.30 – 8.24 (m, 2H), 7.48 (dd, *J* = 1.9, 0.8 Hz, 1H), 7.41 – 7.35 (m, 2H), 6.54 (dd, *J* = 3.2, 0.8 Hz, 1H), 6.41 (dd, *J* = 3.3, 1.9 Hz, 1H), 5.26 (s, 2H); ^{13}C NMR (125 MHz, Chloroform-*d*) δ 155.6, 152.4 147.9, 145.6, 144.2, 125.4, 121.9, 112.3, 110.9, 62.6; IR 3120, 3086, 2973, 1748, 1594, 1523, 1492, 1345, 1263, 1214, 923, 744, 499 cm^{-1}.

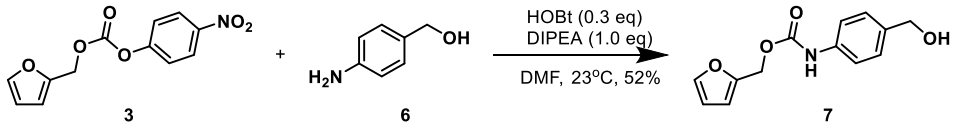

Furan-2-ylmethyl (4-(hydroxymethyl)phenyl)carbamate (7): To a 100 mL oven dried round bottom flask is added **3** (2.4 g, 9.1 mmol, 1.0 eq), 4-aminobenzyl alcohol **6** (1.24 g, 10.0 mmol, 1.1 eq), and hydroxy benzotriazole (0.42 g, 2.7 mmol, 0.3 eq) in DMF (anhydrous, 10 mL). Through a septa cap, *N*,*N*-diisopropylethylamine (1.6 mL, 9.1 mmol, 1.0 eq) is added and the reaction is allowed to stir at room temperature for 48 hours. The solution is diluted with a

solution of 9:1 ethyl acetate: isopropyl alcohol (20 mL) and set to stir for one additional hour. The solution is then quenched with saturated sodium bicarbonate (1 x 30 mL), saturated sodium bisulfite (1 x 30 mL), and brine (3 x 30 mL). The organic layer is dried over magnesium sulfate and concentrated *in vacuo*. The crude product was dry loaded onto Celite and purified via flash chromatography with an increasing gradient of ethyl acetate in hexanes (40 → 70%) to afford **7** as a light tan solid (1.2 g, 52%). ^{1}H NMR (500 MHz, Chloroform-*d*) δ 7.43 (dd, *J* = 1.8, 0.9 Hz, 1H), 7.35 (d, *J* = 8.3 Hz, 2H), 7.30 – 7.26 (m, 2H), 6.75 (s, 1H), 6.45 (dd, *J* = 3.2, 0.7 Hz, 1H), 6.37 (dd, *J* = 3.3, 1.8 Hz, 1H), 5.15 (s, 2H), 4.62 (s, 2H), 1.80 (s, 1H); ^{13}C NMR (125 MHz, Chloroform-*d*) δ 153.1, 149.7, 143.5, 137.3, 136.2, 128.1, 119.0, 110.9, 110.8, 65.0, 58.9; IR 3317, 3119, 2944, 1697, 1610, 1540, 1413, 1220, 1042, 1004, 918, 750, 599 cm^{-1}; HRMS (ESI), calculated for $C_{13}H_{13}NO_4$: ($M+Na^+$) 270.0742; observed 270.0735.

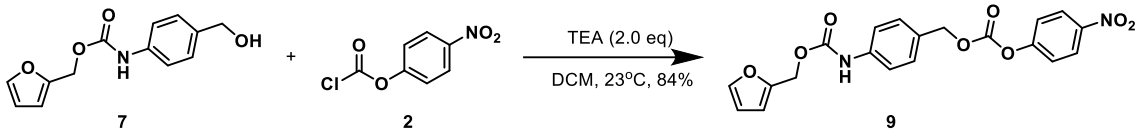

Furan-2-ylmethyl (4-((((4-nitrophenoxy)carbonyl)oxy)methyl)phenyl)carbamate (9): To a 100 mL oven dried round bottom flask is added **7** (1.8 g, 7.28 mmol, 1.0 eq) and **2** (1.76 g, 8.74 6 mmol, 1.2 eq) in DCM (anhydrous, 30 mL). While under an atmosphere of nitrogen, triethylamine (2.03 mL, 14.56 mmol, 2.0 eq) is added dropwise to the reaction via syringe. The reaction is allowed to stir at room temperature for 1.5 hours before being quenched with 1 M HCl (1 x 30 mL) and saturated potassium carbonate (3 x 30 mL). The organic layer is dried over magnesium sulfate and concentrated *in vacuo* to afford a white solid (2.52 g, 84%). ^{1}H NMR (500 MHz, Chloroform-*d*) δ 8.29 – 8.24 (m, 2H), 7.47 – 7.33 (m, 7H), 6.76 (s, 1H), 6.46 (dd, *J* = 3.2, 0.7 Hz, 1H), 6.38 (dd, *J* = 3.2, 1.8 Hz, 1H), 5.24 (s, 2H), 5.16 (s, 2H); ^{13}C NMR

(125 MHz, Chloroform-*d*) δ 155.7, 153.0, 152.6, 149.5, 145.5, 143.6, 138.7, 130.1, 129.6, 129.3, 125.4, 121.9, 111.0, 110.8, 70.8, 59.0; IR 3347, 3117, 2924, 1754, 1711, 1523, 1270, 1211, 1054, 863, 759, 663 cm^{-1}; HRMS (ESI), calculated for $C_{20}H_{16}N_2O_8$: ($M+Na^+$) 435.0804; observed 435.0806.

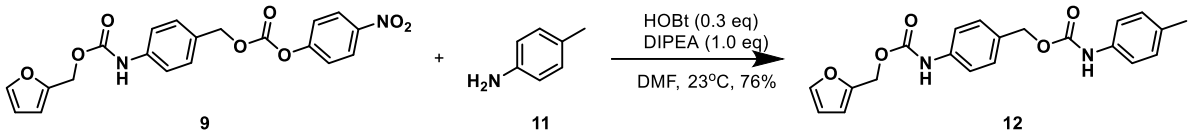

9 11 12

Furan-2-ylmethyl (4-(((p-tolylcarbamoyl)oxy)methyl)phenyl)carbamate (12): To a 15 mL oven dried round bottom flask is added **9** (200 mg, 0.49 mmol, 1.0 eq), 4-methylaniline **11** (57 mg, 0.53 mmol, 1.1 eq), and hydroxy benzotriazole (22 mg, 0.15 mmol, 0.3 eq) in DMF (anhydrous, 2 mL). Through a septa cap, *N*,*N*-diisopropylethylamine (84 μL, 0.49 mmol, 1.0 eq) is added and the reaction is allowed to stir at room temperature for 48 hours. The solution is diluted with a solution of 9:1 ethyl acetate: isopropyl alcohol (10 mL) and set to stir for one additional hour. The solution is then washed with saturated sodium bicarbonate (1 x 10 mL), saturated sodium bisulfite (1 x 10 mL), and brine (3 x 10 mL). The organic layer is dried over magnesium sulfate and concentrated *in vacuo*. The crude product was dry loaded onto Celite and purified via flash chromatography with an increasing gradient of ethyl acetate in hexanes (5 → 40%) to afford **12** as a light tan solid (141 mg, 76%). ^{1}H NMR (400 MHz, Chloroform-*d*) δ 7.46 – 7.42 (m, 1H), 7.36 (q, *J* = 8.5 Hz, 5H), 7.24 (s, 2H), 7.10 (d, *J* = 8.1 Hz, 2H), 6.70 (s, 1H), 6.59 (s, 1H), 6.46 (d, *J* = 3.2 Hz, 1H), 6.38 (dd, *J* = 3.3, 1.9 Hz, 1H), 5.16 (s, 2H), 5.13 (s, 2H), 2.30 (s, 3H); ^{13}C NMR (125 MHz, Chloroform-*d*) δ 162.0, 153.2, 149.5, 143.5, 137.8, 133.5, 131.4, 129.7, 129.5, 126.3, 115.8, 111.0, 110.8, 66.8, 59.0, 20.9; IR 3329, 2963, 1704,

1599, 1536, 1314, 1226, 1045, 817, 509 cm^{-1}; HRMS (ESI), calculated for $C_{21}H_{20}N_2O_5$: ($M+Na^+$) 403.1270; observed 403.1282.

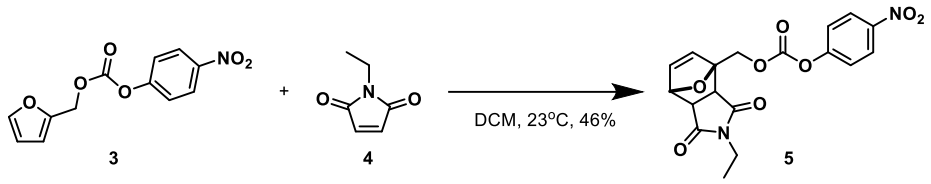

((3aS,4R,7R,7aR)-2-ethyl-1,3-dioxo-1,2,3,3a,7,7a-hexahydro-4H-4,7-epoxyisoindol-4-yl)methyl (4-nitrophenyl) carbonate (5): To a 15 mL oven dried round bottom flask is added **3** (1 g, 3.8 mmol, 1.0 eq) and *N*-ethylmaleimide **4** (1.43 g, 11.4 mmol, 3.0 eq) in DCM (anhydrous, 5 mL). The solution is allowed to stir at room temperature for five days. The solution is then concentrated *in vacuo* and dry loaded onto Celite and purified via flash chromatography with an increasing gradient of ethyl acetate in hexanes (10 → 50%) to afford **5** as a white solid (674 mg, 46%). ^{1}H NMR (500 MHz, Chloroform-*d*) δ 8.31 – 8.26 (m, 2H), 7.45 – 7.40 (m, 2H), 6.51 (dd, *J* = 5.8, 1.7 Hz, 1H), 6.38 (d, *J* = 5.8 Hz, 1H), 5.35 (dd, *J* = 5.5, 1.7 Hz, 1H), 4.92 (dd, *J* = 101.5, 12.3 Hz, 2H), 3.68 (dd, *J* = 7.7, 5.5 Hz, 1H), 3.46 (d, *J* = 7.7 Hz, 1H), 3.40 (q, *J* = 7.2 Hz, 2H), 1.05 (t, *J* = 7.2 Hz, 3H); ^{13}C NMR (125 MHz, Chloroform-*d*) δ 174.3, 155.5, 152.4, 145.7, 136.2, 133.9, 125.5, 121.9, 89.1, 79.9, 66.5, 47.8, 46.9, 33.8, 12.8; IR 3086, 1761, 1691, 1533, 1347, 1260, 1210, 1131, 863, 722, 636, 434 cm^{-1}; HRMS (ESI), calculated for $C_{18}H_{16}N_2O_8$: ($M+Na^+$) 411.0804; observed 411.0795.

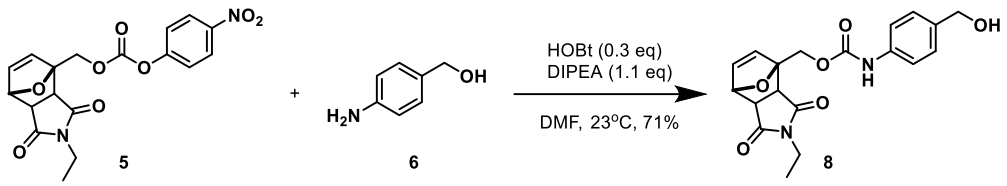

((3aS,4R,7R,7aR)-2-ethyl-1,3-dioxo-1,2,3,3a,7,7a-hexahydro-4H-4,7-epoxyisoindol-4-yl)methyl (4-(hydroxymethyl)phenyl)carbamate (8): To a 15 mL oven dried round bottom flask is added **5** (300 mg, 0.77 mmol, 1.0 eq), **6** (105 mg, 0.85 mmol, 1.1 eq), and hydroxy benzotriazole (35 mg, 0.23 mmol, 0.3 eq) in DMF (anhydrous, 3 mL). Through a septa cap *N,N*-diisopropylethylamine (0.14 mL, 0.77 mmol, 1.0 eq) is added and the reaction is allowed to stir for 48 hours. The solution is diluted with a solution of 9:1 ethyl acetate: isopropyl alcohol (10 mL) and set to stir for one additional hour. The solution is then washed with saturated sodium bicarbonate (1 x 10 mL), saturated sodium bisulfite (1 x 10 mL), and brine (3 x 10 mL). The organic layer is dried over magnesium sulfate and concentrated *in vacuo*. The crude product was dry loaded onto Celite and purified via flash chromatography with an increasing gradient of ethyl acetate in hexanes (30 → 70%) to afford **8** as a light tan solid (203 mg, 71%). ^{1}H NMR (500 MHz, Chloroform-*d*) δ 7.41 – 7.27 (m, 4H), 6.90 (s, 1H), 6.45 (dd, *J* = 5.8, 1.6 Hz, 1H), 6.35 (d, *J* = 5.7 Hz, 1H), 5.34 – 5.28 (m, 1H), 4.96 (d, *J* = 12.5 Hz, 1H), 4.68 (d, *J* = 12.6 Hz, 1H), 4.63 (s, 2H), 3.63 (dd, *J* = 7.7, 5.5 Hz, 1H), 3.42 – 3.33 (m, 3H), 1.04 (t, *J* = 7.2 Hz, 3H); ^{13}C NMR (125 MHz, Chloroform-*d*) δ 174.5, 174.3, 137.1, 136.4, 135.8, 134.5, 129.8, 128.1, 90.0, 79.8, 65.0, 62.9, 47.8, 46.9, 33.7, 12.8; IR 3353, 2952, 2871, 1736, 1692, 1525, 1399, 1245, 1135, 1057, 630 cm^{-1}; HRMS (ESI), calculated for $C_{19}H_{20}N_2O_6$: ($M+Na^+$) 395.1219; observed 395.1232.

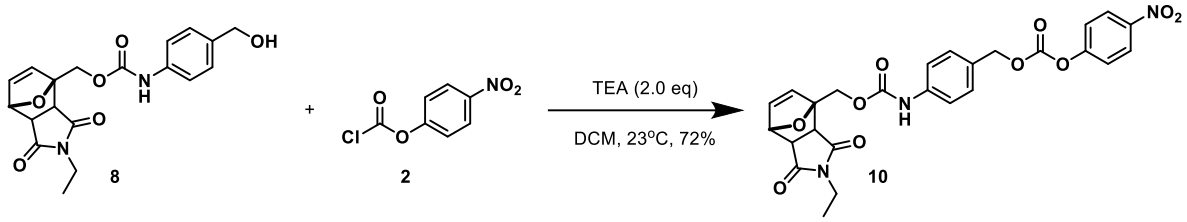

((3aS,4R,7R,7aR)-2-ethyl-1,3-dioxo-1,2,3,3a,7,7a-hexahydro-4H-4,7-epoxyisoindol-4-yl)methyl (4-((((4-nitrophenoxy)carbonyl)oxy)methyl)phenyl)carbamate (10): To a 15 mL oven dried round bottom flask was added **8** (175 mg, 0.47 mmol, 1.0 eq) and **2** (114 mg, 0.56 mmol, 1.2 eq) in DCM (anhydrous, 5 mL). While under an atmosphere of nitrogen, triethylamine (0.13 mL, 0.94 mmol, 2.0 eq) was added dropwise to the reaction via syringe. The reaction is allowed to stir at room temperature for 1.5 hours before being quenched with 1 M HCl (1 x 10 mL) and saturated potassium carbonate (3 x 10 mL). The organic layer is dried over magnesium sulfate and concentrated *in vacuo* to afford a white solid (126 mg, 72%). ^{1}H NMR (500 MHz, Chloroform-*d*) δ 8.31 – 8.23 (m, 2H), 7.48 – 7.34 (m, 6H), 6.88 (s, 1H), 6.47 (dd, *J* = 5.7, 1.7 Hz, 1H), 6.36 (d, *J* = 5.8 Hz, 1H), 5.33 (dd, *J* = 5.5, 1.7 Hz, 1H), 5.24 (s, 2H), 4.84 (dd, *J* = 139.6, 12.5 Hz, 2H), 3.65 (dd, *J* = 7.7, 5.5 Hz, 1H), 3.43 – 3.34 (m, 3H), 1.05 (t, *J* = 7.2 Hz, 3H); ^{13}C NMR (125 MHz, Chloroform-*d*) δ 174.42, 174.26, 155.65, 152.65, 152.57, 145.54, 138.47, 135.85, 134.45, 130.09, 129.53, 125.43, 121.91, 118.89, 89.94, 79.79, 77.41, 77.16, 76.91, 70.76, 63.06, 47.84, 46.94, 33.71, 12.79; IR 3327, 3083, 2953, 1764, 1735, 1691, 1523, 1345, 1201, 1057, 862, 724 cm^{-1}; HRMS (ESI), calculated for $C_{26}H_{23}N_3O_{10}$: ($M+Na^+$) 560.1281; observed 560.1283.

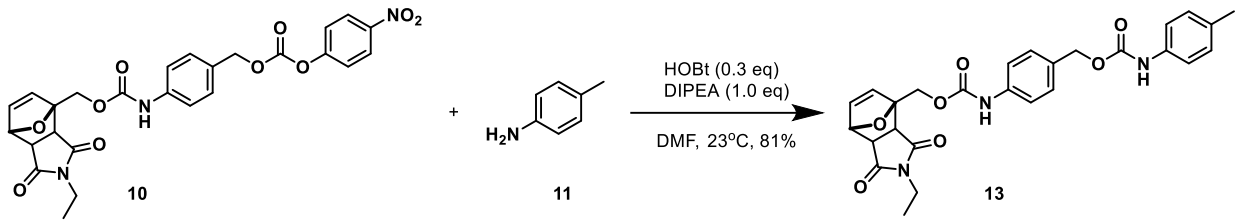

((3aS,4R,7R,7aR)-2-ethyl-1,3-dioxo-1,2,3,3a,7,7a-hexahydro-4H-4,7-epoxyisoindol-4-yl)methyl (4-(((p-tolylcarbamoyl)oxy)methyl)phenyl)carbamate (13): To a 15 mL oven dried round bottom flask was added **10** (210 mg, 0.39 mmol, 1.0 eq), **11** (46 mg, 0.43 mmol, 1.1 eq), and hydroxy benzotriazole (18 mg, 0.12 mmol, 0.3 eq) in DMF (anhydrous, 2 mL). Through a septa cap *N*,*N*-diisopropylethylamine (68 µL, 0.39 mmol, 1.0 eq) is added and the solution is allowed to stir for 48 hours. The solution is diluted with a solution of 9:1 ethyl acetate: isopropyl alcohol (10 mL) and set to stir for one additional hour. The solution is then washed with saturated sodium bicarbonate (1 x 10 mL), saturated sodium bisulfite (1 x 10 mL), and brine (3 x 10 mL). The organic layer is dried over magnesium sulfate and concentrated *in vacuo*. The crude product was dry loaded onto Celite and purified via flash chromatography with an increasing gradient of ethyl acetate in hexanes (30 → 70%) to afford **13** as a light tan solid (155 mg, 81%). ^{1}H NMR (500 MHz, Chloroform-*d*) δ 7.43 – 7.30 (m, 4H), 7.25 (s, 1H), 7.09 (d, *J* = 8.1 Hz, 2H), 6.91 (s, 1H), 6.72 – 6.63 (m, 1H), 6.45 (dd, *J* = 5.7, 1.7 Hz, 1H), 6.35 (d, *J* = 5.8 Hz, 1H), 5.31 (dd, *J* = 5.5, 1.7 Hz, 1H), 5.12 (s, 2H), 4.82 (dd, *J* = 142.7, 12.5 Hz, 2H), 3.63 (dd, *J* = 7.7, 5.5 Hz, 1H), 3.42 – 3.31 (m, 3H), 2.29 (s, 3H), 1.04 (t, *J* = 7.2 Hz, 3H); ^{13}C NMR (125 MHz, Chloroform-*d*) δ 174.48, 174.28, 152.73, 137.75, 135.78, 135.29, 134.47, 131.56, 129.67, 129.55, 118.82, 89.97, 79.75, 77.41, 77.16, 76.91, 66.64, 62.94, 47.82, 46.88, 33.68, 20.87, 12.77; IR 3335, 3083, 2974, 1764, 1734, 1691, 1523, 1345, 1201, 1058, 862, 725 cm^{-1}; HRMS (ESI), calculated for C27H27N3O7: (M+Na^{+}) 528.1747; observed 528.1755.

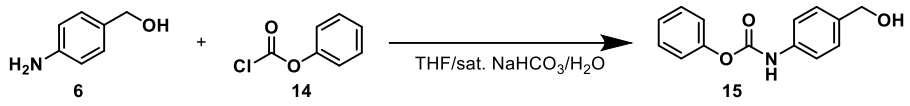

Phenyl (4-(hydroxymethyl)phenyl)carbamate (15): 6 (3 g, 24.4 mmol, 1.0 eq) was suspended in a mixture of THF: sat. $NaHCO_3$: water (45 mL, ratio 2:2:1). Phenyl chloroformate **14** (3.12 mL, 24.85 mmol, 1.02 eq) was added dropwise over five minutes. Once the reaction reached completion, ethyl acetate was added, and the organic phase was washed twice with saturated NH_4Cl solution. The solution was concentrated *in vacuo*. The crude product was dry loaded onto Celite and purified via flash chromatography to afford **15** as a white solid (4.61 g, 78%). Spectral data matches literature values.[3]

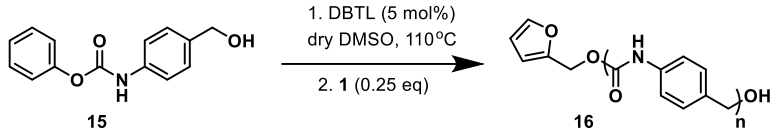

Furan end capped polyurethane (16): To a 25 mL flame dried round bottom flask was added **15** (1.5 g, 6.2 mmol, 1.0 eq) and DBTL (0.183 mL, 0.31 mmol, 0.05 eq) in DMSO (anhydrous, 2.0 mL). The flask was heated to 85 °C for 2.5 hours. **1** (0.134 mL, 1.54 mmol, 0.25 eq) was added to the reaction and stirred overnight. After cooling to room temperature, the polymer was precipitated into cold methanol (30 mL), filtered and dried. In order to obtain completely end capped polymer, the crude polymer is then subjected to 9:1 DMSO:H_2O with 10% piperidine for 2 days at 60 °C prior to being precipitated a second time into cold methanol. Polymer **16** was obtained as a light tan solid (870 mg). ^{1}H NMR (600 MHz, DMSO-d_6) δ 9.80 (s, 1H), 9.74 (s, 15H), 9.61 (s, 1H), 7.66 (s, 1H), 7.43 (d, J = 8.1 Hz, 30H), 7.36 (d, J = 8.1 Hz,

2H), 7.30 (d, *J* = 8.2 Hz, 30H), 7.16 (d, *J* = 7.8 Hz, 2H), 6.52 (s, 1H), 6.43 (s, 1H), 5.07 (s, 2H), 5.01 (s, 30H), 4.36 (d, *J* = 5.7 Hz, 2H). GPC: M_n = 4.6 kg/mol, M_w = 8.8 kg/mol, $Đ$ = 1.9.

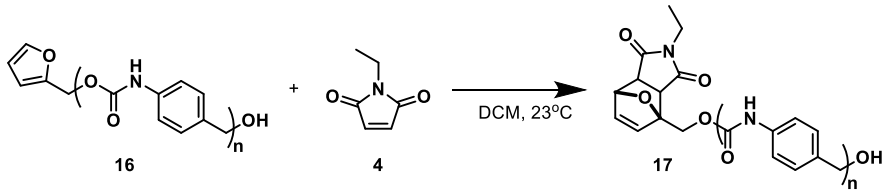

16 4 17

Diels–Alder end capped polyurethane (17): To a 15 mL oven dried round bottom flask is added **16** (250 mg, 0.104 mmol, 1.0 eq) and **4** (130 mg, 1.04 mmol, 10.0 eq) in DMSO (anhydrous, 2 mL). The solution is allowed to stir for one week at room temperature. The polymer is then precipitated into cold methanol, filtered, and dried to afford polymer **17** as a tan solid (125 mg; 25 % no conversion, 25 % *exo* adduct, and 50 % *endo* adduct). GPC: M_n = 5.1 kg/mol, M_w = 7.8 kg/mol, $Đ$ = 1.9.

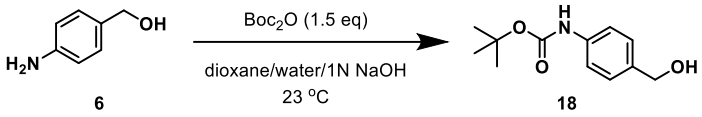

6 18

***Tert*-butyl (4-(hydroxymethyl)phenyl)carbamate (18):** 4-aminobenzyl alcohol (0.5 g, 4.06 mmol, 1 eq) was dissolved in a 1:2:3 mixture of Dioxane:H_2O:1N NaOH (15 mL total). Boc_2O (1.33 g, 6.09 mmol, 1.5 eq) was dissolved in 2.5 mL dioxane and added dropwise. The mixture was stirred at room temperature overnight. After confirmation of reaction completion by TLC, the dioxane was removed *in vacuo* and the remaining solution was extracted with ethyl acetate (3 x 10 mL). After removing the ethyl acetate *in vacuo*, the product was purified via column chromatography (1:1 hexanes:ethyl acetate) to yield **18** (0.706 g) as a white powder. Spectral data matches literature values.[1]

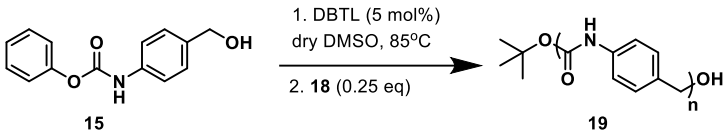

Boc end capped polyurethane (19): To a 25 mL flame dried round bottom flask was added **15** (1.5 g, 6.17 mmol, 1.0 eq) and DBTL (0.183 mL, 0.31 mmol, 0.05 eq) in DMSO (anhydrous, 2 mL). The flask was heated to 85 °C for 2.5 hours. **18** (0.346 g, 1.55 mmol, 0.25 eq) was added to the reaction and stirred overnight. After cooling to room temperature, the polymer was precipitated into cold methanol (20 mL), filtered and dried. In order to obtain completely end capped polymer, the crude polymer is then subjected to 9:1 DMSO:H_2O with 10% piperidine for 2 days at 60 °C prior to being precipitated a second time into cold methanol. Polymer **19** was obtained as a light tan solid (740 mg). Spectral data matches literature values.[1]

3.5.3 Small Molecule Studies

Thermal Stability of furan small molecule model

Compound 12 (10 mg) was dissolved in MeCN-d_3 (0.7 mL). The sample was placed in a preheated heating block at 80 °C. The sample was allowed to stir between NMR spectra taken to monitor the sample. NMR spectra were obtained at t=0 (prior to heating) and t=6 (hours). As demonstrated by having no observable change via NMR at elevated temperature, this indicates that heat alone is not a suitable trigger.

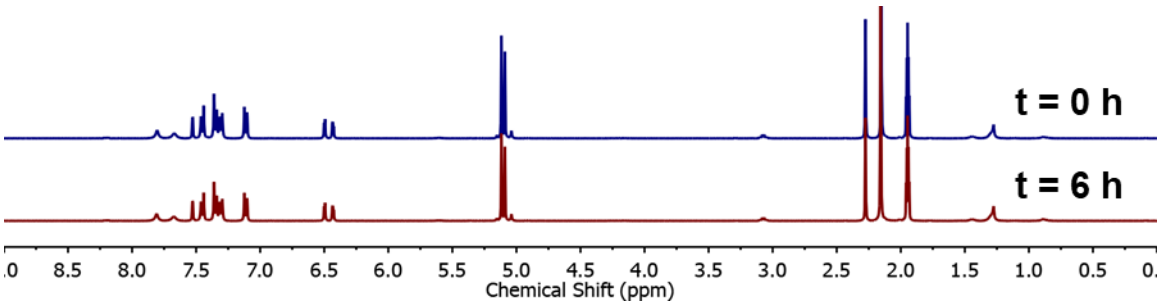

Figure S3.1. Full NMR spectra for compound 12 before and after being heated at 80 °C. There is no structural change from its initial state (navy) after 6 hours of heating at 80 °C (red), supporting our need for a dual-stimuli system.

Quantitative retro-Diels–Alder on small molecule model

Compound 13 (10 mg) was dissolved in MeCN-d_3 (0.7 mL). The sample was placed in a preheated heating block at 80 °C. The sample was allowed to stir, and NMR spectra were obtained prior to heating and every 2 hours after for a total of 6 hours of heating.

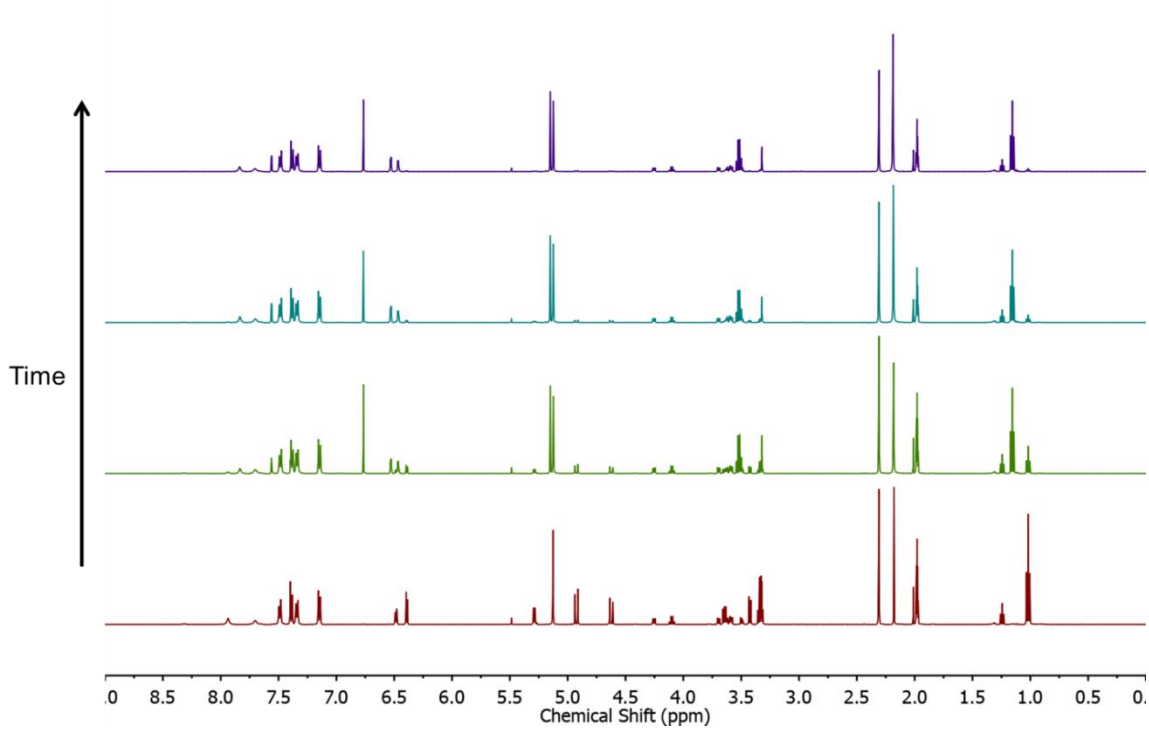

Figure S3.2. NMR spectra for compound 13 at its initial state (red), after 2 hours (green), 4 hours (teal), and 6 hours (purple). Protons for the maleimide appear at 6.77 ppm and a shift in furan peaks is seen between 6.54-6.38 ppm. As demonstrated by the NMR spectrum, near quantitative retro Diels-Alder can be observed over this time period supporting the successful "unlocking" of the trigger system.

Acid Stability of Diels–Alder model

Compound 13 (10 mg) was dissolved in MeCN-d_3 (0.7 mL) with $Sc(OTf)_3$ (1 mg). An initial t0 ^{1}H NMR spectrum was obtained, and the sample was left to stir at room temperature over 48 hours. A t48 ^{1}H NMR spectrum was obtained and shows there was no structural changes to 13 over the 48-hour period while in an acidic environment. This was also done with 13 in DMSO-d_6 (0.7 mL) with TFA-d (0.1 mL) as shown in Figure 3.2c. This stability supports the advantage of using the Diels–Alder lock to ensure long term stability as well as prohibit any premature depolymerization from occurring.

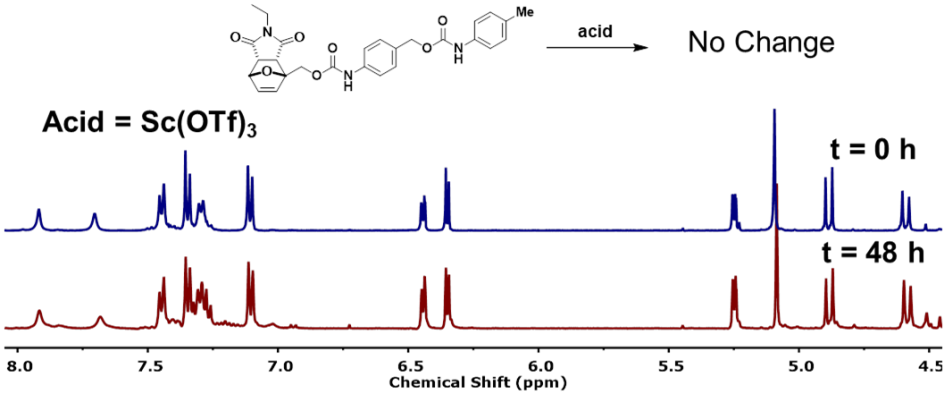

Figure S3.3. ^{1}H NMR spectra of 13 at t0 and t48 hours of being exposed to the acid catalyst $Sc(OTf)_3$. No structural changes were observed indicating that the Diels–Alder lock on the furan adduct acts as a protecting group to eliminate premature activation of the furan cleavage.

Controlled retro-Diels–Alder and release

Compound 13 (10 mg) in DMSO-d_6 (0.7 mL) with TFA-d (0.1 mL) was placed in a preheated heating block at 80 °C. After one hour of heating, the sample is cooled in an ice bath (0 °C) for one minute before being left to reach room temperature. After sitting at room temperature for

one hour the sample is placed back into the heating block. These cycles continue until the sample has reached quantitative release (some time periods are longer than one hour and shown below). NMR spectra are obtained after each heating and each room temperature time period to monitor the progress of the release.

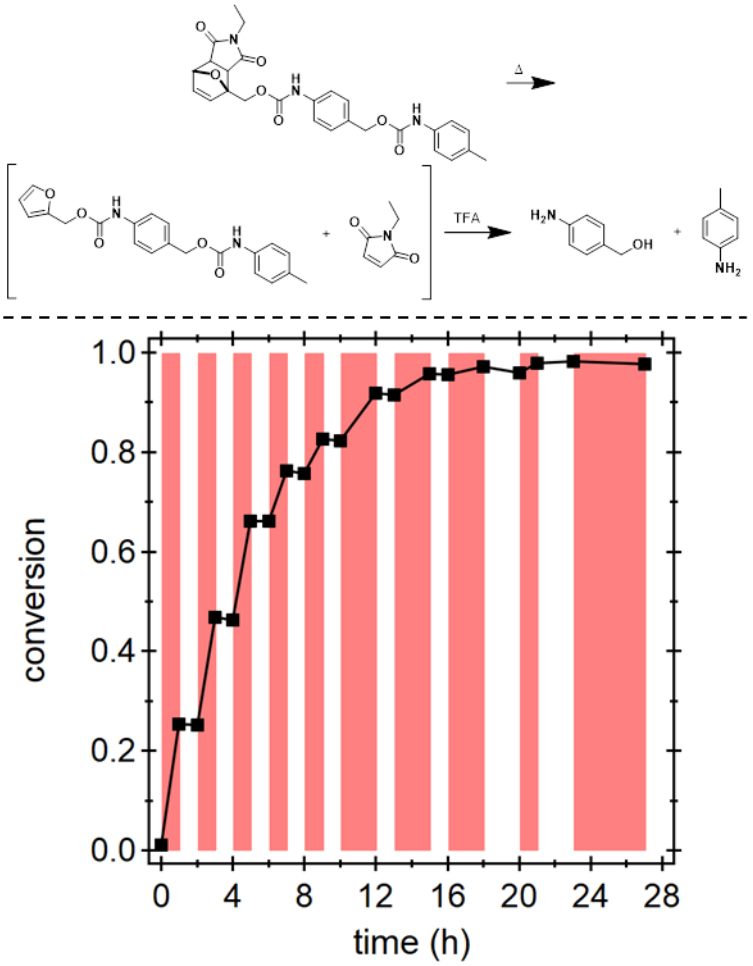

Figure S3.4. Controlled release of the reporter molecule 11 using TFA. The red bars representing heating at 80 °C and the white bars represent holding at room temperature. For this ON/OFF study, 98% conversion was observed after 10 cycles of heating.

Kinetics Studies

Diels–Alder adducts

An NMR sample of 5 (10 mg) with 10 mol% $Sc(OTf)_3$ (1 mg) in MeCN-d_3 (0.7 mL) is monitored overnight (14 h 31 min 10 s) with NMR spectra saved every 2.9 minutes. This was repeated for samples to be run at 50 °C, 60 °C, 65 °C, and 70 °C.

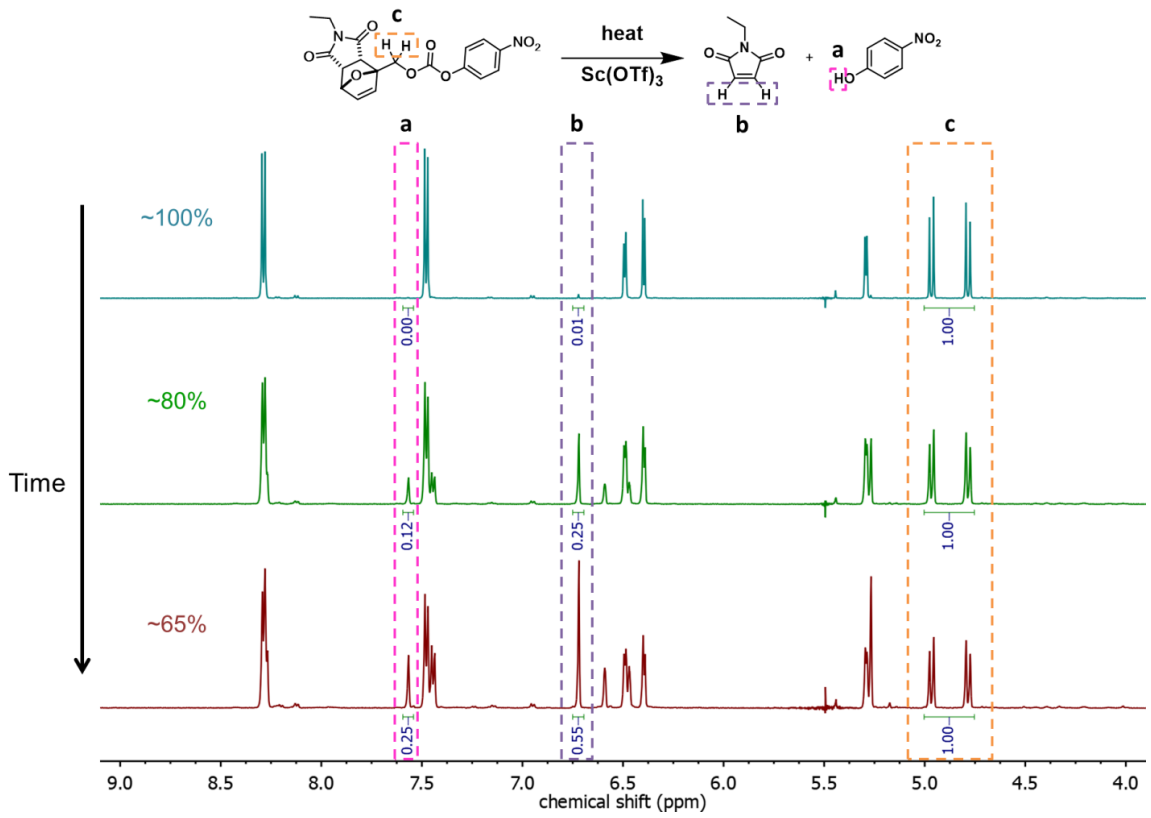

Figure S3.5. NMR spectra of three different states of progress through the kinetics studies at 60 °C showing the peaks used for conversion calculations. The percent shown indicates the amount of our starting Diels–Alder (DA) adduct is still present.

NMR processing: Samples as described above were prepared and then placed in an NMR spectrometer and equilibrated at the given temperature for about 5 minutes before collecting the data. The disappearance of the starting DA adduct was tracked over time. The data was collected as an array collecting 300 scans on the Varian Unity Inova AS600 600 MHz spectrometer. This data was then processed in MestReNova software. A spectrum that was

roughly in the middle of the overall transformation was chosen to phase and baseline the entire data set. In MeCN-d_3, the peaks with δ = 4.78 and 4.97 ppm were integrated as the starting material and the peaks with δ = 6.72 and 7.57 ppm were integrated as the released material. These integrations were then exported as a Script: 1D Integral series. The ratio of the remaining DA adduct was determined by the following equation:

Equation 1:

$$\frac{[DA\ adduct]}{[DA\ adduct]_o} = \frac{\int peak\ c}{\int peak\ c + \frac{2}{3}\int (peaks\ a + b)}$$

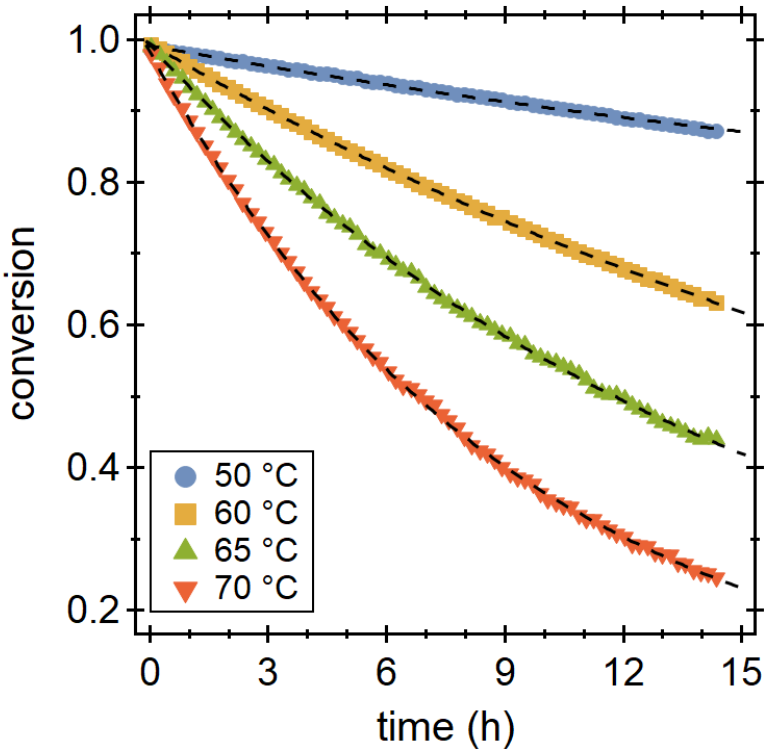

Figure S3.6. Conversion vs time data for adduct 5 at various temperatures as described above in the Kinetics Studies section.

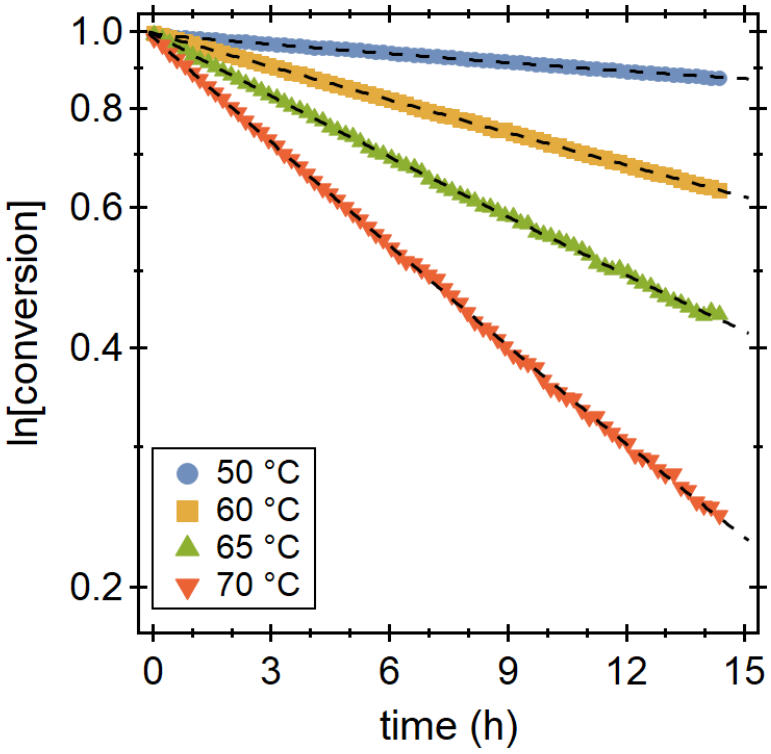

Figure S3.7. Linearized kinetics data for adduct 5 at various temperatures to extrapolate the rate values for further calculations.

The data was then fit onto a logarithmic scale and the reaction rate constants were determined from the slopes of the reaction progression. A t_{lag} value was added to the model to extrapolate all the starting data points to 0% of the reporter molecule for each sample. By plotting the rate constants relative to 1/T, we could use the Arrhenius expression to extract the activation energy.

T(°C)	k
50	0.0087
60	0.0317
65	0.0581
70	0.0983
80*	0.3090

Table S3.1. A_o and k values for the rate order equations found in Figure S3.7. All rate order equations are all in the form of $A = A_o e^{-k*t}$, where $A_o = 1.0$ for all temperatures. *The 80 °C k value was determined from Figure S3.6.

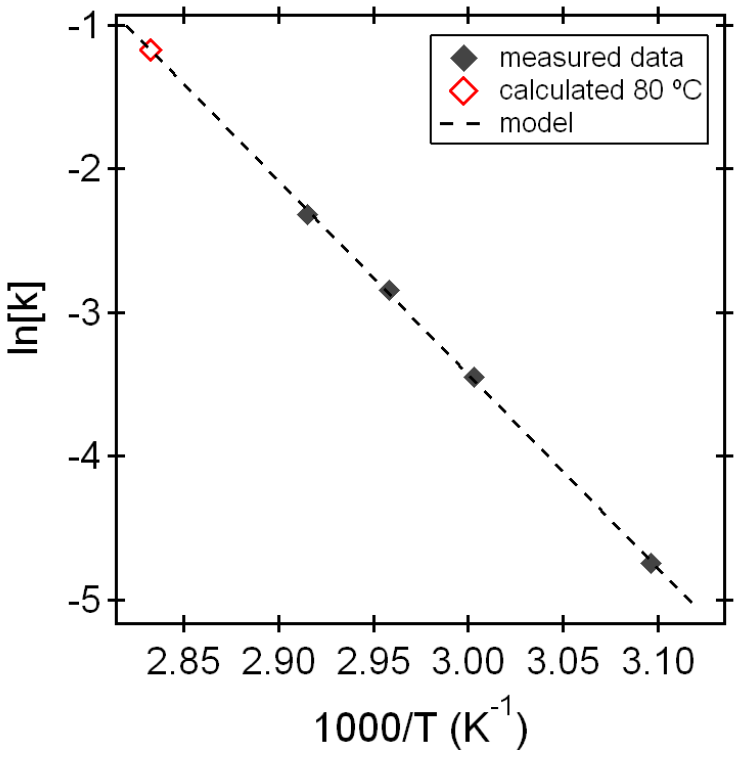

Figure S3.8. Arrhenius plot for the kinetics studies done on 5 to calculate the activation energy of the overall rDA and release of the trigger system, as well as the calculated data point for 80 °C.

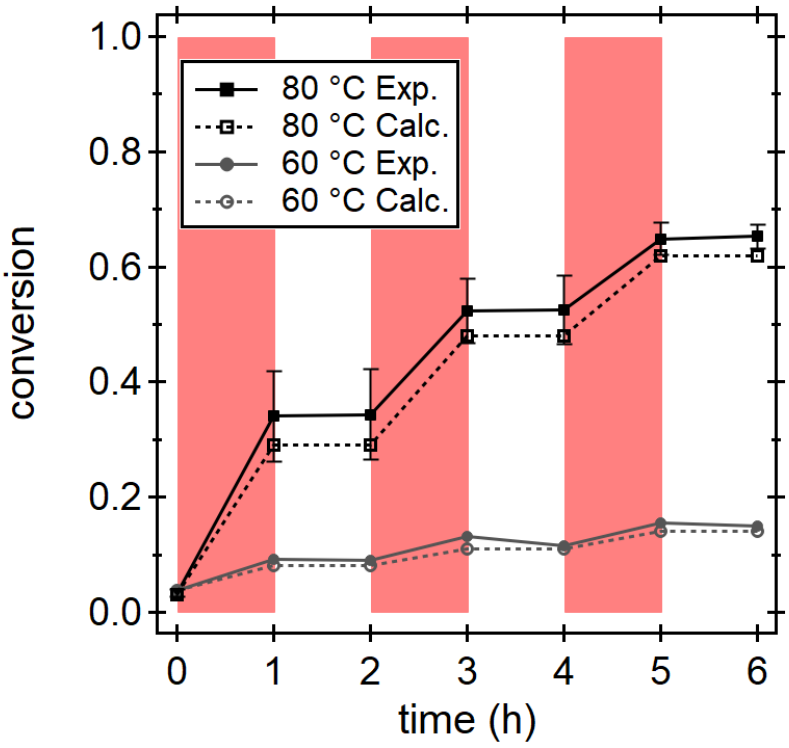

Figure S3.9. Experimental and calculated data for the controlled rDA and release of 13 at 60 °C and 80 °C as described in the Controlled retro-Diels–Alder and release section. The calculated data was determined from models described above in the Kinetics Studies section (Table S3.1).

Furan adducts

An NMR sample of 7 (10 mg) in DMSO-d_6 (0.7 mL) with TFA-d (0.1 mL) is monitored overnight (14 h) with NMR spectra saved every 2.8 minutes. This was repeated for samples which were ran at 50 °C, 60 °C, 65 °C, and 70 °C.

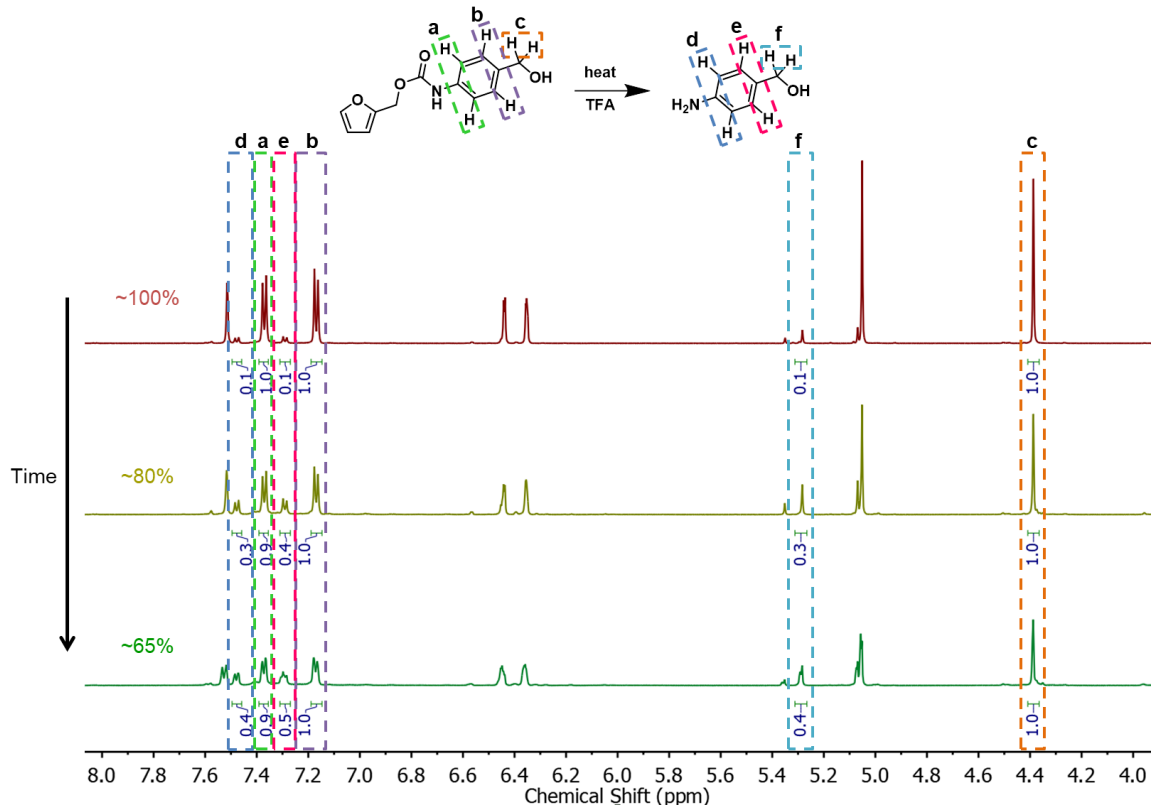

Figure S3.10. NMR spectra of three different states of progress through the kinetics studies at 60 °C showing the peaks used for conversion calculations. The percent shown indicates the amount of our starting furan adduct is still present.

NMR processing: Samples as described above were prepared and then placed in an NMR spectrometer and equilibrated at the given temperature for about 5 minutes before collecting the data. The disappearance of the starting furan adduct was tracked over time. The data was collected as an array collecting 300 scans on the Varian Unity Inova AS600 600 MHz spectrometer. This data was then processed in MestReNova software. A spectrum that was roughly in the middle of the overall transformation was chosen to phase and baseline the entire data set. In DMSO-d_6, the peaks with δ = 4.39, 7.17, and 7.37 ppm were integrated as the starting material and the peaks with δ = 5.29, 7.29, and 7.48 ppm were integrated as the released

material. These integrations were then exported as a Script: 1D Integral series. The ratio of the remaining DA adduct was determined by the following equation:

Equation 2:

$$\frac{[furan\ adduct]}{[furan\ adduct]_o} = \frac{\int(peak\ a + peak\ b + peakc)}{\int(peak\ a + peak\ b + peak\ c + peak\ d + peak\ e + peak\ f)}$$

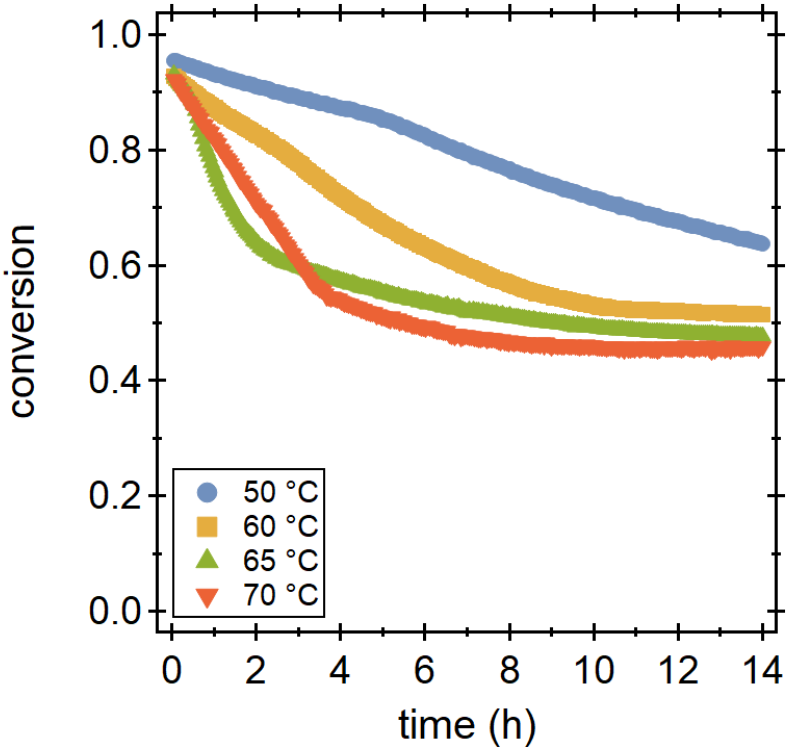

Figure S3.11. Conversion vs time for 7 at various temperatures as described above in the Kinetics Studies section. This acid catalyzed release mimics that of the aza-Piancatelli rearrangement. From previous studies in our group on the aza-Piancatelli mechanism, the rate changes observed are due to the release of the aniline reporter 6. As previous studies show, the concentration of aniline present can alter the rate at which the reaction takes place due to off-cycle binding between the aniline and acid catalyst.[33] With an increased concentration of aniline vs furan adduct, the rate of reaction decreases, similar to the kinetics data shown above.

3.5.4 Polymer Studies

Heat and Acid Release

Diels–Alder trigger

A sample of polymer 17 (10 mg) with TFA-d (0.1 mL) in DMSO-d_6 (0.7 mL) was placed in a preheated heating block at 80 °C. After one hour of heating, the sample is cooled in an ice bath for one minute before being left to reach room temperature. After sitting at room temperature for one hour the sample is placed back into the heating block. These cycles continue until the sample has reached quantitative release (some time periods are longer than one hour and shown below). NMR spectra are obtained after each heating and each room temperature time period to monitor the progress of the release.

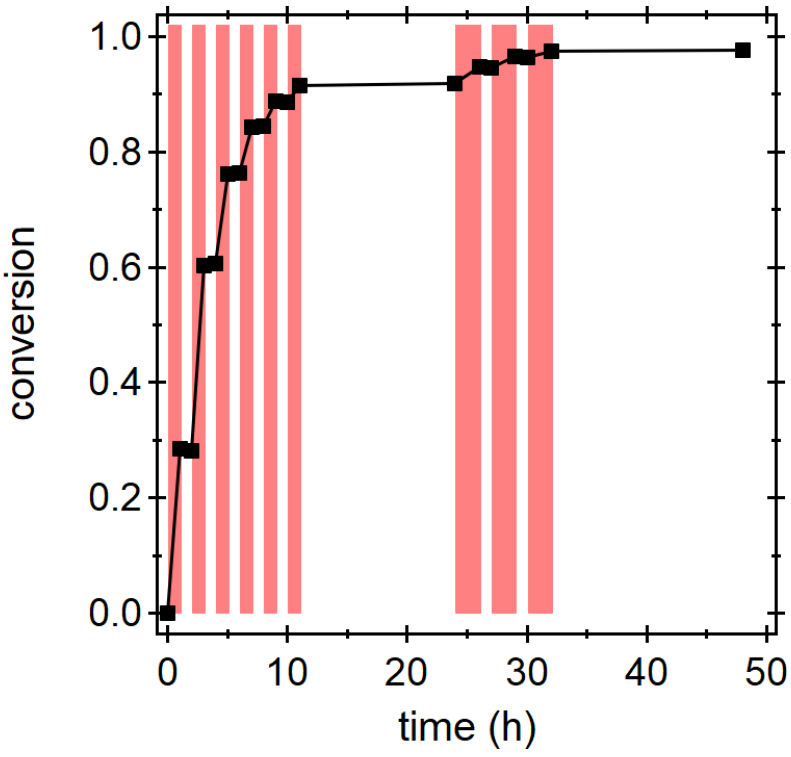

Figure S3.12. Controlled degradation of the DA locked polymer 17 during cycles of heating at 80 °C (red) and room temperature in the presence of acid.

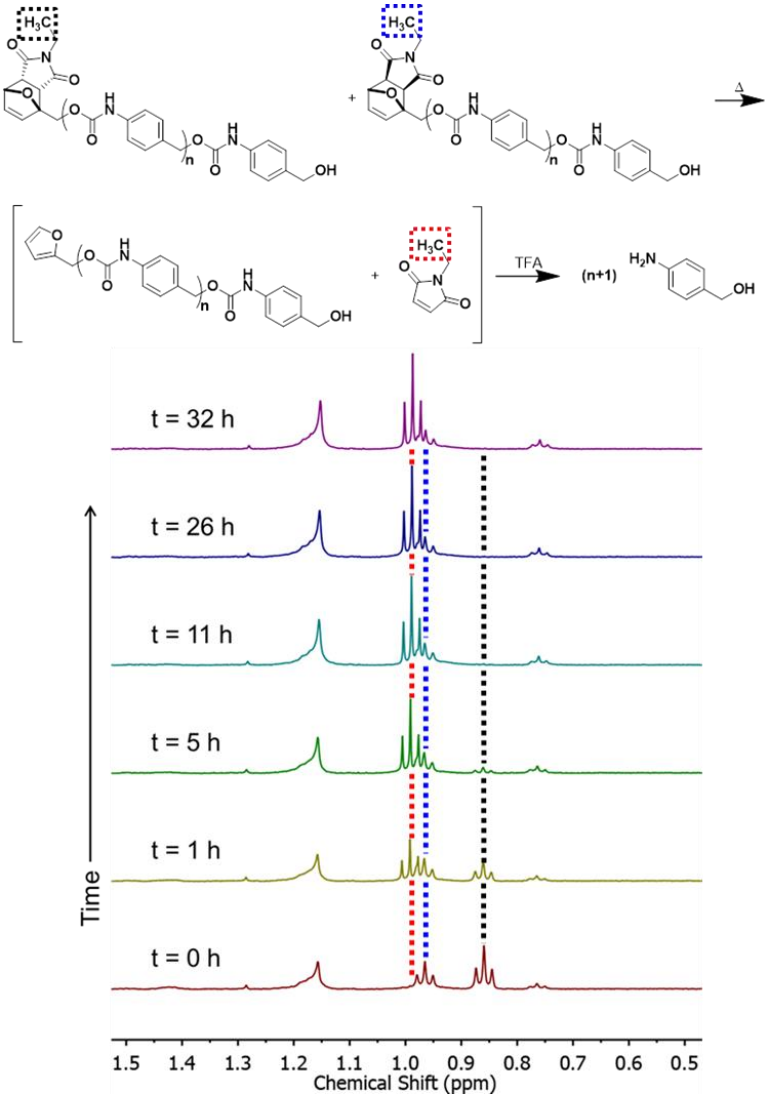

Figure S3.13. Stacked NMR spectra of polymer 17 at various times throughout the experiment shown in Figure S3.9. This shows that the DA adducts are still present throughout the experiment until cleavage takes place allowing for the pausing effect. The methyl group from the maleimide substrates are seen within this spectral range—the endo DA adduct of polymer 17 is seen at 0.86 ppm, the exo DA adduct of polymer 17 is seen at 0.96 ppm, and the maleimide small molecule being thermally cleaved begins to appear at 0.99 ppm.

Furan trigger

A sample of polymer 16 (10 mg) with TFA-d (0.1 mL) in DMSO-d_6 (0.7 mL) was placed in a preheated heating block at 80 °C. After one hour of heating, the sample is cooled in an ice bath for one minute before being left to reach room temperature. After sitting at room temperature for one hour the sample is placed back into the heating block. These cycles continue until the sample has reached quantitative release (some time periods are longer than one hour and shown below). NMR spectra are obtained after each heating and each room temperature time period to monitor the progress of the release.

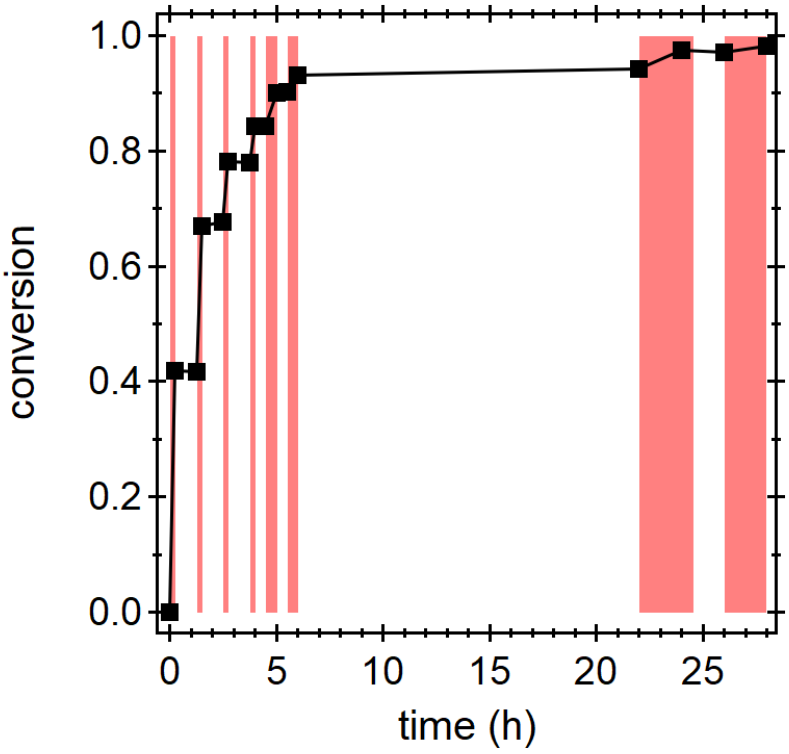

Figure S3.14. Controlled degradation of the furan capped polymer 16 during cycles of heating at 80 °C (red) and room temperature in the presence of acid.

Temperature Studies

A sample of polymer 16 and 17 (10 mg) in DMSO-d_6 (0.7 mL) with TFA-d (0.1 mL) was placed in a preheated heating block. Conversion of the sample is monitored via ^{1}H NMR spectroscopy every hour. This was done with 16 and 17 at 50 °C and 80 °C.

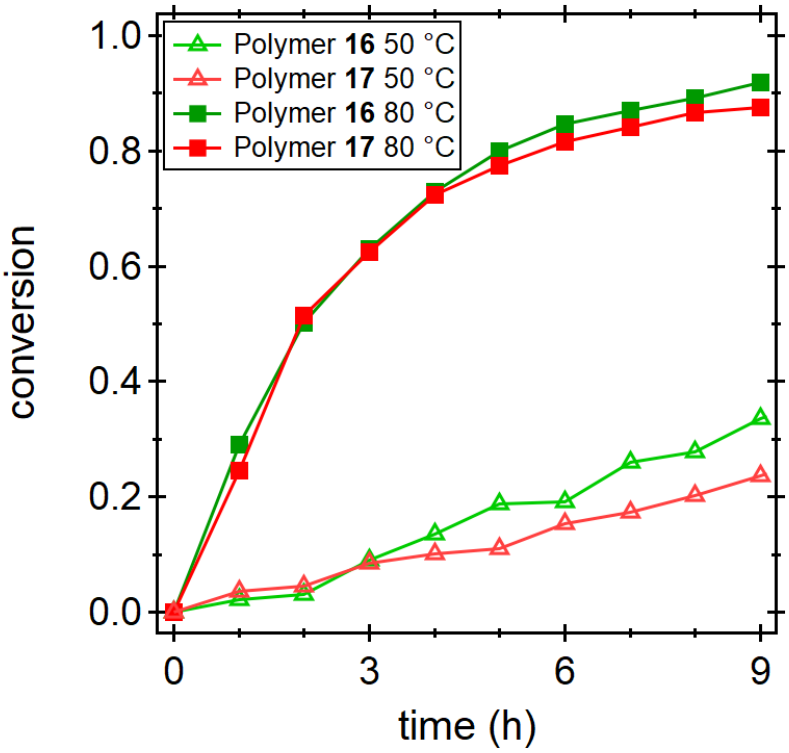

Figure S3.15. Conversion of 16 and 17 at 50 °C and 80 °C in the presence of acid over a 9-hour period.

Kinetics Studies

An NMR sample of 16 (10 mg) in DMSO-d_6 (0.7 mL) with TFA-d (0.1 mL) is monitored overnight (14 h) with NMR spectra saved every 2.8 minutes. This was repeated for samples which were ran at 50 °C, 60 °C, 65 °C, and 70 °C.

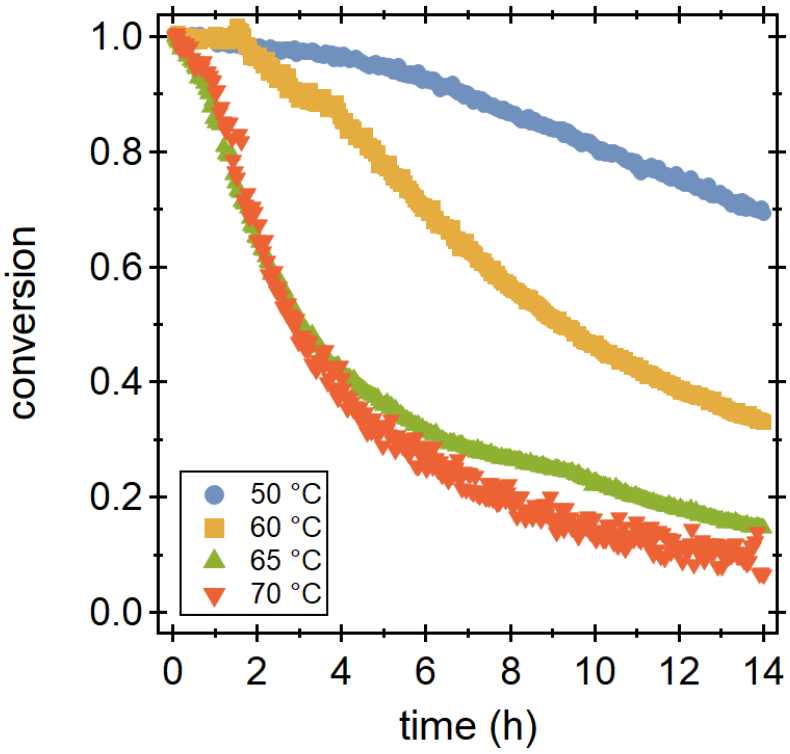

Figure S3.16. Conversion vs time of polymer 16 at various temperatures as described above in the Kinetics Studies section.

Acid-Triggered Release

A sample of polymer 16 (10 mg) with TFA (0.1 mL) in DMSO-d_6 (0.7 mL) was placed in a preheated heating block at 50 °C. The reaction was monitored via NMR at various time intervals spanning a 10-day period. This indicates that the polymer behaves as a SIP by going through full end-to-end depolymerization.

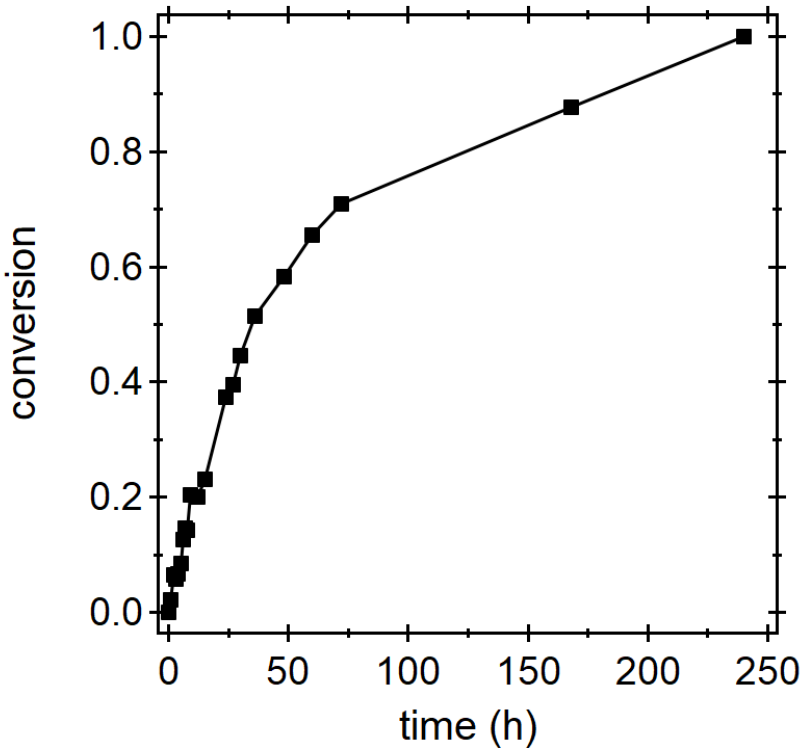

Figure S3.17. Degradation of the non-Diels–Alder furan polymer 16 monitored over time when exposed to an acid stimulus at 50 ºC, showing that when exposed to the triggering stimulus (acid + heat), the SIP can undergo complete depolymerization.

Trigger Stability to Acidic Environment

An NMR sample of polymer 16 (10 mg) in DMSO-d_6 (0.7 mL) with TFA-d (0.1 mL) was prepared and kept at room temperature. A sample of polymer 17 was prepared as well. Both polymer samples were monitored via ^{1}H NMR spectroscopy over a 4-day period to show stability to an acidic environment.

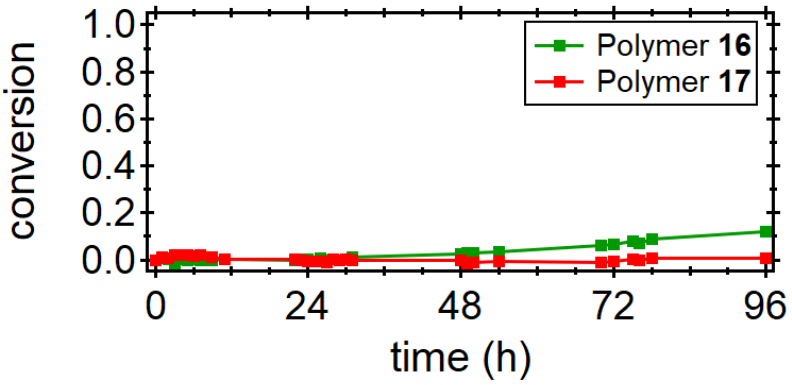

Figure S3.18. Conversion of 16 (■) and 17 (■) over a 4-day period when left at ambient temperatures in an acidic environment.

Acid Sensitive Boc-SIP Control Study

A sample of polymer 19 (10 mg) was dissolved in DMSO-d_6 (0.7 mL). An initial ^{1}H NMR spectrum was obtained. TFA-d (0.1 mL) was added to the polymer sample at room temperature and a ^{1}H NMR spectrum was obtained after 5 min to observe the deprotection and depolymerization.

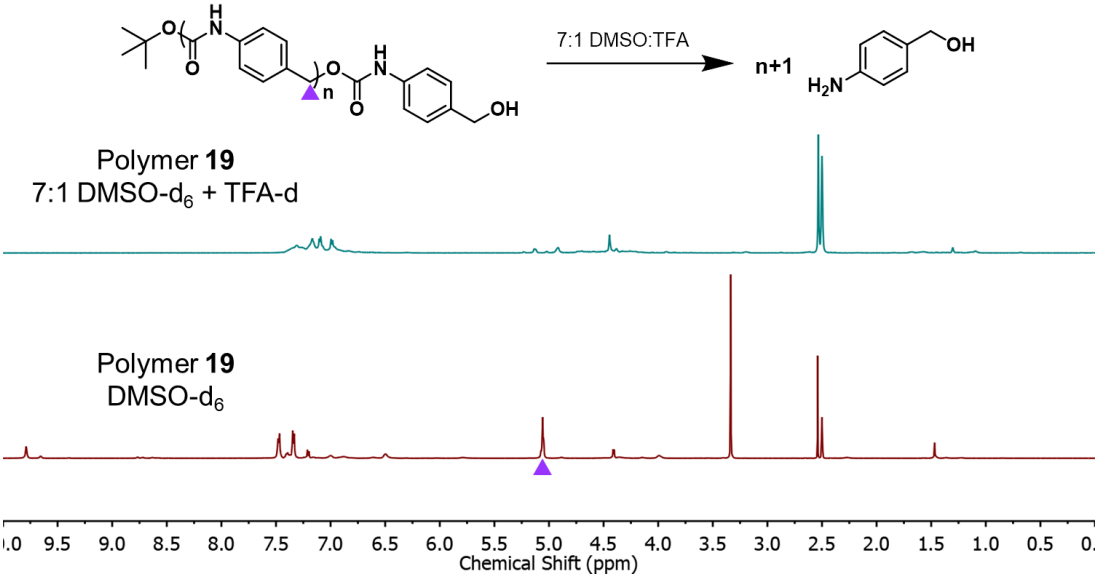

Figure S3.19. NMR spectra of polymer 19 before and after addition of the TFA-d catalyst at room temperature. Depolymerization is expressed by the loss of the backbone benzylic protons (▲).

3.5.5 ^{1}H NMR and ^{13}C NMR Spectra

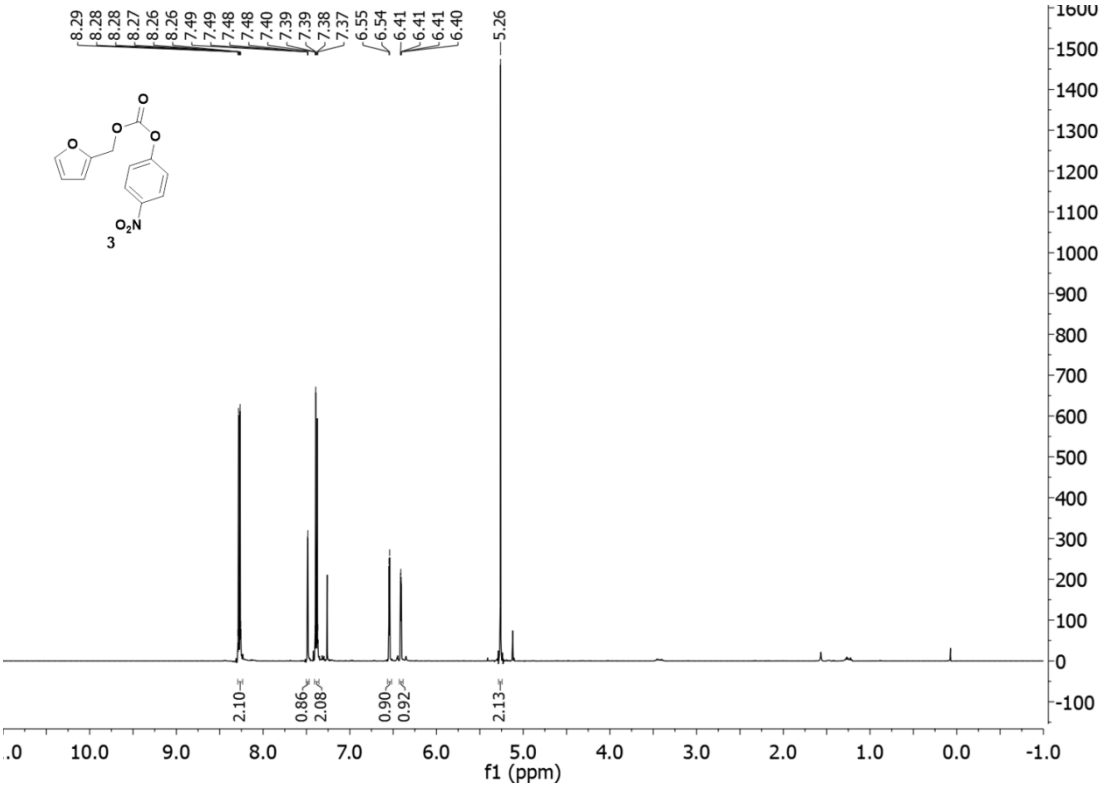

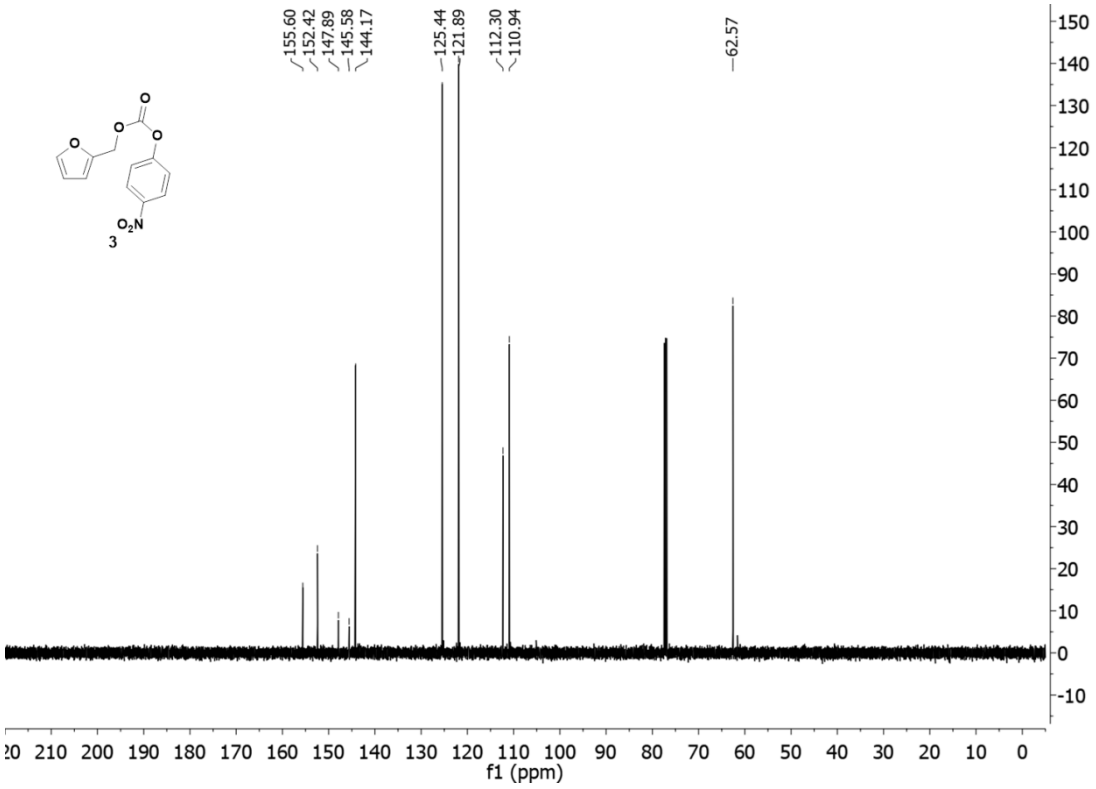
155.60
152.42
147.89
145.58
144.17
125.44
121.89
112.30
110.94
62.57
O
O
O
O
O2N
3
150
140
130
120
110
100
90
80
70
60
50
40
30
20
10
0
-10
210 200 190 180 170 160 150 140 130 120 110 100 90 80 70 60 50 40 30 20 10 0
f1 (ppm)

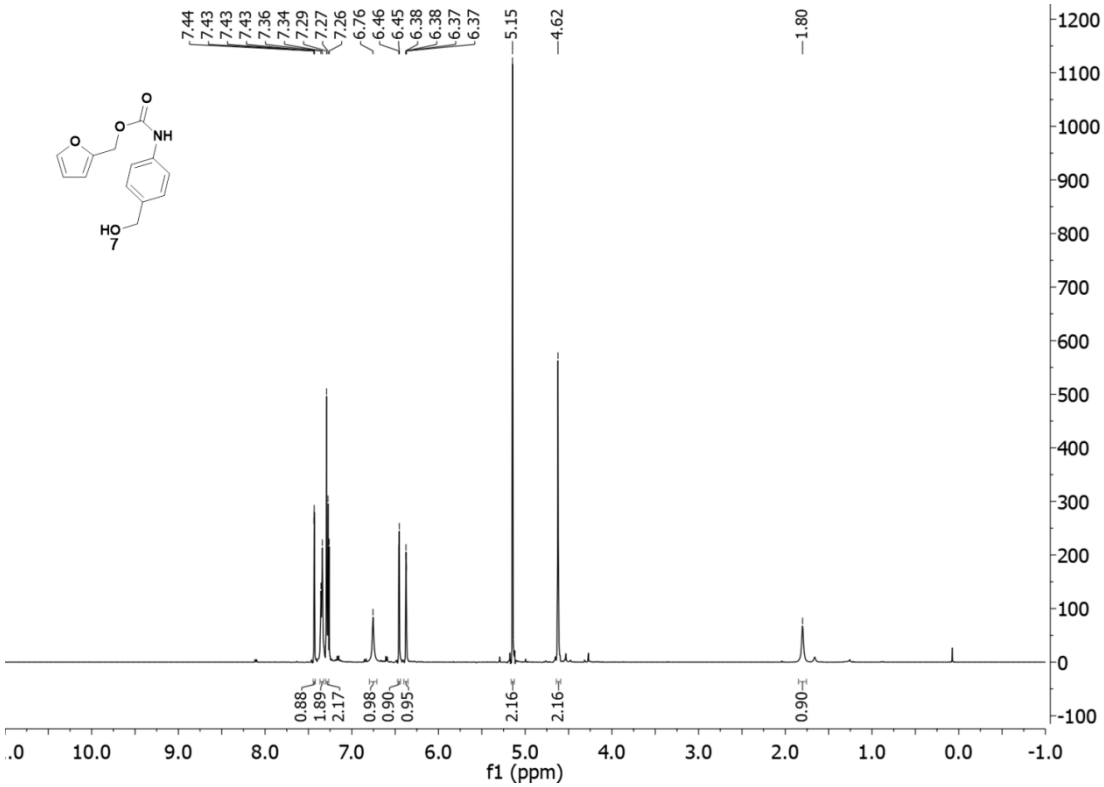
7.44
7.43
7.43
7.43
7.36
7.34
7.29
7.27
7.26
6.76
6.46
6.45
6.38
6.38
6.37
6.37
5.15
4.62
1.80
O
O
NH
O
HO
7
0.88
1.89
2.17
0.98
0.90
0.95
2.16
2.16
0.90
f1 (ppm)

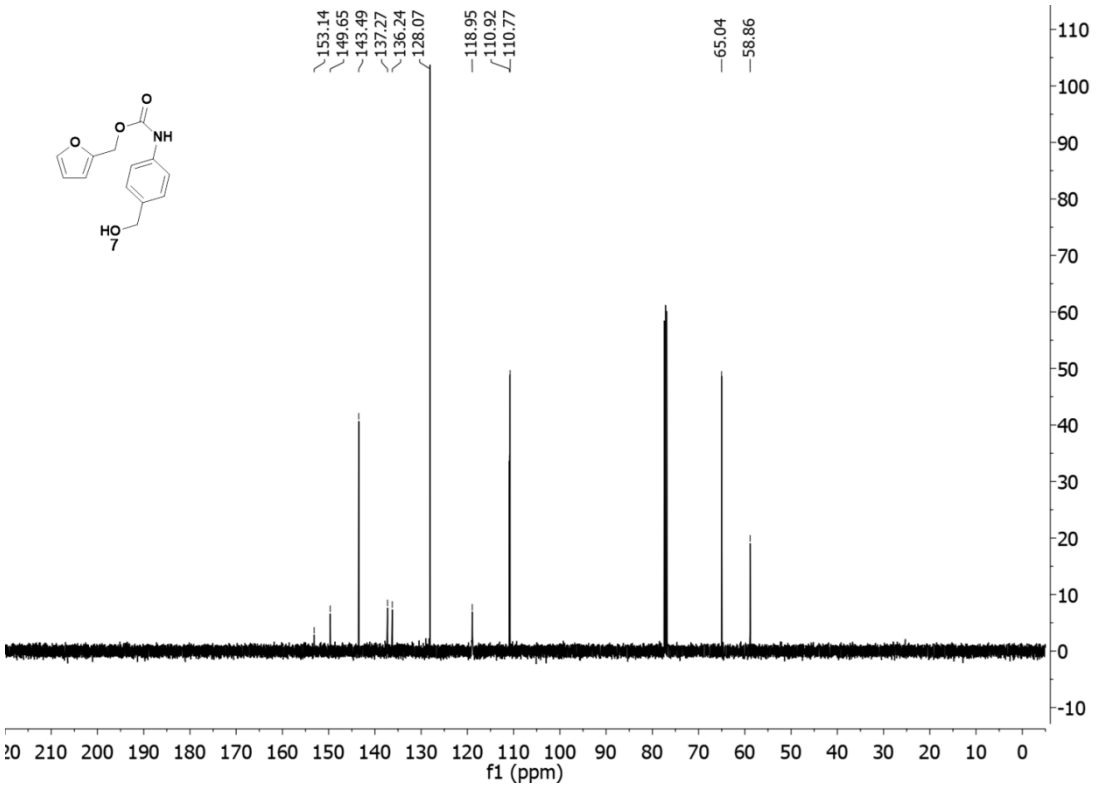
153.14
149.65
143.49
137.27
136.24
128.07
118.95
110.92
110.77
65.04
58.86
O
O
NH
O
HO
7
f1 (ppm)

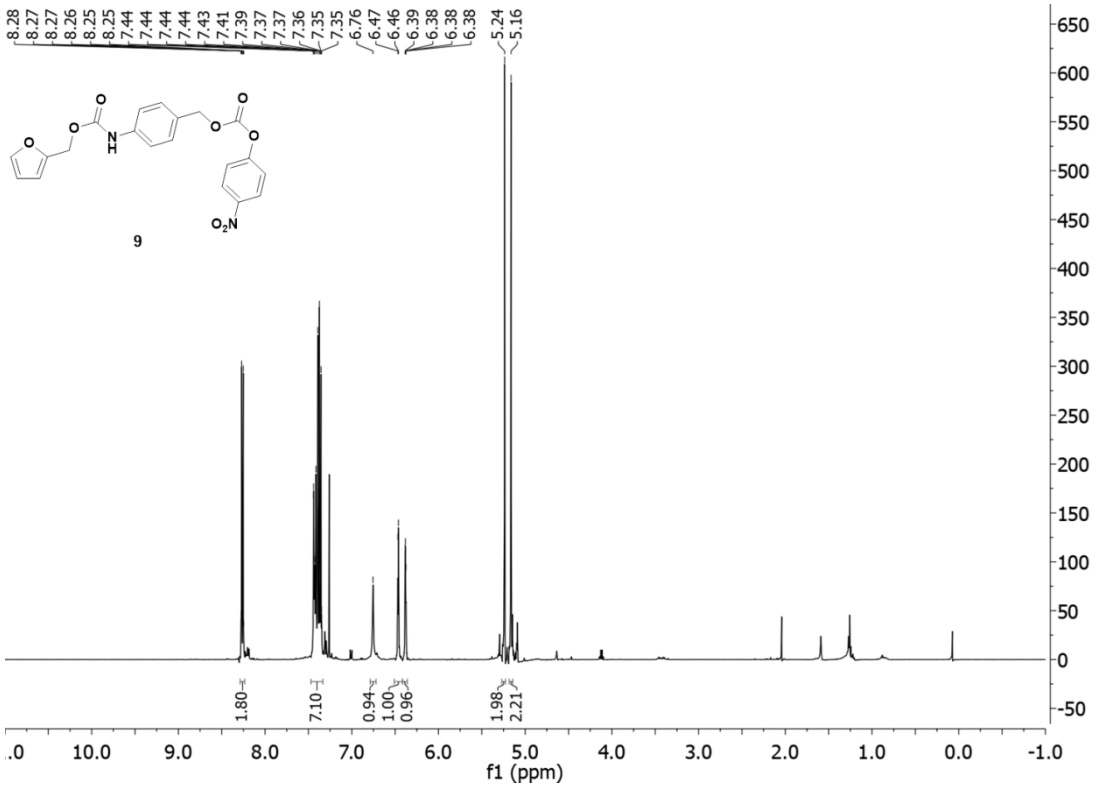
8.28
8.27
8.27
8.26
8.25
8.25
7.44
7.44
7.44
7.44
7.44
7.43
7.41
7.39
7.37
7.37
7.36
7.35
7.35
6.76
6.47
6.46
6.39
6.38
6.38
6.38
5.24
5.16
9
1.80
7.10
0.94
1.00
0.96
1.98
2.21
f1 (ppm)

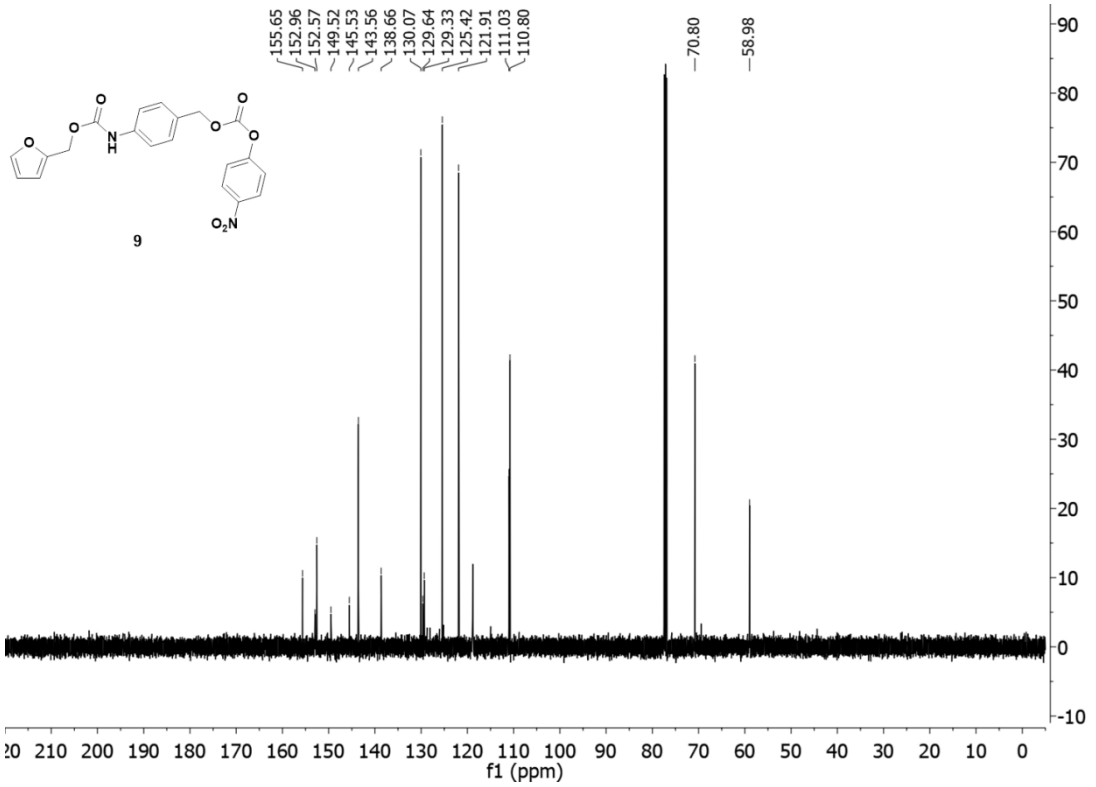
155.65
152.96
152.57
149.52
145.53
143.56
138.66
130.07
129.64
129.33
125.42
121.91
111.03
110.80
70.80
58.98
9
f1 (ppm)

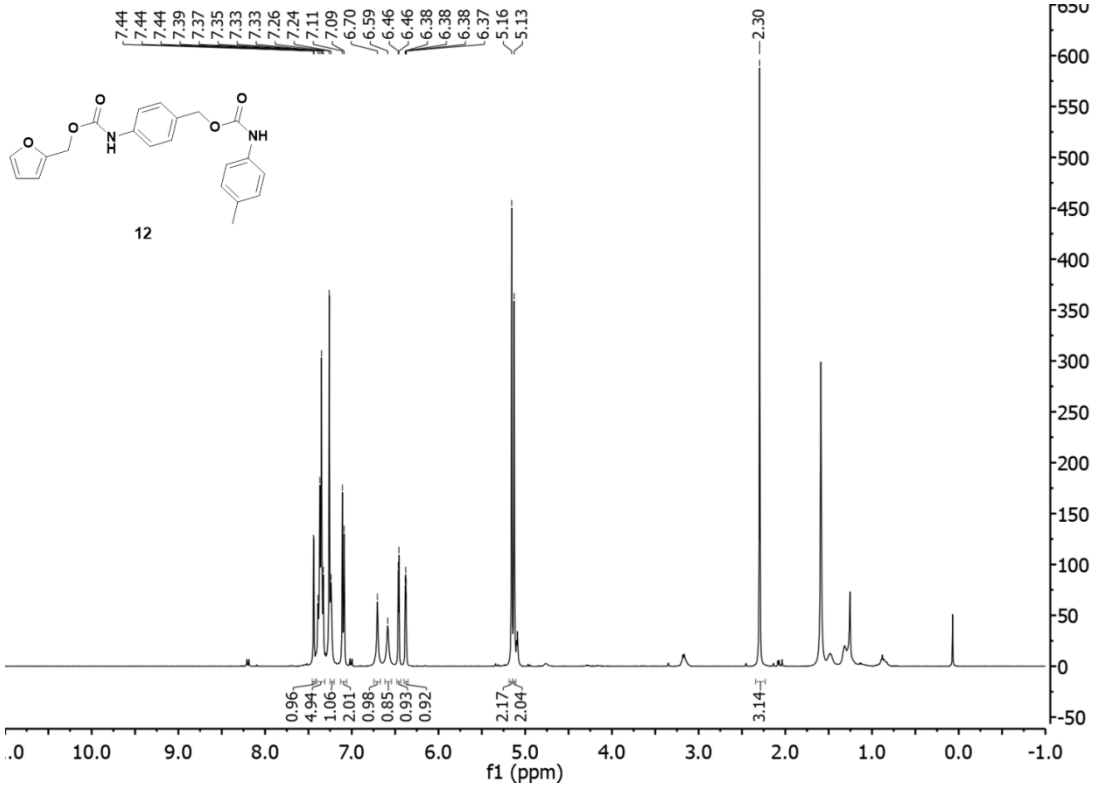
7.44
7.44
7.44
7.39
7.37
7.35
7.33
7.33
7.26
7.24
7.11
7.09
6.70
6.59
6.46
6.46
6.38
6.38
6.38
6.37
5.16
5.13
2.30
12
0.96
4.94
1.06
2.01
0.98
0.85
0.93
0.92
2.17
2.04
3.14
f1 (ppm)

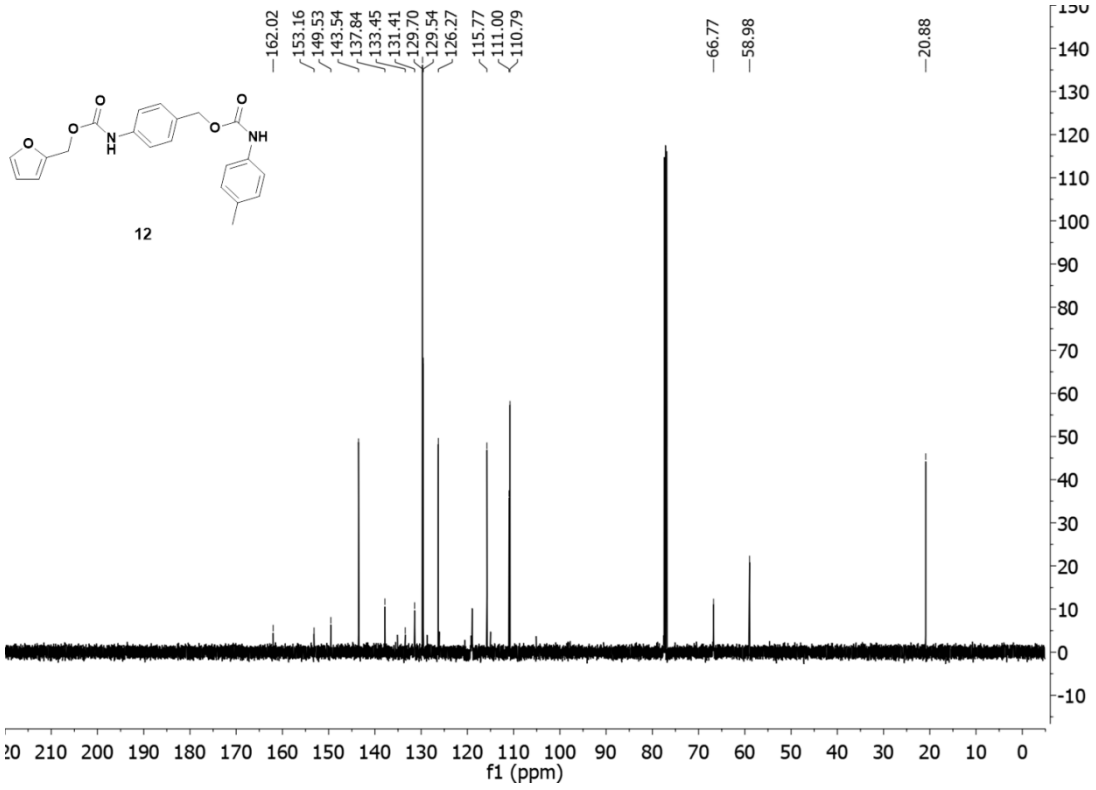
162.02
153.16
149.53
143.54
137.84
133.45
131.41
129.70
129.54
126.27
115.77
111.00
110.79
66.77
58.98
20.88
12
f1 (ppm)

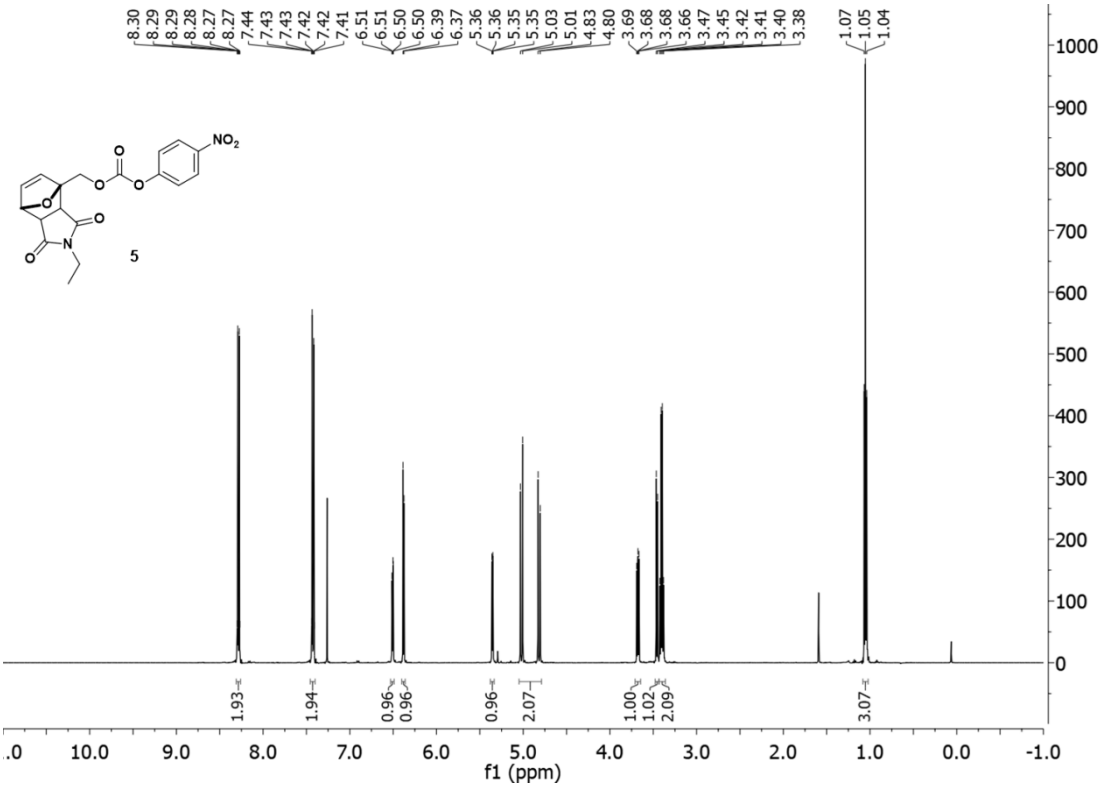
8.30
8.29
8.29
8.28
8.27
8.27
7.44
7.43
7.43
7.42
7.42
7.41
6.51
6.51
6.50
6.50
6.39
6.37
5.36
5.36
5.35
5.35
5.03
5.01
4.83
4.80
3.69
3.68
3.68
3.66
3.47
3.45
3.42
3.41
3.40
3.38
1.07
1.05
1.04
NO2
5
1.93
1.94
0.96
0.96
0.96
2.07
1.00
1.02
2.09
3.07
f1 (ppm)

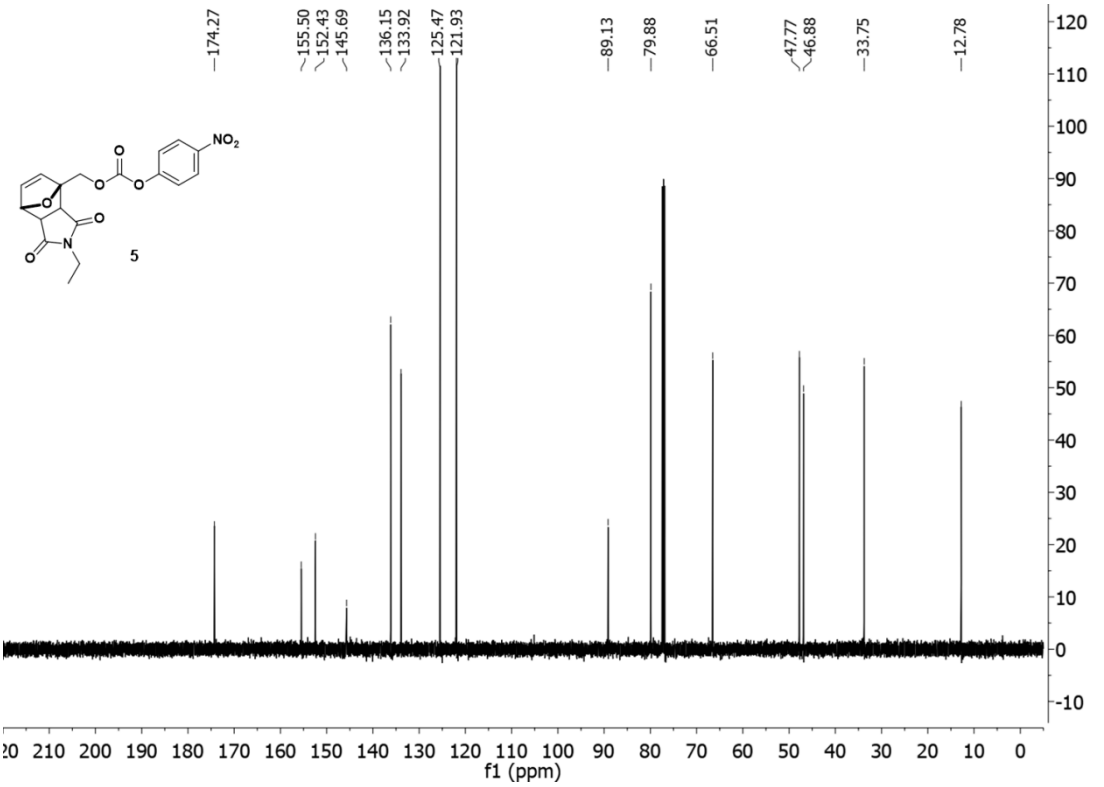
174.27
155.50
152.43
145.69
136.15
133.92
125.47
121.93
89.13
79.88
66.51
47.77
46.88
33.75
12.78
NO2
5
f1 (ppm)

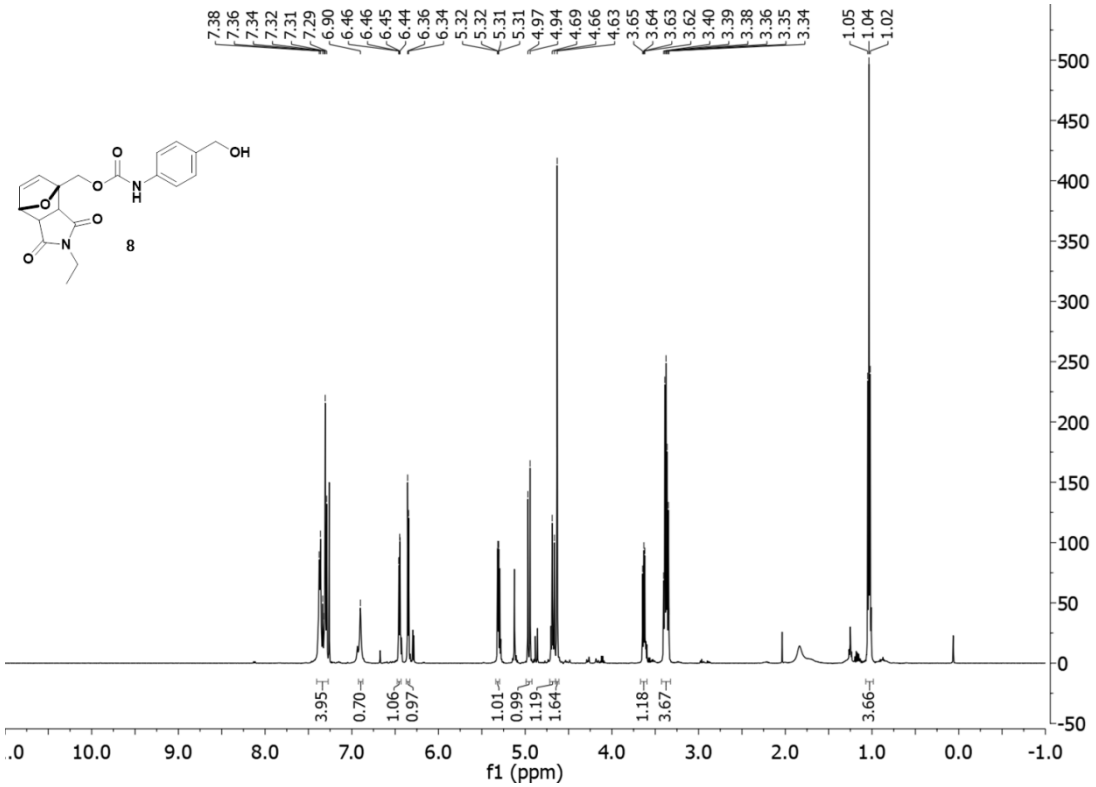
7.38
7.36
7.34
7.32
7.31
7.29
6.90
6.46
6.46
6.45
6.44
6.36
6.34
5.32
5.32
5.31
5.31
4.97
4.94
4.69
4.66
4.63
3.65
3.64
3.63
3.62
3.40
3.39
3.38
3.36
3.35
3.34
1.05
1.04
1.02
OH
O
N
H
O
O
O
N
8
3.95
0.70
1.06
0.97
1.01
0.99
1.19
1.64
1.18
3.67
3.66
f1 (ppm)

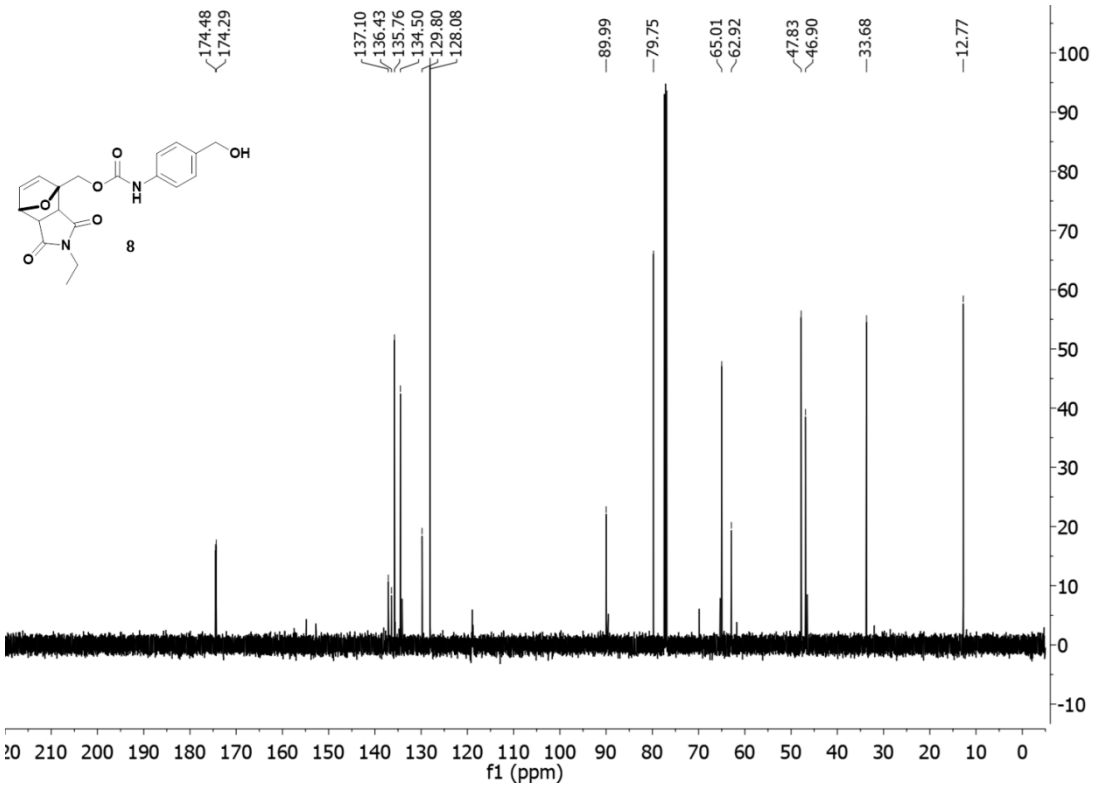
174.48
174.29
137.10
136.43
135.76
134.50
129.80
128.08
89.99
79.75
65.01
62.92
47.83
46.90
33.68
12.77
OH
O
N
H
O
O
O
N
8
f1 (ppm)

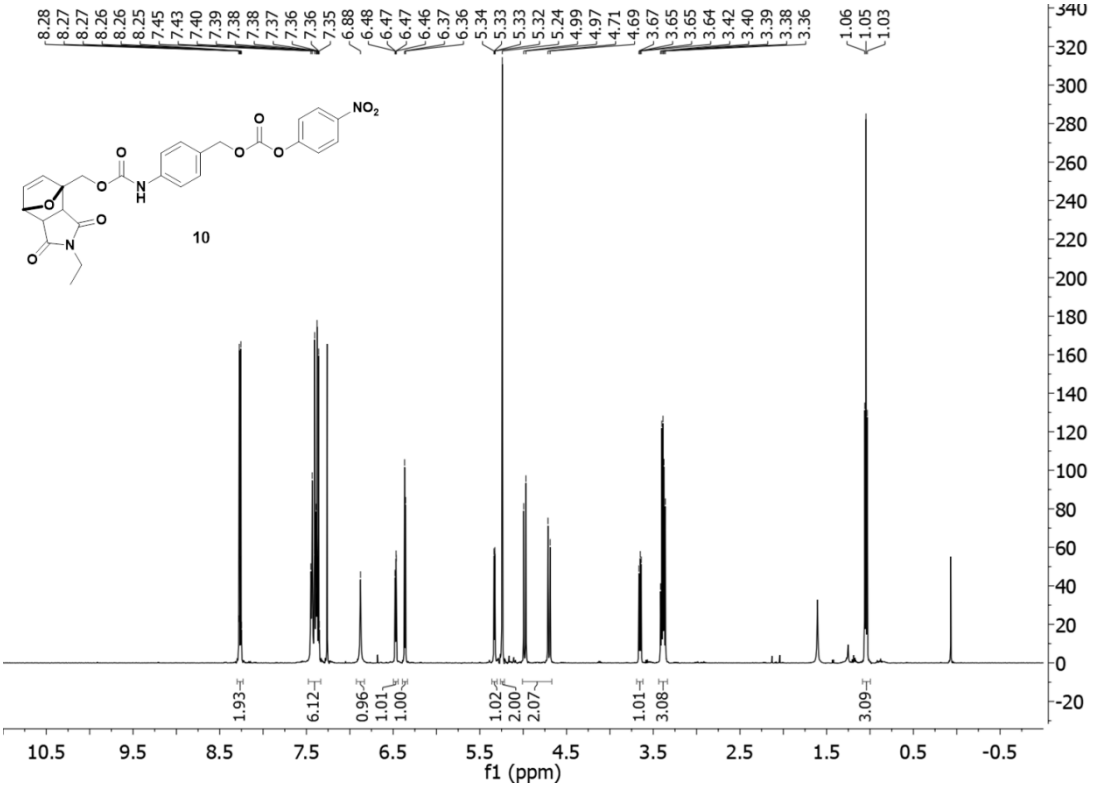
8.28 8.27 8.27 8.26 8.26 8.25 7.45 7.43 7.40 7.39 7.38 7.38 7.37 7.36 7.36 7.35 6.88 6.48 6.47 6.47 6.46 6.37 6.36 5.34 5.33 5.33 5.32 5.24 4.99 4.97 4.71 4.69 3.67 3.65 3.65 3.64 3.42 3.40 3.39 3.38 3.36 1.06 1.05 1.03
NO2
10
1.93 6.12 0.96 1.01 1.00 1.02 2.00 2.07 1.01 3.08 3.09
f1 (ppm)

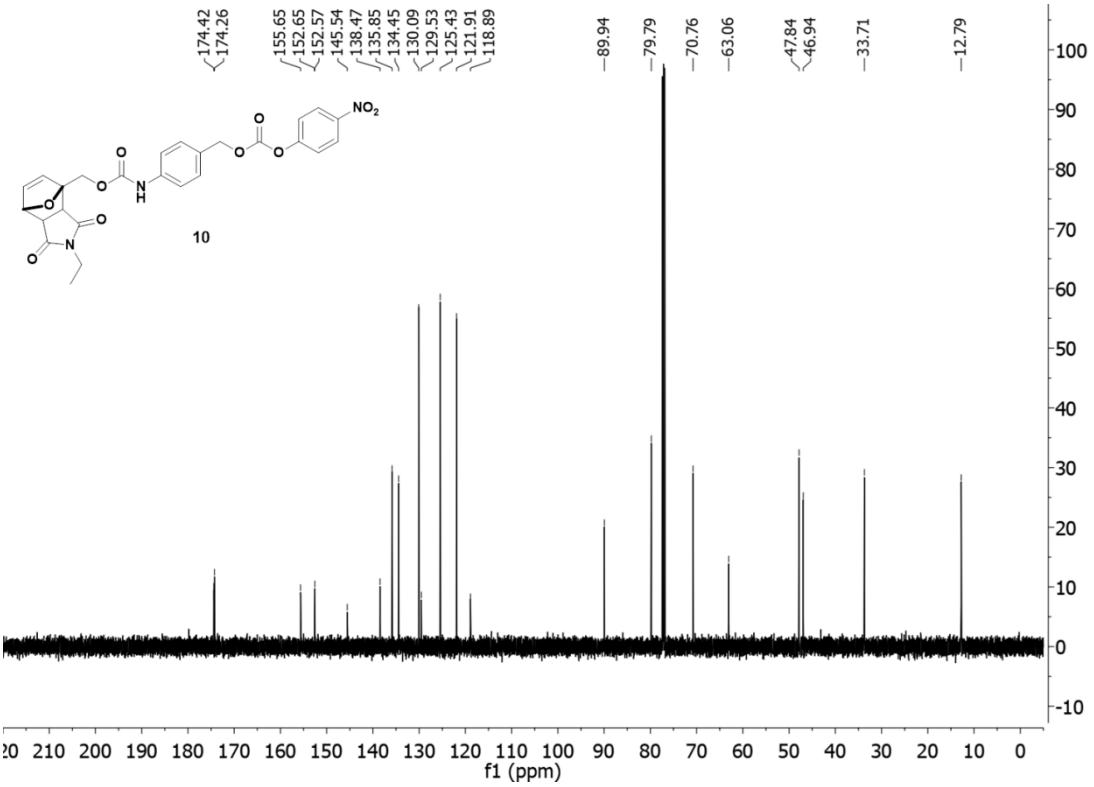
174.42 174.26 155.65 152.65 152.57 145.54 138.47 135.85 134.45 130.09 129.53 125.43 121.91 118.89 89.94 79.79 70.76 63.06 47.84 46.94 33.71 12.79
NO2
10
f1 (ppm)

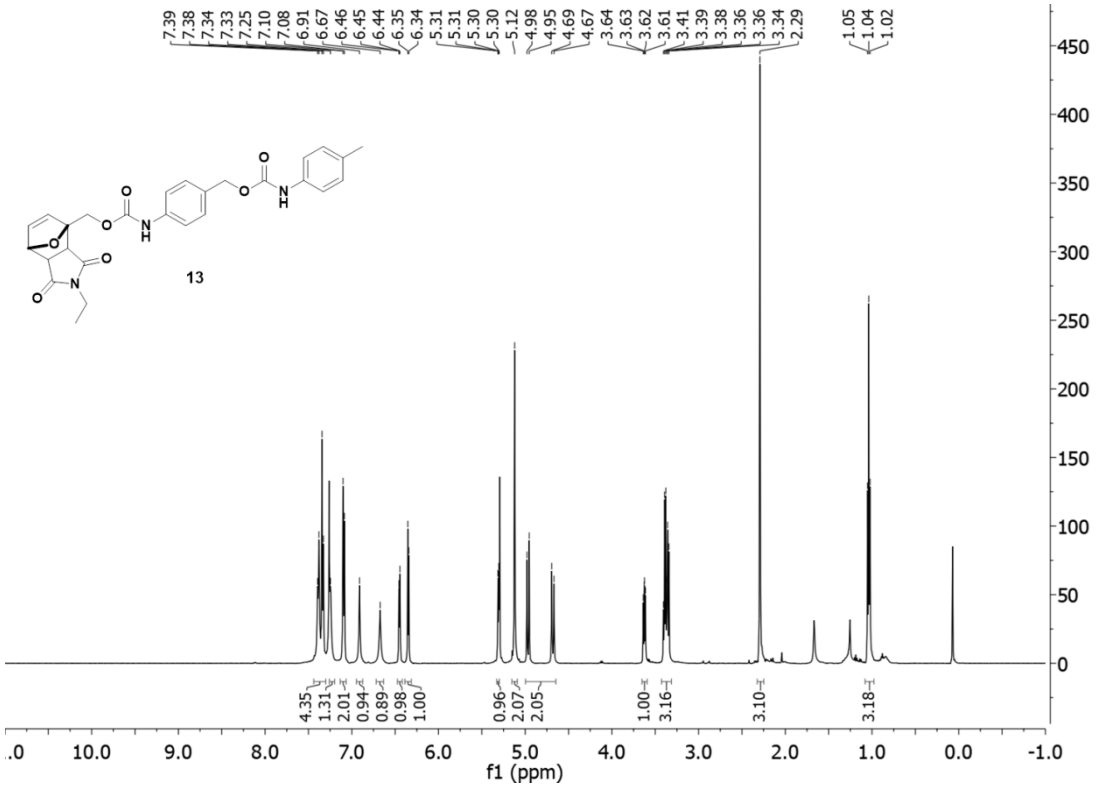
7.39
7.38
7.34
7.33
7.25
7.10
7.08
6.91
6.67
6.46
6.45
6.44
6.35
6.34
5.31
5.31
5.30
5.30
5.12
4.98
4.95
4.69
4.67
3.64
3.63
3.62
3.61
3.41
3.39
3.38
3.36
3.36
3.34
2.29
1.05
1.04
1.02
13
4.35
1.31
2.01
0.94
0.89
0.98
1.00
0.96
2.07
2.05
1.00
3.16
3.10
3.18
f1 (ppm)

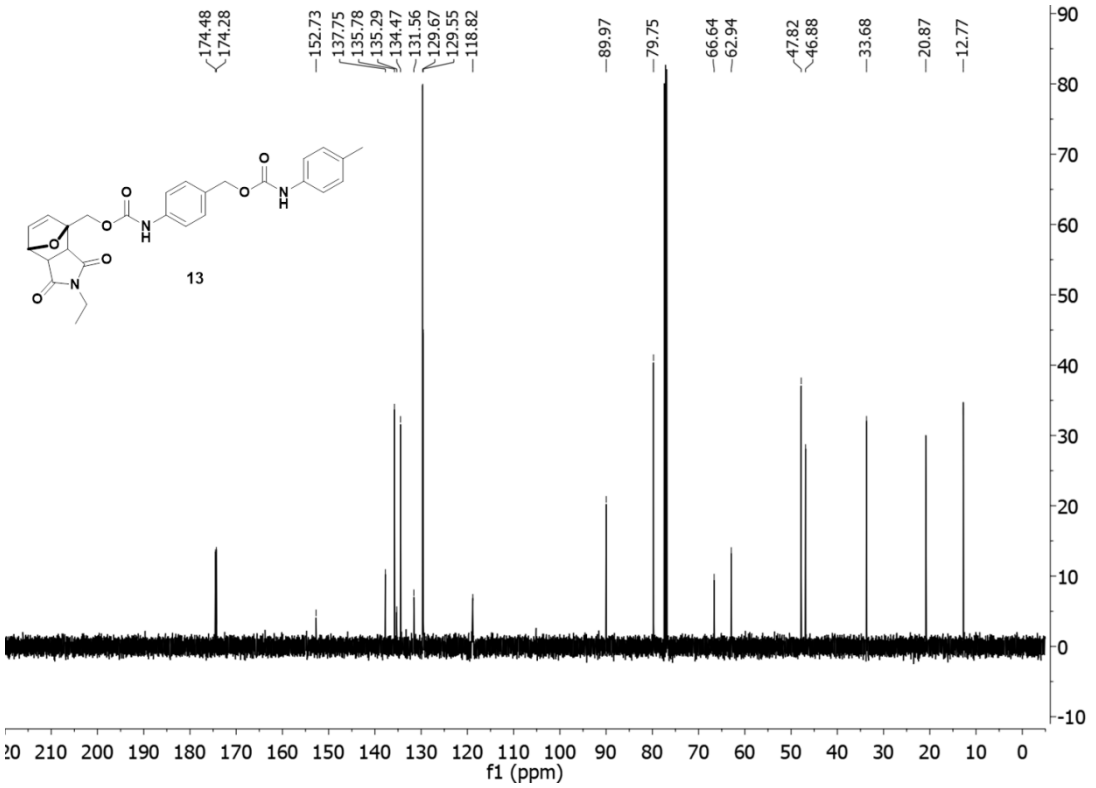
174.48
174.28
152.73
137.75
135.78
135.29
134.47
131.56
129.67
129.55
118.82
89.97
79.75
66.64
62.94
47.82
46.88
33.68
20.87
12.77
13
f1 (ppm)

3.6 References

1 Gisbert-Garzarán, M.; Lozano, D. Vallet-Regí, M.; Manzano, M. *RSC Adv.* **2016**, 7, 132–136.

2 Esser-Kahn, A. P.; Sottos, N. R.; White, S. R.; Moore, J. S. *J. Am. Chem. Soc.* **2010**, 132, 10266–10268.

3 Sagi, A.; Weinstain, R.; Karton, N.; Shabat, D. *J. Am. Chem. Soc.* **2008**, 130, 5434–5435.

4 Roth, M. E.; Green, O.; Gnaim, S.; Shabat, D. *Chem. Rev.* **2015**, 116, 1309–1352.

5 Peterson, G. I.; Larsen, M. B.; Boydston, A. J. *Macromolecules* **2012**, 45, 7317–7328.

6 DeWit, M. A.; Gillies, E. R. *J. Am. Chem. Soc.* **2009**, 131, 18327–18334.

7 DiLauro, A. M.; Lewis, G. G.; Phillips, S. T. *Angew. Chem., Int. Ed.* **2015**, 54, 6200–6205.

8 Seo, W.; Phillips, S.T. *J. Am. Chem. Soc.* **2010**, 132, 9234–9235.

9 de Groot, F. M.; Albrecht, C.; Koekkoek, R.; Beusker, P. H.; Scheeren, H. W. *Angew. Chem., Int. Ed.* **2003**, 42, 4490– 4494.

10 Li, S.; Szalai, M. L.; Kevwitch, R. M.; McGrath, D. V. *J. Am. Chem. Soc.* **2003**, 125, 10516–10517.

11 Fan, B.; Trant, J. F.; Gillies, E. R. *Macromolecules* **2016**, 49, 9309–9319.

12 Weinstain, R.; Baran, P. S.; Shabat, D. *Bioconjugate Chem.* **2009**, 20, 1783–1791.

13 de Groot, F. M.; Loos, W. J.; Koekkoek, R.; van Berkom, L. W.; Busscher, G. F.; Seelen, A. E.; Albrecht, C.; de Bruijn, P.; Scheeren, H. W. *J. Org. Chem.* **2001**, 66, 8815–8830.

14 Amir, R. J.; Pessah, N.; Shamis, M.; Shabat, D. *Angew. Chem., Int. Ed.* **2003**, 42, 4494–4499.

15 de Gracia Lux, C.; McFearin, C. L.; Joshi-Barr, S.; Sankaranarayanan, J.; Fomina, N.; Almutairi, A. *ACS Macro Lett.* **2012**, 1, 922–926.

16 Liu, G.; Wang, X.; Hu, J.; Zhang, G.; Liu, S. *J. Am. Chem. Soc.* **2014**, 136, 7492–7497.

17 Peterson, G. I.; Church, D. C.; Yakelis, N. A.; Boydston, A. J. *Polymer* **2014**, 55, 5980–5985.

18 Fan, B.; Trant, J. F.; Hemery, G.; Sandre, O.; Gillies, E. R. *Chem. Commun.* **2017**, 53, 12068–12071.

19 Yardley, R. E.; Gillies, E. R. *J. Polym. Sci., Part A: Polym. Chem.* **2018**, 56, 1868–1877.

20 McBride, R. A.; Gillies, E. R. *Macromolecules* **2013**, 46, 5157–5166.

21 Palmer, L. I.; Read de Alaniz, J. *Org. Lett.* **2013**, 15, 476– 479.

22 Fisher, D.; Palmer, L. I.; Cook, J. E.; Davis, J. E.; Read de Alaniz, J. *Tetrahedron* **2014**, 70, 4105–4110.

23 Palmer, L. I.; Read de Alaniz, J. *Angew. Chem., Int. Ed.* **2011**, 50, 7167–7170.

24 Veits, G. K.; Wenz, D. R.; Read de Alaniz, J. *Angew. Chem., Int. Ed.* **2010**, 49, 9484–9487.

25 Wenz, D. R.; Read de Alaniz, J. *Org. Lett.* **2013**, 15, 3250–3253.

26 Palmer, L. I.; Read de Alaniz, J. *Synlett* **2014**, 25, 08–11.

27 Piutti, C.; Quartieri, F. *Molecules* **2013**, 18, 12290– 12312.

28 Gandini, A. *Prog. Polym. Sci.* **2013**, 38, 1–29.

29 Taimoory, S. M.; Sadraei, S. I.; Fayoumi, R. A.; Nasri, S.; Revington, M.; Trant, J. F. *J. Org. Chem.* **2018**, 83, 4427– 4440.

30 Fan, B.; Trant, J. F.; Wong, A. D.; Gillies, E. R. *J. Am. Chem. Soc.* **2014**, 136, 10116–10123.

31 Zhuang, J.; Gordon, M. R.; Ventura, J.; Li, L.; Thayumanavan, S. *Chem. Soc. Rev.* **2013**, 42, 7421–7435.

32 Discekici, E. H.; St. Amant, A. H.; Nguyen, S. N.; Lee, I.-H.; Hawker, C. J.; Read de Alaniz, J. *J. Am. Chem. Soc.* **2018**, 140, 5009–5013.

33 Yu, D.; Thai, V. T.; Palmer, L. I.; Veits, G. K.; Cook, J. E.; Read de Alaniz, J.; Hein, J. E. *J. Org. Chem.* **2013**, 78, 12784–12789.

4 Utilizing Blocked Isocyanates for Controlled Polyurethane Formation

4.1 Abstract

Isocyanate chemistry is used prominently in polyurethane materials such as those used for solid propellant formulations. This chemistry is advantageous due to the high reactivity of isocyanates with polyols; however, this reactivity can also be detrimental. Not only are isocyanates rather toxic, but due to the high reactivity of the isocyanates, reaction rates and kinetics are difficult to control. Seen in literature and used widely in industrial patents is the concept of blocked isocyanates where a protecting group is used to alter the isocyanate functionality that can later be thermally removed and allow for the isocyanate's reactivity to be utilized. Not only can altering the isocyanate and the blocking group allow for more tunability in cure rates and reaction kinetics, these alterations can be utilized to adapt the chemistry to the desired application needs as we aim to push polymer binder materials into the realm of 3D printing processes.

4.2 Introduction

Isocyanate functionalized compounds have driven the field of polyurethanes and polyurethane formation. Polyurethanes derived from isocyanates are found in a wide range of applications including automobile primers, automobile topcoats, sealants, foams, insulation, adhesives, and polymer binders.[46] (Figure 4.1) Utilizing isocyanates for the formation of polyurethanes is quite common due to the high reactivity and fast kinetics that isocyanates offer when in the presence of a nucleophile, typically a polyol. The variety of

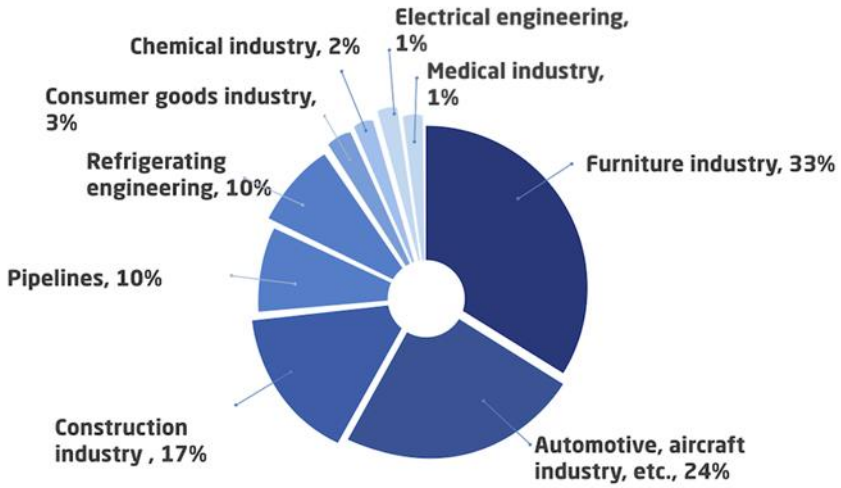

Figure 4. 1

World-wide isocyanate consumption per industry according to the Engineering Chemical Technological Center (ECTC). Engineering Chemical Technologies Center, 2019. *Global Isocyanate Market*. [image] Available at: <https://ect-center.com/blog-en/global-isocyanate-market> [Accessed November 2020].

applications utilizing isocyanates is possible due to the diversity in isocyanate structures—di- or tri-functional—as well as their reactivity. The kinetics between isocyanates and polyols offer formation of a library of polyurethanes. Although this reactivity is advantageous for the formation of polyurethanes and their many uses, this same reactivity can be detrimental as well. Not only are isocyanates found to be highly toxic, but their kinetics can make these materials unfavorable due to the lack of controllability and selectivity over the reaction.[35] Isocyanates can react with themselves creating dimers and trimers which leads to decreased shelf life and usability.[35]

The application of isocyanates in materials we find of interest is their use in the formation of polymer binders. Specifically, we want to study polymer binder materials that are commonly used in energetic materials, specifically solid rocket propellants.[36,88] Typically, polymer binders are made of a polyol, isocyanate, catalyst, and plasticizer while containing a high level of solids loading (80-90 wt%) of oxidizers and energetics.[88] Since

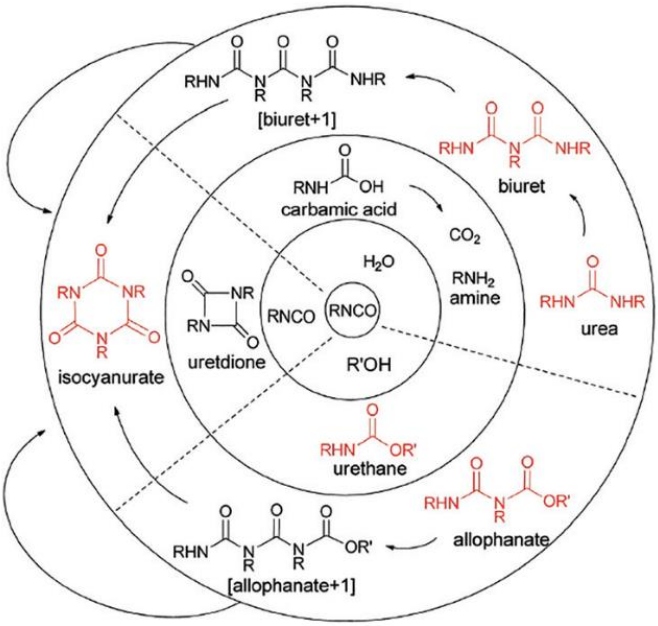

Figure 4. 2

Structural representation of isocyanate reactivity with water, other isocyanates, and alcohols. Reproduced from Reference #6 with permission from the Royal Society of Chemistry.

the 1940's, the most utilized polyol for binder materials is hydroxyl terminated polybutadiene (HTPB).[89] HTPB has become the most extensively studied material due to its many advantages including that HTPB has excellent mechanical properties to allow for its use with a wide range of temperatures while maintaining good aging qualities.[88] While utilizing the well-studied components and formulations of polymer binders, there is a new interest in transferring this chemistry to 3D printing processes. Currently the classic batch processing for curing of polymer binders is not feasible because of the longer working times needed. Batch processing requires time for formulation mixing, degassing, and mold pouring, whereas the ideal material for 3D printing would allow for little to no reactivity at the print head while offering near instant curing into a solid structure that is capable of holding shape once printed. In order to overcome these challenges, we are looking to adapt the current polymer binder formulations to offer more controllability over the material's curing and reactivity. Our work will focus on the

design and development of a new class of polymer binders that will provide opportunities in 3D printing for applications such as propellants and energetics.

Solid propellant formulations generally rely on the high reactivity of isocyanate chemistry and polyols to drive polyurethane formation. Control over polyurethane formation for these systems has mainly focused on temperature, time, stoichiometry, and catalyst activity to control reaction rates and kinetics. However, for many applications such as 3D printing it is necessary to delay the desired isocyanate-hydroxyl reactions and develop on-demand curing. Although predominantly used in industry to eliminate the isocyanate moisture sensitivity problem,[43] the use of "blocked", or "masked" isocyanates holds tremendous potential for 3D printing rocket propellants. Blocked isocyanates are a class of materials resulting from the addition of a protecting group on the isocyanate functionality. By using a nucleophilic compound containing an active hydrogen, the high reactivity of the isocyanate is blocked, and a new functional group is present (Scheme 4.1). The resulting functional group is typically a carbonate or carbamate by reaction with a hydroxyl or amine containing compound, respectively. Through a facile synthesis, an isocyanate can have a range of blocking groups including phenols,[44] anilines,[4543] oximes,[43] imidazoles,[43] pyrazoles,[43] and more.[43] Blocked isocyanates have gained interest due to the many advantages they offer. Not only does blocking the isocyanate diminish the free isocyanate's toxicity, but the pot life of the isocyanate also increases making it inert at room temperature for long-term storage while still being able to access the desired isocyanate reactivity at elevated temperatures.

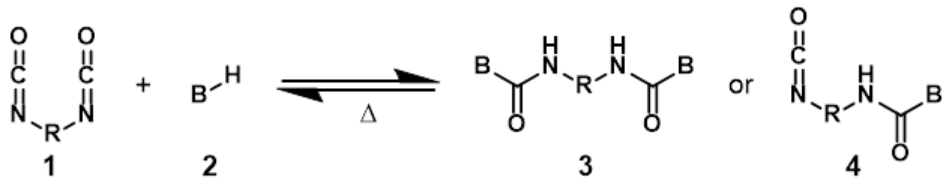

Scheme 4. 1

General scheme for the synthesis of blocked isocyanates.

Taken together, blocked isocyanates provide a synthetic handle for controlled solid propellant formulations and open up new opportunities for additive manufacturing. For solid rocket propellant applications, which contain energetic materials, it is necessary to use a blocking agent that can be removed to reveal the reactive isocyanate functionality at temperatures less than 80 ºC. It is widely accepted that an aromatic blocked isocyanate, such as electron deficient phenols or anilines, undergo deblocking at lower temperatures compared to an aliphatic blocked isocyanate, as a consequence of both steric and electronic effects. For example, Nasar and Kalaimani demonstrated that deblocking temperature of phenol (130 ºC) can be lowered to 85 ºC (*o*-chlorophenol) by incorporating electron withdrawing chloro-substituent into the *ortho* position.[44] However, the lower deblocking temperature is not simply an electronic effect, as incorporating the same electron withdrawing chloro-substituent into the *para* position only lowers the deblocking temperature by 10 ºC (deblocking temperature of *p*-chlorophenol is 120 ºC). As a result of numerous studies, it is possible to tailor the deblocking temperature simply by selecting the correct blocking group.

Critical to the development of blocking groups specifically for 3D printing of solid rocket propellants will be the deblocking kinetics. Hot-stage FTIR spectroscopy is a straightforward and readily available analytical tool for studying deblocking kinetics of -NCO functional groups. The IR spectra exhibit strong bands near ν = 2270 cm^{-1} attributed to free N=C=O, the

appearance of which can be compared to the disappearance during deblocking of the bands associated with the blocked isocyanate (C=O between ν = 1640 cm^{-1} to ν = 1720 cm^{-1} and N–H band at approximately ν = 1535 cm^{-1} and at 3300 cm^{-1}). Analogous to tuning the deblocking temperature, the rate of deblocking can also be readily tuned. However here, evidence supports that electronics is the dominate effect in controlling deblocking rate, with electron withdrawing groups leading to increased rates. While studying the kinetics of phenol-based blocking groups, Nasar and Kalaimani, observed that the reaction rates increased with the addition of an electron withdrawing group and rates decreased with electron donating groups as substituents.[44] By running deblocking studies at 120 °C, 130 °C, and 140 °C, activation energies were collected for various phenol-based blocking groups on toluene diisocyanate. Phenol as a blocking group gives an activation energy of 50.05 kJ mol^{-1}. With the addition of a chloro-substituent in the *ortho* position, this activation energy is decreased to 48.23 kJ mol^{-1}, whereas a methoxy-substituent in the same position causes the activation energy to significantly increase to 57.98 kJ mol^{-1}.[44] These activation energies translate to *o*-chlorophenol having a reaction rate twice that of phenol supporting the idea that electronics play a crucial role in designing blocking groups to have tunable and controlled reactivity.

Comparing both the kinetics of the forward blocking reaction with the deblocking reaction there is an overlapping temperature range where both blocking and deblocking can occur. This range, the equilibrium temperature range (ETR), can be used to aid in the determination of the reactivity of the blocked isocyanates (Figure 4.3). For example, *p*-chlorophenol has an ETR of 80-90 °C. This narrow range shows that any temperature below 80 °C there will be no reaction of the blocked isocyanate, but above 90 °C the only reaction occurring will be deblocking the isocyanate. This control will be advantageous for additive manufacturing due to the narrow

ON/OFF curing window that can be readily accessed by heating or cooling a material during processing.

Initial studies on blocked isocyanates by the Air Force in 1986 has demonstrated that (1) the facile synthesis of blocked isocyanates—blocked isocyanates can be prepared on scale in 1-step by reacting desired isocyanate with corresponding blocking group enabling a library of blocked isocyanates to be accessed,[46,90] (2) blocked isocyanates with a range of structures can be used to cure both carbon filled and non-carbon filled gumstocks on-demand,[49] (3) temperature can be used to "trigger" on-demand curing, with rapid polyurethane formation occurring at 145 ºF but not at 130 ºF.[49] Herein, we discuss the current investigation of the development of blocked isocyanates (BICs) for low temperature deblocking to be used in 3D printing of polymer binders for energetic materials.

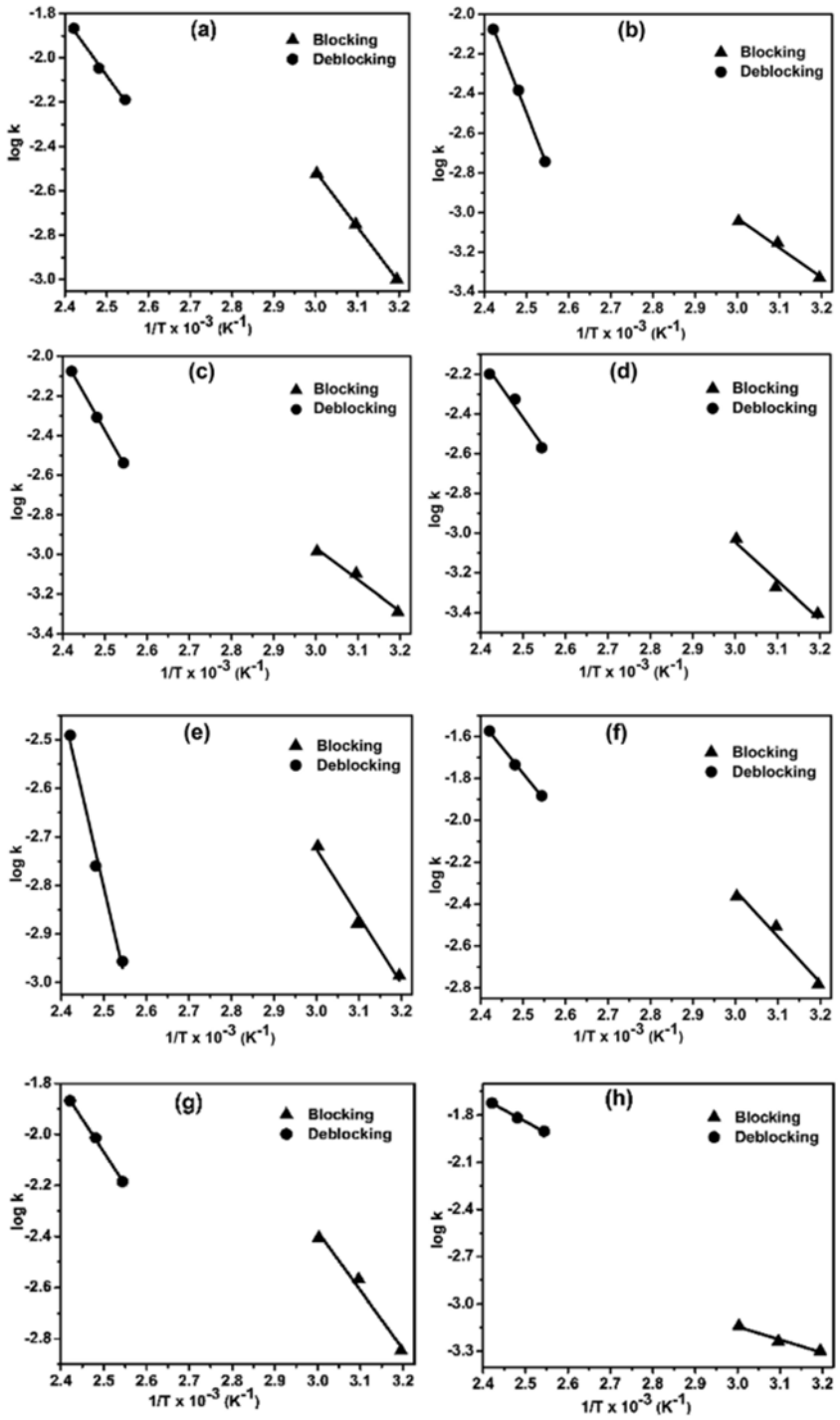

Figure 4. 3

Arrhenius plots of Nasar and Kalaimani's forward and reverse reactions of blocked polyisocyanates with blocking agents: a) phenol, b) o-cresol, c) p-cresol, d) o-methoxyphenol, e) p-methoxyphenol, f) o-chlorophenol, g) p-chlorophenol, and h) methyl 4-hydroxybenzoate. Reprinted from Reference #7 with permission from the Royal Society of Chemistry.

4.3 Results and Discussion

Prior to developing a library of BICs, we set forth in studying the kinetics and reactivity of isocyanate with our polyol, HTPB. Due to the distinct N=C=O peak visible via FTIR, we were able to monitor the reaction of 2,4-toluene diisocyanate (TDI) with HTPB in the presence of our tin catalyst (DBTL). As seen in Figure 4.4, the isocyanate functionality is present in our initial measurements near $\nu = 2300\ cm^{-1}$. This peak then decreases in intensity as the isocyanate readily reacts with the hydroxyl groups of our polymer network. We studied this reactivity at ambient temperatures as well as elevated temperature to begin understanding the curing kinetics expected once we incorporate BICs. In our room temperature sample, we see significant decrease in the isocyanate presence after 60 minutes; however, at 70 °C (158 °F), we see complete conversion of the isocyanate within 15 minutes. As expected, the isocyanate functionality is very reactive with hydroxyl groups and we hypothesized that as we begin to develop BICs and study their kinetics, that our rate limiting reaction with be the deblocking step allowing for this quick curing with HTPB. We then investigated how this reactivity would change if our isocyanate is in the presence of a competing nucleophile—such as the blocking group once removed. Via FTIR we again study the conversion of our isocyanate peak. Unfortunately, this technique does not differentiate between which nucleophile our isocyanate is reacting with, but we were able to discover a change in the conversion kinetics. When we

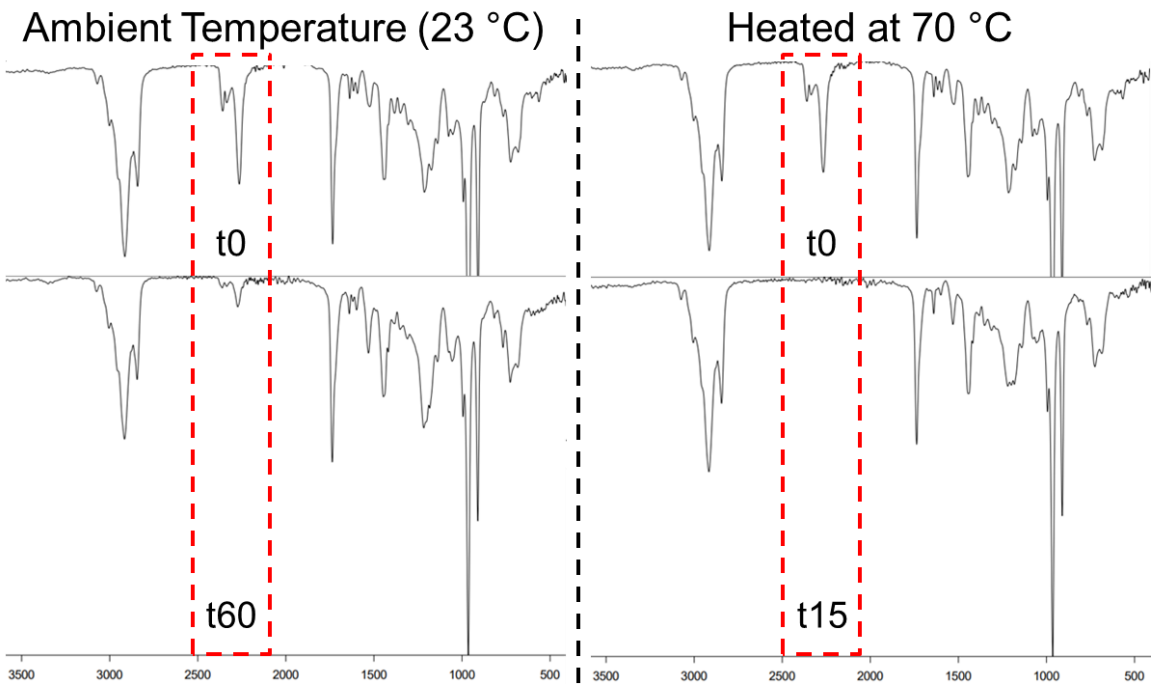

Figure 4. 4

FTIR spectra monitoring the consumption of isocyanate within a polymer binder formulation containing HTPB, TDI, catalyst, and plasticizer at ambient temperature and elevated temperature.

studied the same network as before, with added 2,4-dinitrophenol (DNP) as the "removed" blocking group, we observed that at ambient conditions the network still shows a significant amount of isocyanate still present after 90 minutes and at elevated temperatures (70 °C) it required 60 minutes before full conversion was achieved. Seeing as how the presence of a blocking group altered the isocyanate reactivity, we wanted to begin the synthesis of various BICs to begin studies on how the reversible nature of these materials can cause fluctuations in the material kinetics.

The synthesis of blocked isocyanates is a generally a straightforward, one-step, facile synthesis that utilizes the readily reactive isocyanate functionality. Scheme 4.2 shows the diversity available in isocyanate synthesis. Due to the common use of these materials in industry and polymer binders, our studies focused on BICs formed from three diisocyanates:

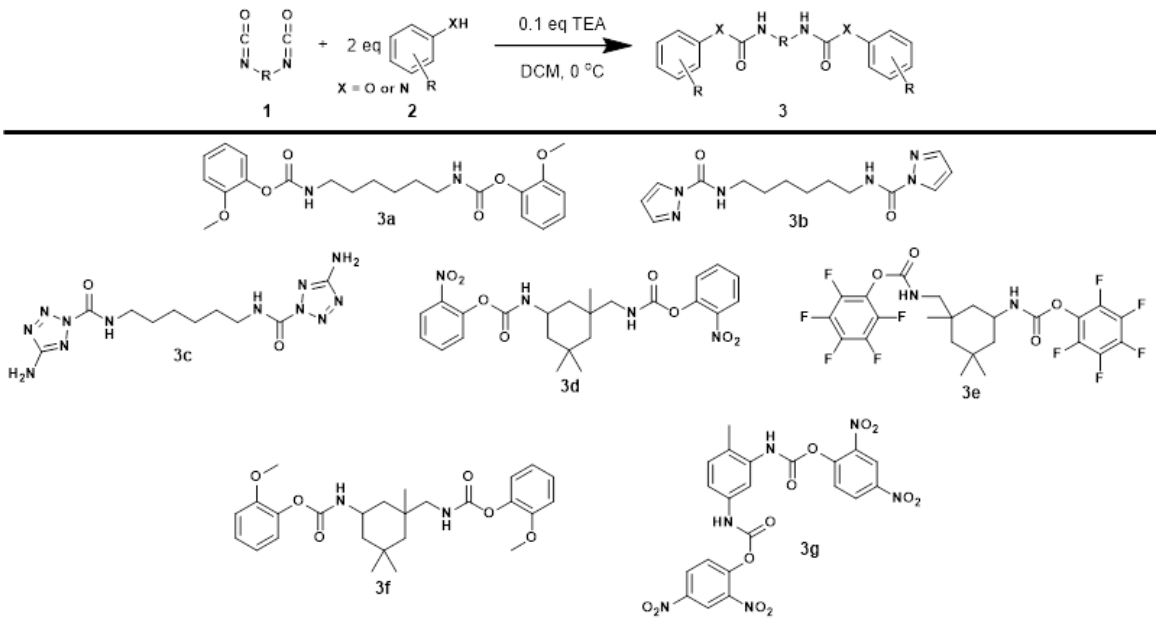

Scheme 4. 2

Substrate scope of di-blocked isocyanates (dBICs) utilizing a one-step reaction.

hexamethylene diisocyanate (HMDI), isophorone diisocyanate (IPDI), and 2,4-toluene diisocyanate (TDI). Our first approach for BICs was studying di-blocked materials to remove all isocyanate reactivity and offer the most control over the release and curing with HTPB. Utilizing ^{1}H NMR, we test the deblocking ability of these materials via a trapping agent. For these studies we used benzyl alcohol as a trapping agent for once the original blocking group is removed from our isocyanate. Benzyl alcohol was chosen due to the significant shift seen in the benzylic protons between the unreacted alcohol and once the alcohol has reacted with our free isocyanate. Initial studies started with **3a**, **3b**, and **3c** due to their use of the same isocyanate, HMDI. Instantly we learn that BICs can have solubility issues as these HMDI derivatives cannot be used in traditional organic solvents but rather this deblocking and trapping experiment was completed in DMSO-d_6. In the presence of 2 equivalents of benzyl alcohol and tin catalyst, the BIC is subjected to heating overnight. For **3a**, it was determined

that the deblocking temperature was 100 °C and this afforded 40% of the BIC to be trapped by benzyl alcohol after 18 hours of heating. **3b** and **3c** were heated at 120 °C for 18 hours affording 23% and 10% trapped isocyanate, respectively. The slow deblocking and trapping taking place with **3b** and **3c** indicate that in order to achieve near instant curing for future 3D printing, the temperatures used must be increased past the limits of polymer binder processing. The 40% trapped isocyanate obtained by **3a** indicates that for quick curing we would also need higher temperatures unless a slow cure was desired to maintain temperatures for polymer binder processing. Continuing this study for **3d**, **3e**, and **3f** we began looking at the reactivity offered from IPDI derived BICs. These materials were all now soluble in traditional solvents and thus the trapping experiments were completed in MeCN-d_3. After being subjected to 80 °C for 2 hours, **3d** and **3e** afforded 78% and 75% of the sample trapped by benzyl alcohol, respectively. This successful release of material pushed the study to lower temperatures (60 °C) where we see **3e** exhibit 36% trapped after 2 hours and 69% after 24 hours of heat. **3d** showed great promise with 52% trapped within 2 hours of heating at 60 °C and 75% after 24 hours. With the ability to achieve deblocking at these temperatures we continued with control studies to ensure the stability of **3d** and **3e**; unfortunately, after both materials were left in ambient conditions for 96 hours, each compound observed 40% of the material reacted with benzyl alcohol. This lack of stability at room temperature lends us to believe that with an IPDI derived blocked isocyanate, we may need a blocking group containing more electron donating character, leading us to **3f**. When left heating at 70 °C for 48 hours, we observed 36% trapping. Although this reactivity is lower than previous materials, we also see that when **3f** is left at ambient conditions for 48 hours there is less than 1% of the BIC trapped by benzyl alcohol (Figure 4.5). These

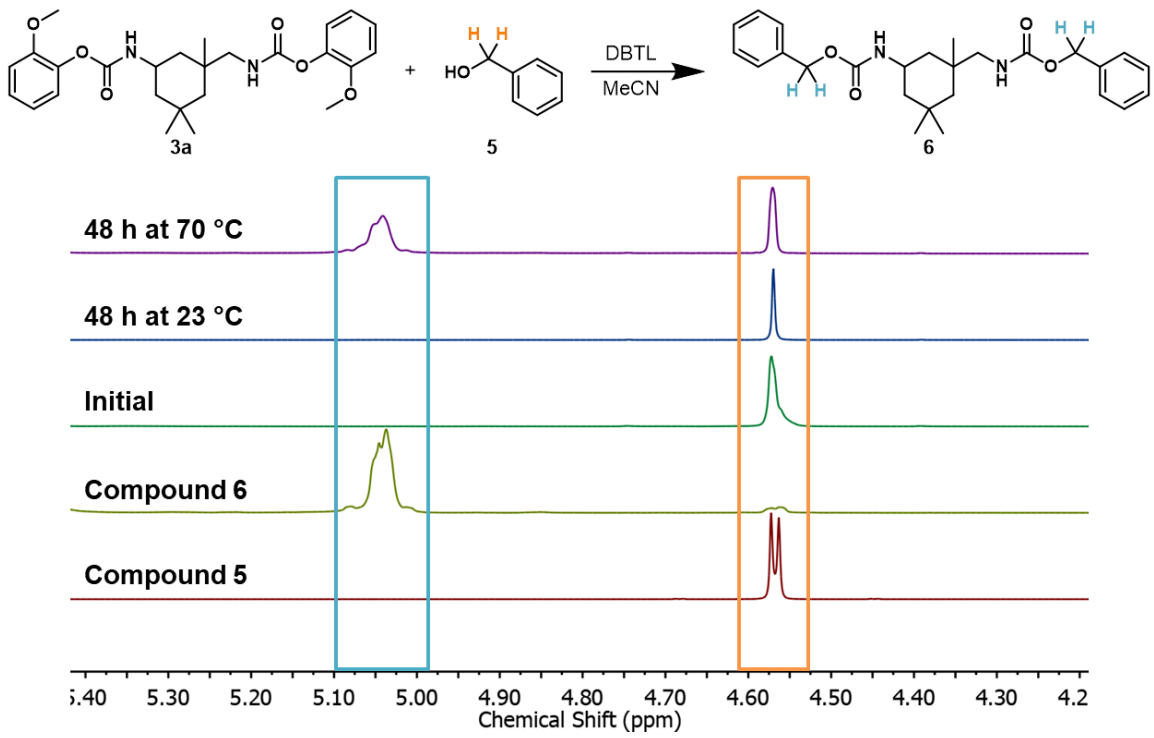

Figure 4. 5

^{1}H NMR monitoring the reactivity of 3a with the benzyl alcohol 5 trapping agent at 23 °C and 70 °C over 48 hours.

promising results from **3f** has led us to begin testing our BIC materials in HTPB polymer binder formulations; however, as we were studying dBICs, we learned of previous work done that utilizes mono-blocked materials within propellant formulas.

Previously we only considered the full blocking of the isocyanate functionality in order to have control over the reaction kinetics. By investigating mono-blocked isocyanates (mBICs) we open the ability to tolerate some "premature" reactions to take place between the free isocyanate site and the hydroxyl groups of the polyol. By having theoretically 50% of our hydroxyl/isocyanate reactions taking place prior to triggering, we can have a partially cured network that can decrease the gel point time; this potential would be advantageous as we bring these materials into 3D printing. We decided that as we worked with di-blocked

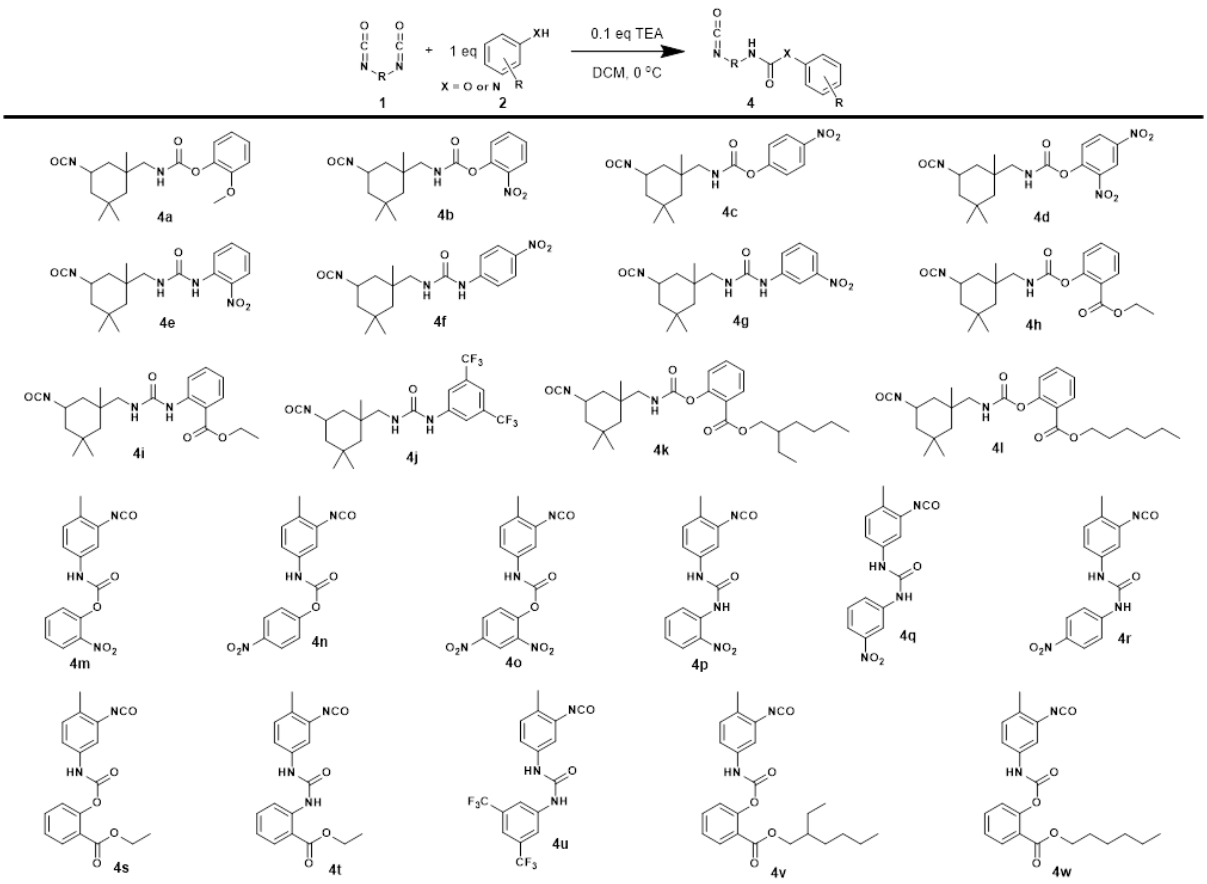

Scheme 4. 3

Mono-blocked isocyanate (mBIC) substrate scope showcasing the ease of synthesis and functional group availability.

isocyanates (dBICs) we would start diving into the option of mBICs. By altering the stoichiometry of our BIC synthesis, we were easily able to access a library of mBICs offering different reactivity (Scheme 4.3). The first mBIC we chose to study was **4a** to compare its reactivity with the success of the di-blocked derivative. Undergoing the same trapping experiment with benzyl alcohol, **4a** shows 59% trapped after 48 hours at 70 °C while at ambient temperature we observe 32% trapped. Trapping at room temperature is anticipated with our mBIC as we have one available reactive isocyanate site to allow for up to 50% trapping without

heat. This combination of IPDI and 2-methoxyphenol has proven to be a plausible route for incorporating BICs into polymer binders.

The next step into moving these materials into formulations and 3D printing is to begin testing the ability for curing to take place. The range of deblocking temperatures for our materials spans 60-120 °C; due to the energetic materials in polymer binders we want to focus on the BICs that activate at lower temperatures of 60-70 °C. From work previously reported by the Air Force Office of Scientific Research, we synthesized **4o** as it has a deblocking temperature of 65 °C and the report used this mBIC in known polymer binder formulations.[49] This material was added to our library of BICs and would become a key material in our future work. From our library of BICs, we began studies with **3f**, **4a**, **3g**, and **4o** in HTPB formulations to investigate how the deblocking and curing reactions occur in HTPB formulations. These HPTB formulations are based off currently used polymer binder networks containing HTPB, an isocyanate source, tin catalyst (DBTL), and a plasticizer (bis(2-ethylhexyl) adipate). By altering the ratios of these components, we expect to observe changes in material properties and curing kinetics. Based off Figure 4.4, we know that isocyanates readily react with HTPB at ambient and elevated temperatures, thus our curing rates will mostly depend on the deblocking of the BICs. Unfortunately, our BICs are generally insoluble in the formulations meaning we not only are relying on our deblocking kinetics to allow for curing, but dispersion within the polymer network may also influence our curing abilities. Due to the ease of monitoring **3f** and **4a** via ^{1}H NMR, our first attempts at polymer curing were completed with these materials. Two sets of samples were prepared in dram vials to obverse reactivity at ambient and elevated (70 °C) temperatures. **3f** and **4a** were quite soluble in the formulations which we hypothesized would aid in the uniform

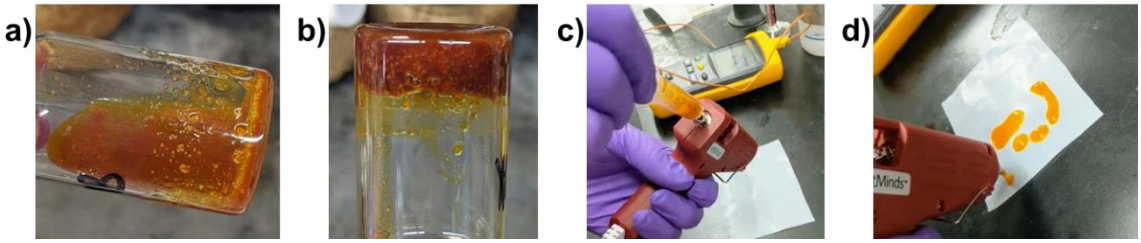

Figure 4. 6

a) Binder formulation containing 4o at ambient temperatures; b) Binder formulation with 4o after heating at 70 °C for 1 hour; c) adapted hot glue gun apparatus with syringe of binder formulation; d) attempt at direct ink writing with binder formulation.

distribution of the isocyanate as it is revealed. As anticipated, over two days the non-heated samples showed no progress towards a gel point or curing; however, we unfortunately did not detect any reaction taking place in our heated samples either. After 48 hours at 70 °C, the samples of **3f** and **4a** were removed from heat to ensure we were not facilitating any reverse reactions between the released IPDI and HTPB. After cooling to ambient temperature, there was no gelation taking place in the samples containing **3f** and **4a.** With these formulations not working, we moved forward with testing **3g** and **4o**. Not only are we now testing the release of a different isocyanate source, but **3g** and **4o** are not soluble within our HPTB formulations. Previously we predicted solubility would aid in the curing process but with these samples we now believe that the presence of an insoluble BIC and thus insoluble blocking group is advantageous. All the isocyanates studied (HMDI, IPDI, and TDI) are liquids without blocking groups present and thus are easily soluble within HTPB and readily reactive. With an insoluble blocking group, we can eliminate the reformation of the BIC due to the isocyanate being easily dispersed within the HTPB and facilitating the curing process. While observing **3g** at room temperature we see no reaction taking place, but with **4o** we begin to see an increase in the formulation viscosity as the available isocyanate begins to react with HTPB. At 70 °C, **3g** continues to show no curing, but **4o** shows curing within an hour for one of the formulations

(Figure 4.6). This specific formulation contains the highest volume of plasticizer that can allow for more dispersion of the isocyanate to assist the curing of HTPB with TDI. With this successful cure of one formulation, we wanted to quickly test out the possibility of this material being pushed forward into 3D printing processes.

Of the 3D printing pathways, we believe that direct ink writing offers the most flexibility in terms of shapes and printing layers of an object. Direct ink writing also utilizes a heated print head that will activate the BIC as the material is being extruded. For our first attempts at any printing, we developed a handheld writing/printing unit using a store-bought hot glue gun (Figure 4.6). By reengineering the heating component and material pathway, we were able to insert a metal syringe into the glue gun that would connect to a syringe containing the HTPB/BIC formulation. Although we were able to extrude material that upon cooling was cured and could be handled, the hot glue gun's apparatus heats up to temperatures higher than we need for **4o** and thus we had curing taking place within the syringe. We believe that if we can control the temperature at which the hot gun operates that this formulation containing **4o** would be a workable starting point for moving BICs into 3D printing of polymer binders.

4.4 Future Work

Studying the reactivity of the blocked isocyanate materials is just the start of developing new polymer binder formulations for use in 3D printing. Although we were able to synthesize a library of dBICs and mBICs, we believe there are still studies to be done before any further printing attempts can be made. Due to the specific needs of polymer binders, future work with BICs would include investigating how the incorporation of these new isocyanate sources affects the cured HTPB's physical properties. Experiments to probe changes in modulus and

stress/strain relationships will be crucial in creating materials that maintain the integrity already achieved by current polymer binders. While working with collaborators we can obtain samples of the current polymer binder networks for test for baseline measurements and begin to investigate the most important properties to maintain. Once material property measurements are completed, we can begin designing the optimal route for transforming our formulation into a 3D printing accessible material.

4.5 Conclusion

In conclusion, we have created a library of blocked isocyanates via a facile, one-step synthesis that includes new low temperature activated materials. These low temperature BICs are ideal for polymer binder materials due to the sensitive energetic materials typically held within the cured HTPB matrix. Blocked isocyanates are the next step in moving polymer binders into 3D printing processes due to their decreased toxicity and extended pot life. The ability to mix binder formulation prior to any curing taking place will facilitate homogeneous curing. As we continue to investigate the reaction kinetics and effects of BIC on the binder's physical properties, we will be able to push polymer binders into the field of user-friendly point-of-use 3D printing.

4.6 Experimental

4.6.1 Materials and Methods

Unless stated otherwise, reactions were conducted in oven dried glassware under an atmosphere of N_2 using reagent grade solvents. All commercially obtained reagents were used as received. Reaction temperatures were controlled using a Heidolph temperature modulator,

and unless otherwise, reactions were performed at room temperature (RT, approximately 23 °C). Thin-layer chromatography (TLC) was conducted with E. Merck silica gel 60 F254 pre-coated plates (0.25 mm) and visualized by exposure to UV light (254 nm) or stained with potassium permanganate or p-anisaldehyde. Flash chromatography was preformed using normal phase silica gel (60 Å, 230–240 mesh, Geduran®). ^{1}H NMR spectra were recorded on Varian Spectrometers (at 400, 500, and 600 MHz) and are reported relative to deuterated solvent signals. Data for ^{1}H NMR spectra are reported as follows: chemical shift (δ ppm), multiplicity, coupling constant (Hz) and integration. ^{13}C NMR spectra were recorded on Varian spectrometers (at 100, 125, and 150 MHz). Data for ^{13}C NMR spectra are reported in terms of chemical shift. IR spectra were recorded on a Perkin Elmer Spectrum 100 FTIR and a Bruker Alpha FTIR and are reported in terms of frequency of absorption (cm^{-1}). High resolution mass spectra were obtained from the UC Santa Barbara Mass Spectrometry Facility.

4.6.2 Experimental Procedures and Data

4.6.2.1 Synthesis Procedures

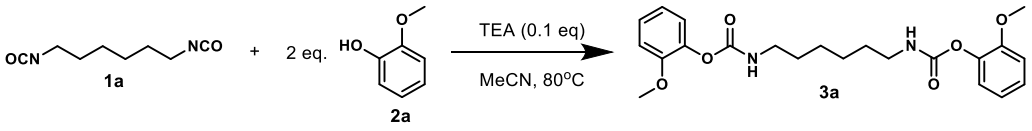

Bis(2-methoxyphenyl) hexane-1,6-diyldicarbamate (3a): To a 50 mL round bottom flask is added 2-methoxyphenol (1.43 mL, 12.8 mmol, 2.0 eq) in acetonitrile (20 mL). Triethylamine (0.09 mL, 0.64 mmol, 0.1 eq) is added to the stirring solution. Lastly, hexamethylene diisocyanate (1.03 mL, 6.4 mmol, 1.0 eq) is added to the reaction. The reaction is left to stir at

reflux overnight. Upon cooling, a precipitate forms. This solid is collected via vacuum filtration and dried to afford PDT (2.4 g, 89%).

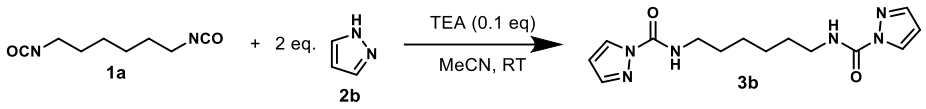

N,N'-(hexane-1,6-diyl)bis(1H-pyrazole-1-carboxamide) (3b): To a 50 mL round bottom flask is added pyrazole (0.85 g, 12.4 mmol, 2.0 eq) in acetonitrile (20 mL). Triethylamine (0.09 mL, 0.62 mmol, 0.1 eq) is added to the stirring solution. Lastly, hexamethylene diisocyanate (1.0 mL, 6.2 mmol, 1.0 eq) is added to the reaction. The reaction is allowed to stir for 1 hour at room temperature. A precipitate formed and was collected via vacuum filtration and dried to afford solid PDT (1.68 g, 89%).

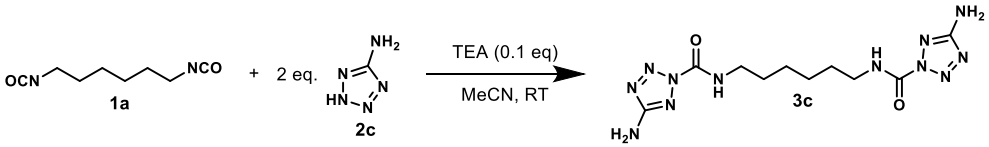

N,N'-(hexane-1,6-diyl)bis(5-amino-2H-tetrazole-2-carboxamide) (3c): To a 50 mL round bottom flask is added 2-aminotetrazole (0.53 g, 6.2 mmol, 2.0 eq) in acetonitrile (10 mL). Triethylamine (0.04 mL, 0.31 mmol, 0.1 eq) is added to the stirring solution. Lastly, hexamethylene diisocyanate (0.5 mL, 3.1 mmol, 1.0 eq) is added to the reaction. The reaction is allowed to stir for 15 minutes at room temperature. A precipitate formed and was collected via vacuum filtration and dried to afford PDT (976 mg, 93%).

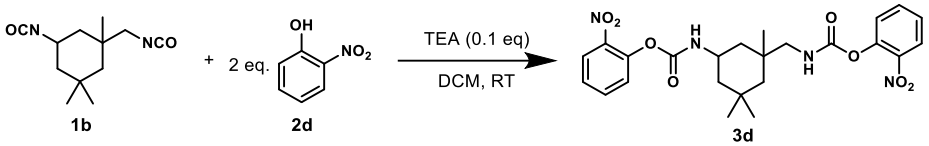

2-nitrophenyl ((1,3,3-trimethyl-5-(((2-nitrophenoxy)carbonyl)amino)cyclohexyl)methyl)carbamate (3d): To a 50 mL round bottom flask is added 2-nitrophenol (1.33 g, 9.5 mmol, 2.0 eq) in acetonitrile (10 mL). Triethylamine (0.07 mL, 0.47 mmol, 0.1 eq) is added to the stirring solution. Lastly, isophorone diisocyanate (1.0 mL, 4.7 mmol, 1.0 eq) is added to the reaction. The reaction is left to stir at reflux overnight. Upon cooling, a precipitate forms. This solid is collected via vacuum filtration and dried to afford PDT (1.34 g, 57%).

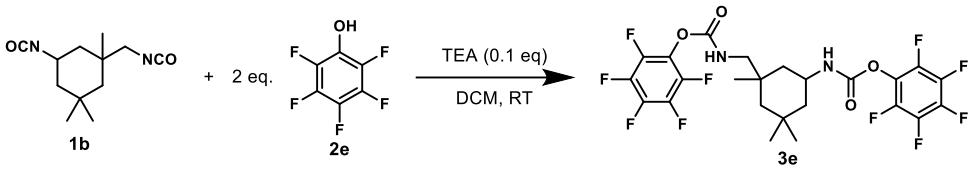

Perfluorophenyl (3,3,5-trimethyl-5-((((perfluorophenoxy)carbonyl)amino)methyl)cyclohexyl)carbamate (3e): To a 50 mL round bottom flask is added 2,3,4,5,6-pentafluorophenol (1.76 g, 9.5 mmol, 2.0 eq) in acetonitrile (10 mL). Triethylamine (0.07 mL, 0.47 mmol, 0.1 eq) is added to the stirring solution. Lastly, isophorone diisocyanate (1.0 mL, 4.7 mmol, 1.0 eq) is added to the reaction. The reaction is left to stir at reflux overnight. Upon cooling, a precipitate forms. This solid is collected via vacuum filtration and dried to afford PDT (694 mg, 25%).

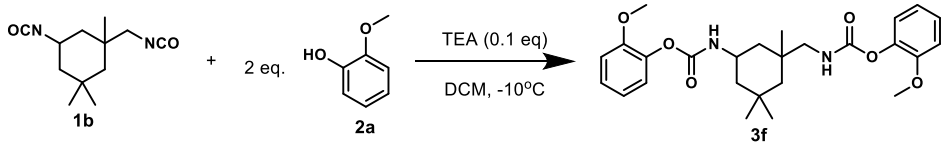

2-methoxyphenyl (3-((((2-methoxyphenoxy)carbonyl)amino)methyl)-3,5,5-trimethylcyclohexyl)carbamate (3f): To a 50 mL round bottom flask is added 2-methoxyphenol (0.95 mL, 8.5 mmol, 2.0 eq) in DCM (5 mL). Triethylamine (0.06 mL, 0.43

mmol, 0.1 eq) is added to the stirring solution. Lastly isophorone diisocyanate (0.89 mL, 4.3 mmol, 1.0 eq) is added to the reaction. The reaction is allowed to stir overnight at -10 °C. Once the reaction reaches room temperature, the reaction was concentrated *in vacuo* and dried to afford solid PDT (1.96 g, 97%).

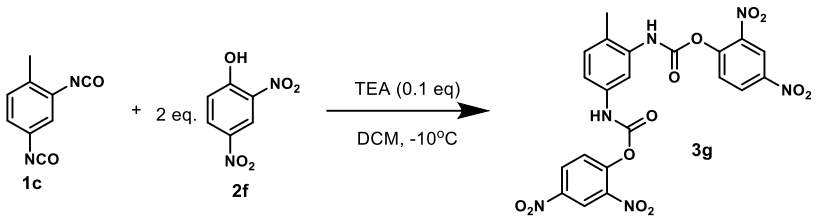

Bis(2,4-dinitrophenyl) (4-methyl-1,3-phenylene)dicarbamate (3g): To a 100 mL round bottom flask is added 2,4-dinitrophenol (2.1 g, 11.4 mmol, 2.0 eq) in DCM (10 mL). Triethylamine (0.08 mL, 0.57 mmol, 0.1 eq) is added to the stirring solution. Lastly, 2,4-toluene diisocyanate (0.82 mL, 5.7 mmol, 1.0 eq) is added to the reaction. The reaction is allowed to stir overnight at -10 °C. Once the reaction reaches room temperature, the reaction was concentrated *in vacuo*. A solid was collected and dried to afford PDT (2.91 g, 94%).

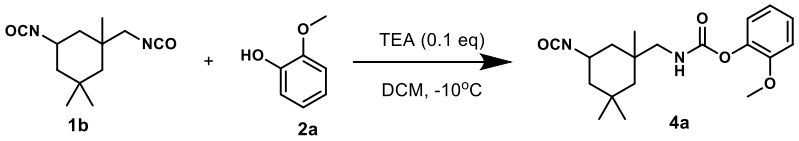

2-methoxyphenyl ((5-isocyanato-1,3,3-trimethylcyclohexyl)methyl)carbamate (4a): To a 50 mL round bottom flask is added 2-methoxyphenol (0.64 mL, 5.7 mmol, 1.0 eq) in DCM (5 mL). Triethylamine (0.08 mL, 0.57 mmol, 0.1 eq) is added to the stirring solution. Lastly, isophorone diisocyanate (1.2 mL, 5.7 mmol, 1.0 eq) is added to the reaction. The reaction is allowed to stir overnight at -10 °C. Once the reaction reaches room temperature, the reaction was concentrated *in vacuo*. A solid was collected and dried to afford PDT (1.91 g, 97%).

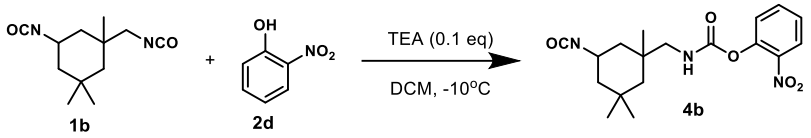

2-nitrophenyl ((5-isocyanato-1,3,3-trimethylcyclohexyl)methyl)carbamate (4b): To a 10 mL round bottom flask is added 2-nitrophenol (0.16 g, 1.12 mmol, 1.0 eq) in DCM (1.5 mL). Triethylamine (0.02 mL, 0.11 mmol, 0.1 eq) is added to the stirring solution. Lastly, isophorone diisocyanate (0.24 mL, 1.12 mmol, 1.0 eq) is added to the reaction. The reaction is allowed to stir overnight at -10 °C. Once the reaction reaches room temperature, the reaction was concentrated *in vacuo*. A solid was collected and dried to afford PDT (389 mg, 96%).

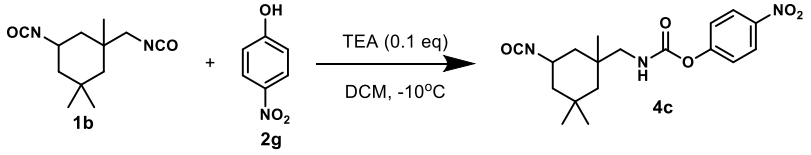

4-nitrophenyl ((5-isocyanato-1,3,3-trimethylcyclohexyl)methyl)carbamate(4c): To a 10 mL round bottom flask is added 4-nitrophenol (0.16 g, 1.12 mmol, 1.0 eq) in DCM (1.5 mL). Triethylamine (0.02 mL, 0.11 mmol, 0.1 eq) is added to the stirring solution. Lastly, isophorone diisocyanate (0.24 mL, 1.12 mmol, 1.0 eq) is added to the reaction. The reaction is allowed to stir overnight at -10 °C. Once the reaction reaches room temperature, the reaction was concentrated *in vacuo*. A solid was collected and dried to afford PDT (397 mg, 98%).

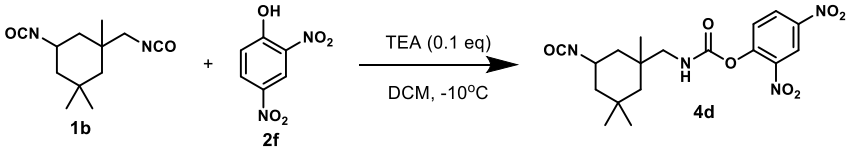

2,4-dinitrophenyl ((5-isocyanato-1,3,3-trimethylcyclohexyl)methyl)carbamate (4d): To a 10 mL round bottom flask is added 2,4-dinitrophenol (0.21 g, 1.12 mmol, 1.0 eq) in DCM (1.5 mL). Triethylamine (0.02 mL, 0.11 mmol, 0.1 eq) is added to the stirring solution. Lastly,

isophorone diisocyanate (0.24 mL, 1.12 mmol, 1.0 eq) is added to the reaction. The reaction is allowed to stir overnight at -10 °C. Once the reaction reaches room temperature, the reaction was concentrated *in vacuo*. A solid was collected and dried to afford PDT (414 mg, 91%).

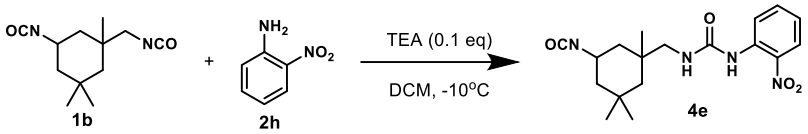

1-((5-isocyanato-1,3,3-trimethylcyclohexyl)methyl)-3-(2-nitrophenyl)urea (4e): To a 10 mL round bottom flask is added 2-nitroaniline (0.16 g, 1.12 mmol, 1.0 eq) in DCM (1.5 mL). Triethylamine (0.02 mL, 0.11 mmol, 0.1 eq) is added to the stirring solution. Lastly, isophorone diisocyanate (0.24 mL, 1.12 mmol, 1.0 eq) is added to the reaction. The reaction is allowed to stir overnight at -10 °C. Once the reaction reaches room temperature, the reaction was concentrated *in vacuo*. A solid was collected and dried to afford PDT (351 mg, 87%).

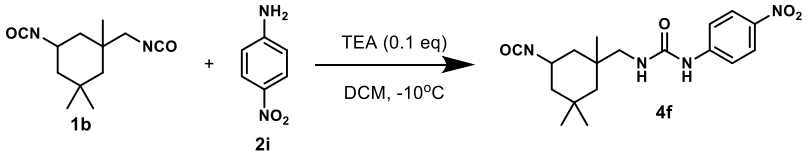

1-((5-isocyanato-1,3,3-trimethylcyclohexyl)methyl)-3-(4-nitrophenyl)urea (4f): To a 10 mL round bottom flask is added 4-nitroaniline (0.16 g, 1.12 mmol, 1.0 eq) in DCM (1.5 mL). Triethylamine (0.02 mL, 0.11 mmol, 0.1 eq) is added to the stirring solution. Lastly, isophorone diisocyanate (0.24 mL, 1.12 mmol, 1.0 eq) is added to the reaction. The reaction is allowed to stir overnight at -10 °C. Once the reaction reaches room temperature, the reaction was concentrated *in vacuo*. A solid was collected and dried to afford PDT (319 mg, 79%).

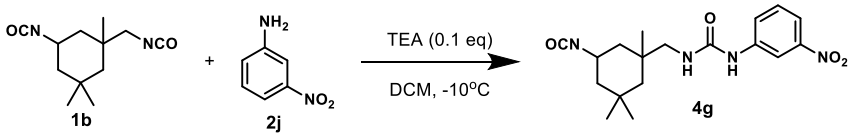

1-((5-isocyanato-1,3,3-trimethylcyclohexyl)methyl)-3-(3-nitrophenyl)urea (4g): To a 10 mL round bottom flask is added 3-nitroaniline (0.16 g, 1.12 mmol, 1.0 eq) in DCM (1.5 mL). Triethylamine (0.02 mL, 0.11 mmol, 0.1 eq) is added to the stirring solution. Lastly, isophorone diisocyanate (0.24 mL, 1.12 mmol, 1.0 eq) is added to the reaction. The reaction is allowed to stir overnight at -10 °C. Once the reaction reaches room temperature, the reaction was concentrated *in vacuo*. A solid was collected and dried to afford PDT (384 mg, 95%).

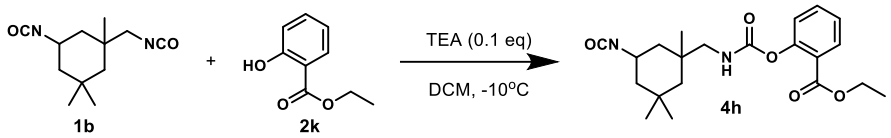

Ethyl 2-((((5-isocyanato-1,3,3-trimethylcyclohexyl)methyl)carbamoyl)oxy)benzoate (4h): To a 10 mL round bottom flask is added ethyl 2-hydroxybenzoate (0.16 mL, 1.12 mmol, 1.0 eq) in DCM (1.5 mL). Triethylamine (0.02 mL, 0.11 mmol, 0.1 eq) is added to the stirring solution. Lastly, isophorone diisocyanate (0.24 mL, 1.12 mmol, 1.0 eq) is added to the reaction. The reaction is allowed to stir overnight at -10 °C. Once the reaction reaches room temperature, the reaction was concentrated *in vacuo*. A solid was collected and dried to afford PDT (392 mg, 90%).

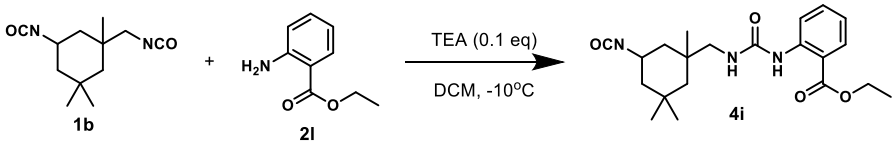

Ethyl 2-(3-((5-isocyanato-1,3,3-trimethylcyclohexyl)methyl)ureido)benzoate (4i): To a 10 mL round bottom flask is added ethyl 2-aminobenzoate (0.17 mL, 1.12 mmol, 1.0 eq) in DCM (1.5 mL). Triethylamine (0.02 mL, 0.11 mmol, 0.1 eq) is added to the stirring solution. Lastly, isophorone diisocyanate (0.24 mL, 1.12 mmol, 1.0 eq) is added to the reaction. The reaction is

allowed to stir overnight at -10 °C. Once the reaction reaches room temperature, the reaction was concentrated *in vacuo*. A solid was collected and dried to afford PDT (286 mg, 66%).

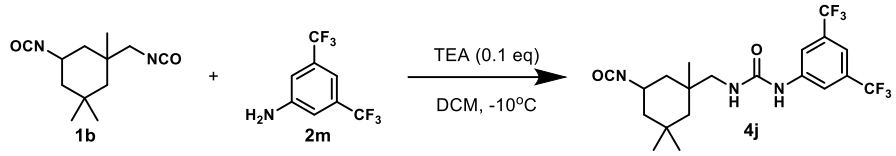

1-(3,5-bis(trifluoromethyl)phenyl)-3-((5-isocyanato-1,3,3-trimethylcyclohexyl)methyl)urea (4j): To a 10 mL round bottom flask is added 3,5-bis(trifluoromethyl)aniline (0.18 mL, 1.12 mmol, 1.0 eq) in DCM (1.5 mL). Triethylamine (0.02 mL, 0.11 mmol, 0.1 eq) is added to the stirring solution. Lastly, isophorone diisocyanate (0.24 mL, 1.12 mmol, 1.0 eq) is added to the reaction. The reaction is allowed to stir overnight at -10 °C. Once the reaction reaches room temperature, the reaction was concentrated *in vacuo*. A solid was collected and dried to afford PDT (450 mg, 89%).

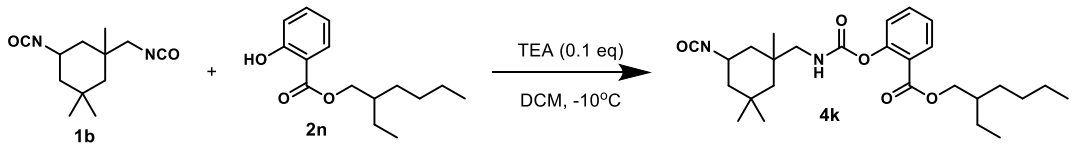

2-ethylhexyl 2-((((5-isocyanato-1,3,3-trimethylcyclohexyl)methyl)carbamoyl)oxy)benzoate (4k): To a 10 mL round bottom flask is added 2-ethylhexyl 2-hydroxybenzoate (0.28 mL, 1.12 mmol, 1.0 eq) in DCM (1.5 mL). Triethylamine (0.02 mL, 0.11 mmol, 0.1 eq) is added to the stirring solution. Lastly, isophorone diisocyanate (0.24mL, 1.12 mmol, 1.0 eq) is added to the reaction. The reaction is allowed to stir overnight at -10 °C. Once the reaction reaches room temperature, the reaction was concentrated *in vacuo*. A solid was collected and dried to afford PDT (503 mg, 95%).

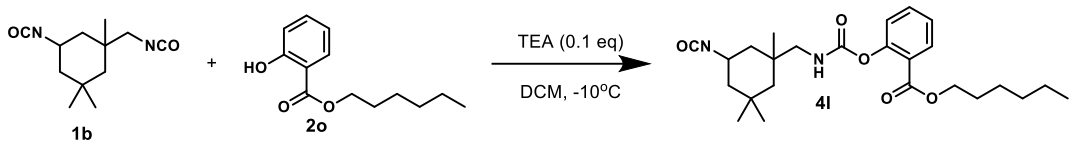

Hexyl 2-((((5-isocyanato-1,3,3-trimethylcyclohexyl)methyl)carbamoyl)oxy)benzoate (4l): To a XX mL round bottom flask is added hexyl 2-hydroxybenzoate (0.24 g, 1.12 mmol, 1.0 eq) in DCM (1.5 mL). Triethylamine (0.02 mL, 0.11 mmol, 0.1 eq) is added to the stirring solution. Lastly, isophorone diisocyanate (0.24 mL, 1.12 mmol, 1.0 eq) is added to the reaction. The reaction is allowed to stir overnight at -10 °C. Once the reaction reaches room temperature, the reaction was concentrated *in vacuo*. A solid was collected and dried to afford PDT (473 mg, 95%).

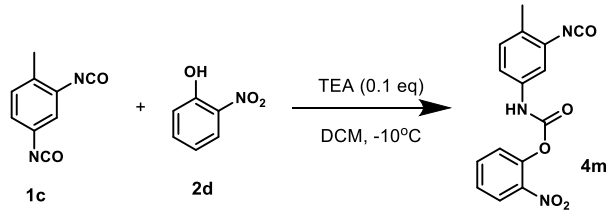

2-nitrophenyl (3-isocyanato-4-methylphenyl)carbamate (4m): To a 10 mL round bottom flask is added 2-nitrophenol (0.20 g, 1.44 mmol, 1.0 eq) in DCM (1.5 mL). Triethylamine (0.02 mL, 0.14 mmol, 0.1 eq) is added to the stirring solution. Lastly, 2,4-toluene diisocyanate (0.21 mL, 1.44 mmol, 1.0 eq) is added to the reaction. The reaction is allowed to stir overnight at -10 °C. Once the reaction reaches room temperature, the reaction was concentrated *in vacuo*. A solid was collected and dried to afford PDT (406 mg, 90%).

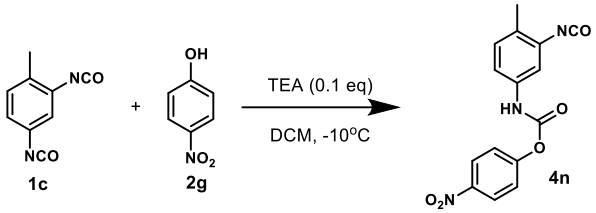

4-nitrophenyl (3-isocyanato-4-methylphenyl)carbamate (4n): To a 10 mL round bottom flask is added 4-nitrophenol (0.20 g, 1.44 mmol, 1.0 eq) in DCM (1.5 mL). Triethylamine (0.02 mL, 0.14 mmol, 0.1 eq) is added to the stirring solution. Lastly, 2,4-toluene diisocyanate (0.21 mL, 1.44 mmol, 1.0 eq) is added to the reaction. The reaction is allowed to stir overnight at -10 °C. Once the reaction reaches room temperature, the reaction was concentrated *in vacuo*. A solid was collected and dried to afford PDT (442 mg, 98%).

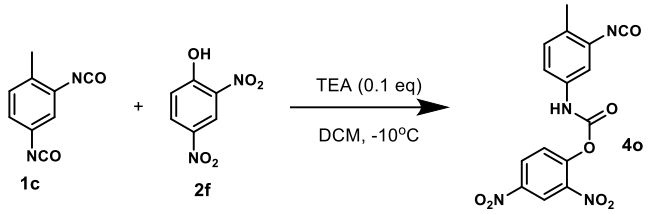

2,4-dinitrophenyl (3-isocyanato-4-methylphenyl)carbamate (4o): To a 250 mL round bottom flask is added 2,4-dinitrophenol (5.29 g, 28.7 mmol, 1.0 eq) in DCM (25 mL). Triethylamine (0.4 mL, 2.87 mmol, 0.1 eq) is added to the stirring solution. Lastly, 2,4-toluene diisocyanate (4.13 mL, 28.7 mol, 1.0 eq) is added to the reaction. The reaction is allowed to stir overnight at -10 °C. Once the reaction reaches room temperature, the reaction was concentrated *in vacuo*. A solid was collected and dried to afford PDT (10.2 g, 99%).

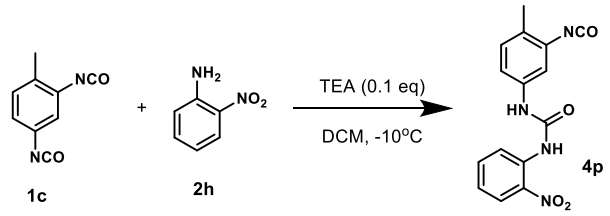

1-(3-isocyanato-4-methylphenyl)-3-(2-nitrophenyl)urea (4p): To a 10 mL round bottom flask is added 2-nitroaniline (0.20 g, 1.44 mmol, 1.0 eq) in DCM (1.5 mL). Triethylamine (0.02 mL, 0.14 mmol, 0.1 eq) is added to the stirring solution. Lastly, 2,4-toluene diisocyanate (0.21

mL, XX mol, 1.0 eq) is added to the reaction. The reaction is allowed to stir overnight at -10 °C. Once the reaction reaches room temperature, the reaction was concentrated *in vacuo*. A solid was collected and dried to afford PDT (405 mg, 90%).

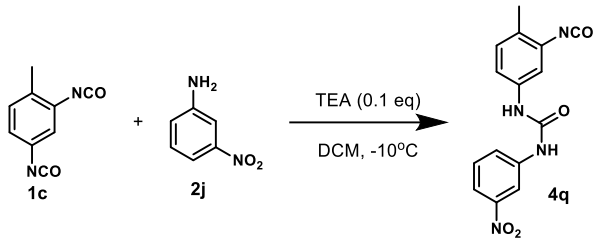

1-(3-isocyanato-4-methylphenyl)-3-(3-nitrophenyl)urea (4q): To a 10 mL round bottom flask is added 3-nitroaniline (0.20 g, 1.44 mmol, 1.0 eq) in DCM (1.5 mL). Triethylamine (0.02 mL, 0.14 mmol, 0.1 eq) is added to the stirring solution. Lastly, 2,4-toluene diisocyanate (0.21 mL, 1.44 mmol, 1.0 eq) is added to the reaction. The reaction is allowed to stir overnight at -10 °C. Once the reaction reaches room temperature, the reaction was concentrated *in vacuo*. A solid was collected and dried to afford PDT (441 mg, 98%).

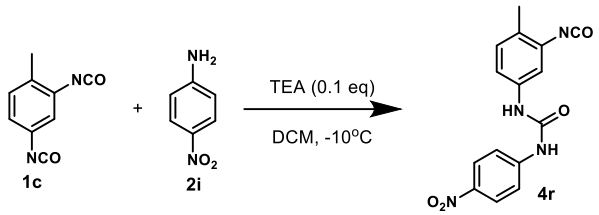

1-(3-isocyanato-4-methylphenyl)-3-(4-nitrophenyl)urea (4r): To a 10 mL round bottom flask is added 4-nitroaniline (0.20 g, 1.44 mmol, 1.0 eq) in DCM (1.5 mL). Triethylamine (0.02 mL, 0.14 mmol, 0.1 eq) is added to the stirring solution. Lastly, 2,4-toluene diisocyanate (0.21 mL, 1.44 mmol, 1.0 eq) is added to the reaction. The reaction is allowed to stir overnight at -10 °C. Once the reaction reaches room temperature, the reaction was concentrated *in vacuo*. A solid was collected and dried to afford PDT (418 mg, 93%).

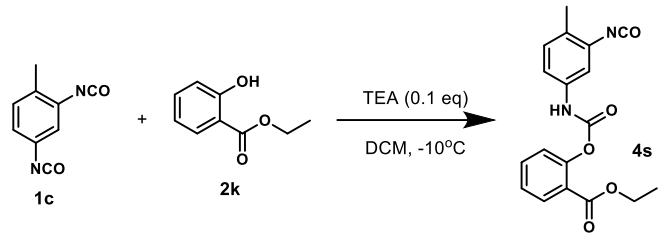

Ethyl 2-(((3-isocyanato-4-methylphenyl)carbamoyl)oxy)benzoate (4s): To a 10 mL round bottom flask is added ethyl 2-hydroxybenzoate (0.21 mL, 1.44 mmol, 1.0 eq) in DCM (1.5 mL). Triethylamine (0.02 mL, 0.14 mmol, 0.1 eq) is added to the stirring solution. Lastly, 2,4-toluene diisocyanate (0.21 mL, 1.44 mmol, 1.0 eq) is added to the reaction. The reaction is allowed to stir overnight at -10 °C. Once the reaction reaches room temperature, the reaction was concentrated *in vacuo*. A solid was collected and dried to afford PDT (470 mg, 96%).

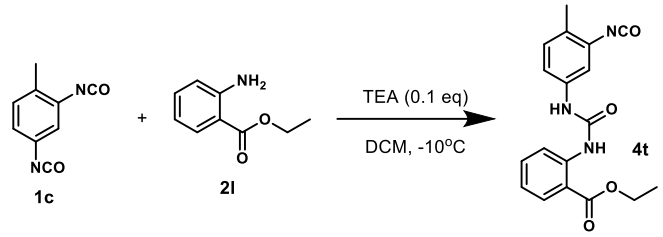

Ethyl 2-(3-(3-isocyanato-4-methylphenyl)ureido)benzoate (4t): To a 10 mL round bottom flask is added ethyl 2-aminobenzoate (0.21 mL, 1.44 mmol, 1.0 eq) in DCM (1.5 mL). Triethylamine (0.02 mL, 0.14 mmol, 0.1 eq) is added to the stirring solution. Lastly, 2,4-toluene diisocyanate (0.21 mL, 1.44 mmol, 1.0 eq) is added to the reaction. The reaction is allowed to stir overnight at -10 °C. Once the reaction reaches room temperature, the reaction was concentrated *in vacuo*. A solid was collected and dried to afford PDT (479 mg, 98%).

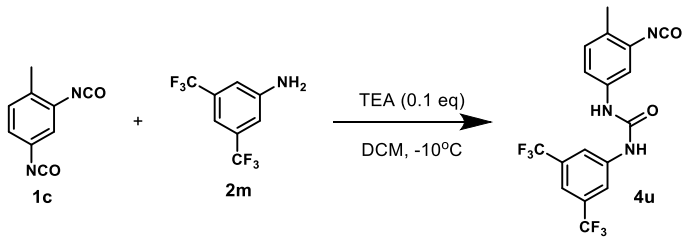

1-(3,5-bis(trifluoromethyl)phenyl)-3-(3-isocyanato-4-methylphenyl)urea (4u): To a 10 mL round bottom flask is added 3,5-bis(trifluoromethyl)aniline (0.22 mL, 1.44 mmol, 1.0 eq) in DCM (1.5 mL). Triethylamine (0.02 mL, 0.14 mmol, 0.1 eq) is added to the stirring solution. Lastly, 2,4-toluene diisocyanate (0.21 mL, 1.44 mmol, 1.0 eq) is added to the reaction. The reaction is allowed to stir overnight at -10 °C. Once the reaction reaches room temperature, the reaction was concentrated *in vacuo*. A solid was collected and dried to afford PDT (534 mg, 92%).

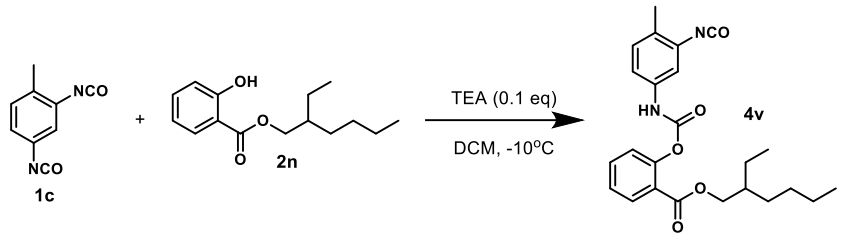

2-ethylhexyl 2-(((3-isocyanato-4-methylphenyl)carbamoyl)oxy)benzoate (4v): To a 10 mL round bottom flask is added 2-ethylhexyl 2-hydroxybenzoate (0.36 mL, 1.44 mmol, 1.0 eq) in DCM (1.5 mL). Triethylamine (0.02 mL, 0.14 mmol, 0.1 eq) is added to the stirring solution. Lastly, 2,4-toluene diisocyanate (0.21 mL, 1.44 mmol, 1.0 eq) is added to the reaction. The reaction is allowed to stir overnight at -10 °C. Once the reaction reaches room temperature, the reaction was concentrated *in vacuo*. A solid was collected and dried to afford PDT (575 mg, 94%).

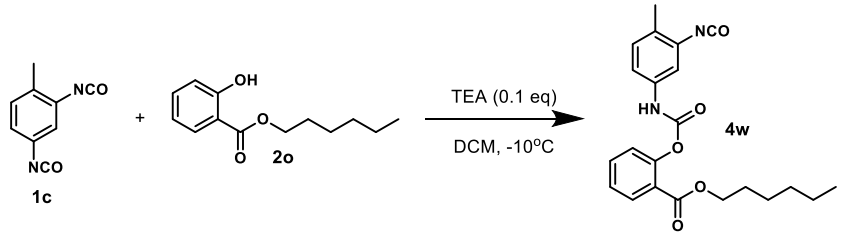

Hexyl 2-(((3-isocyanato-4-methylphenyl)carbamoyl)oxy)benzoate (4w): To a 10 mL round bottom flask is added hexyl 2-hydroxybenzoate (0.31 mL, 1.44 mmol, 1.0 eq) in DCM (1.5 mL). Triethylamine (0.02 mL, 0.14 mmol, 0.1 eq) is added to the stirring solution. Lastly, 2,4-toluene diisocyanate (0.21 mL, 1.44 mmol, 1.0 eq) is added to the reaction. The reaction is allowed to stir overnight at -10 °C. Once the reaction reaches room temperature, the reaction was concentrated *in vacuo*. A solid was collected and dried to afford PDT (502 mg, 88%).

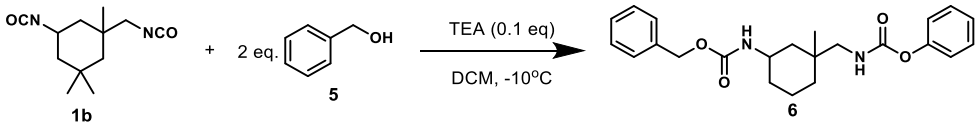

Benzyl (3,3,5-trimethyl-5-(((phenoxycarbonyl)amino)methyl)cyclohexyl)carbamate (6): To a 50 mL round bottom flask is added benzyl alcohol (1.0 g, 9.5 mmol, 2.0 eq) in acetonitrile (10 mL). Triethylamine (0.13 mL, 0.95 mmol, 0.1 eq) is added to the stirring solution. Lastly, isophorone diisocyanate (1.0 mL, 4.8 mmol, 1.0 eq) is added to the reaction. The reaction is allowed to stir overnight at room temperature. The reaction was concentrated *in vacuo* and dried to afford solid PDT (1.69 g, 83%).

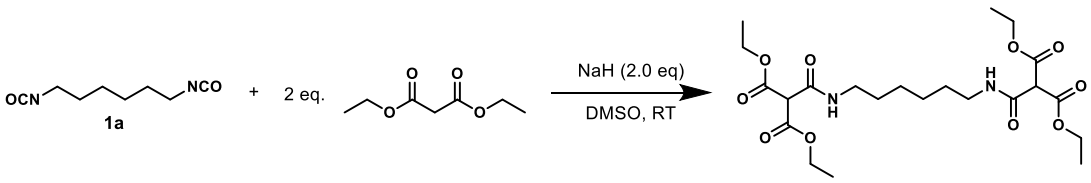

Tetraethyl 2,2'-((hexane-1,6-diylbis(azanediyl))bis(carbonyl))dimalonate: To an oven 50 mL round bottom flask is added ethyl malonate (0.31 mL, 2.0 mmol, 2.0 eq) in dry DMSO (5 mL). Sodium hydride (60 wt% in oil dispersion; 80 mg, 2.0 mmol, 2.0 eq) is added and the solution is capped and allowed to stir until homogenous. Hexamethylene diisocyanate (0.16 mL, 1.0 mmol, 1.0 eq) is added dropwise via syringe through a septa and the reaction is allowed to stir for 2 hours at ambient temperature. The reaction solution is added to cold DI water (50

mL) and extracted with DCM (3 x 50 mL). The combined organic layers were dried over magnesium sulfate and concentrated *in vacuo* to afford solid PDT (176 mg, 36%).

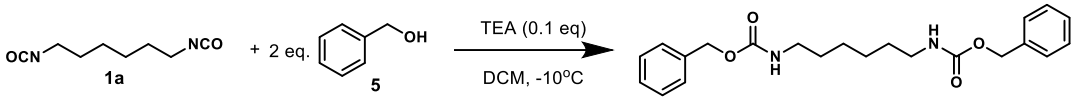

Dibenzyl hexane-1,6-diyldicarbamate: To a 50 mL round bottom flask is added benzyl alcohol (0.26 mL, 2.5 mmol, 2.0 eq) in acetonitrile (5 mL). Triethylamine (0.02 mL, 0.13 mmol, 0.1 eq) is added to the stirring solution. Lastly, hexamethylene diisocyanate (0.20 mL, 1.25 mmol, 1.0 eq) is added to the reaction. The reaction is allowed to stir overnight at room temperature. The reaction was concentrated *in vacuo* and dried to afford solid PDT (366 mg, 76%).

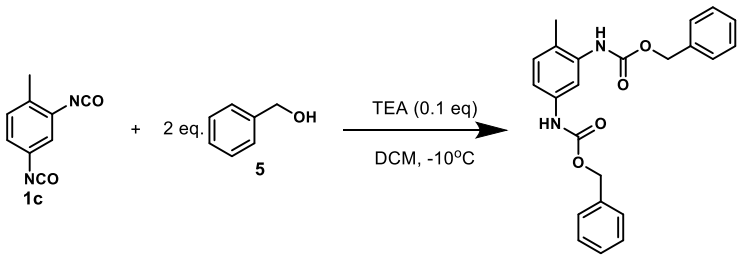

Dibenzyl (4-methyl-1,3-phenylene)dicarbamate: To a 50 mL round bottom flask is added benzyl alcohol (0.53 mL, 5.1 mmol, 2.0 eq) in DCM (5 mL). Triethylamine (0.04 mL, 0.25 mmol, 0.1 eq) is added to the stirring solution. Lastly, 2,4-toluene diisocyanate (0.36 mL, 2.5 mmol, 1.0 eq) is added to the reaction. The reaction is allowed to stir overnight at room temperature. The reaction was concentrated *in vacuo* and dried to afford solid PDT (849 mg, 87%).

4.7 References

1 D. A. Wicks and Z. W. Wicks, *Prog. Org. Coatings*, 2001, **41**, 1–83.

2 E. Delebecq, J. P. Pascault, B. Boutevin and F. Ganachaud, *Chem. Rev.*, 2012, **113**, 80–118.

3 A. K. Mahanta and D. D. Pathak, *Polyurethane*.

4 S. Chaturvedi and P. N. Dave, *Arab. J. Chem.*, 2019, **12**, 2061–2068.

5 J. D. Hunley, *35th Jt. Propuls. Conf. Exhib.*

6 M. S. Rolph, A. L. J. Markowska, C. N. Warriner and R. K. O'Reilly, *Polym. Chem.*, 2016, **7**, 7351–7364.

7 A. S. Nasar and S. Kalaimani, *RSC Adv.*, 2016, **6**, 76802–76812.

8 A. S. Nasar, S. Subramani and G. Radhakrishnan, *J. Polym. Sci. Part A Polym. Chem.*, 1999, **37**, 1815–1821.

9 C. K. Bina, K. G. Kannan and K. N. Ninan, *J. Therm. Anal. Calorim.*, 2004, **78**, 753–760.

10 W. H. Graham and R. E. Boothe, *Control of the Urethane Cure Reaction with Solid, Blocked Isocyanates*, 1986.